

Investigating regional recharge dynamics through the use of tritium and radiocarbon isotopes to assess the hydrological resilience of groundwater in southern Africa

by

Jared D. van Rooyen

This is submitted in fulfilment of the requirements of a



DOCTOR OF EARTH SCIENCE IN THE FACULTY OF SCIENCE

at Stellenbosch University

March 2021

Department of Earth Science, Stellenbosch University

Supervisor: Dr. Jodie Miller

DECLARATION

I hereby declare that the entirety of the work contained herein is my own, original work, that I am the authorship owner thereof (unless to the extent explicitly otherwise stated) and that I have not previously in its entirety or in part submitted it for obtaining any qualification. This thesis is submitted in fulfillment of a Doctor of Earth Science in the department of Earth Science, Stellenbosch University.

Full name: Jared D. van Rooyen

Signature:

Signed on.....22nd..... Day of.....October.....2020

Copyright © 2021 Stellenbosch University
All rights reserved

ABSTRACT

Water resources are integral in the global pursuit of equitable growth and sustainability. Although groundwater is the most abundant freshwater resource accessible to humans and the environment, it is often underrepresented in water management strategies and policy. Furthermore, groundwater reservoirs are not only vulnerable to contamination, but to depletion through climate change, land use change and increased water demand. As groundwater monitoring in southern Africa is sparse and long-term records are rarely available, it is difficult to constrain the groundwater system on a regional scale. Radioactive isotope tracers have proven effective in estimating recharge and residence times of groundwater over a local to global scale and could provide insight to regional groundwater vulnerability in an otherwise data poor region. The use of tritium (^3H) and radiocarbon (^{14}C) isotopes requires a comprehensive understanding of initial tracer abundance in recharge as well as subsurface physiochemical processes that affect the accuracy of predicted recharge rates and residence times. The release of ^3H and ^{14}C from thermo-nuclear bomb tests during the 1950's and 1960's changed the applications of these tracers in hydrology. However, the 'bomb peak' has been mostly attenuated in modern times and the return of atmospheric tracers to background levels presents new challenges and applications in hydrological studies. To constrain the natural variability of ^3H in South African rainfall, backward trajectories of 'water parcels' that produced sampled rainfall events were modelled to assess the controls of water mass origin on ^3H activity. It was found that ~90% of ^3H variability could be completely or partially explained by the origin of the water mass. By understanding the variability of ^3H in South African rainfall, the theoretical activity of ^3H in groundwater can be predicted through lumped parameter models. When combined with ^{14}C theoretical abundances, measured tracer abundance can be assessed as the proportion of modern groundwater and age of the fossil component in major aquifers across southern Africa. It was found that aquifers across southern Africa have diverse proportions of mixed groundwater (0.6 - 100%) that are mixed within a wide range of older groundwater, that range in calculated ages (105 - 59400 years) and mean residence times for each aquifer system (4698 - 27841 years). The distribution of ^3H activity in groundwater across South Africa was modelled using geostatistics that evaluated the effects of ^3H variability in precipitation and unsaturated zone travel time. The predicted ^3H surface agrees well to expected controls, with proximal (<100km) coastal regions, winter rainfall zones and deeper depth to groundwater predicted to have lower ^3H activities. Conversely, inland localities with shallower depth to groundwater and/or summer rainfall are predicted to have elevated ^3H activities. The predictive surface was then included as a recharge indicator in a novel groundwater vulnerability assessment, that incorporates both the risk of reducing groundwater quantity but also a deterioration in quality through modern contamination and sustained salinization. The assessment found that large portions of South Africa (22.4%) have a very high vulnerability to depletion in quantity and deterioration in quality, adding that this will likely increase (+3-6%) in the next 50 years as a result of climate change. This thesis outlines the need for an improved understanding of the vulnerability, sustainability and resilience of South Africa's groundwater resources and offers insight through an investigation to the efficacy of ^3H and ^{14}C as tracers of regional recharge dynamics.

LIST OF PUBLICATIONS

Peer reviewed articles

- van Rooyen, J.D.**, Palscu, L., Visser, A., Vennemann, T.W., Miller, J.A., 2020. Spatial and temporal variability of tritium in precipitation in South Africa and It's bearing on hydrological studies, *Journal of Environmental Radioactivity*, <https://doi.org/10.1016/j.jenvrad.2020.106354> Impact factor: 2.16
- van Rooyen, J.D.**, Miller, J.A., (2020). Using tritium and radiocarbon activities to constrain modern groundwater proportions in southern Africa. *J. Hydrol.* (Submitted, 29th August 2020) Impact factor: 4.50
- van Rooyen, J.D.**, Palscu, L., Watson, A.P., & Miller, J. A. (2020). Constraining the spatial distribution of tritium in groundwater and its bearing on modern recharge in South Africa. *Water Resources research*, (Submitted, 7th October 2020) Impact factor: 4.31
- van Rooyen, J.D.**, Watson, A.P. & Miller, J.A. Combining quantity and quality controls to determine groundwater vulnerability to depletion and deterioration throughout South Africa. *Environ Earth Sci* 79, 255 (2020). <https://doi.org/10.1007/s12665-020-08998-1> Impact factor: 2.18

Book Sections

Miller, J.A., Watson, A.P., Fleischer, M., Eilers, A., Sigidi, N.T., Van Gend, J., **van Rooyen, J.D.**, Clarke, C.E. & De Clercq, W.P. (2018) Groundwater quality, quantity, and recharge estimation on the West Coast of South Africa In: *Climate change and adaptive land management in southern Africa – assessments, changes, challenges, and solutions* (ed. by Revermann, R., Krewenka, K.M., Schmiedel, U., Olwoch, J.M., Helmschrot, J. & Jürgens, N.), pp. 86–95, *Biodiversity & Ecology*, 6, Klaus Hess Publishers, Göttingen & Windhoek.

Reports

Miller, Jodie A., Andrew P. Watson, Melanie Fleischer, Anya Eilers, Nthabeliseni T. Sigidi, Jani van Gend, **Jared D. van Rooyen**, Catherine E. Clarke, and Willem P. de Clercq. "Groundwater quality, quantity, and recharge estimation on the West Coast of South Africa. *Biodiversity & Ecology* (2018): 86-95.

van Rooyen, J.D., Miller, J.A., Watson, A.P., and Butler, M., 2018. Salinisation and groundwater vulnerability on the west coast of South Africa. In: *Application of Isotope Hydrology to understand saline groundwater and surface water systems and the interaction between them in the Western and Northern Cape provinces of South Africa* (ed. by Miller, J.A. and Watson, A.P.), pp 157-172, Water Research Commission, Pretoria.

TABLE OF CONTENTS

Declaration	i
Abstract.....	ii
List of Publications	iii
Table of Contents.....	iv
List of Figures	vii
List of Tables	xi
Acknowledgements.....	xii
Funding Contributors	xii
Data Contributors.....	xiii
CHAPTER 1 Introduction.....	1
1. Problem statement	4
2. Aims and objectives.....	4
3. Study premise	5
3.1. Isotope tracers.....	5
3.2. Techniques and models for tracers.....	10
4. Thesis outline.....	13
References	13
CHAPTER 2 Tritium in Precipitation	19
1. Introduction	20
2. Environmental context	22
3. Methodology.....	22
3.1. Sampling strategy	22
3.2. Analysis	23
3.3. HYSPLIT modelling structure	23
3.4. Statistical assessment of data.....	23
4. Results.....	23
4.1. Stable isotopes of oxygen and hydrogen.....	23
4.3. Tritium activity	24
4.4. Moisture origin through HYSPLIT models	25
5. Discussion.....	26
5.1. Seasonal effects on tritium activity in precipitation	26
5.2. Origin of water masses that form precipitation.....	28

5.3.	Event based spatial variability of tritium in precipitation	30
5.4.	Implication for hydrological studies	30
6.	Conclusions	30
	References	31
CHAPTER 3 Modern and Fossil Groundwater		32
1.	Introduction	33
2.	Methodology.....	36
2.1.	Construction of ^{14}C and ^3H abundance curves for southern Africa.....	36
2.2.	Compilation of groundwater reference data	38
2.3.	Correction of tracer activity in groundwater reference data.....	40
2.4.	Modelling modern vs fossil groundwater proportions.....	42
3.	Results.....	44
4.	Discussion.....	46
4.1.	Predicting tracer abundance in recharge and flow over time	46
4.2.	The dissolution of ‘dead’ carbon	47
4.3.	The variability of tritium in rainfall	47
4.4.	The distribution of modern and fossil groundwater in southern Africa	47
4.5.	Global suitability and implications	48
5.	Conclusions	49
	References	49
CHAPTER 4 Tritium in Groundwater		54
1.	Introduction	55
2.	Materials and methods	57
2.1.	Sampling strategy	57
2.2.	Analysis	58
2.3.	Measured ^3H in groundwater	58
2.4.	Environmental co-variables.....	58
2.5.	Data pre-processing.....	59
2.6.	Derivation of ^3H distribution surfaces.....	60
3.	Results.....	61
3.1.	Prediction variances and external drift	61
3.2.	Predicted activity of ^3H in groundwater.....	61
4.	Discussion.....	62
4.1.	Model validation and prediction variance.....	63

4.2.	Groundwater ³ H anomalies	63
4.3.	³ H and modern groundwater distributions	64
4.4.	Current and future context of ³ H distributions.....	65
5.	Conclusions	65
	References	66
CHAPTER 5	Groundwater Vulnerability.....	70
1.	Introduction	71
2.	Methodology.....	73
2.1.	Input parameters	74
2.2.	Model construction	76
2.3.	Sensitivity analysis.....	79
3.	Results.....	79
3.1.	Groundwater vulnerability	80
3.2.	Projected vulnerability	81
3.3.	Parameter sensitivity.....	82
4.	Discussion.....	82
4.1.	Model sensitivity	83
4.2.	Comparison to other South African GW vulnerability assessments.....	83
4.3.	Assessing groundwater vulnerability	86
4.4.	Application to groundwater management.....	87
5.	Conclusions	87
	References	88
CHAPTER 6	Conclusions and Recommendations	91
1.	Synopsis.....	91
2.	Major contributions.....	91
3.	Recommendations and future work.....	92
	References	93
Appendix	95

LIST OF FIGURES

Chapter 1 - Introduction

- Figure 1 – Conceptual diagram of the tritium cycle from its production in the upper atmosphere, incorporation in precipitation, recharge to decay in the subsurface. 2
- Figure 2 – A simplified framework of the study approach, breakdown of publications and their contributions to the research objectives. 3
- Figure 3 – The naturally occurring isotopes of hydrogen and their abundance. 5
- Figure 4 – The tritium time series and neutron monitor data in the Northern and Southern Hemisphere (László et al., 2020). 6
- Figure 5 – The naturally occurring isotopes of carbon and their abundance. 8
- Figure 6 – The fraction of modern carbon change during a) the onset of the industrial revolution, ~1900-1950 (Reimer et al., 2013) and b) the testing of above ground thermonuclear weapons, 1953-1964 (Hua et al., 2013). 8
- Figure 7 - The range of ^{14}C isotope ratios (black numbers) among different reservoirs of the Earth system, expressed relative to the atmospheric ^{14}C content defined in the preindustrial as 1.0, specifically based on wood from 1890. The percent of total ^{14}C atoms in the Earth system (red numbers) is a combination of the total C pool size and the ^{14}C age of the pool (Schuur et al., 2016). 9

Chapter 2 - Tritium in Precipitation

- Figure 1 – Schematic of the natural controls on tritium activity in global precipitation. (1) Geomagnetic modulation of cosmic bombardment of nitrogen to produce tritium in the upper atmosphere; (2) increases in tropo-stratospheric mixing in spring; (3) varying amounts of convective vs stratiform rainfall; (4) moisture recycling over continent and (5) anthropogenic production through nuclear processes and radioactive waste. 21
- Figure 2 – Site map of collection locations for (a) regional precipitation samples and (b) Western Cape temporal and storm samples. Graded blue colour represents rainfall amount and rainfall zones are delineated by dashed lines in panel (a) for summer, winter and all year rainfall. 21
- Figure 3 – Stable isotope plots of summer and winter rainfall from Paarl. Bubble sizes represent rainfall in panel (a) and tritium activity in panel b. Plots include the Global Meteoric Water Line (GMWL) where $\delta\text{D} = 8 \times \delta^{18}\text{O} + 10$ and the Local Meteoric Water Line (LMWL) where $\delta\text{D} = 6.8 \times \delta^{18}\text{O} + 10.5$. 24
- Figure 4 – Box and Whisker plot showing the modal distributions of sample tritium activity populations for precipitation from Paarl (n=80), storm events 1 and 2 (n=34 and 32) and regional samples (n=57). Median values are represented by a solid horizontal line and mean values by an 'x'. 24
- Figure 5 – Daily rainfall collected in Paarl for the one year period from October 2017 to October 2018. Tritium activities for sampled rainfall for events are plotted in panel (a) and divided into rainfall events larger than 5 mm. Stable isotope values are plotted in panel (b) and divided into δD and $\delta^{18}\text{O}$. 25
- Figure 6 – Measured tritium activity [TU] of precipitation events as a function of the amount of precipitation [mm/d]. 26
- Figure 7 – Tritium activities sampled from a single precipitation event over a 3 day period collected in Paarl. Included is the monthly weighted average of tritium from the same location for the month of June 2018. Lengths of the bars represent the duration over which the sample was taken and heights present the analytical error. 26
- Figure 8 – HYSPLIT particle tracks (top) from three separate precipitation events (Panels a, b, c) collected from the temporal sampling location in Paarl, Western Cape. Particles record hourly meteorological data (middle) which enables the model to calculate expected spatial contributions of water mass origin (bottom). Each example was selected to show

distinct precipitation origin mechanisms that result in local precipitation. Panel (a) represents a high altitude, low latitude origin with evidence of continental recycling of moisture, panel (b) represents a typical winter frontal system of mixed altitude origins originating from the nearby ocean and panel (c) represents a low altitude, high latitude origin in the Southern Ocean. 27

Figure 9 – Monthly averages and weighted monthly averages of tritium activity in precipitation sampled in Paarl, plotted with (a) monthly precipitation amounts (bars) and cumulative precipitation (lines) of total (blue) and sampled (grey) precipitation and (b) monthly averages of δD and $\delta^{18}O$ from sampled events (squares and circles) and historical stable isotope records from the nearest GNIP station approx. 43km away (connected squares and circles). Dashed lines represent the annual mean and weighted mean of tritium in precipitation. 28

Figure 10 – Combine moisture origin heat maps of precipitation received in Paarl, Western Cape, in summer (a) and winter (b). Moisture sources are characterized as volume [mm] proportions of individual precipitation events and combine to show the moisture origins of the total precipitation received in a season. 29

Chapter 3 -Modern and Fossil Groundwater

Figure 1 – The spatial distribution of alluvial and major rock aquifers that contain 3H and ^{14}C reference data in relation to the SADC. Rainfall isohyets are included to give context to the large variability in regional recharge potential. 35

Figure 2 – Simplified model framework depicting the steps followed to predict the presence of mixed groundwater and the range of mean residence times (MRT) from historical atmospheric and soil data records and measured tracer abundances of ^{14}C and 3H in groundwater. 36

Figure 3 – The atmospheric record of ^{14}C and 3H in precipitations from six GNIP stations for 3H and three published records for ^{14}C . The weight moving average is calculated for 3H activity (stippled black line). 37

Figure 4 – Predicted activity of ^{14}C and 3H from a renewal rate model (a) and exponential flow models (b). Atmospheric (blue) and Soil zone (brown) data was used for renewal rate models. Exponential flow models were calculated for $f=0.6$ (green), $f=0.8$ (blue) and $f=1$ (yellow). Lines for carbonate dissolution and decadal mixing of modern and fossil components are shown in panel b. 38

Figure 5 – The distribution of $\delta^{13}C$ in C3 and C4 plants (Green) (O'Leary, 1988) and in groundwater samples included in this study. Samples are stacked according to their country of origin. 40

Figure 6 – The distribution of carbonate bearing lithologies: according to lithologies that contain significant coal deposits (black), secondary carbonate bearing rocks that contains calcareous rich sands and or clays (light blue) and primary carbonate rocks such as limestones, chert beds, marls and karstic aquifers (panel a), C4 proportion of vegetation derived from satellite data, field observations and known plant distributions (panel b) and winter (WRZ) vs all year (YRZ) vs summer (SRZ) rainfall zones, represented as a percentages of consensus of previous literature that delineated rainfall zones in southern Africa (c), with reference to spatial groundwater data 41

Figure 7 – Theoretical corrections scenarios for $\delta^{13}C/^{14}C$ that plot left (a) and right (b) of the closed system dissolution line. Uncorrected (white square) and corrected (red square) samples are connected by open, open & closed and closed system correction lines (black with arrow). 41

Figure 8 – $\delta^{13}C$ and ^{14}C of samples separate by country, dot colours are according to the proportion of C4 in surface vegetation from <5% (Green) to 30% (yellow) >60% (blue). Dilution lines calculated using eq. 3 are shown for <5% C4 (Green line) and >60% C4 (blue line) with 5% range lines (stippled lines). 42

Figure 9 – Predicted mixed and unmixed groundwater (white and grey boxes) from actual mean residence time (MRT) in mixed water from corrected tracer input, using a tracer abundance curves. Dotted black lines represent the array of mixing scenarios, should the mixing be binary. 43

Figure 10 – Groundwater sample ^{14}C and ^3H separated into decadal groups with predicted atmospheric (blue line) and soil zone (orange line) renewal rate models and exponential flow model, $f=0.6$ (grey line). Ranges of unmixed groundwater are represented by transparent grey sections, delineated by the range of predicted abundance curves produced from renewal rate and groundwater flow models. 44

Figure 11 – The percentage of mixed wells (pie charts) with a range of MRTs for the given aquifer system. Samples with evidence of modern and Holocene/fossil groundwater mixing are coloured in blue whereas samples that indicated that no significant mixing are coloured in red. 45

Chapter 4 – Tritium in Groundwater

Figure 1 - The distribution of ^3H in groundwater sample locations as well as the major towns in South Africa. Mean annual precipitation is represented in mm in ten classes (Schulze et al., 2006). 56

Figure 2 - Box plot showing the basic ^3H model statistics of the seven sampling campaigns used to collect groundwater in this study as well as the DWA database used to supplement the collected groundwater data. 57

Figure 3 - The semivariance of point pairs computed as a variogram cloud in the data outlier analysis. Semivariance is represented as the average γ for a point pair as calculated in equation 1. 58

Figure 4 - The frequency distribution of a) measured ^3H (Tritium Units) in groundwater and b) the predicted depth to groundwater (meters below ground level) of all 722 samples. The relationship of ^3H and depth to groundwater is plotted in c). 59

Figure 5 - The geostatistical results for variogram fit, predicted ^3H activity and prediction variance of a) the empirical calculation of ^3H distribution independent on external controls on activity and the residuals calculations of ^3H distribution dependent on external controls on activity for b) depth to water, c) summer vs winter rainfall and d) Euclidean distance from the ocean. 60

Figure 6 - The predicted distribution of ^3H in groundwater by KED with all environmental co-variables. The geostatistical results for variogram fit and prediction variance (top left) and the uranium deposit extents are overlaid onto the distribution surface as well as the location of the South African escarpment. Locations of interest are included for a radioactive waste disposal site (Vaalputs) and a managed aquifer recharge location (Atlantis). 61

Figure 7 - Measured vs predicted ^3H activity in groundwater from the out-of-sample verification method. 62

Figure 8 - Autocorrelation results for ^3H in groundwater which determines low and high clusters of samples as well as high-low and low-high outliers in the spatial dataset. Included are depth to water contours on the interpolated surface computed for this study. 63

Chapter 5 – Groundwater Vulnerability

Figure 1 – The distribution of South Africa's population per province (dark boundaries) represented as percentage of total population (Census, 2011). South Africa is also divided into nineteen water management areas (WMA's), determined by the National Water Resource Strategy one (NWRS-1), shaded areas represent the new nine Catchment Management Agency (CMA) boundaries developed in NWRS-2. Major river systems across South Africa are represented with thickness according to the order of the river from source (note: some provincial boundaries are marked by major river systems and overlap in the figure). 72

Figure 2 – Model framework of the thematic layers, divided into two major subheadings and five minor subheadings, representing major and minor strategies. Major headings are divided according to parameters that are: (1) controlled by climatic indicators and (2) indicate the pollution potential of a groundwater system. Minor subheadings are divided under major heading (1) into: (3) GCM regional parameters and (4) recharge indicators and under major heading (2) into: (5) physical attributes; (6) chemical characteristics and (7) human groundwater dependence. 73

- Figure 3 – Reclassification scheme utilized to calculate the vulnerability index for each input parameter on a scale of 1-8, with a visualization of reclassified thematic layers. Each input variable was reclassified on a predetermined linear scale that either applies an equal interval weighting of the source data range or aligns to typical reported ranges associated with the parameter. 77
- Figure 4 – Framework of sensitivity analysis for groundwater vulnerability MCE methods. Adapted from (Napolitano and Fabbri, 1996) to test the sensitivity of the model to a single parameter at a time by adjusting each parameter individually and comparing the output. 79
- Figure 5 – The distribution of sensitivity shown across South Africa and divided into the nineteen water management areas (WMAs) according to the National Water Resource Strategy one (NWRS-1). Areas of low sensitivity are marked in blue and areas of high sensitivity in red. 79
- Figure 6 – Model sensitivity divided by parameter contribution to total sensitivity of each water management area (WMA) according to the National Water Resource Strategy one (NWRS-1). The order of WMAs is according to the official labels given in NWRS-1 and correspond to regions from the north east of the country to the south west. 80
- Figure 7 – Outputs of all 36 scenarios, grouped under major strategies as three main column groups and minor strategy combinations as maps within the columns, the presented scenario (MI/C-2/P-2) is outlined in red and the scenario that has been future projected in section 3.2 is highlighted in blue. 81
- Figure 8 – Percentage of total area of South Africa for five different categories of groundwater vulnerability (Very low, low, moderate, high and very high) per unit area. Results are presented as: (1) an equally weighted scenario or base scenario (light grey stippled); (2) the mean if all 36 scenarios (dark grey dot stippled) with range bars to show the ranges of included scenarios and (3) the presented MI/C-2/P-2 model scenario (solid black line). 82
- Figure 9 – Distribution of: a) groundwater vulnerability from the presented scenario MI/C-2/P-2, where major strategies are weighted equally and minor strategies are skewed toward recharge indicators and physical attributes; b) groundwater drought risk produced from Villholth et al., 2013 and c) DRASTIC groundwater vulnerability produced by Musekiwa and Majola, 2013. Water management areas are overlaid on the presented scenario to indicate the spatial distribution of groundwater vulnerabilities. 83
- Figure 10 – Groundwater vulnerability per water management area (WMA) produced from scenario MI/C-2/P-2 as a proportion of the total percentage vulnerability per an area. The order of the presented WMAs is according to the official labels given in NWRS-1 and correspond to regions from the north east of the country to the south west. 84
- Figure 11 – A comparative map showing an example scenario output (left) MI/C-3/P-2 of current groundwater vulnerability with of future (50 years) projected maps: (1) from the UKMO-HanCM3 GCM; (2) the lowest ensemble of 16 GCMs and (3) the highest ensemble of 16 GCMs. Outputs for all prediction models are presented under two emission scenarios: (1) SRES B1 low CO₂ emissions and (2) SRES A2 high CO₂ emissions. 84
- Figure 12 – A combined plot showing the percentage of total area of groundwater vulnerability for a current groundwater vulnerability (MI/C-3/P-2) with 6 projected maps 50 years into the future from : (1) the UKMO-HanCM3 GCM; (2) the lowest ensemble of 16 GCMs and (3) the highest ensemble of 16 GCMs. Outputs for all prediction models are presented under two emission scenarios: (1) SRES B1 low CO₂ emissions and (2) SRES A2 high CO₂ emissions. 84

LIST OF TABLES

Chapter 2 – Tritium in Precipitation

Table 1 – Statistically moments of precipitations data for (1) temporal precipitation events in Paarl, Western Cape divided into summer and winter seasonal precipitation, (2) two Storm events in the Western Cape (2017 and 2018) and (3) regional precipitation data from across South Africa.	23
Appendix Table 1 – Analysis results of samples collected in Paarl, Western Cape.	95
Appendix Table 2 – Analysis results of samples collected in single storm events.	97
Appendix Table 3 – Analysis results of regional samples.	99

Chapter 3 – Modern and Fossil Groundwater

Appendix Table 1 - ^{14}C and ^3H data, from across Namibia, Botswana, Mozambique and South Africa, collated from published and unpublished literature producing 624 data points.	101
Appendix Table 2 – Data sources for ^{14}C and ^3H data collated from previous studies.	108

Chapter 4– Tritium in Groundwater

Appendix Table 1 – Analysis results of samples collected in by authors over seven sampling campaigns.	121
Appendix Table 2 – Analysis results of samples collated by iThemba LABS and the Department of Water Affairs (DWA).	125

Chapter 5– Groundwater Vulnerability

Table 1 - Data sources utilized in the modelling framework. The table describes the attributes of the data source utilized as well as the reference period and source of the data.	74
Table 2 - Major and Minor strategy weightings that are possible in the 36 presented scenarios as well as the example scenario M-I/C-2/P-2.	77
Table 3 - Sensitivity analysis results presented with the effective weights of the base output and the example output MI/C-2/P-2.	85

ACKNOWLEDGEMENTS

First and foremost, I would like to extend my deepest gratitude to my supervisor, Prof. Jodie Miller. It has been a pleasure to have had the opportunity to complete this PhD and progress as a scientist under your guidance. Your unwavering patience for my development, as well as my quirks, is commendable and I trust that nothing will change as we move forward onto new and exciting prospects. In particular, your insights into the subtle, and not so subtle, nuances of science have encouraged my pursuit of an academic career and in turn made for a memorable postgraduate journey. I shall look back fondly on the endless debates, chit-chats, master plans, dreams and personal anecdotes we have shared during my time in Stellenbosch. This thesis, and my postgraduate work in its entirety, would not have been possible without your efforts to secure financial support and the resources necessary for sample collection, analysis, skills development, conference attendance and scientific exposure that formed the backbone of my research. I look forward to continuing a fruitful academic partnership in the future.

I would also like to acknowledge my close friend and mentor, Dr. Andrew Watson. The plethora of time and effort you have put into my development as a scientist has been integral to my development. A large portion of my understanding of the hydrogeological system is a direct result of your continued interest in my success. I also appreciate the personal support you have provided throughout my postgraduate studies, on and off the bike. To my other colleagues in the Earth Science department, I cannot thank you enough for the support in both my scientific and social endeavours.

I would like to mention a few specific mentors and colleagues that have, in their own ways, been instrumental in the success of this PhD. Prof. Gabriel Bowen and his team at the University of Utah, who's spatial short course provided the knowledge and skills necessary for the geostatistical undertakings of this study. To Prof. Torsten Vennemann from the University of Lausanne, your guidance and insight into the intricacies of stable isotopes in hydrology were the cornerstone of understanding tritium's journey in the atmosphere. To Dr. Ate Visser, without your supervision and insights into coding in R, the novel tritium models presented in this thesis would not have been possible, I cannot thank you enough for sharing your insights and experience in this regard. To Dr. Lazslo Palscu, without your analysis and guidance the majority this work would not be possible, your attention to detail has produced a one-of-a-kind dataset to be proud of.

The IAH and ECHN community has always been a constant pillar of support in my studies as well as my academic development. Your voluntary service is worth its weight in gold. To the past chairs and co-chairs who have guided our community and myself into such a strong position, I ensure you that your legacy of excellence, equity and support will be upheld in my tenure in the community. I would also like to indirectly thank the pioneers of research into tritium as a modern tracer, as your efforts formed the foundation on which this thesis is built.

Lastly, to my friends and family that have supported me throughout this journey, I am eternally grateful. To my wonderful life partner, I cannot thank you enough for always being there when I needed you, supporting my work and facilitating a wonderful home to nurture our relationship. The mostest. To my dearest Brother, you have always been a source of advice and a guiding light in the darkest times, ready to celebrate my success and dust me off when I fall. This is as much your success as it is mine. To my steadfast Mom, your unending support both emotionally and financially, as well as your continued interest in my life, is testament to your wealth of love and patience. I cannot wait to return the favour. To my beloved grandparents, your unwavering support and willingness to sacrifice on my behalf has truly been an inspiration. Your investment in my life and education is boundless and I hope that this work is only the beginning of my remuneration. Thank you all.

FUNDING CONTRIBUTORS

I would like to thank the Water Research Commission South Africa for initial funding support and the iPahakade program and National Research Foundation (NRF) South Africa for bursary support. I would also like to thank the 'backers' of the Know Your Water crowdfunding campaign that enabled this study to begin in 2016. This work is based on the research supported wholly/in part by the *National Research Foundation of South Africa* (Grant Number: 118594) and the Southern African Science

Centre for Climate Change and Adaptive Land Management (SASSCAL). Analysis was partly supported by the European Union and the State of Hungary, co-financed by the European Regional Development. These publication forms part of the output of the Biogeochemistry Research Infrastructure Platform (BIOGRIP) of the Department of Science and Innovation of South Africa.

DATA CONTRIBUTORS

The author and co-authors would like to thank all the data contributors that were used in this study. A portion of the data provided in this thesis was kindly made available by Dr. Roger Diamond on behalf of the late Mr. Siep Talma as well as Mike Butler (iThemba LABS) on behalf of the Department of Water Affairs (DWA) who also provided access to borehole information that was gathered in the National Groundwater Archive (NGA) as well as water level accessed from their website. The South African Weather Services (SAWS) and the Agricultural Research Council (ARC) provided access to climate and rainfall data. The author would like to thank the CGA for access to high resolution digital elevation model and the Council for Geosciences (CGS) for access to geological maps of the areas. Farmers within the study catchment provided access to boreholes, rainfall and climate information that was required for the modelling. Citizen scientists who collected water samples as part of the Know Your Water campaign.

CHAPTER 1 INTRODUCTION

The availability of freshwater represents the cornerstone of equitable, stable and productive societies and ecosystems (Rodell et al., 2018). As water demand and stress increase on a global scale, owing principally to climate change and population growth, the security of water resources has become a priority. The United Nations have recognized water security as one of the seventeen sustainable development goals (No.6) and predicts that large regions of the world are going to experience 'low water security' in the coming decades (United Nations, 2015). To mitigate water resource related socio-economic and environmental issues, stakeholders and policymakers need to ensure the sustainable procurement, development and remediation of global freshwater resources. Groundwater represents the most abundant freshwater resource accessible to both humans and the environment (Gleeson et al., 2016; Rodell et al., 2018), especially in semi-arid to arid regions where surface water is scarce (Mazzoni et al., 2018; Taylor et al., 2013). The use of groundwater is rapidly increasing as a result of anthropogenic climate change, increased food production and population growth (Cuthbert et al., 2019; Díaz-Cruz and Barceló, 2008; Ferguson and Gleeson, 2012; Gleeson et al., 2015; Zhang et al., 2001). As a result, groundwater is becoming increasingly vulnerable to depletion and contamination (Villholth et al., 2013; Wada et al., 2010), phenomena that are becoming more evident as the realities of climate change become apparent and attention turns to the resilience of the global water cycle.

The assessment of groundwater vulnerability is typically associated with the potential for a contaminant to enter a groundwater resource (Al-Adamat and Al-Shabeeb, 2017; Aller et al., 1987; Liu et al., 2003; Panagopoulos et al., 2006). Recent research suggests groundwater resources are not only vulnerable to contamination but are also vulnerable to depletion. The Gravity Recovery and Climate Experiment (GRACE) has enabled the quantifications of groundwater stress, carrying capacity, inter-annual fluctuation and storage of global groundwater resources (Gao et al., 2020; Richey et al., 2015; Thomas et al., 2017; Voss et al., 2013; Yeh et al., 2006). This data, supported by numerous local-scale investigations, indicates that global aquifers are under threat of groundwater depletion (GWD). The abstraction of groundwater faster than it is naturally replenished has caused an unremitting decline in local and regional water tables. This disparity between abstraction and recharge was quantified in northwest India, where the rate of water table decline was estimated at $4\pm 1 \text{ cm yr}^{-1}$ (equi. $17.7\pm 4.5 \text{ km}^3\text{yr}^{-1}$) (Rodell et al., 2015). Similar, albeit slower, rates of depletion have been documented in North China (Feng et al., 2013), the Middle East (Voss et al., 2013), U.S.A (Scanlon et al., 2012, 2005) and North Africa (Hamed et al., 2014). However, not all GWD is induced by abstraction and climate change effects on recharge can be significant (Thomas and Famiglietti, 2019).

A recent evaluation of GRACE derived data suggests that GWD estimates may be non-representative and the role of extreme precipitation events, intensified by climate change, is causing non-linearity in modern changes in groundwater storage (Shamsudduha and Taylor, 2019). The uncertainty associated with groundwater depletion estimates suggests that evaluating the response of groundwater to climate change is critical in the development of groundwater management strategies. As groundwater residence times are generally longer than other facets of the hydrological cycle, the groundwater response to change, both natural and anthropogenic, is often delayed. A useful metric to assess if a change is permanent or not is to constrain hydrological resilience, which is defined as a catchment's ability to absorb disturbance and maintain or quickly regain hydrologic function (Mao et al., 2017). A permanent change would in turn affect the vulnerability of local and regional groundwater to both depletion and deterioration. Although holistic groundwater vulnerability assessments are difficult to perform on a regional scale, vulnerability assessments that include the risk of GWD are now necessary. Additionally, modern recharge mechanics, which control a catchment's hydrological resilience, are changing as a result of climate change, land-use change and shifts in resource utilization (Hu et al., 2019). Understanding recharge is important for stakeholders and policymakers to assess groundwater vulnerability and in turn hydrological resilience, in a more robust manner.

The South African government outlines two basic principles of the National Water act; (1) equity and (2) sustainability, that are critical to the sustainable development goals of the country. Climate change is expected to adversely affect South Africa's hydrological resources and potentially add stress to the already fragile water supply. South Africa is a water scarce country with an average mean annual precipitation of 464mm (Global = 768mm) (Schulze et al., 2006), which ranges from below 100 mm in the Northern Cape to over 3200 mm in the high-altitude eastern interior. Rainfall is highly variable in spatial distribution and unpredictable, both within and between years. When combined with high evapotranspiration and run-off rates, water is

considered a major limiting resource for sustainable development in the country (Blamey et al., 2017). All nine of South Africa's catchment management agencies (CMA) have experienced varying degrees of drought crisis in the past two decades. As groundwater resources already form a cornerstone of water supply for agricultural, industrial, and urban use, it is paramount that groundwater dependent hydrological resilience is constrained on a regional scale. From 2015-2018, the City of Cape Town experienced a severe, prolonged drought that left surface water resources dangerously low (24.7%). The Western Cape government approved the augmentation of nearby groundwater resources to curtail the supply deficit. Such, groundwater supplementation schemes are becoming more common, not only in South Africa but also globally. As arid regions are predicted to be affected by climate change disrupting to the stationarity of recharge, constraining the vulnerability and resilience of regional groundwater is particularly important.

A myriad of investigative tools has been developed to assess aquifer recharge rates, yet there is no single instrument or method that can measure recharge accurately enough to be used exclusively (Cartwright et al., 2017; McGuire and McDonnell, 2006). Recharge estimates are typically performed using a combination of data collected and modelled through diverse approaches (Nimmo et al., 2005; Scanlon et al., 2002). Quantitative methods include water mass balances and numerical modelling, which carry with them substantial uncertainties and differ in approach according to the availability of data (surface vs groundwater). Chemical tracer methods are effective as a supplementary method of calibration and/or validation of typical recharge investigative techniques (Sanford, 2011). In regions where physical monitoring data availability is low, isotopic tracers have proven to be effective indicators of recharge, residence time and hydrological response to climate change (Cartwright et al., 2017; Zuber et al., 2011). Furthermore, isotopic methods are becoming more prevalent in hydrological studies due to advances in analytical capabilities and spatial statistics (West et al., 2009). Isotope tracers, both stable and radioactive, represent effective indicators of exchange between major components of the hydrological cycle that control hydrological resilience. Although a large suite of isotopes is used in hydrology, studies that investigate residence time typically use radioactive isotopes due to their predictable rate of decay/production in the subsurface. Additionally, noble gases such as krypton (^{85}Kr) and Argon (^{39}Ar) (including parent-daughter isotope methods) and compound tracers, such as chlorofluorocarbons or sulphur hexafluoride, are also used to predict residence time and recharge rates (Cartwright et al., 2017).

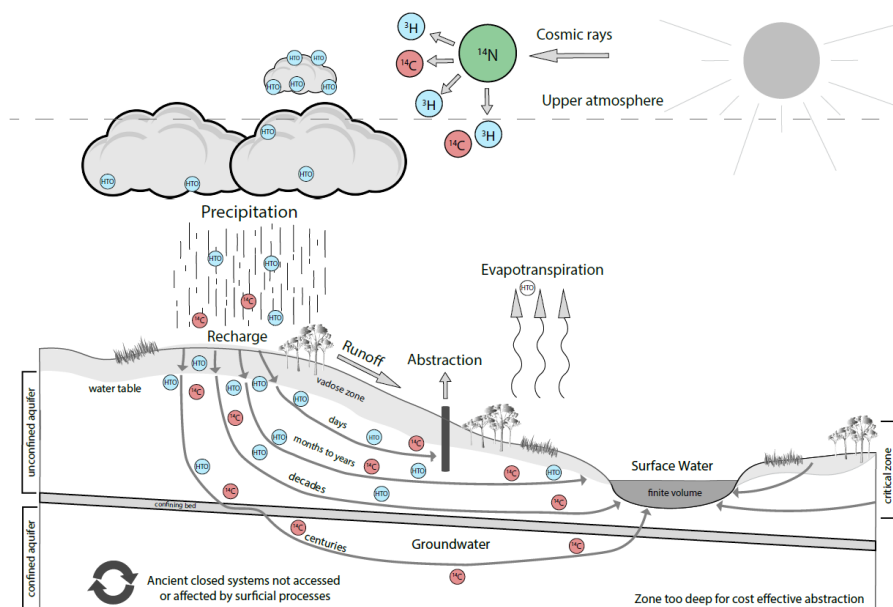


Figure 1 - Conceptual diagram of tritium and radiocarbon in the hydrological cycle, from the production in the upper atmosphere, incorporation in precipitation, recharge to decay in the subsurface

Groundwater residence times can be difficult to constrain as aquifers vary significantly in flow and recharge rate, from days to millennia (Fig.1). In order to capture this extremely wide range, the appropriate isotope and associated decay rate must be used. Additionally, each isotopic method incurs uncertainties associated with its residence time calculation due to isotope specific rates of production, incorporation and interaction within the aquifer system (e.g. carbonate dissolution in radiocarbon dating). Perhaps the least affected isotope systems are those that are within the water molecule itself. Stable isotopes of oxygen

(^{18}O) and hydrogen (^2H) are used extensively in the literature due to their conservative nature and predictable fractionation (Barbieri, 2019; Dansgaard, 1964; Fontes, 1980; Gonfiantini et al., 1998). Subsequently, the radioactive isotope of hydrogen, tritium (^3H), presents a unique opportunity for residence time and recharge investigations. ^3H is produced naturally in the upper atmosphere, incorporated into the water cycle, and falls out of secular equilibrium once isolated in the subsurface (Fig.1). The finite lifespan of ^3H in groundwater enables residence time studies to date relatively young/modern groundwater flow paths. Whereas radiocarbon (^{14}C) is a useful residence time tracer for older groundwater due to carbon's ubiquitous presence in the hydrological cycle and a substantially longer half-life (5730 years) than that of ^3H (12.312 years) (Fig.1). This enables ^{14}C to be used to date waters that have much older, fossil residence times (up to ~50 000 years)(Kalin, 2000). The capabilities of isotope tracers increase over smaller spatial extents and with more information about local climate, vadose zone and aquifer properties. To estimate modern groundwater proportions over a regional extent and its interaction with fossil groundwater, isotope systems and model approaches must be carefully selected to optimize predictions and in turn, assess the groundwater vulnerability of large catchments and watersheds.

Current approaches to groundwater vulnerability assessment treat risks associated with climate change, depletion, anthropogenic pollution and natural deterioration independently. These groundwater vulnerability models do not include isotope tracers, even though isotopes are ideal tracers of the hydrological cycle. The central goal of this project is to develop a model that incorporates hydrological tracers, which adds a layer of information about the hydrological cycle, to constrain the vulnerability of groundwater to a change in quantity and quality caused through various natural and anthropogenic processes. Before such a model can be developed the efficacy of hydrological tracers in southern Africa must be determined. In this study, ^3H and ^{14}C in precipitation and groundwater data are used to: (1) constrain the variability of ^3H in precipitation using an adapted model from HYSPLIT based trajectories, (2) relate modern and fossil groundwater through lumped parameter modelling, (3) predict the spatial distribution of ^3H in groundwater using geostatistics and (4) use ^3H in groundwater distributions within a holistic groundwater vulnerability assessment (Fig.2). The results of this study are not only relevant to groundwater management strategies in South Africa but apply to other water-scarce regions globally. The novel approaches and methods in this study showcase the potential for multi-isotope approaches that use ^3H and ^{14}C to support the assessment of groundwater vulnerability and hydrological resilience.

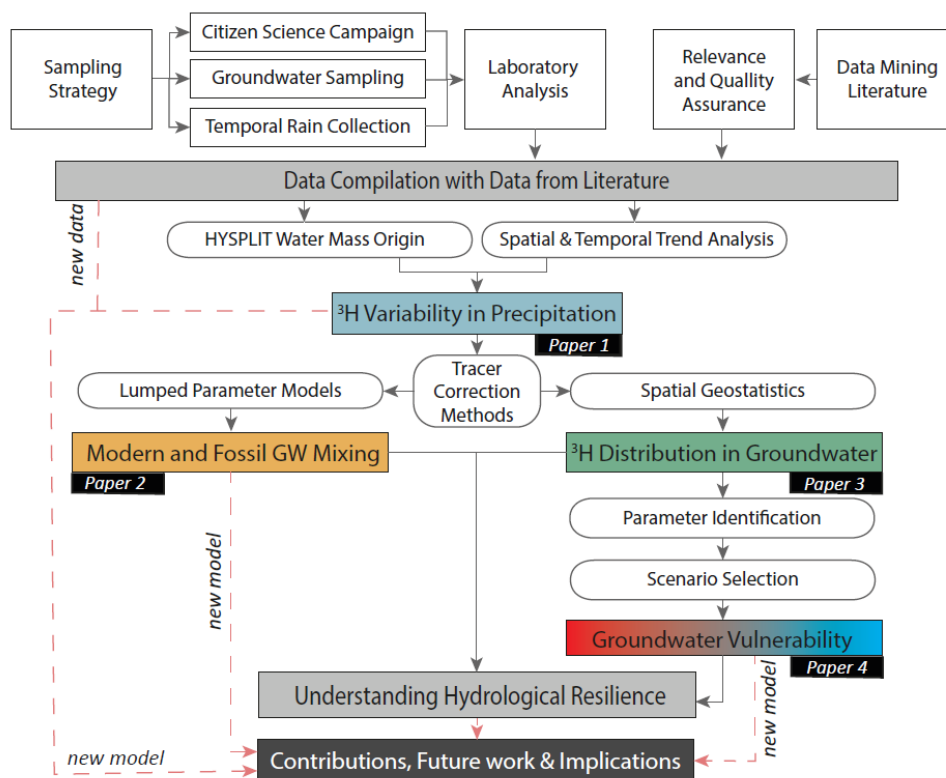


Figure 2 – A simplified framework of the study approach, breakdown of publications and their contributions to the research objectives.

1. Problem statement

In regions where long-term monitoring data is scarce, it is difficult to examine the response of the groundwater system to changes in climate and recharge dynamics. The efficacy of isotope studies to supplement the assessment of groundwater vulnerability and hydrological resilience is dependent on the selection of a well-suited isotope tracer or tracers, the ability to collect/collate regional data pertinent to each tracer and the development of an approach that mitigates the inherent uncertainty associated with the tracer. Although tritium is well suited and extensively used as a modern groundwater tracer, due to its short half-life and chemically conservative nature in recharge and groundwater flow, local and regional controls on its variability are still poorly constrained in southern Africa. Similarly, radiocarbon dating has seen progressive improvement in corrections of groundwater ages of older groundwater associated with carbonate dissolution, yet substantial uncertainty is still associated with corrections in arid regions and/or silicate dominated aquifers. Although groundwater vulnerability methods have been developed to assess pollution and drought risk independently, without the assistance of isotope tracers, a combined approach that assesses vulnerability in the context of quantity and quality is yet to be developed.

2. Aims and objectives

To understand how ^3H and ^{14}C could be used to interpret regional recharge dynamics and better constrain regional groundwater vulnerability within southern Africa, four key aims and objectives have been identified and are addressed as outcomes of the four publications in this thesis (Fig.2). These aims and objectives outline several key questions that need to be interrogated and constrained before groundwater vulnerability can be assessed:

Aim & Paper [1]: To constrain the variability and distribution of tritium in South African precipitation

- Which dominant factors that control the variability of ^3H in precipitation across South Africa?
- Is there a spatial and temporal dependence of ^3H variability on the identified dominant controls?
- Could the distribution and variability of ^3H in precipitation be modelled from the identified controls and predicted in different climatic environments?

Aim & Paper [2]: To calculate the proportion of modern and fossil groundwater mixing

- What is the temporal and spatial density of ^3H and ^{14}C atmospheric records in southern Africa?
- Are these records representative of tracer abundance in modern recharge and if not, what corrections could be made to mitigate this?
- How likely is closed system carbonate dilution and can initial $\delta^{13}\text{C}$ be predicted over a regional extent?
- What is the proportion of modern groundwater mixing in samples collected in southern Africa?

Aim & Paper [3]: To predict and interpolate the distribution of tritium in groundwater in South Africa

- Is the variation of ^3H in precipitation transferred into the ^3H activity of groundwater in South Africa?
- To what extent does travel time in the unsaturated zone affect ^3H activity in groundwater?
- How accurately can the ^3H distribution in groundwater, considering the known controls on activity, be predicted and what does this distribution imply in terms of modern recharge in South Africa?

Aim & Paper [4]: To assess regional groundwater vulnerability to a decrease in quality and quantity

- What environmental indicators are important for predicting the vulnerability of groundwater to a decrease in quantity and a deterioration in quality?
- How can isotope tracers contribute to the assessment of groundwater vulnerability in the context of modern recharge and groundwater distribution?
- Can the vulnerability of groundwater be predicted for future climate scenarios and how can this supplement sustainable groundwater management?

3. Study premise

The methodologies followed in this study to assess the variability, proportions and distributions of tracers as well as the implications that tracer abundance has on other research objectives, are synthesized below. These summaries provide the appropriate background information for the selection of: [1] hydrological tracers for modern and fossil groundwater and [2] new model approaches to constrain atmospheric controls, mixing relationships, spatial distributions and groundwater vulnerability, as described in the subsequent chapters.

3.1. Isotope tracers

The selection of isotopic tracers to achieve the aims of this study was carefully considered during the project's conception. The vulnerability of groundwater is synonymous with the potential of modern contaminants to infiltrate into an aquifer, and in this case also the risk of depletion, hence the appropriate tracer must be chemically conservative as well as temporally non-conservative. As ^3H forms part of the water molecule, its behaviour in an aquifer would be independent of that of a contaminant and its radioactive nature provides a temporal indicator for groundwater residence time. Although the short half-life of tritium enables a clear indication of modern groundwater, it cannot constrain mixing relationships with older groundwater, hence a radio-isotope with a longer lifespan should be included. ^{14}C was identified as an ideal indicator of fossil groundwaters as its abundance can be predicted with known atmospheric records. The details of these isotope systems are explored further below.

3.1.1. Tritium

Hydrogen has three naturally occurring isotopes, of which two are stable and one radioactive. Stable isotopes of hydrogen include protium (^1H , one proton) and deuterium (^2H , one proton and one neutron) and represent almost all of hydrogen's natural abundance with 99.972% and 0.028% respectively (Fig.3) (Schimmelmann and Sauer, 2018). The radioactive isotope of hydrogen, tritium (^3H , one proton and 2 neutrons), is only found naturally in trace amounts in the atmosphere and hydrosphere (Fig.3). The ^3H atom decays into helium-3 (^3He) through beta-decay and has a half-life of 12.312 years (Lucas and Unterweger, 2000; MacMahon, 2006). Tritium is most commonly found in nature as part of the water molecule (HTO) or organically bound tritium (OBT).

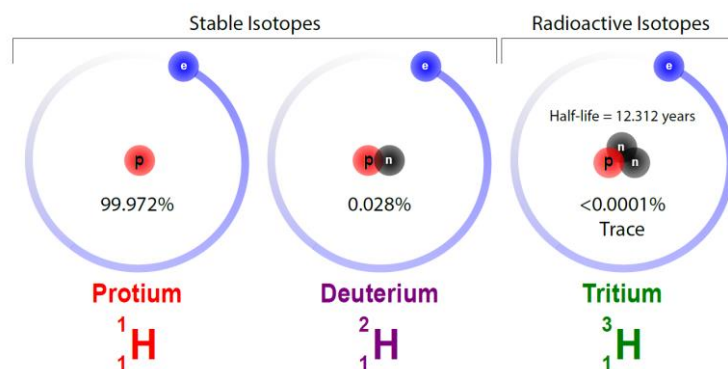


Figure 3 - The naturally occurring isotopes of hydrogen and their abundance.

3.1.1.1. Production and fall out rates

The production of naturally occurring tritium is largely attributed to the interaction of cosmic radiation with atmospheric gases (Craig and Lal, 1961; Grosse et al., 1951; Kaufman and Libby, 1954). Cosmic rays are produced and omitted from both processes outside of our solar system (Galactic cosmic rays, GCR) as well as lower energy solar cosmic rays (SCR) which are comprised of an array of high energy charged particles. When cosmic rays reach the earth's atmosphere, they produce a cascade of nuclear reactions between secondary particles and atmospheric nuclei. Isotopes that are formed in this manner are called cosmogenic isotopes and are formed through either the reaction of atmospheric gases or the spallation of oxygen and nitrogen. ^3H is produced in the upper atmosphere through the reaction of $^{14}\text{N}(n,^3\text{H})^{12}\text{C}$. The production and fallout rates of this process are controlled by numerous cosmogenic, atmospheric and geochemical processes. Tritium production in the upper atmosphere requires at least $\sim 4\text{MeV}$ energy of the neutron before ^{14}N can produce a ^3H atom, thus the rate of production is largely regulated

by the modulation of cosmic rays by earth's geomagnetic field. This modulation causes the increased production of ^3H from the equator to the polar regions, where production rates can be around 17 times higher and the intensity is controlled by the Sun's magnetic field alternation every 11 years (Palcsu et al., 2018). The average natural production rate of tritium in the upper atmosphere is estimated to be ~ 2500 atoms/m 2 /s 2 (Craig and Lal, 1961; Masarik and Beer, 2009), two-thirds of which is produced in the stratosphere and one third in the upper troposphere.

Tritium produced in the upper atmosphere reacts with stratospheric oxygen and hydroxide ions, in the form of $\text{T}^+ + \text{OH}^- = \text{HTO}$, and the tritiated water molecule (HTO) enters the global hydrological cycle (Rozanski et al., 1991). The estimated tritium concentration of the stratosphere is several orders of magnitude higher than that of the troposphere, at $5\text{-}9 \times 10^5$ tritium unit (TU, one tritium unit corresponds to one ^3H to 10^{18} H atoms) (Palcsu et al., 2018). The elevated abundance of ^3H in the stratosphere is due to a high production rate and low water content, allowing ^3H to remain suspended in the thin upper atmosphere. Although some ^3H is produced in the troposphere, the majority of HTO is incorporated through mixing at the tropopause (Zahn et al., 1998). The transport of ^3H is moderated by stratospheric-tropospheric interaction and can be seen indirectly through the seasonality of ^3H in rainfall (Zahn et al., 1998). Additionally, a significant increase of stratospheric-tropospheric mixing is prominent in the springtime of the northern hemisphere, where elevated tritium fallout is evident and termed the 'spring leak' (Harms et al., 2016; Suess, 1969). Thereafter the natural activity of ^3H in precipitation is controlled by processes within the hydrological cycle (Rozanski et al., 2013).

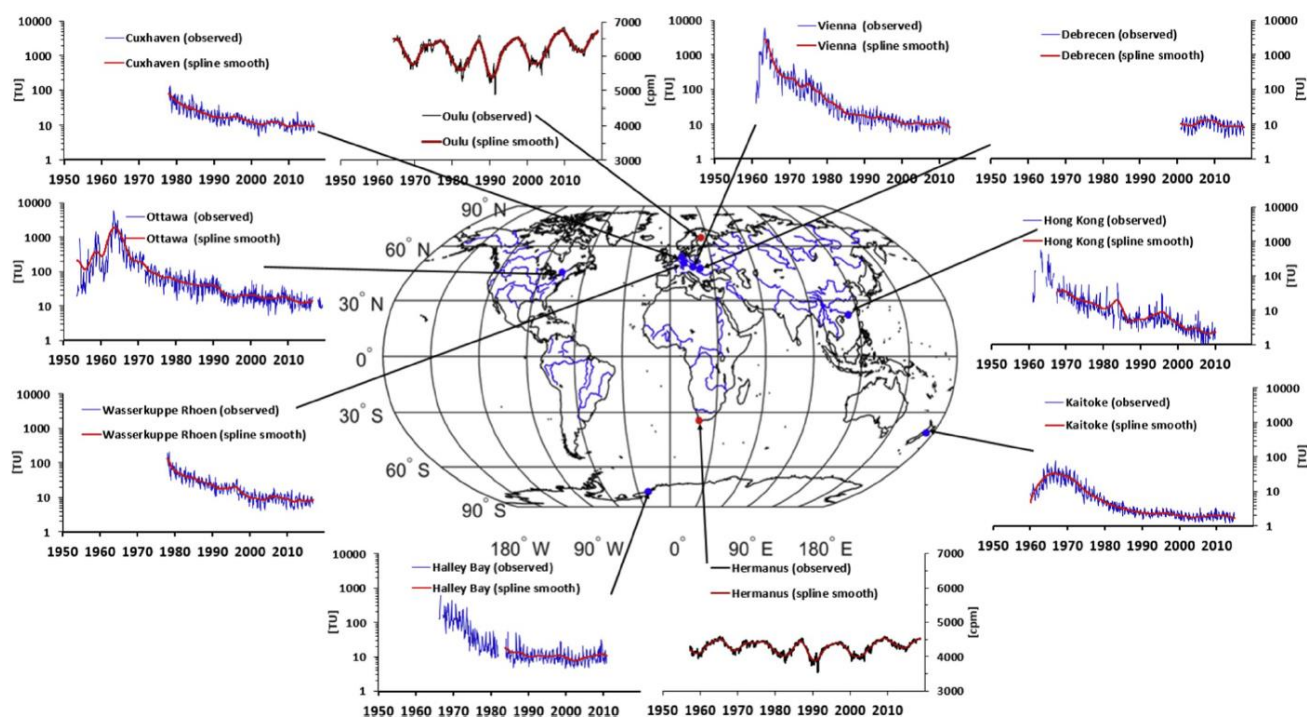


Figure 4 - The tritium time series and neutron monitor data in the Northern and Southern Hemisphere (László et al., 2020)

Massive amounts of anthropogenically produced ^3H were introduced into the atmosphere through thermal-nuclear bomb testing in the 1950's and early 1960's (Rozanski et al., 1991; Unesco, 1966). This resulted in the ^3H concentration in the northern hemisphere, mid-latitude precipitation to exceed 3000 TU. Approximately 520-550 kg of ^3H was introduced into the atmosphere, dwarfing the stratospheric estimated steady-state abundance of 3.8 kg (Palcsu et al., 2018). Since the banning of atmospheric nuclear tests in 1963, the activity of ^3H has declined due to decay and dilution in the hydrosphere/atmosphere (Kern et al., 2020). Anthropogenic ^3H is also produced on a local scale from nuclear facilities but at much smaller amounts and only affects localized environments (Fiévet et al., 2013; Köllö et al., 2011). Modern precipitation has since returned to background activities over much of the world, as the majority of the 'bomb peak' has been attenuated (Fig.4) (Cauquoin et al., 2016; Eastoe et al., 2012; Harms et al., 2016; Healy, 2010; Kern et al., 2020; Rahn et al., 2017; Visser et al., 2018).

3.1.1.2. ^3H in the hydrological cycle

More than 99% of tropospheric tritium is in the form of HTO and is incorporated into the water cycle. ^3H is then deposited into the earth's surficial water systems through either precipitation or vapor exchange. HTO follows the water cycle pathways almost exactly as un-tritiated water does, with only small perturbations as a result of fractionation effects during phase changes (Michel and Survey, 2005). In the case of ocean water, the predominant process is vapor exchange, due to the massive surface area of the ocean and ocean ^3H activity is in secular equilibrium with atmospheric activity (0.60 ± 0.10 TU) (Oms et al., 2019). ^3H in terrestrial water bodies is predominantly controlled by the activity of ^3H in local precipitation. As the lifespan of ^3H often exceeds the residence time of river systems, terrestrial contributions to ocean HTO are estimated to be around 10% of ocean HTO (Oms et al., 2019). Larger lake systems, that have residence times that exceed the lifespan of ^3H form a similar secular equilibrium to atmospheric ^3H yet are more largely controlled by river input rather than vapor exchange (Morgenstern et al., 2010; Suess, 1969).

The ubiquitous presence of ^3H in surface waters facilitates the uptake of HTO into the biosphere, where HTO can either be stored in water form or converted to OBT. The ratios of which are specific to the organic mechanism that incorporates the water molecule into the organism, most commonly through exchange processes during photosynthesis and digestion. The reintroduction of HTO into the atmosphere through transpiration is often fast enough to have negligible effects on atmospheric concentrations yet the effects of continental moisture recycling can be substantial in the concentration of ^3H in precipitation (Harms et al., 2016). Ultimately the variability of ^3H in local precipitation is controlled to varying degrees by: (1) geomagnetic modulation of cosmic bombardment of nitrogen to produce ^3H in the upper atmosphere (Palcsu et al., 2018); (2) increases in tropo-stratospheric mixing during the spring months (Visser et al., 2018); (3) varying amounts of convective vs stratiform rainfall, as storm cells that interact through the tropopause can entrain higher tritium activities (Aggarwal et al., 2016); (4) moisture recycling over continents, where ^3H is further enriched through exchange with re-evaporated continental moisture and continued stratospheric fall out (C. V. Tadros et al., 2014) and (5) anthropogenic production through nuclear processes and radioactive waste (Rozanski et al., 1991).

The secular equilibrium of ^3H in the atmosphere is less apparent in the unsaturated zone, where vapor exchange with the atmosphere is limited and ^3H begins to decay faster than it is replenished. This phenomenon led to numerous unsaturated zone travel time studies to be conducted after the 'bomb peak', where the extremely elevated atmospheric activity could be traced along the infiltration pathway in the unsaturated zone. It was initially thought that the infiltration of HTO in the unsaturated zone behaved in a piston flow manner with minor dispersion, yet further investigation suggested that the vapor transport of ^3H in the unsaturated zone is more significant (Phillips et al., 1988). The effect of the unsaturated zone travel is now attributed to many factors including vapor exchange, diffusion, pore water storage, ^3H soil inventory and infiltration rate (Li et al., 2019). Irrigation practices also have significant effects on local ^3H variability in the unsaturated zone as irrigation waters can have a significantly different ^3H activity as local precipitation (Currell et al., 2010).

Once ^3H reaches the subsurface through recharge, its abundance is predominantly dependent on decay as the subsurface production of ^3H is limited to areas nearby landfills, radioactive mineral deposits or radioactive waste sites (Hughes et al., 2011; Nigro et al., 2017; Palcsu et al., 2010). Furthermore, granitic rocks that contain Li rich minerals can produce and maintain significant amounts of ^3H in fracture fluids (>2 TU) (Andrews and Kay, 1982). However, geogenic production of ^3H in permeable rocks is only significant in rocks with low matrix porosity, limiting the contribution of geogenic ^3H to most aquifer systems. If an aquifer system does not contain detectable levels of ^3H is either no longer being actively recharged or its isolated flow path is long enough (>100 a) to allow for ^3H to decay below detection limits. However, ^3H activities are not likely to represent the actual residence time of all groundwater, as the mixing of fossil and modern groundwater can result in very old (>10000 a) groundwater containing detectable ^3H (Jasechko et al., 2017). In systems where mixed groundwaters are common, lumped parameter models with a different radioactive isotope, that can constrain older waters, is necessary.

3.1.2. Radiocarbon

Carbon has many naturally occurring isotopes yet only three are significant in the context of this study. Two of which are stable and one radioactive. Stable isotopes of carbon include carbon-12 (^{12}C , six protons and six neutrons) and carbon-13 (^{13}C ,

six protons and seven neutrons) and represent almost all of carbon's natural abundance with 98.89% and 1.109% respectively (Fig.5) (Schuur et al., 2016). The radioactive isotope of carbon pertinent to this study is carbon-14 (^{14}C , six protons and 8 neutrons), is only found naturally in trace amounts in the atmosphere, hydrosphere, biosphere and lithosphere (Fig.5). The ^{14}C atom decays into nitrogen-14 (^{14}N) through beta-decay and has a half-life of 5730 ± 80 years (Godwin, 1962). ^{14}C is most commonly found in nature as part of the carbon-dioxide molecule (CO_2) or inorganic material in various forms. ^{14}C is predominantly found in the hydrosphere as dissolved CO_2 , dissolved organic carbon (DOC) or dissolved inorganic carbon (DIC).

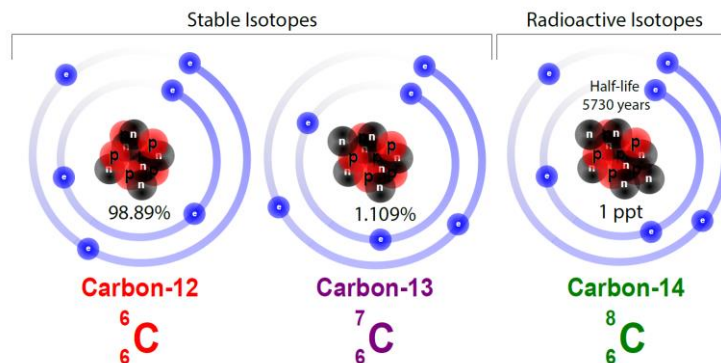


Figure 5 - The naturally occurring isotopes of carbon and their abundance.

3.1.2.1. Production and fall out rates

The natural production of ^{14}C is largely isolated to the upper atmosphere, where cosmic rays interact with atmospheric gases. ^{14}C is produced in the upper atmosphere through the reaction of $^{14}\text{N}(n,p)^{14}\text{C}$. The rate at which this reaction occurs is controlled by the same modulation as ^3H yet requires less energy ($\sim 1\text{MeV}$) and forms only a small part of the large atmospheric reservoir, thus is less sensitive to sunspot cycles as ^3H production is (0.25%) (Palcsu et al., 2018). Due to mixing between the upper and lower atmosphere, the distribution of ^{14}C in the lower atmosphere is relatively uniform (Clark, 2015; Clark and Fritz, 1997; Kalin, 2000). Although ^{14}C essentially behaves the same as ^{12}C chemically, differences in mass result in a slightly different distribution of ^{14}C in the global carbon cycle. ^{14}C is oxidised to form CO_2 and incorporated into the natural biosphere through photosynthesis and a large proportion returned through the decay of organic matter and root respiration. The long half-life of ^{14}C means that it can move through many C reservoirs in the global cycle before decaying below detection limits. To define a reference atmospheric abundance of ^{14}C , pre-industrial wood samples were used as a reference as initial radiocarbon (a^{14}C) or 100 percent modern carbon (pmc). Much older samples that contain low ^{14}C abundance are also affected by millennial-scale fluctuation in the production of atmospheric ^{14}C .

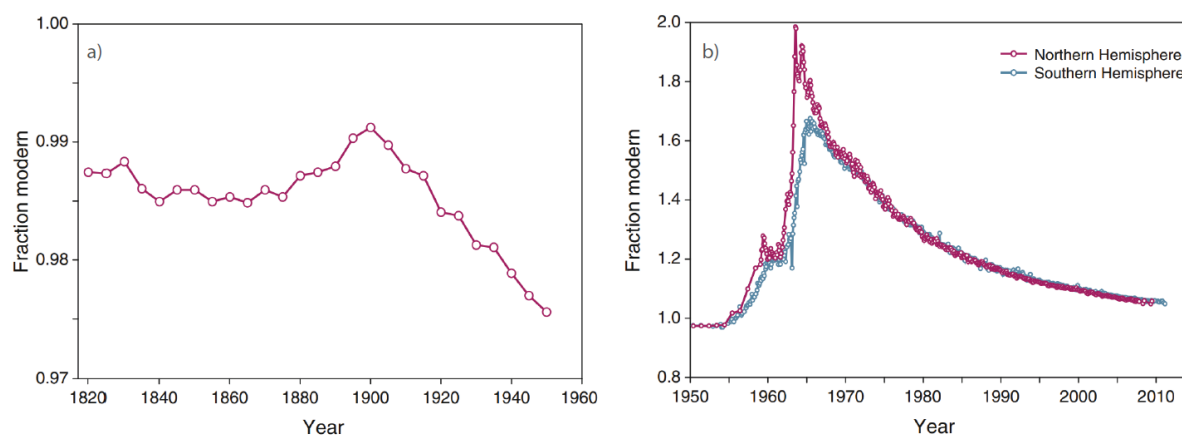


Figure 6 - The fraction of modern carbon change during a) the onset of the industrial revolution, ~ 1900 -1950 (Reimer et al., 2013) and b) the testing of above ground thermonuclear weapons, 1953-1964 (Hua et al., 2013)

Although the natural abundance of ^{14}C has varied significantly since the last glacial maximum (LGM), anthropogenic effects on ^{14}C atmospheric abundance over the last two centuries are prominent, especially over such a short time (Schuur et al., 2016).

After 1850, human activities within the 'industrial revolution' prompted the release of large amounts of stored C that had a lower abundance of ^{14}C through fossil fuel combustion and land-use change. This ^{14}C dilution in the atmosphere resulted in a decrease in atmospheric ^{14}C below 100 pmc (Fig.6a) (Hua et al., 2013). Thus, as the pool of total C introduced into the atmosphere through human activities increased and the abundance of ^{14}C did not, the ratio of ^{12}C to ^{14}C declined. During this decline, the testing of thermonuclear weapons saw a similar 'bomb peak' effect as was measured in ^3H activity. Where above ground testing introduced massive amounts of ^{14}C into the stratosphere, almost double in the northern hemisphere, through a similar process as described for the cosmogenic production of ^{14}C . The one year delay in the 'bomb peak' in the southern hemisphere is a result of the majority of tests being performed in the northern hemisphere and only an annual rate of turnover at the equator of air masses (Levin et al., 1995; Manning and Melhuish, 1994). The global attenuation of the bomb-peak was facilitated through the exchange of C in the carbon cycle and atmospheric levels have largely returned to pre-bomb pmc in the mid-latitude northern hemisphere where the peak was highest (Levin et al., 2013).

3.1.2.2. ^{14}C in the carbon cycle

As ^{14}C moves through the carbon cycle in a largely similar fashion as ^{12}C , researchers can predict its abundance by measuring the abundance of ^{14}C in each earth reservoir and by factoring in the known production of ^{14}C in the upper atmosphere and radioactive decay. Although mixing of the upper and lower atmosphere is not instantaneous, it is much faster than that of the ocean and land C reservoirs (Broecker and Peng, 1982). Despite the production of ^{14}C in the upper atmosphere, only ~2% of all ^{14}C (pre-1850) is contained in the atmosphere (Fig.7). Over two-thirds (65%-78%) are captured in deep ocean sediments, 8-10% in the surface ocean and 2-18% in marine sediments, largely a result of the oceanic carbon pump (Volk and Hoffert, 1985). Although, the deep ocean contains the largest proportion of ^{14}C , the mixing of this reservoir is relatively slow and the modern fraction is lower than the terrestrial biosphere which shows very similar modern fractions to the atmosphere (Fig.7). The unique ability of ^{14}C to trace both the interaction of C reservoirs as well as the residence time of C in the reservoir, has been applied across many scientific disciplines for a large array of purposes (Schuur et al., 2016).

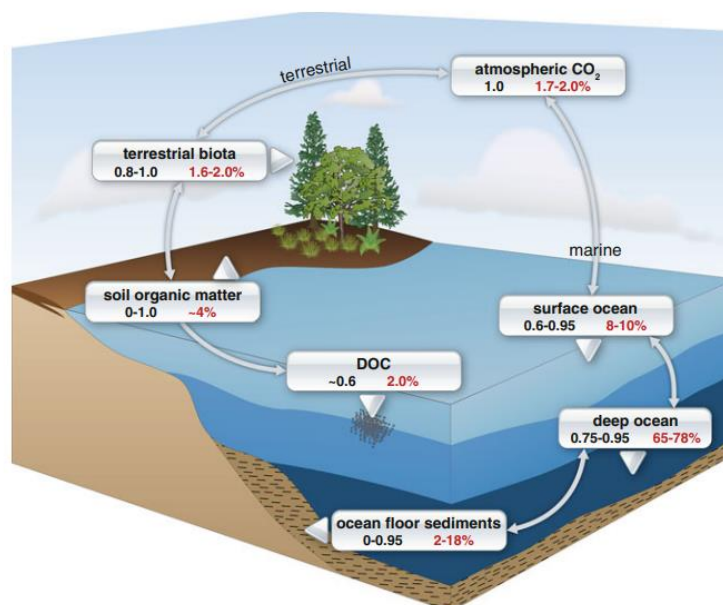


Figure 7 - The range of ^{14}C isotope ratios (black numbers) among different reservoirs of the Earth system, expressed relative to the atmospheric ^{14}C content defined in the preindustrial as 1.0, specifically based on wood from 1890. The percent of total ^{14}C atoms in the Earth system (red numbers) is a combination of the total C pool size and the ^{14}C age of the pool (Schuur et al., 2016)

Over and above the global scale effects on the ^{14}C abundance in different reservoirs (glacial cycles, industrialization, nuclear bomb testing, etc.), localized processes also capture and store ^{14}C . By using the same decay methodology, the allocation of C in local cycles can be dated over varying timescales (Schuur et al., 2016). Cosmogenic radiocarbon dating is useful for assessing residence times between 300 – 50 000 years based on the comparison of measured ^{14}C with modern C (Stenström et al., 2011). Younger systems that capture and store ^{14}C are likely affected by the 'bomb peak', which enables the measured ^{14}C to be

compared to the known atmospheric change and residence time can be accurately estimated ($\pm 1-2$ years). However, the determination of an age is dependent on the system being closed, allowing for only decay once C enters the system with no further atmospheric exchange (Schoor et al., 2016). One such system is that of groundwater, where residence times have been successfully calculated as atmospheric ^{14}C is isolated once it enters the water table as DIC (Kalin, 2000). The variability of atmospheric ^{14}C is reflected in the groundwater record and has helped distinguish younger and older groundwater reservoirs (Cartwright et al., 2017; Plummer and Sprinkle, 2001). Unfortunately, atmospheric ^{14}C variability is often trumped by the introduction of ^{14}C -free carbon into groundwater, which includes the dissolution of carbonate minerals, isotopic exchange with carbonates, oxidation of old organic matter (methanogenesis) and the CO_2 -rich volcanic gases.

In order to best interpret calculated ^{14}C groundwater ages, the addition of ^{14}C -free carbon must be accounted for to avoid the over-estimation of residence times and the under-estimation of recharge rates (Kalin, 2000). Fortunately, several methods are used to account for this dissolution which includes ion geochemistry, stable carbon isotopes and other geochemical tracers such as $^{87}\text{Sr}/^{86}\text{Sr}$ ratios (Coetsiers and Walraevens, 2009; Meredith et al., 2012). As the $\delta^{13}\text{C}$ of groundwater is initially controlled by the soil horizon from which carbon is dissolved, it can be predicted through the soil processes that fractionate carbon isotopes, e.g. photosynthesis and respiration. Vegetation is a major control of $\delta^{13}\text{C}$ in the soil zone as carbon isotope fractionation in the photosynthetic pathways of plants is significant and distinct between C_3 and C_4 type plants (O'Leary, 1988).

Studies that have been undertaken in the southern hemisphere (Australia and New Zealand), in semi-arid and/or silicate dominated terrains, have found that $\delta^{13}\text{C}$ values are extremely variable and can result in gross over/under correction of ^{14}C residence times (Cartwright et al., 2017). However, it is still important to note that it is likely that closed system carbonate dissolution is still contributing 'dead' carbon to the collected sample. Additionally, ^{14}C corrections could be made more accurate if coupled with another isotopic or geochemical measurement, e.g. $^{87}\text{Sr}/^{86}\text{Sr}$ or HCO_3 (Cartwright, 2010; Cartwright et al., 2013). Despite the potential issues surrounding the use of ^{14}C as a residence time indicator, it is still commonly used as a tracer for estimating long-term recharge rates and residence times over regional settings (A P Atkinson et al., 2014; Cartwright et al., 2013; Corcho Alvarado et al., 2007; Currell et al., 2010; McMahon et al., 2011; Plummer and Sprinkle, 2001; Zhu et al., 2000).

3.2. Techniques and models for tracers

The selection of model methodologies to achieve the aims of this study were carefully considered during the project's progression. As the objectives of this study intend to interpret tracer abundance and decay throughout the hydrological cycle, methods and models must be selected for each reservoir of the tracer's lifespan as well as the implications of measured tracer abundance on the interconnectivity of reservoirs and their residence times. This includes: [1] the production and fall out of tracers in the atmosphere and subsequent incorporation into precipitation, [2] the abundance of tracers in groundwater over time under different groundwater flow conditions and [3] the implications on modern recharge mechanics derived from tracers on groundwater vulnerability assessments.

3.2.1. Particle trajectory models

One of the most extensively used atmospheric particle trajectory models is the Hybrid Single-Particle Lagrangian Integrated Trajectory model (HYSPPLIT), developed by the National Oceanic and Atmospheric Administration (NOAA) Air Resources Laboratory (ARL) (Draxler and Hess, 1998). It is defined as a complete system for computing simple air parcel trajectories as well as complex transport, dispersion chemical transformation and deposition simulations (Stein et al., 2015). One of the most common model applications is the use of back-trajectory analysis to determine the origins of particles, this method has been used to describe atmospheric transport of radioactive material, smoke, dust pollutants, ash and water masses. The calculation of the HYSPPLIT model is a hybrid of the Lagrangian approach and the Eulerian methodology. The Lagrangian approach uses a moving frame of reference when computing the movement of the air parcel, computing advection and diffusion to predict the migration of a particle across modelled conditions. The Eulerian methodology uses a fixed three-dimensional grid as a frame of reference and is typically used for the tracking of pollutant air concentrations. The basis from which trajectories are calculated can be mathematically described as:

$$P_{mean}(t + \Delta t) = P_{mean}(t) + \frac{1}{2}[V(P_{mean}, t) + V(\{P_{mean}(t) + [V(P_{mean}, t)\Delta t]\}, t + \Delta t)]\Delta t \quad (1)$$

where P is the position at time t and V is the average of the three-dimensional velocity vectors at the initial or 'first guess' positions. In this case, only the advection component is considered in the prediction of particle/parcel trajectories. In order to capture atmospheric movement and mixing, a turbulent dispersion component is added. These diffusion equations are constructed by adding the mean velocity obtained from meteorological data (Fay et al., 1995); namely,

$$X_{final}(t + \Delta t) = X_{mean}(t + \Delta t) + U'(t + \Delta t)\Delta t \quad (2)$$

$$Z_{final}(t + \Delta t) = Z_{mean}(t + \Delta t) + W'(t + \Delta t)\Delta t \quad (3)$$

where U' and W' correspond with the turbulent velocity components, X_{mean} and Z_{mean} are the mean components of particle positions and X_{final} and Z_{final} are the final positions in the horizontal and vertical, respectively. It must also be noted that the turbulence component is only added after the advection computation. The U' and W' components are calculated according to a modified discrete-time Langevin equation (Chock and Winkler, 1996). Furthermore the inclusion of calculations concerning how wet and dry deposition as well as in cloud estimates as outlined in the inclusion of a co-efficient described in other studies (Leadbetter et al., 2015; Visser et al., 2016). The methodology outlined in this thesis contributed to a model developed at the Lawrence Livermore National Laboratory in California, U.S.A, and can be found in more detail in Visser et al., 2018.

3.2.2. Lumped parameter models

Lumped parameter models (LPMs) are mathematical models that determine the concentration of a tracer over a simplified groundwater flow path. This is done by setting an aquifer geometry and flow configuration to account for hydrodynamic dispersion or mixing within an aquifer, well bore, or discharge area. LPMs are generally used for determining ages for groundwater by including one or more residence time tracers and predicting mixing relationships of younger and older aquifer components. The addition of unsaturated zone travel time can be included in LPMs but must be predetermined by another method, typically through particle tracking by numerical groundwater flow models. The major benefit of LPMs is that tracers of both young and old groundwater can be interpreted simultaneously so that a wide range of residence times can be constrained in a single system.

The tracer LPM workbook, developed by the USGS, contains five LPMs that can be used to determine groundwater residence time relationships for different groundwater flow conditions (Jurgens et al., 2012). The five primary LPMs are: [1] piston-flow model (PFM), [2] exponential mixing model (EMM), [3] exponential piston flow model (EPM), [4] partial exponential model (PEM), and [5] dispersion model (DM). If tracers are particularly suited to one model, any combination of primary LPMs can be used in a binary mixing model (BMM), to estimate tracer abundances over time for multiple tracers. The workbook has expanded functionality to facilitate hydrogeologic conceptualization, visualizations and best-fit parameter estimation. The distributions of groundwater age can be evaluated in two ways: [1] two or more tracers can be evaluated against one another to measure the concordance with expected abundances or [2] data collected as a time series can be compared to modelled trends of tracer abundance.

Each individual LPM corresponds to an input (recharge) location and an output (discharge location), which is typically the well or spring that a groundwater sample was collected from. An LPM calculates using either transit-time distribution functions or exit-age distribution functions $[g(t)]$ (Maloszewski and Zuber, 1993). In these methods, the collected water sample is assumed to consist of many water "parcels" that have mixed from different flow paths with discrete residence time and tracer abundance. The simulated tracer concentration at the outlet position, within a steady-state aquifer, can be calculated from the tracer abundance at the inlet position using $[g(t)]$ in the function:

$$C_{out}(t) = \int_{-\infty}^t C_{in}(t')e^{-\lambda(t-t')} g(t-t')dt' \quad (4)$$

where $C_{out}(t)$ is the outlet tracer concentration at the time of collection (t) and $C_{in}(t')$ is the tracer concentration at the inlet at the time in which the tracer entered the system (t'), λ the decay constant if the tracer is radioactive and $t - t'$ is the mean residence time of the water parcel. The LPM approach assumes that tracers are injected and detected in the fluid flux and, other than decay, behave conservatively in the system traveling with the water parcel. The inferred mean ages calculated from tracer abundance is thus equal to the mean residence time of water being discharged from the system or to a screened interval.

3.2.3. Groundwater vulnerability models

With the development of initial basic methods for assessing groundwater vulnerability to contamination, several other methods have been adapted from it. Each method that is developed has been carefully catered to a specific problem that earlier methods were insufficient in addressing effectively. The most popular techniques are described below:

The GOD rating system (Foster, 1987), one of the earliest and most rudimentary methods, was developed in an attempt to simplify the existing groundwater vulnerability to contamination index (SGVI) and included only 3 main input parameters: the groundwater occurrence, the lithology of overlying layers and the depth to groundwater. In the same year, the U.S. Environmental Protection Agency (EPA) developed DRASTIC (Aller et al., 1987) to characterize groundwater pollution potential. The method incorporates seven input parameters namely: depth to water, net recharge, aquifer media, topography, the impact of the vadose zone and hydraulic conductivity. Each input parameter was assigned a rating for pollution potential from 1 - 10 and then calculated as a weighted sum to determine the final vulnerability index. The DRASTIC method also had two variations that could be used for natural areas and for areas of pesticide heavy agriculture, which changes the various weighting of the input parameters.

One vulnerability method suggests that one need not over complicate the evaluation and that an aquifer's vulnerability is so overwhelmingly controlled by its physical morphology that only a few inputs are needed. The AVI (Aquifer Vulnerability Index) rating system (Stempvoort et al., 1993) only uses two inputs: the thickness of each sedimentary layer above the uppermost aquifer and the estimated hydraulic conductivity to assess the vulnerability of an aquifer to pollution. Alternatively, the SINTACS method (Civita, 1994) was derived from the DRASTIC methodology and has the same seven input parameters but has a much more complicated structure. The method isolates different weighting strings and runs them in parallel allowing for rating to be divided into intervals, which result in six vulnerability classes. It, therefore, allows for new weighting classes to be created for sufficiently variable areas, whereas the rating classes in the DRASTIC model were fixed.

Some researchers have even combined several methods into one, the ISIS method (Civita and De Regibus, 1995) combines elements from DRASTIC, SINTACS and GOD methods, the method allows for a more flexible structure for the user. It does this by having inputs grouped, for instance 'the annual mean of net recharge' can be represented by a recharge estimate or a complex calculation including mean annual rainfall, surface temperature and other related parameters. Other methods have also been developed for specific hydrogeological environments, for instance the EPIK (Doerfliger and Zwahlen, 1997) method was created to assess the vulnerability of karst aquifers in Switzerland.

Gogu and Dassargues, 2000 have summarized in detail these methods and have begun to tackle some of the past and future issues surrounding groundwater vulnerability assessments in the context of overlay and index methods. Several comparative studies (Corniello et al., 1997) have been done to evaluate the strengths and weaknesses of the methods and although the findings have been interesting they have been inconclusive in determining the best method.

In addition to investigations that focus their vulnerability index on determining pollution potentials, other assessments are more primarily focused on the vulnerability of groundwater resources to drought. Villholth et al., (2013) developed the GRiMMS methods for groundwater drought risk (GWDR) which is another variation of an overlay index method or multi-criteria evaluation using a set of algorithms in a pre-set framework to estimate a vulnerability index. The study was done over the Southern African Development Community (SADC) region and estimated what portion of the population that is dependent on groundwater is vulnerable to more severe and regular drought periods as a result of climate change.

To constrain the vulnerability of groundwater on a regional scale, that encompasses both the risk of contamination and groundwater depletion, multiple aspects of the hydrological cycle need to be investigated. Groundwater quality indicators have been used in groundwater vulnerability studies before and methods are well constrained in the literature. However, indicators of groundwater quantity are somewhat less explored, with only a few groundwater drought risk and local abstraction studies available. As regional hydrological studies need large amounts of spatial and temporal data to be accurate, the degree and distribution of groundwater vulnerability to depletion is difficult to constrain. Isotopic systems are particularly useful, due to the ability of isotopes to be proxies for climate, recharge and residence time. Modern recharge dynamics can be interpreted as both indicators of (1) renewable, actively recharged groundwater and (2) potential for surface pollutants to enter the

groundwater system. This dual-purpose makes modern recharge indicators particularly useful in assessing groundwater vulnerability. Furthermore, as most groundwater is a mix of younger and older groundwater, it is important to understand the proportion of modern groundwater with groundwater recharged a long time ago. To better understand the mixing relationships of modern groundwater with fossil groundwater, residence time tracers that can constrain much older groundwater residence times must also be investigated.

4. Thesis outline

The thesis is comprised of six chapters, the first is an introductory chapter that outlines the context of the study and synthesizes the aims and ideas that form the premise of the study. Chapters 2 through 5 are comprised of four papers which logically follow on from each other. Papers 1 and 4 are published, papers 2 and 3 have been submitted and are under review. Paper 4 was published first, as it forms a proof of concept for incorporating tritium based modern groundwater assessments into groundwater vulnerability assessments. The first contribution (Chapter 2) "Spatial and temporal variability of tritium in precipitation in South Africa and its bearing on hydrological studies" develop novel techniques to investigate the variability of ^3H in event-based precipitation in South Africa. The second contribution (Chapter 3) "Using tritium and radiocarbon activities to constrain modern groundwater proportions in southern Africa" compares predicted abundances of ^3H and ^{14}C in groundwater with collated data to estimate the proportion of modern groundwater and the age of the fossil mixing component distributed across southern Africa. The third contribution (Chapter 4) "Constraining the spatial distribution of tritium in groundwater across South Africa" develops a spatial interpolation model to predict the distribution of tritium activity in groundwater within South Africa. The fourth contribution (Chapter 5) "Combining quantity and quality controls to determine groundwater vulnerability to depletion and deterioration throughout South Africa" develops a novel model framework, which incorporates both quantity and quality controls, to assess groundwater vulnerability to contamination/pollution and depletion. The model approach is then applied to South Africa and forecasted using climate change prediction models. The final chapter summarizes the findings, developments, conclusions and implications for future research, addressing which aims and objectives were achieved as well as the associated limitations.

References

- Aggarwal, P.K., Romatschke, U., Araguas-Araguas, L., Belachew, D., Longstaffe, F.J., Berg, P., Schumacher, C., Funk, A., 2016. Proportions of convective and stratiform precipitation revealed in water isotope ratios. *Nat. Geosci.* 9, 624–629. <https://doi.org/10.1038/ngeo2739>
- Al-Adamat, R., Al-Shabeeb, A.A.-R., 2017. A Simplified Method for the Assessment of Groundwater Vulnerability to Contamination. *J. Water Resour. Prot.* 09, 305–321. <https://doi.org/10.4236/jwarp.2017.93020>
- Aller, L., Lehr, J.H., Petty, R., 1987. A Standardized System to Evaluate Ground Water Pollution Potential Using Hydrogeologic Settings. *Natl. Water Well Assoc.*
- Andrews, J.N., Kay, R.L.F., 1982. Natural production of tritium in permeable rocks. *Nature* 298, 361–363. <https://doi.org/10.1038/298361a0>
- Atkinson, A.P., Cartwright, I., Gilfedder, B.S., Cendón, D.I., Unland, N.P., Hofmann, H., 2014. ^{14}C and ^3H to understand groundwater flow and recharge in an aquifer window. *Hydrol. Earth Syst. Sci.* 18, 4951–4964. <https://doi.org/10.5194/hess-18-4951-2014>
- Barbieri, M., 2019. Isotopes in hydrology and hydrogeology. *Water (Switzerland)* 11. <https://doi.org/10.3390/w11020291>
- Blamey, R.C., Middleton, C., Lennard, C., Reason, C.J.C., 2017. A climatology of potential severe convective environments across South Africa. *Clim. Dyn.* 49, 2161–2178. <https://doi.org/10.1007/s00382-016-3434-7>
- Böhlke, J.K., 2002. Groundwater recharge and agricultural contamination. *Hydrogeol. J.* 10, 153–179. <https://doi.org/10.1007/s10040-001-0183-3>
- Böhlke, J.K., Denver, J.M., 1995. Combined use of groundwater dating, chemical, and isotopic analyses to resolve the history and fate of nitrate contamination in two agricultural watersheds, Atlantic coastal plain, Maryland. *Water Resour. Res.* 31, 2319–2339.
- Broecker, W.S., Peng, T.-H., 1982. Tracers in the Sea.
- Cartwright, I., 2010. Using groundwater geochemistry and environmental isotopes to assess the correction of ^{14}C ages in a silicate-dominated aquifer system. *J. Hydrol.* 382, 174–187. <https://doi.org/10.1016/j.jhydrol.2009.12.032>
- Cartwright, I., Cendón, D., Currell, M., Meredith, K., 2017. A review of radioactive isotopes and other residence time tracers in understanding groundwater recharge: Possibilities, challenges, and limitations. *J. Hydrol.* 555, 797–811. <https://doi.org/10.1016/j.jhydrol.2017.10.053>

- Cartwright, I., Fifield, L.K., Morgenstern, U., 2013. Using ^3H and ^{14}C to constrain the degree of closed-system dissolution of calcite in groundwater. *Appl. Geochemistry* 32, 118–128. <https://doi.org/10.1016/j.apgeochem.2012.10.023>
- Cauquoin, A., Jean-Baptiste, P., Risi, C., Fourré, Landais, A., 2016. Modeling the global bomb tritium transient signal with the AGCM LMDZ-iso: A method to evaluate aspects of the hydrological cycle. *J. Geophys. Res.* 121, 12,612–12,629. <https://doi.org/10.1002/2016JD025484>
- Chock, D.P., Winkler, S.L., 1996. A Particle-Grid Air Quality Modeling Approach 99, 97–132. https://doi.org/10.1007/978-1-4613-8492-2_4
- Civita, M., 1994. Le carte di vulnerabilità degli acquiferi all'inquinamento: teoria e pratica. *Quad. di Tec. di Prot. Ambient.* Pitagora ed.
- Civita, M., De Regibus, C., 1995. Sperimentazione di alcune metodologie per la valutazione della vulnerabilità degli acquiferi. *Atti 2° Conv. Naz.*
- Clark, I., 2015. *Groundwater geochemistry and isotopes.* CRC press.
- Clark, I.D., Fritz, P., 1997. *Environmental isotopes in hydrogeology.* CRC press.
- Coetsiers, M., Walraevens, K., 2009. A new correction model for ^{14}C ages in aquifers with complex geochemistry—application to the Neogene Aquifer, Belgium. *Appl. Geochemistry* 24, 768–776.
- Corcho Alvarado, J.A., Purtschert, R., Barbecot, F., Chabault, C., Rueedi, J., Schneider, V., Aeschbach-Hertig, W., Kipfer, R., Loosli, H.H., 2007. Constraining the age distribution of highly mixed groundwater using ^{39}Ar : A multiple environmental tracer ($^3\text{H}/^3\text{He}$, ^{85}Kr , ^{39}Ar , and ^{14}C) study in the semiconfined Fontainebleau Sands Aquifer (France). *Water Resour. Res.* <https://doi.org/10.1029/2006WR005096>
- Corniello, A., Ducci, D., Napolitano, P., 1997. Comparison between parametric methods to evaluate aquifer pollution vulnerability using GIS: an example in the “Piana Campana”, southern Italy. *Eng. Geol. Environ.* Balkema, Rotterdam 1721–1726.
- Craig, H., Lal, D., 1961. The Production Rate of Natural Tritium. *Tellus* 13, 85–105. <https://doi.org/10.1111/j.2153-3490.1961.tb00068.x>
- Currell, M.J., Cartwright, I., Bradley, D.C., Han, D., 2010. Recharge history and controls on groundwater quality in the Yuncheng Basin, north China. *J. Hydrol.* 385, 216–229. <https://doi.org/10.1016/j.jhydrol.2010.02.022>
- Cuthbert, M.O., Gleeson, T., Moosdorf, N., Befus, K.M., Schneider, A., Hartmann, J., Lehner, B., 2019. Global patterns and dynamics of climate–groundwater interactions. *Nat. Clim. Chang.* 9, 137–141. <https://doi.org/10.1038/s41558-018-0386-4>
- Dansgaard, W., 1964. Stable isotopes in precipitation. *Tellus* 16, 436–468. <https://doi.org/10.3402/tellusa.v16i4.8993>
- Díaz-Cruz, M.S., Barceló, D., 2008. Trace organic chemicals contamination in ground water recharge. *Chemosphere* 72, 333–342. <https://doi.org/10.1016/j.chemosphere.2008.02.031>
- Doerfliger, N., Zwahlen, F., 1997. EPIK: a new method for outlining of protection areas in karstic environment, in: *International Symposium and Field Seminar on “Karst Waters and Environmental Impacts”*, Edited by: Günay, G. and Jonshon, AI, Antalya, Turkey, Balkema, Rotterdam. pp. 117–123.
- Draxler, R.R., Hess, G.D., 1998. An overview of the HYSPLIT₄ modelling system for trajectories, dispersion and deposition. *Aust. Meteorol. Mag.* 47, 295–308.
- Eastoe, C.J., Watts, C.J., Ploughe, M., Wright, W.E., 2012. Future use of tritium in mapping pre-bomb groundwater volumes. *Ground Water* 50, 87–93. <https://doi.org/10.1111/j.1745-6584.2011.00806.x>
- Fay, B., Glaab, H., Jacobsen, I., Schrodin, R., 1995. Evaluation of Eulerian and Lagrangian atmospheric transport models at the Deutscher Wetterdienst using anateX surface tracer data. *Atmos. Environ.* 29, 2485–2497. [https://doi.org/10.1016/1352-2310\(95\)00144-N](https://doi.org/10.1016/1352-2310(95)00144-N)
- Feng, W., Zhong, M., Lemoine, J.M., Biancale, R., Hsu, H.T., Xia, J., 2013. Evaluation of groundwater depletion in North China using the Gravity Recovery and Climate Experiment (GRACE) data and ground-based measurements. *Water Resour. Res.* 49, 2110–2118. <https://doi.org/10.1002/wrcr.20192>
- Ferguson, G., Gleeson, T., 2012. Vulnerability of coastal aquifers to groundwater use and climate change. *Nat. Clim. Chang.* 2, 342–345. <https://doi.org/10.1038/nclimate1413>
- Fiévet, B., Pommier, J., Voiseux, C., Bailly Du Bois, P., Laguionie, P., Cossonnet, C., Solier, L., 2013. Transfer of tritium released into the marine environment by french nuclear facilities bordering the english channel. *Environ. Sci. Technol.* 47, 6696–6703. <https://doi.org/10.1021/es400896t>
- Fontes, J.C., 1980. *Environmental isotopes in groundwater hydrology.* Elsevier, Netherlands.
- Foster, S., 1987. Fundamental concepts in aquifer vulnerability, pollution risk and protection strategy. *Vulnerability of soil and groundwater to pollutants*, Proc Inf 38:69–86. van

- Duijvenbooden W, van Waegeningh HG TNO Comm. Hydrol. Res. Hague. Vulnerabil, 69–86.
- Gao, F., Wang, H., Liu, C., 2020. Long-term assessment of groundwater resources carrying capacity using GRACE data and Budyko model. *J. Hydrol.* 588, 125042. <https://doi.org/10.1016/j.jhydrol.2020.125042>
- Gleeson, T., Befus, K.M., Jasechko, S., Luijendijk, E., Cardenas, M.B., 2016. The global volume and distribution of modern groundwater. *Nat. Geosci.* 9, 161–164. <https://doi.org/10.1038/ngeo2590>
- Gleeson, T., Befus, K.M., Jasechko, S., Luijendijk, E., Cardenas, M.B., 2015. The global volume and distribution of modern groundwater. *Nat. Geosci. Advance on*, 1–15. <https://doi.org/10.1038/ngeo2590>
- Godwin, H., 1962. Half-life of radiocarbon. *Nature* 195, 984.
- Gogu, R., Dassargues, A., 2000. Current and future trends in groundwater vulnerability assessment using overlay and index methods. Springer-Verlag 39.
- Gonfiantini, R., Fröhlich, K., Araguás-Araguás, L., Rozanski, K., 1998. Isotopes in groundwater hydrology, in: *Isotope Tracers in Catchment Hydrology*. Elsevier, pp. 203–246.
- Grosse, A. V., Johnston, W.M., Wolfgang, R.L., Libby, W.F., 1951. Tritium in nature. *Science* (80-). 113, 1–2. <https://doi.org/10.1126/science.113.2923.1>
- Hamed, Y., Ahmadi, R., Hadji, R., Mokadem, N., Dhia, H. Ben, Ali, W., 2014. Groundwater evolution of the Continental Intercalaire aquifer of Southern Tunisia and a part of Southern Algeria: use of geochemical and isotopic indicators. *Desalin. Water Treat.* 52, 1990–1996. <https://doi.org/10.1080/19443994.2013.806221>
- Harms, P.A., Visser, A., Moran, J.E., Esser, B.K., 2016. Distribution of tritium in precipitation and surface water in California. *J. Hydrol.* 534, 63–72. <https://doi.org/10.1016/j.jhydrol.2015.12.046>
- Healy, R.W., 2010. Estimating groundwater recharge. Cambridge University Press.
- Hu, K.X., Awange, J.L., Kuhn, M., Saleem, A., 2019. Spatio-temporal groundwater variations associated with climatic and anthropogenic impacts in South-West Western Australia. *Sci. Total Environ.* 696. <https://doi.org/10.1016/j.scitotenv.2019.133599>
- Hua, Q., Barbetti, M., Rakowski, A.Z., 2013. Atmospheric radiocarbon for the period 1950–2010. *Radiocarbon* 55, 2059–2072.
- Hughes, C.E., Cendón, D.I., Harrison, J.J., Hankin, S.I., Johansen, M.P., Payne, T.E., Vine, M., Collins, R.N., Hoffmann, E.L., Loosz, T., 2011. Movement of a tritium plume in shallow groundwater at a legacy low-level radioactive waste disposal site in eastern Australia. *J. Environ. Radioact.* 102, 943–952. <https://doi.org/10.1016/j.jenvrad.2010.05.009>
- Jasechko, S., Perrone, D., Befus, K.M., Bayani Cardenas, M., Ferguson, G., Gleeson, T., Luijendijk, E., McDonnell, J.J., Taylor, R.G., Wada, Y., Kirchner, J.W., 2017. Global aquifers dominated by fossil groundwaters but wells vulnerable to modern contamination. *Nat. Geosci.* 10, 425–429. <https://doi.org/10.1038/ngeo2943>
- Jurgens, B.C., Böhlke, J.K., Eberts, S.M., Survey, U.S.G., 2012. TracerLPM (Version 1): An Excel® workbook for interpreting groundwater age distributions from environmental tracer data. *Tech. Methods.* <https://doi.org/10.3133/tm4F3>
- Kalin, R.M., 2000. Radiocarbon dating of groundwater systems, in: *Environmental Tracers in Subsurface Hydrology*. Springer, pp. 111–144.
- Kaufman, S., Libby, W.F., 1954. The natural distribution of tritium. *Phys. Rev.* 93, 1337–1344. <https://doi.org/10.1103/PhysRev.93.1337>
- Kern, Z., Erdélyi, D., Vreča, P., Krajcar Bronić, I., Fórizs, I., Kanduč, T., Štok, M., Palcsu, L., Süveges, M., Czuppon, G., Kohán, B., Gábor Hatvani, I., 2020. Isoscape of amount-weighted annual mean precipitation tritium (^3H) activity from 1976 to 2017 for the Adriatic–Pannonian region – AP $^3\text{H}_v1$ database. *Earth Syst. Sci. Data* 12, 2061–2073. <https://doi.org/10.5194/essd-12-2061-2020>
- Köllo, Z., Palcsu, L., Major, Z., Papp, L., Molnár, M., Ranga, T., Dombóvári, P., Manga, L., 2011. Experimental investigation and modelling of tritium washout by precipitation in the area of the nuclear power plant of Paks, Hungary. *J. Environ. Radioact.* 102, 53–59. <https://doi.org/10.1016/j.jenvrad.2010.09.002>
- László, E., Palcsu, L., Leelóssy, Á., 2020. Estimation of the solar-induced natural variability of the tritium concentration of precipitation in the Northern and Southern Hemisphere. *Atmos. Environ.* 233. <https://doi.org/10.1016/j.atmosenv.2020.117605>
- Leadbetter, S.J., Hort, M.C., Jones, A.R., Webster, H.N., Draxler, R.R., 2015. Sensitivity of the modelled deposition of Caesium-137 from the Fukushima Dai-ichi nuclear power plant to the wet deposition parameterisation in NAME. *J. Environ. Radioact.* 139, 200–211. <https://doi.org/10.1016/j.jenvrad.2014.03.018>
- Levin, I., Graul, R., Trivett, N.B.A., 1995. Long-term observations of atmospheric CO₂ and carbon isotopes at continental sites in Germany. *Tellus B* 47, 23–34.

- Levin, I., Kromer, B., Hammer, S., 2013. Atmospheric $\delta^{14}\text{C}$ trend in Western European background air from 2000 to 2012. *Tellus, Ser. B Chem. Phys. Meteorol.* 65. <https://doi.org/10.3402/tellusb.v65i0.20092>
- Li, Z., Jasechko, S., Si, B., 2019. Uncertainties in tritium mass balance models for groundwater recharge estimation. *J. Hydrol.* 571, 150–158. <https://doi.org/10.1016/j.jhydrol.2019.01.030>
- Liu, C.W., Lin, K.H., Kuo, Y.M., 2003. Application of factor analysis in the assessment of groundwater quality in a blackfoot disease area in Taiwan. *Sci. Total Environ.* 313, 77–89. [https://doi.org/10.1016/S0048-9697\(02\)00683-6](https://doi.org/10.1016/S0048-9697(02)00683-6)
- Lucas, L.L., Unterweger, M.P., 2000. Comprehensive Review and Critical Evaluation of the Half-Life of Tritium. *J. Res. Natl. Inst. Stand. Technol.* 105, 541–549. <https://doi.org/10.6028/jres.105.043>
- MacMahon, D., 2006. Half-life evaluations for ^3H , ^{90}Sr , and ^{90}Y . *Appl. Radiat. Isot.* 64, 1417–1419. <https://doi.org/10.1016/j.apradiso.2006.02.072>
- Maloszewski, P., Zuber, A., 1993. Tracer experiments in fractured rocks: matrix diffusion and the validity of models. *Water Resour. Res.* 29, 2723–2735.
- Manning, M.R., Melhuish, W.H., 1994. Atmospheric $\Delta^{14}\text{C}$ Record from Wellington (1954–1993). *Environmental System Science Data Infrastructure for a Virtual Ecosystem*
- Mao, F., Clark, J., Karpouzoglou, T., Dewulf, A., Buytaert, W., Hannah, D., 2017. HESS Opinions: A conceptual framework for assessing socio-hydrological resilience under change. *Hydrol. Earth Syst. Sci.* 21, 3655–3670. <https://doi.org/10.5194/hess-21-3655-2017>
- Masarik, J., Beer, J., 2009. An updated simulation of particle fluxes and cosmogenic nuclide production in the Earth's atmosphere. *J. Geophys. Res. Atmos.* 114, 1–9. <https://doi.org/10.1029/2008JD010557>
- Mazzoni, A., Heggy, E., Scabbia, G., 2018. Forecasting water budget deficits and groundwater depletion in the main fossil aquifer systems in North Africa and the Arabian Peninsula. *Glob. Environ. Chang.* 53, 157–173. <https://doi.org/10.1016/j.gloenvcha.2018.09.009>
- McGuire, K.J., McDonnell, J.J., 2006. A review and evaluation of catchment transit time modeling. *J. Hydrol.* 330, 543–563. <https://doi.org/10.1016/j.jhydrol.2006.04.020>
- McMahon, P.B., Plummer, L.N., Böhlke, J.K., Shapiro, S.D., Hinkle, S.R., 2011. A comparison of recharge rates in aquifers of the United States based on groundwater-age data. *Hydrogeol. J.* 19, 779–800. <https://doi.org/10.1007/s10040-011-0722-5>
- Meredith, K., Cendón, D.I., Pigois, J.P., Hollins, S., Jacobsen, G., 2012. Using ^{14}C and ^3H to delineate a recharge “window” into the Perth Basin aquifers, North Gngangara groundwater system, Western Australia. *Sci. Total Environ.* 414, 456–469. <https://doi.org/10.1016/j.scitotenv.2011.10.016>
- Michel, R.L., Survey, U.S.G., 2005. Tritium in the Hydrologic Cycle 53–66. https://doi.org/https://doi.org/10.1007/1-4020-3023-1_5
- Morgenstern, U., Stewart, M.K., Stenger, R., 2010. Dating of streamwater using tritium in a post nuclear bomb pulse world: Continuous variation of mean transit time with streamflow. *Hydrol. Earth Syst. Sci.* 14, 2289–2301. <https://doi.org/10.5194/hess-14-2289-2010>
- Nigro, A., Sappa, G., Barbieri, M., 2017. Application of boron and tritium isotopes for tracing landfill contamination in groundwater. *J. Geochemical Explor.* 172, 101–108. <https://doi.org/10.1016/j.gexplo.2016.10.011>
- Nimmo, J.R., Healy, R.W., Stonestrom, D.A., 2005. Aquifer Recharge. *Encycl. Hydrol. Sci.* 1–18. <https://doi.org/10.1002/0470848944.hsa161a>
- O’Leary, M.H., 1988. Carbon Isotopes in Photosynthesis Fractionation techniques may reveal new aspects of carbon dynamics in plants. *Bioscience* 38, 328–336.
- Oms, P.E., Bailly du Bois, P., Dumas, F., Lazure, P., Morillon, M., Voiseux, C., Le Corre, C., Cossonnet, C., Solier, L., Morin, P., 2019. Inventory and distribution of tritium in the oceans in 2016. *Sci. Total Environ.* 656, 1289–1303. <https://doi.org/10.1016/j.scitotenv.2018.11.448>
- Palcsu, L., Molnár, M., Major, Z., Svingor, E., Veres, M., Barnabás, I., Kapitány, S., 2010. Detection of tritium and alpha decaying radionuclides in L/ILW by measurements of helium isotopes. *J. Radioanal. Nucl. Chem.* 286, 483–487. <https://doi.org/10.1007/s10967-010-0741-z>
- Palcsu, L., Morgenstern, U., Sültenfuss, J., Koltai, G., László, E., Temovski, M., Major, Z., Nagy, J.T., Papp, L., Varlam, C., Faurescu, I., Túri, M., Rinyu, L., Czuppon, G., Botyán, E., Jull, A.J.T., 2018. Modulation of Cosmogenic Tritium in Meteoric Precipitation by the 11-year Cycle of Solar Magnetic Field Activity. *Sci. Rep.* 8, 1–9. <https://doi.org/10.1038/s41598-018-31208-9>
- Panagopoulos, G.P., Antonakos, A.K., Lambrakis, N.J., 2006. Optimization of the DRASTIC method for groundwater vulnerability assessment via the use of simple statistical methods and GIS. *Hydrogeol. J.* 14, 894–911. <https://doi.org/10.1007/s10040-005-0008-x>
- Phillips, F.M., Mattick, J.L., Duval, T.A., Elmore, D., Kubik, P.W., 1988. Chlorine 36 and tritium from nuclear weapons fallout as tracers for long-term liquid and vapor movement in

- desert soils. *Water Resour. Res.* 24, 1877–1891. <https://doi.org/10.1029/WR024i011p01877>
- Plummer, L.N., Sprinkle, C.L., 2001. Radiocarbon dating of dissolved inorganic carbon in groundwater from confined parts of the Upper Floridan aquifer, Florida, USA. *Hydrogeol. J.* 9, 127–150. <https://doi.org/10.1007/s100400000121>
- Rahn, P.H., Detwiler, A.G., Davis, A.D., 2017. Tritium in groundwater in the Black Hills of South Dakota. *Environ. Earth Sci.* 76, 1–11. <https://doi.org/10.1007/s12665-017-7082-y>
- Reimer, P.J., Bard, E., Bayliss, A., Beck, J.W., Blackwell, P.G., Ramsey, C.B., Buck, C.E., Cheng, H., Edwards, R.L., Friedrich, M., 2013. IntCal13 and Marine13 radiocarbon age calibration curves 0–50,000 years cal BP. *Radiocarbon* 55, 1869–1887.
- Richey, A.S., Thomas, B.F., Lo, M.H., Reager, J.T., Famiglietti, J.S., Voss, K., Swenson, S., Rodell, M., 2015. Quantifying renewable groundwater stress with GRACE. *Water Resour. Res.* 51, 5217–5237. <https://doi.org/10.1002/2015WR017349>
- Rodell, M., Famiglietti, J.S., Wiese, D.N., Reager, J.T., Beaudoin, H.K., Landerer, F.W., Lo, M.H., 2018. Emerging trends in global freshwater availability. *Nature* 557, 651–659. <https://doi.org/10.1038/s41586-018-0123-1>
- Rodell, M., Velicogna, I., Famiglietti, J.S., 2015. Satellite-based estimates of groundwater depletion in India. *Curr. Sci.* 109, 610–617. <https://doi.org/10.1038/nature08238>
- Rozanski, K., Araguás-Araguás, L., Gonfiantini, R., 2013. Isotopic Patterns in Modern Global Precipitation 1–36. <https://doi.org/10.1029/GM078p0001>
- Rozanski, K., Gonfiantini, R., Araguas-Araguas, L., 1991. Journal of Physics G : Nuclear and Particle Physics Related content Tritium in the global atmosphere : distribution patterns and recent trends. *J. Phys. G Nucl. Part. Phys.* 17, S523–S536.
- Sanford, W., 2011. Calibration of models using groundwater age 13–16. <https://doi.org/10.1007/s10040-010-0637-6>
- Scanlon, B.R., Faunt, C.C., Longuevergne, L., Reedy, R.C., Alley, W.M., McGuire, V.L., McMahon, P.B., 2012. Groundwater depletion and sustainability of irrigation in the US High Plains and Central Valley. *Proc. Natl. Acad. Sci.* 109, 9320–9325. <https://doi.org/10.1073/pnas.1200311109>
- Scanlon, B.R., Healy, R.W., Cook, P.G., 2002. Choosing appropriate technique for quantifying groundwater recharge. *Hydrogeol. J.* 10, 18–39. <https://doi.org/10.1007/s10040-0010176-2>
- Scanlon, B.R., Reedy, R.C., Stonestrom, D.A., Prudic, D.E., Dennehy, K.F., 2005. Impact of land use and land cover change on groundwater recharge and quality in the southwestern US. *Glob. Chang. Biol.* 11, 1577–1593. <https://doi.org/10.1111/j.1365-2486.2005.01026.x>
- Schimmelmann, A., Sauer, P.E., 2018. Hydrogen Isotopes BT - Encyclopedia of Geochemistry: A Comprehensive Reference Source on the Chemistry of the Earth, in: White, W.M. (Ed.), . Springer International Publishing, Cham, pp. 696–701. https://doi.org/10.1007/978-3-319-39312-4_326
- Schulze, R.E., Lynch, S.D., Maharaj, M., 2006. Annual Precipitation. South African Atlas Climatol. Agrohydrology. Water Res. Comm. Pretoria, RSA, WRC Rep. 489/1/06, Section 6.2.
- Schuur, E.A.G., Druffel, E.R.M., Trumbore, S.E., 2016. Radiocarbon and climate change. Switz. Springer Int. Publ. Switz.
- Shamsudduha, M., Taylor, R., 2019. Groundwater storage dynamics in the world's large aquifer systems from GRACE: uncertainty and role of extreme precipitation. *Earth Syst. Dyn. Discuss.* 1–36. <https://doi.org/10.5194/esd-2019-43-supplement>
- Stein, A.F., Draxler, R.R., Rolph, G.D., Stunder, B.J.B., Cohen, M.D., Ngan, F., 2015. NOAA's hysplit atmospheric transport and dispersion modeling system. *Bull. Am. Meteorol. Soc.* 96, 2059–2077. <https://doi.org/10.1175/BAMS-D-14-00110.1>
- Stempvoort, D. Van, Ewert, L., Wassenaar, L., 1993. Aquifer Vulnerability Index: a Gis - Compatible Method for Groundwater Vulnerability Mapping. *Can. Water Resour. J.* 18, 25–37. <https://doi.org/10.4296/cwrj1801025>
- Stenström, K.E., Skog, G., Georgiadou, E., Genberg, J., Johansson, A., 2011. A guide to radiocarbon units and calculations. *Lunfd* 6, 0–17.
- Suess, H.E., 1969. Tritium geophysics as an international research project. *Science (80-)*. 163, 1405–1410.
- Tadros, C. V., Hughes, C.E., Crawford, J., Hollins, S.E., Chisari, R., 2014. Tritium in Australian precipitation: A 50 year record. *J. Hydrol.* 513, 262–273. <https://doi.org/10.1016/j.jhydrol.2014.03.031>
- Taylor, R.G., Todd, M.C., Kongola, L., Maurice, L., Nahozya, E., Sanga, H., Macdonald, A.M., 2013. Evidence of the dependence of groundwater resources on extreme rainfall in East Africa. *Nat. Clim. Chang.* 3, 374–378. <https://doi.org/10.1038/nclimate1731>
- Thomas, B.F., Famiglietti, J.S., 2019. Identifying Climate-Induced Groundwater Depletion in GRACE Observations. *Sci. Rep.* 9, 1–9. <https://doi.org/10.1038/s41598-019-40155-y>
- Thomas, B.F., Famiglietti, J.S., Landerer, F.W., Wiese, D.N., Molotch, N.P., Argus, D.F., 2017. Remote Sensing of

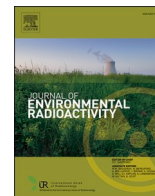
- Environment GRACE Groundwater Drought Index : Evaluation of California Central Valley groundwater drought. *Remote Sens. Environ.* 198, 384-392. <https://doi.org/10.1016/j.rse.2017.06.026>
- Unesco, 1966. 5 - Tritium in the Atmosphere 3, 63-74.
- United Nations, 2015. United Nations. The UN Sustainable Development Goals. New York Available.
- Villholth, K.G., Tøttrup, C., Stendel, M., Maherry, A., 2013. Integrated mapping of groundwater drought risk in the Southern African Development Community (SADC) region. *Hydrogeol. J.* 21, 863-885. <https://doi.org/10.1007/s10040-013-0968-1>
- Visser, A., Moran, J.E., Hillegonds, D., Singleton, M.J., Kulongoski, J.T., Belitz, K., Esser, B.K., 2016. Geostatistical analysis of tritium, groundwater age and other noble gas derived parameters in California. *Water Res.* 91, 314-330. <https://doi.org/10.1016/j.watres.2016.01.004>
- Visser, A., Thaw, M., Esser, B., 2018. Analysis of air mass trajectories to explain observed variability of tritium in precipitation at the Southern Sierra Critical Zone Observatory, California, USA. *J. Environ. Radioact.* 181, 42-51. <https://doi.org/10.1016/j.jenvrad.2017.10.008>
- Volk, T., Hoffert, M.I., 1985. Ocean carbon pumps: Analysis of relative strengths and efficiencies in ocean-driven atmospheric CO₂ changes. *carbon cycle Atmos. CO₂ Nat. Var. Archean to Present* 32, 99-110.
- Voss, K.A., Famiglietti, J.S., Lo, M., De Linage, C., Rodell, M., Swenson, S.C., 2013. Groundwater depletion in the Middle East from GRACE with implications for transboundary water management in the Tigris-Euphrates-Western Iran region. *Water Resour. Res.* 49, 904-914. <https://doi.org/10.1002/wrcr.20078>
- Wada, Y., Van Beek, L.P.H., Van Kempen, C.M., Reckman, J.W.T.M., Vasak, S., Bierkens, M.F.P., 2010. Global depletion of groundwater resources. *Geophys. Res. Lett.* 37, 1-5. <https://doi.org/10.1029/2010GL044571>
- West, J.B., Bowen, G.J., Dawson, T.E., Tu, K.P., 2009. *Isoscapes: understanding movement, pattern, and process on Earth through isotope mapping.* Springer.
- Yeh, P.J., Swenson, S.C., Famiglietti, J.S., Rodell, M., 2006. Remote sensing of groundwater storage changes in Illinois using the Gravity Recovery and Climate Experiment (GRACE) 42, 1-7. <https://doi.org/10.1029/2006WR005374>
- Zahn, A., Barth, V., Pfeilsticker, K., Platt, U., 1998. Deuterium, Oxygen-18, and Tritium as Tracers for Water Vapour Transport in the Lower Stratosphere and Tropopause Region. *J. Atmos. Chem.* 30, 25-47. <https://doi.org/10.1023/A:1005896532640>
- Zhang, L., Dawes, W.R., Walker, G.R., 2001. Response of mean annual evapotranspiration to vegetation changes at catchment scale. *Water Resour. Res.* 37, 701-708.
- Zhu, H.W., Chen, A., Mao, Z.Q., Xu, C.L., Xiao, X., Wei, B.Q., Liang, J., Wu, D.H., 2000. Effect of surface treatments on hydrogen storage of carbon nanotubes. *J. Mater. Sci. Lett.* 19, 1237-1239. <https://doi.org/10.1023/A:1006713228929>
- Zuber, A., Ró, K., Purtschert, R., 2011. On some methodological problems in the use of environmental tracers to estimate hydrogeologic parameters and to calibrate flow and transport models 53-69. <https://doi.org/10.1007/s10040-010-0655-4>

CHAPTER 2 TRITIUM IN PRECIPITATION

PAPER PUBLICATION HISTORY	
Title	Spatial and temporal variability of tritium in precipitation in South Africa and its bearing on hydrological studies
Journal	Journal of Environmental Radioactivity, IF= 2.161 (2020)
Status	Published
Authors and roles	J.D. van Rooyen – PhD Candidate J.A. Miller – Primary Supervisor L. Palscu – Co-Author A. Visser – Co-Author T.W. Vennemann - Co-Author
Applicant Contribution	Collected rainfall samples, collated data, co-developed and constructed the model, interpreted results and wrote the manuscript.

Contents lists available at [ScienceDirect](https://www.sciencedirect.com)

Journal of Environmental Radioactivity

journal homepage: <http://www.elsevier.com/locate/jenvrad>

Spatial and temporal variability of tritium in precipitation within South Africa and its bearing on hydrological studies

J.D. van Rooyen^{a,*}, L. Palcsu^b, A. Visser^c, T.W. Vennemann^d, J.A. Miller^a

^a Department of Earth Sciences, Faculty of Sciences, University of Stellenbosch, Private Bag X1, Matieland, 7601, South Africa

^b Isotope Climatology and Environmental Research Centre (ICER), Institute for Nuclear Research, H-4026, Debrecen, Bem tér 18/c, Hungary

^c Lawrence Livermore National Laboratory, Nuclear and Chemical Sciences Division, 7000 East Ave, Livermore, CA, 94550, United States

^d Institute of Earth Surface Dynamics, University of Lausanne, Lausanne, Switzerland

ABSTRACT

Tritium, the radioactive isotope of hydrogen, has been used to understand groundwater recharge processes for decades. The current variation of tritium in the atmosphere is largely attributed to stratospheric production and fall out rates as well as global circulation phenomena controlling the hydrological cycle. Global controls on the variability in atmospheric tritium activity are poorly suited to explain local variation and tritium activities in precipitation are often assumed to be uniform over both local and regional catchments and watersheds. This assumption can result in both over and under estimation of modern recharge within an aquifer when using tritium as the recharge proxy. In order to minimize the inherent prediction residuals associated with tritium based recharge investigations, the variability of tritium in precipitation was modelled from 127 spatial precipitation samples taken over a two year period, combined with a 76 precipitation sample group-set taken over a one year period in a single location. Precipitation events were traced backward in time, from the point of collection, using HYSPLIT modelling to ascertain the origins of moisture content as well as the altitudes of moisture origin reached along the particle track. Tritium activities, collected over a one year period in Paarl, range from 0.45 to 4.16 TU and have a mean of 1.59 TU. Spatial storm events in the Western Cape in 2017 and 2018 had a range from 0 to 2.2 and 0.37 to 3.27 TU, respectively, with mean activities of 1.18 ($n = 34$) and 1.25 TU ($n = 32$). Both storm events had similar tritium variability ($\sigma = 0.5$ $n = 35$ and 0.48 $n = 32$). Regional precipitation events had the largest range of tritium activities (0.55–12.2 TU). Although not all tritium activities can be explained by interrogating the water mass origin, this study suggests that approximately 90% of events can be completely or partially attributed to the origin of the water mass. The variability of tritium, both spatially and temporally, was higher than expected, confirming that when uniform tritium inputs are used, the groundwater system would provide inaccurate modern recharge estimates. Higher spatial resolution of tritium variation in precipitation for a particular region will improve our ability to relate tritium activities in groundwater to local precipitation.

1. Introduction

Cosmogenic radioactive isotope tracers are produced at, and decay at, different rates that make radio-isotope tracers uniquely dynamic and robust for the purpose of hydrogeological investigations. The suite of radio-isotope tracers available in modern isotope hydrology to evaluate recharge include ^3H , ^{14}C , ^{36}Cl and the radioisotopes of the noble gases (^{85}Kr , ^{81}Kr , and ^{39}Ar). These isotopes allow for the characterization of recharge that occurred within the last couple of years to hundreds of thousands of years (Busenberg and Plummer, 2008; Clark, 2015; Clark and Fritz, 2013; Cook and Solomon, 1997; Darling et al., 2012; Kalin, 2000; Loosli et al., 2000; McGuire and McDonnell, 2006; Phillips, 2000; Scanlon et al., 2002). However, radio-isotopes with short half-lives are uniquely positioned to provide information on recent recharge processes and hence can be used to track the impact of modern climate change on

groundwater systems (Cartwright et al., 2017). Modern recharge can occur over a period of weeks in shallow alluvial aquifers to decades and older in deeper confined systems or in aquifers with low hydraulic conductivity. Tritium has been identified as an ideal residence time indicator of modern processes because it is dominantly a function of atmospheric processes and typically not produced underground along groundwater flow paths (Cartwright et al., 2017). On this basis, the activity of tritium in groundwater has been used to differentiate modern vs fossil groundwater (Gleeson et al., 2016), track the contamination of fossil groundwater by modern recharge (Jaschecko et al., 2017), and measure groundwater residence times (Cartwright and Morgenstern, 2015). However, for recharge investigations using tritium, the input activity or concentration of precipitation derived tritium, is usually presumed to be relatively uniform or constant over a given region and timeframe (e.g. one rainfall season in a groundwater catchment) but this

* Corresponding author.

E-mail addresses: jvanrooyen121@gmail.com (J.D. van Rooyen), palcsu@atomki.mta.hu (L. Palcsu), visser3@llnl.gov (A. Visser), torsten.vennemann@unil.ch (T.W. Vennemann), jmiller@sun.ac.za (J.A. Miller).

<https://doi.org/10.1016/j.jenvrad.2020.106354>

Received 6 March 2020; Received in revised form 2 July 2020; Accepted 6 July 2020

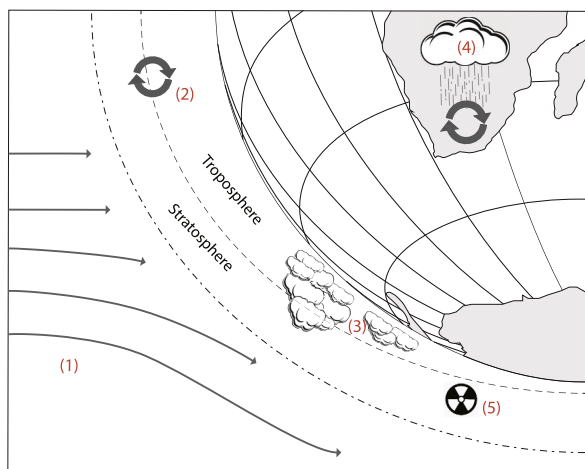


Fig. 1. Schematic of the natural controls on tritium activity in global precipitation. (1) Geomagnetic modulation of cosmic bombardment of nitrogen to produce tritium in the upper atmosphere; (2) increases in tropo-stratospheric mixing in spring; (3) varying amounts of convective vs stratiform rainfall; (4) moisture recycling over continent and (5) anthropogenic production through nuclear processes and radioactive waste.

assumption seems unlikely to be valid (Stewart et al., 2010).

Tritium is the radioactive isotope of hydrogen with a half-life of 12.312 years (MacMahon, 2006). Large amounts of anthropogenic tritium were produced as a result of atmospheric testing of thermonuclear weapons during the period 1950–1970 (Eastoe et al., 2012; Tadros et al., 2014; Thatcher, 1962). Atmospheric tritium activity has since decayed back to background levels and is now largely controlled by variable stratospheric production and fall out rates, as well as ocean

water dilution and moisture recycling (Tadros et al., 2014). As a result, there is significant variability in the activity of tritium in global precipitation. This variation may be a function of: (1) geomagnetic modulation of cosmic bombardment of nitrogen to produce tritium in the upper atmosphere (Palcsu et al., 2018); (2) increases in tropo-stratospheric mixing during the spring months (Visser et al., 2018); (3) varying amounts of convective vs stratiform rainfall, as storm cells that interact through the tropopause can entrain higher tritium activities (Aggarwal et al., 2016); (4) moisture recycling over continents, where tritium is further enriched through exchange with re-evaporated continental moisture and continued stratospheric fall out (Tadros et al., 2014) and (5) anthropogenic production through nuclear processes and radioactive waste (Rozanski et al., 1991) (Fig. 1). Moreover, due to landmass distribution, ocean/atmospheric circulation and anthropogenic production, the processes that control atmospheric tritium activity in the northern hemisphere will differ from those in the southern hemisphere. Similarly, high-latitude regions produce more stratospheric tritium than equatorial areas and in turn contribute more tritium to precipitation through fall out and mixing. How these processes interact to govern the activity of tritium in precipitation at different locations around the planet is central to understanding the variability of tritium in the groundwater system and how this impacts our understanding of recharge dynamics.

Before this can happen though, a better understanding of the behavior of tritium in the hydrological cycle is required to assess the spatial variability of tritium in surface and subsurface hydrology as well as any anthropogenic contributions derived from nuclear activity (Visser et al., 2018). To do this, tritium data must be collected and investigated on a regional scale and at a variety of time-steps (Harms et al., 2016). Tritium has long been collected as part of nuclear monitoring programs but also via the Global Network of Isotopes in Precipitation (GNIP) program of the International Atomic Energy Agency (IAEA). Multiple studies have reported monthly tritium activities and successfully constrained the potential controls on tritium variability in precipitation in

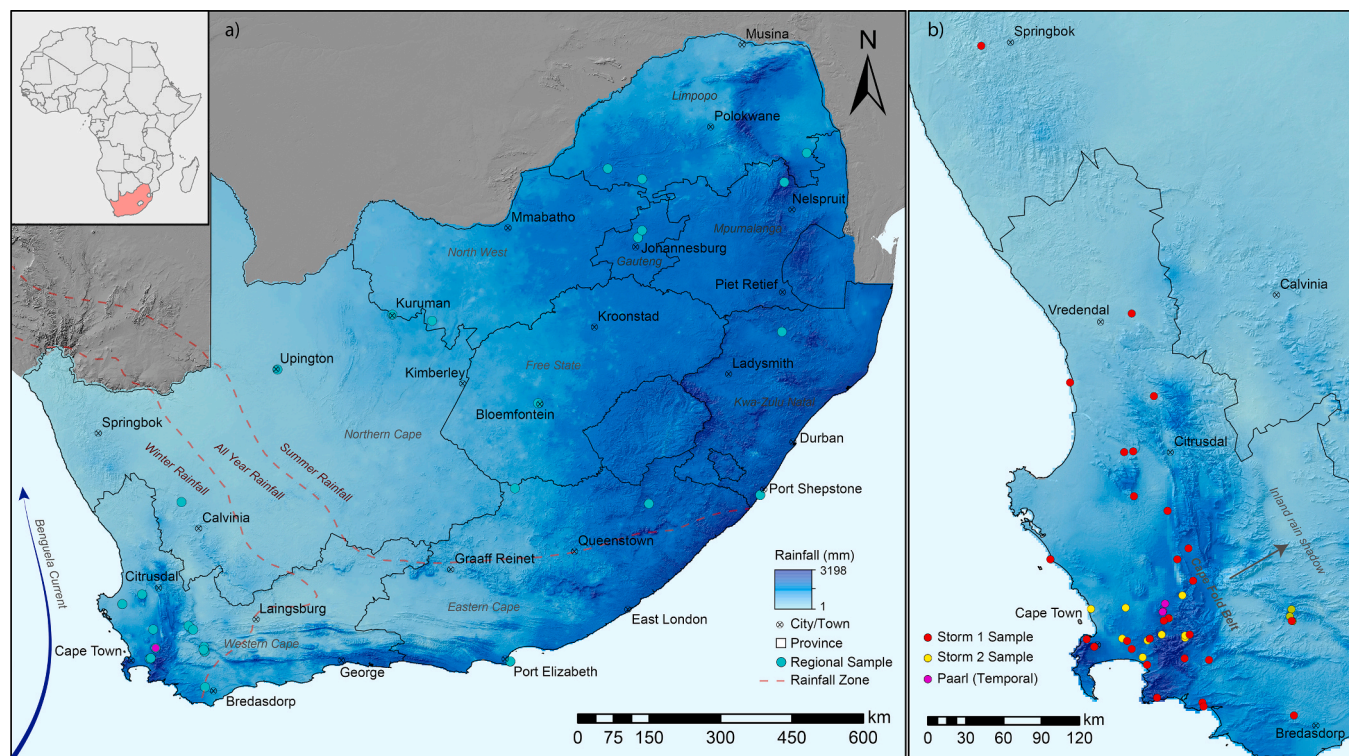


Fig. 2. Site map of collection locations for (a) regional precipitation samples and (b) Western Cape temporal and storm samples. Graded blue color represents rainfall amount and rainfall zones are delineated by dashed lines in panel (a) for summer, winter and all year rainfall. (For interpretation of the references to color in this figure legend, the reader is referred to the Web version of this article.)

spatially diverse locations and scales (Mair et al., 2013; Tadros et al., 2014; Visser et al., 2018). Although trends on a monthly temporal scale are evident and explain macro-processes, this temporal resolution cannot characterize event based tritium variability. To investigate the extent, magnitude and significance of the established trends and effects on tritium activity in precipitation, a higher temporal resolution is required.

This study investigates the temporal and spatial variations of tritium activity in daily precipitation and single storm events in South Africa through the sampling of: (1) daily precipitation over a one year period at a single location (Paarl, Western Cape Province); (2) two major storm events in two different years sampled at multiple locations in the Western Cape Province; and (3) regional precipitation events across South Africa. Stable isotopes of O and H were also analyzed from the same samples as the tritium, to link the type of rainfall received at each sample location to the tritium activity. The source of moisture within the air mass was investigated using data produced from HYSPLIT trajectories to evaluate the latitude and altitude effects of source water to the tritium activity of precipitation. Using the above information and data to investigate major controls on tritium activity in South African precipitation may aid in constraining the actual input of tritium into the local hydrological cycle. Expanding our understanding of tritium variability in precipitation, particularly in the southern hemisphere, will contribute to our understanding of hydrological resilience, an increasingly important global concept used to evaluate climate change driven alteration of hydrological cycles.

2. Environmental context

South Africa has a diverse climate, ranging from semi-arid to arid zones in the central and western reaches to sub-tropical zones on the east coast and temperate (dry winter) zones in the north-east. The country also receives variable rainfall, divided into summer and winter rainfall areas (Fig. 2). Mean annual precipitation ranges from below 100 mm in the Northern Cape to over 3200 mm in the high altitude eastern interior. In the last five years, drought conditions have been prevalent throughout much of the country, with the Western, Eastern and Northern Cape provinces being the worst affected (Baudoin et al., 2017). The inter-annual variability of rainfall is often attributed to larger-scale phenomena including the El Niño-Southern Oscillation (Philippon et al., 2012) and the Southern Annual Mode (Reason and Rouault, 2005). However, the specific controls on the variability of rainfall origin, intensity and regularity is debated in the literature (e.g. Synodinos et al., 2018). Recently, it has been proposed that in South Africa, the source of moisture is predominantly controlled by “atmospheric rivers” that facilitate the mass transport of moisture from equatorial regions towards the poles. These processes appear to be dynamically linked to the formation and movement of extratropical cyclones (Blamey et al., 2018; Ralph et al., 2004).

The Western Cape Province of South Africa (Fig. 2) generally experiences a warm, temperate mediterranean climate, where the majority of the province’s rainfall is received in the austral winter months (May–Sep) (Ndebele et al., 2019). Rainfall amount is heterogeneous across the province, ranging from relatively wet (>1500 mm/yr⁻¹) on mountainous windward slopes that form part of the Cape Fold Belt, to semi-arid (<150 mm/yr⁻¹) regions on the west coast and within the inland rain shadow (Fig. 2). The far eastern reaches, near the border with the Eastern Cape, receive sporadic year round rainfall and represent a transition zone between winter and summer rainfall regions (Fig. 2). Climate heterogeneity is attributed to the province’s geographical location, topography and cold seawater upwelling from the Benguela Current (Philippon et al., 2012) (Fig. 2). Rainfall origins are generally associated with cold frontal systems that are dependent on the occurrence of extratropical cyclones and cut off lows south-west of South Africa (Blamey et al., 2017).

The stable isotope composition of precipitation in the Western Cape

has a range from moderately positive to more negative δD and $\delta^{18}O$ values (12 to -40‰ and 2 to -7‰ respectively) (Diamond and Harris, 2019; Harris et al., 2010). Winter precipitation is distinctly depleted in the heavy isotopes as a result of lower temperatures and increased amounts of precipitation. Isotopic variation can be delineated by a seasonal effect rather than specific temperature and precipitation amount, and this is likely a result of monthly averages that include hot days without precipitation in the winter months (Harris et al., 2010). Orographically forced precipitation, which has less fluctuation in temperature, also has a minor influence on isotopic variability, whereas frontal systems can result in pronounced isotopic variation independent of temperature and pressure as a result of fractionation effects related to the rainout (Harris et al., 2010).

3. Methodology

Samples were collected over a period of 18 months between June 2017 and November 2018 in a series of collection campaigns. Precipitation was collected on a daily basis in containers with large surface areas to maximize sample size for low precipitation events. The data was interrogated statistically to highlight trends in isotopic composition in relation to temporal, spatial and meteorological variations. Temporal samples were collected at a collection point managed by the authors, whilst storm and regional samples were collected by both members of the research team as well as citizen scientists. The Hybrid Single Particle Lagrangian Integrated Trajectory model (HYSPLIT) used in this study was developed by the Air Resources Laboratory (ARL), a division of the National Oceanic and Atmospheric Administration (NOAA), to compute air parcel trajectories through atmospheric circulation patterns (Stein et al., 2015). The model is publically available and defines the trajectory of an infinitely small particle by integrating its vertical and horizontal movement in time (either backwards or forwards).

3.1. Sampling strategy

Collection campaigns are separated into three classes: (1) temporal data collected on a daily basis at a single location (Paarl); (2) storm data collected at multiple locations for two individual storm events (Western Cape Province); and (3) opportunistic sampling of regional precipitation collected at different times and locations across South Africa (Fig. 2). Daily samples were collected from a single location in the town of Paarl in the Western Cape Province of South Africa, over a one year period between October 2017 and October 2018. The sample location in Paarl ($-33.7348S$, $18.9588E$) is about 170 masl and received 1080.8 mm of precipitation during the sample period from 129 days of rainfall, 96 of 129 precipitation events were successfully sampled and analyzed (839.8 mm/1080.8 mm - 77.7%), as smaller events (<1 mm) usually did not produce enough water for the 1 L requirement for analysis. In addition, seven precipitation events greater than 5 mm were missed and three samples were lost in transit to the laboratory where the tritium analyses were performed. For the storm events, two large storm events in the Western Cape, one in June 2017 and one in June 2018, were sampled. The storm from June 2017 was sampled at 29 locations over a 48 h period. The storm from June 2018 was sampled at 10 locations over a 72 h period combined with samples from two sites that were sampled several times during the storm to assess hourly isotopic variation at a single location. All samples were transferred to 1 L amber HDPE containers after collection.

Regional precipitation spot sampling was completed opportunistically by either organized sampling participants (citizen scientists) or through established sampling locations from the research group. The latter were collected during coupled groundwater sampling campaigns and represent a far larger regional distribution across the country. A total of 57 samples were collected in this way, from March 2017 to December 2018, at 25 spatially distinct locations with 7 locations being sampled multiple times ($n = 3-8$) within a one year period. All collected

Table 1

Statistical moments of precipitation data for (1) temporal precipitation events in Paarl, Western Cape divided into summer and winter seasonal precipitation, (2) two Storm events in the Western Cape (2017, 2018) and (3) regional precipitation data from across South Africa.

	$\delta^2\text{H}$		$\delta^{18}\text{O}$		^3H (TU)	
	Summer ¹⁶	Winter ³⁵	Summer ¹⁶	Winter ³⁵	Summer ³¹	Winter ⁴⁵
Temporal Data (Paarl)						
Mean	-2.52	-9.48	-2.28	-3.34	1.86	1.43
Max	11.29	17.26	2.03	2.88	4.16	3.27
Min	-19.25	-35.02	-4.74	-6.97	0.62	0.45
Std.Dev	9.02	11.9	1.68	1.76	0.97	0.57
Single Storm Events						
	2017 ³⁴	2018 ³²	2017 ³⁴	2018 ³²	2017 ³⁴	2018 ³²
Mean	-4.86	-4.08	-18.04	-13.52	1.18	1.25
Max	-1.57	3.07	2.77	17.08	2.2	3.27
Min	-7.85	-8.66	-35.53	-39.35	0	0.37
Std.Dev	1.4	2	9.5	10.4	0.5	0.48
Regional Data					Snow ⁴	Rain ⁵⁷
Mean	-2.89		-9.7		3.97	2.21
Max	10.96		29.63		5.88	12.2
Min	-8.53		-57.37		2.56	0.55
Std.Dev	17.98		3.45		0.98	1.85

samples were recorded with the date of the precipitation event, the duration of the event and the volume of precipitation received. It is also important to note that South Africa was experiencing drought conditions during the sampling period, and as a result many stations did not receive sufficient precipitation for analysis of tritium. In addition, four snow samples were collected from high altitude regions in the Western Cape during the winter of 2018 by hiking groups.

3.2. Analysis

Analysis for stable and radioactive isotopes were done at the University of Lausanne (UNIL), Switzerland, and the Institute for Nuclear Research (ATOMKI), Debrecen, Hungary, respectively. Samples at UNIL were analyzed using a Picarro L2140i CO₂ laser CRDS (Cavity-Ring-Down-Spectroscopy) technique to measure the stable isotope compositions of hydrogen and oxygen. This method determines isotopologue concentrations using cavity ringdown spectroscopy by injecting approximately 1.2 μL of water into a vaporizing unit and transferred into the cavity of the spectroscopic analyzer (Gupta et al., 2009). Measured samples are validated against known IAEA water standards (VSMOW, VSLAP) as well as laboratory standards from the University of Lausanne, Switzerland. Results are reported as the conventional delta values against the international standard VSMOW/SLAP (Nelson, 2000). Replicate samples, normalized against international standards, had an average analytical uncertainty of $\pm 0.4\text{‰}$ and $\pm 0.07\text{‰}$, respectively for their δD and $\delta^{18}\text{O}$ values. Samples analyzed for tritium at ATOMKI were analyzed using the ^3He ingrowth method (Palcsu et al., 2010; Papp et al., 2012). This is done by degassing the water sample and measuring the newly produced ^3He gas from tritium decay using a dual collector (noble gas) mass spectrometer, after a predetermined length of time. The method has a detection limit of 0.012 TU and expectation values are within 2% for samples between 1 and 20 TU.

3.3. HYSPLIT modelling structure

The HYSPLIT method used in this study was adapted from the analysis of air mass trajectories performed to investigate moisture origin effects on tritium activity in precipitation in California (U.S.A) (Visser et al., 2018). Particles were released every hour over 24 h at six release altitudes (1000–6000 m) and traced backward over 240 h (10 days). The particle location was recorded every hour together with pressure, altitude, temperature and humidity at that time and location. Specific humidity was calculated from temperature and relative humidity at each particle location and assigned to the immediate air mass. The automated R-code ran all the desired trajectories and calculate the change in water vapor pressure between two time steps for a single particle along its

trajectory. This allowed for the estimation of precipitation as a function of the loss of water content over time and assigned a weighting equivalent to water content loss of the six released particles at $t=0$. The moisture content of the water vapor mass was calculated using the water vapor pressure, temperature and altitude. Precipitation data, for the purpose of partitioning origin locations, was used from the South African National Weather Service for the town of Paarl, where a weather data station is approx. 7 km away from the sampling location. The equation used to determine the moisture content was defined as in the original model development (Visser et al., 2018).

Once the moisture origin of the measured volume of precipitation per event was determined and distributed spatially by the model, all the sampled precipitation events were combined into frequency maps to display the moisture origins over the one year period as well as summer vs winter precipitation origins. This method was also used to investigate the moisture origins of the two storm events and regional sampling events.

3.4. Statistical assessment of data

Standard modal statistics were applied to the compiled data. Temporal samples were later interrogated as aggregates of weighted values according to precipitation amount. The resulting weighted averages were compared to identify the potential controls on tritium, δD and $\delta^{18}\text{O}$ variation over time. Additional approaches include adding thresholds of precipitation amount equivalent to local interception and assessing winter and summer precipitation independently. Storm and regional samples underwent a series of spatial autocorrelation techniques in order to identify spatial trends and statistically significant correlations between isotopic signatures and environmental parameters.

4. Results

Results below are presented as: (1) δD and $\delta^{18}\text{O}$ values and (2) tritium activity of daily precipitation, storm events and regional samples, followed by (3) HYSPLIT particle tracks to determine moisture origin. Results are summarized using standard statistical moments as outlined above in Table 1 with the full results available in online supplementary files A1-A3.

4.1. Stable isotopes of hydrogen and oxygen

δD and $\delta^{18}\text{O}$ values for daily precipitation collected in Paarl had a range from -35.0‰ to 17.3‰ and -6.97‰ – 2.88‰ respectively, with mean values of -7.4‰ and -3.02‰ ($n=50$, Table A1). Winter values for δD and $\delta^{18}\text{O}$ were more negative than summer precipitation values

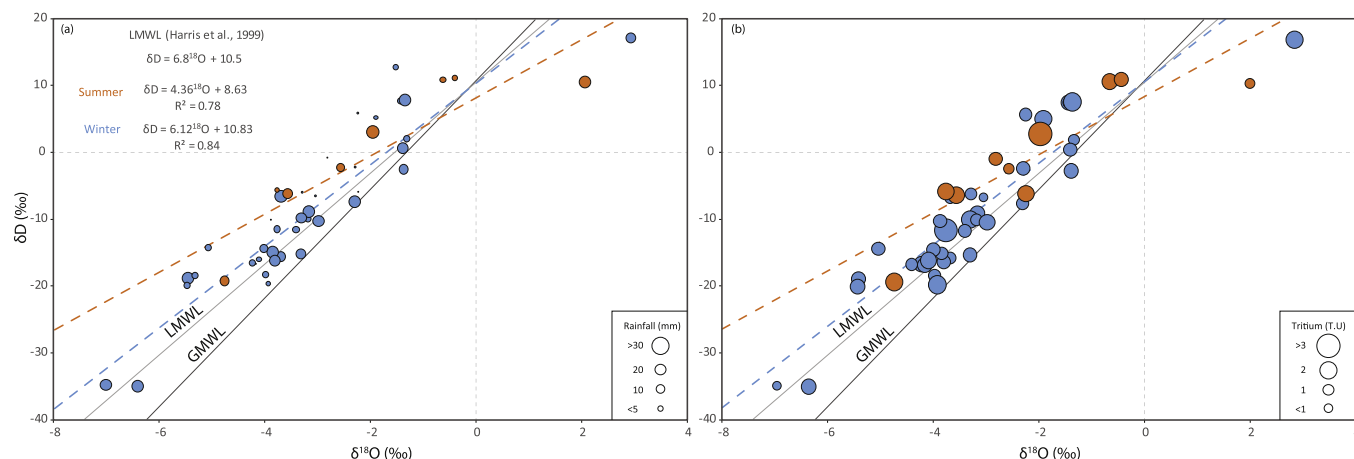


Fig. 3. Stable isotope plots of summer and winter rainfall from Paarl. Bubble sizes represent rainfall in panel (a) and tritium activity in panel b. Plots include the Global Meteoric Water Line (GMWL) where $\delta\text{D} = 8x\delta^{18}\text{O} + 10$ and the Local Meteoric Water Line (LMWL) where $\delta\text{D} = 6.8x\delta^{18}\text{O} + 10.5$.

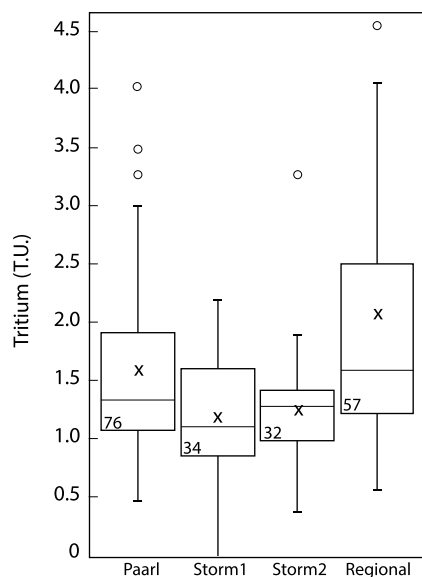


Fig. 4. Box and Whisker plot showing the modal distributions of sample tritium activity populations for precipitation from Paarl ($n = 80$), storm events 1 and 2 ($n = 34$ and 32) and regional samples ($n = 57$). Median values are represented by a solid horizontal line and mean values by an 'x'.

with means of -9.5‰ and -3.34‰ respectively in the winter and -2.5‰ and -2.28‰ respectively in the summer (Table 1). In general, larger precipitation events were received in winter and had more negative δD and $\delta^{18}\text{O}$ values, whereas large precipitation events in the summer generally had enriched positive values (Fig. 3). Both summer and winter precipitation data had local meteoric water lines that deviate from the LMWL defined for Cape Town by Harris et al. (2010). δD and $\delta^{18}\text{O}$ values had little correlation to precipitation amount (Fig. 3a).

Results for precipitation samples from the single storm event in 2017 (about 25 mm, 7th to 9th of June) had a mean δD value of -18.0‰ and a mean $\delta^{18}\text{O}$ value of -4.86‰ ($n = 34$, Table A.2). A similar storm event in the winter of 2018 (about 60 mm, 14th-18th of June) had a mean δD value of -13.5‰ and a mean $\delta^{18}\text{O}$ value of -4.08‰ ($n = 32$, Table A.2). Deuterium excess was investigated as a potential indicator of water vapor origin but showed random spatial distributions (Moran's $I = -0.08$). Stable isotope data from the regional precipitation samples had a mean δD value of -9.7‰ and a $\delta^{18}\text{O}$ value of -2.89‰ ($n = 47$, Appendix: Table A.3) and ranges -57.4‰ – -29.6‰ for δD values and from -8.53‰

to 10.96‰ for $\delta^{18}\text{O}$. δD values were highly variable with a standard deviation of 17.98 while $\delta^{18}\text{O}$ values were less variable ($\sigma = 3.5$, $n = 57$).

4.2. Tritium activity

The mean activity of tritium for the 76 daily precipitation samples collected at the single location in Paarl was 1.67 TU and ranged from 0.45 to 4.16 TU, with a median value of 1.47 TU (Fig. 4). Precipitation tritium data for summer and winter months had mean values of 1.86 and 1.52 TU respectively. Summer months showed increased variability in tritium activity ($\sigma = 0.93$, $n = 31$) when compared to winter ($\sigma = 0.62$, $n = 45$). Although summer precipitation had generally more positive $\delta^{18}\text{O}$ and δD values, tritium activity had poor correlation when compared to $\delta^{18}\text{O}$ and δD (Fig. 3b). Tritium activity for individual daily precipitation was plotted against precipitation amount and separated by precipitation amounts larger than 5 mm, equal to the estimated precipitation amount needed for recharge in the region derived from Watson et al. (2018) (Fig. 5). Potential recharge events had a mean tritium activity of 1.46 TU ($n = 45$) and precipitation amounts <5 mm had a mean tritium activity of 2.17 TU ($n = 31$). Despite a clear difference in the tritium activities of precipitation above and below 5 mm, tritium activities showed poor correlation with precipitation amount ($r^2 = 0.09$, Fig. 6).

Storm 1 samples had a mean tritium activity of 1.18 TU ($n = 34$) and a range of 2.2 TU (0–2.2 TU) and showed a poor spatial autocorrelation with a Moran's I value of 0.03. Storm 2 samples had a mean tritium activity of 1.25 TU ($n = 32$) with a range of 2.9 TU (0.37–3.27), also showing poor spatial autocorrelation (Moran's $I = 0.05$). However, both storm events showed similar tritium variability (Storm 1 - $\sigma = 0.5$ $n = 35$ and Storm 2 - $\sigma = 0.48$ $n = 32$). Additionally, samples were collected at time-based intervals (2 h) during storm 2 at the Paarl collection site, apart from three samples that were collected at longer intervals due to not enough sample volume during these periods. Fifteen samples were collected over a three-day period as the frontal system passed through (Fig. 7). Tritium activities from the three day storm event ranged from 0.91 to 3.27 TU and averaged 1.37 TU. $\delta^{18}\text{O}$ and δD during the 3 day storm event again show poor correlation to tritium activities with r^2 values of <0.01 .

Regional precipitation events had the largest range of tritium activities (0.55–12.2 TU). These samples also had the largest ranges of collection altitudes, precipitation amounts and stable isotope variance. The highest recorded tritium activity in the dataset was collected in Randburg, Johannesburg with a tritium activity of 12.2 TU, which was a significant outlier ($P < 0.05$), and the lowest recorded tritium activity in precipitation was in Uvongo on the East coast of Kwa-Zulu Natal of 0.55 TU. The mean tritium activity of regional precipitation is 2.21 TU. In

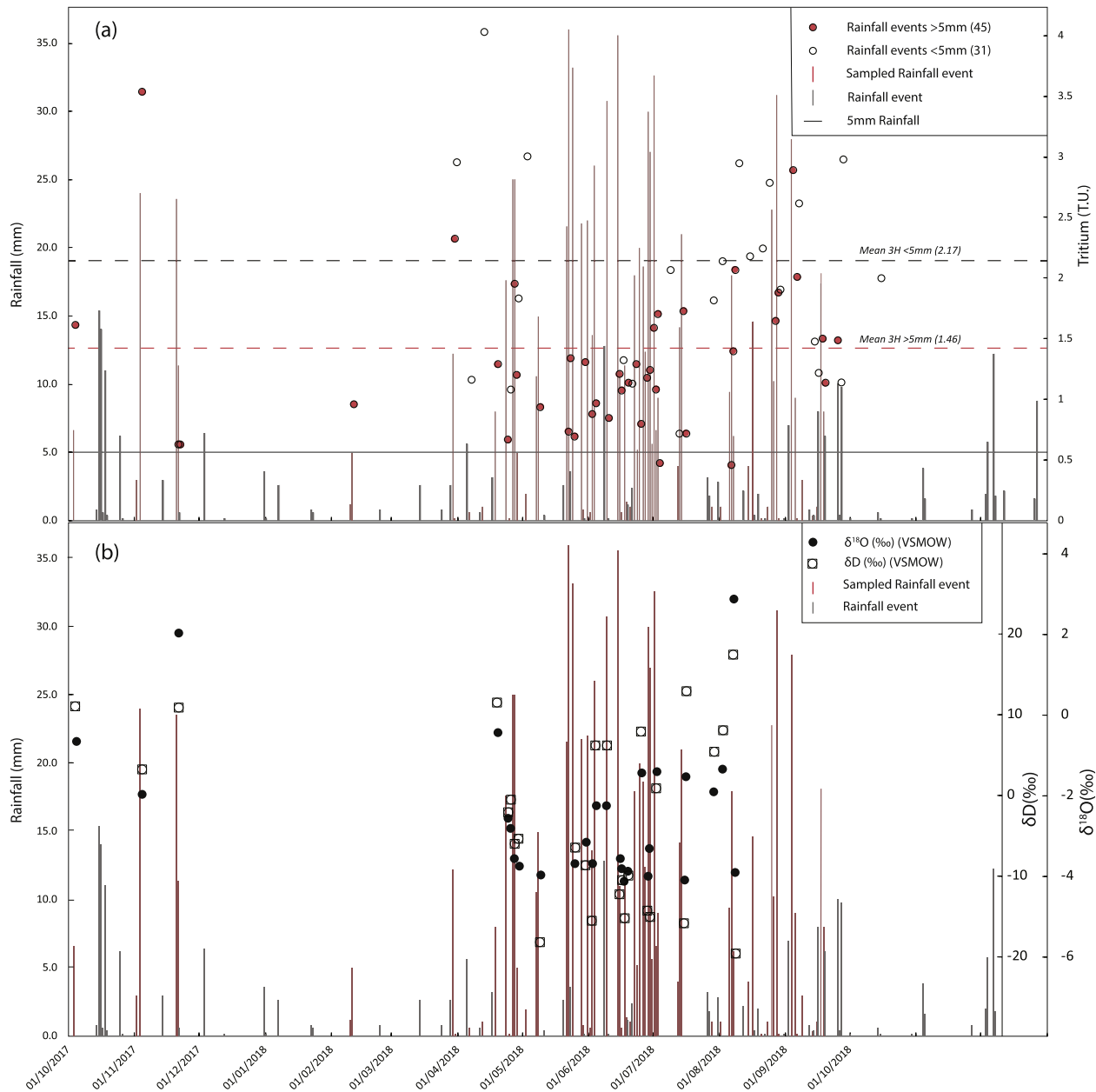


Fig. 5. Daily rainfall collected in Paarl for the one year period from October 2017 to October 2018. Tritium activities for sampled rainfall for events are plotted in panel (a) and divided into rainfall events larger than 5 mm. Stable isotope values are plotted in panel (b) and divided into δD and $\delta^{18}O$.

general, tritium activities were distributed as increasing values from the south-west of the country to the north-east. Snow samples showed elevated tritium activities with a mean of 3.97 TU ($n = 4$).

4.3. Moisture origin through HYSPLIT models

HYSPLIT particle tracks (Fig. 8) of all precipitation events sampled ($n = 76$) indicated that the majority of precipitation originates to the west and south-west of South Africa, over the Atlantic and Southern Oceans ($n = 62$). There was also evidence from the frequency of water mass origin, that 66% of precipitation in the summer months typically originated from higher altitudes and lower latitudes ($n = 24$, e.g. Fig. 8a). Both summer and winter precipitation were effected by ocean

water dilution with late uptake into the cloud system before precipitation ($n = 31$ e.g. Fig. 8b). However, 55% precipitation in the winter months originated from lower altitudes and mid to high latitudes ($n = 27$ e.g. Fig. 8c). Precipitation events that originated from continental moisture recycling were uncommon ($n = 5$), but typically had elevated tritium activity ($\bar{x} = 2.29$ TU). HYSPLIT particle tracks for single storm events showed that the majority of the precipitation sample sites had similar precipitation origin areas (within a 1×1 degree area) in the Southern Ocean, south-west of Cape Town. Sample locations further away from Cape Town (e.g. Springbok) had origins further to the west, yet aligned to the same storm event. Tritium activities showed moderate correlation with maximum moisture contribution altitudes at t_0 ($R^2 = 0.506$).

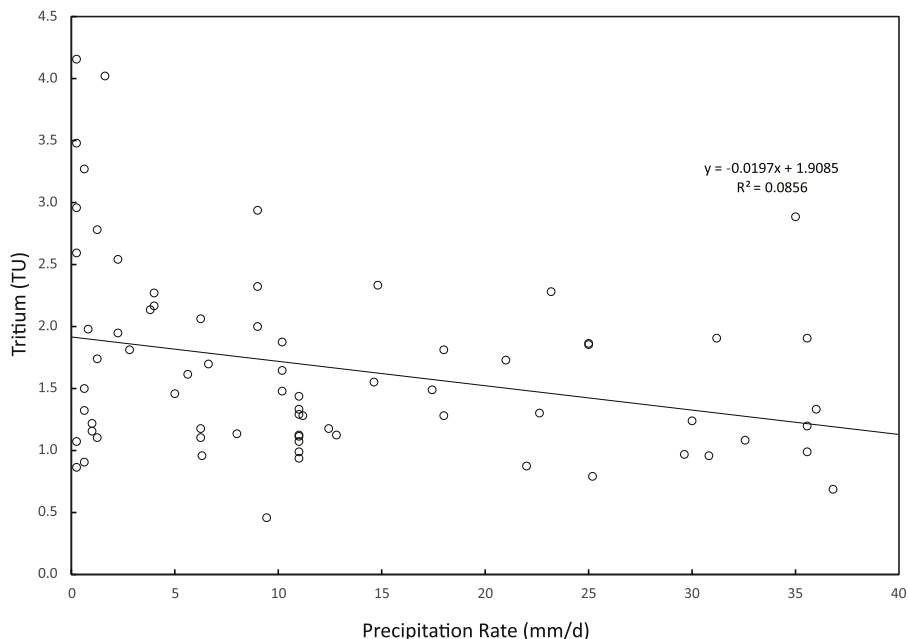


Fig. 6. Measured tritium activity [TU] of precipitation events as a function of the amount of precipitation [mm/d].

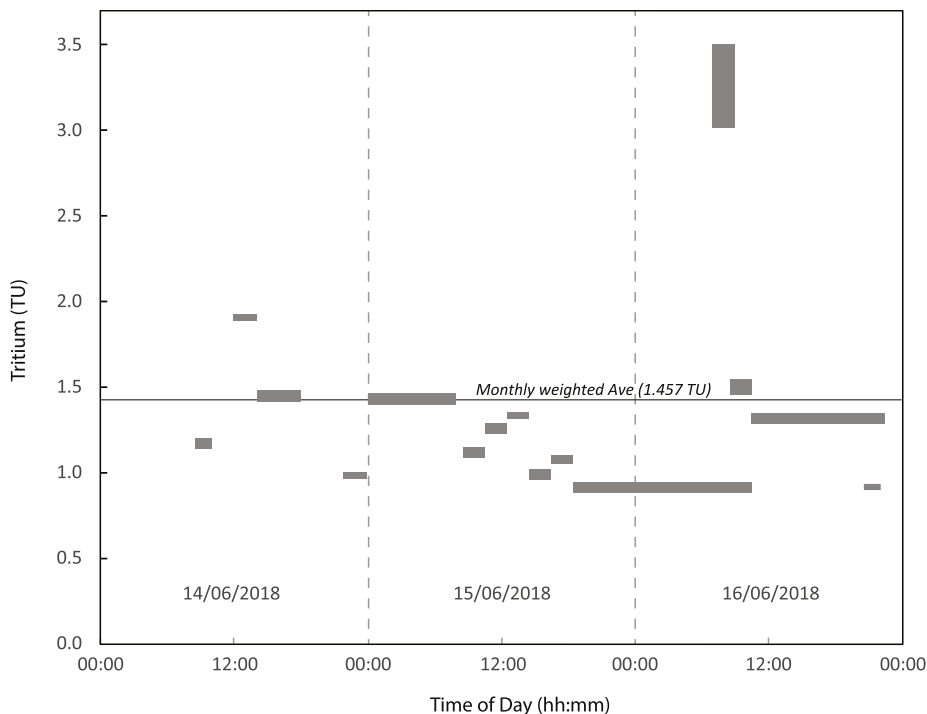


Fig. 7. Tritium activities sampled from a single precipitation event over a 3 day period collected in Paarl. Included is the monthly weighted average of tritium from the same location for the month of June 2018. Lengths of the bars represent the duration over which the sample was taken and heights present the analytical error.

5. Discussion

The variability of tritium data related to seasonality in Paarl and the spatial distribution in the Western Cape and across South Africa, is clearly evident and likely related to both regional and global processes. Our understanding of the controls on tritium activity in precipitation is largely based on aggregated monthly data from GNIP stations or established monitoring systems, yet daily tritium data shows a new layer of variability that has not been well characterized. The following discussion highlights key trends in the results, compares these to those that

have been previously observed using monthly collection protocols and evaluates the reliability of the HYSPLIT methodology to understand tritium distribution and variability and what this tells us about hydrological resilience.

5.1. Seasonal effects on tritium activity in precipitation

Temporal data collected in Paarl shows a large range of values for δD , $\delta^{18}O$ and tritium. Comparison of monthly averages of δD and $\delta^{18}O$ from Paarl data shows the same seasonal trend of monthly averages of the

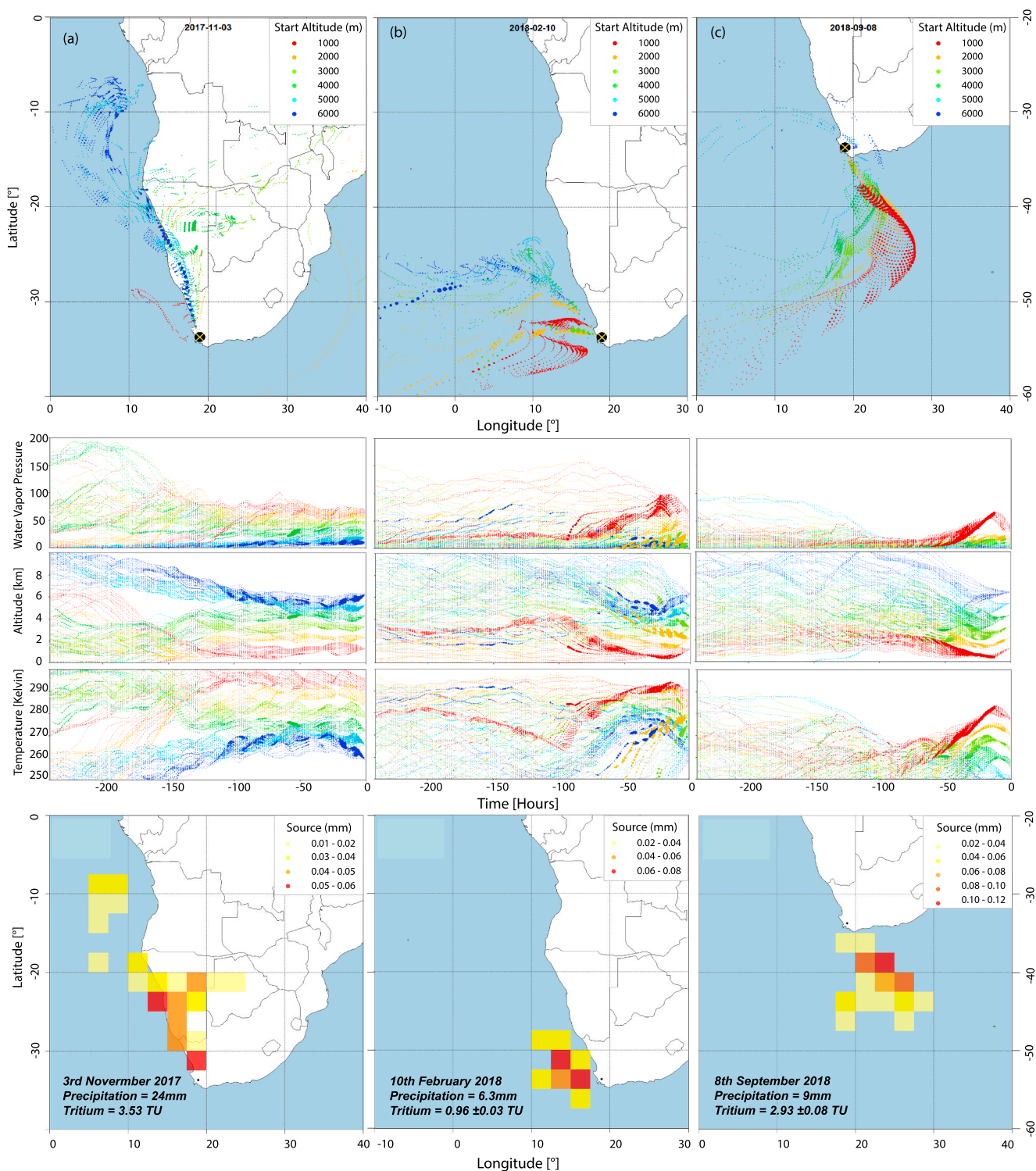


Fig. 8. HYSPLIT particle tracks (top) from three separate precipitation events (Panels a, b, c) collected from the temporal sampling location in Paarl, Western Cape. Particles record hourly meteorological data (middle) which enables the model to calculate expected spatial contributions of water mass origin. Each example was selected to show distinct precipitation origin mechanisms that result in local precipitation. Panel (a) represents a high altitude, low latitude origin with evidence of continental recycling of moisture, panel (b) represents a typical winter frontal system of mixed altitude origins originating from the nearby ocean and panel (c) represents a low altitude, high latitude origin in the Southern Ocean.

GNIP station at Cape Town International Airport approximately 42 km away (Fig. 9). This wide range of δD and $\delta^{18}O$ is a result of different precipitation type, temperature and intensity in the summer vs winter months (Harris et al., 2010). δD and $\delta^{18}O$ in Paarl show poor

correlations to precipitation amounts on a daily time step, yet show much clearer relationships with seasonal monthly averages. This suggests that isotopic fractionation processes could have stronger correlations with seasonal temperature fractionation effects, as opposed to

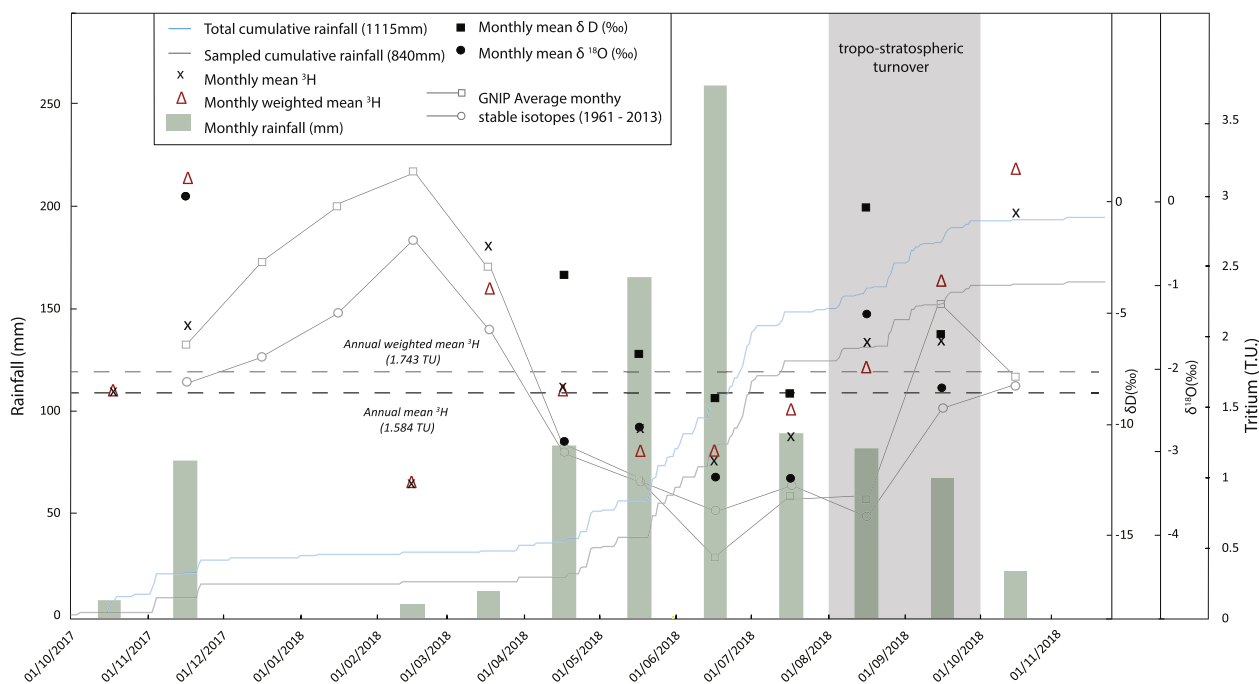


Fig. 9. Monthly averages and weighted monthly averages of tritium activity in precipitation sampled in Paarl, plotted with (a) monthly precipitation amounts (bars) and cumulative precipitation (lines) of total (blue) and sampled (grey) precipitation and (b) monthly averages of δD and $\delta^{18}O$ from sampled events (squares and circles) and historical stable isotope records from the nearest GNIIP station approx. 43 km away (connected squares and circles). Dashed lines represent the annual mean and weighted mean of tritium in precipitation. (For interpretation of the references to color in this figure legend, the reader is referred to the Web version of this article.)

precipitation out effects. While water mass origins are typically from the Southern Ocean, where δD and $\delta^{18}O$ should be near zero, significant enrichment of δD and $\delta^{18}O$ was observed in Paarl in some events ($n = 12$), particularly in the summer months. This may be a result of: (1) continental recycling phenomena in the summer months where precipitation origins occur at lower latitudes/higher altitudes and/or (2) large extratropical cyclonic systems raining out significant amounts of isotopically heavier precipitation before landfall in the winter months (Blamey et al., 2018). A similar lack of correlation can be seen with δD and $\delta^{18}O$ values and the activity of tritium in precipitation for daily events. This may be a result of the origin of moisture at higher latitudes as well as higher altitudes and increased residence time of moisture, allowing for the accumulation of regional tritium fall out as opposed to kinetic and temperature related fractionation (Aggarwal et al., 2016).

Variation in tritium values in the Western Cape, is most pronounced between summer and winter precipitation. Although tritium activity in daily precipitation samples showed poor correlation to precipitation amount, weighted monthly averages of tritium activities show distinct seasonal trends, mimicking the typical seasonal variation of tritium activities reported elsewhere in the world (Mair et al., 2013; Tadros et al., 2014; Visser et al., 2018). Monthly averages of tritium in precipitation, weighted by the precipitation volume, show a steady decline in activity from March to June as rainfall increases and temperature decreases and an equivalent rise in tritium activity through the spring months of July through October. The rise in tritium activities in spring can be related to the tropo-stratospheric turnover during this period (Fig. 9) (Black et al., 2006). The degree of tritium seasonality shows strong correlation to more negative winter δD and $\delta^{18}O$, shown as monthly averages (1961–2013) from the nearby GNIIP station (Fig. 9). This suggests the macro seasonal processes that control δD and $\delta^{18}O$ could affect tritium activities as well. Although seasonal trends of tritium activity are clear, it is still unclear as to why tritium activities are so variable between individual events. Consequently, characterizing the tritium activity in precipitation for a region is difficult without considering the origin of the water mass, its potential interaction with

stratospheric tritium, the effect of ocean water dilution and the residence time of the water mass in the atmosphere.

5.2. Origin of water masses that form precipitation

The use of HYSPLIT backward trajectories to investigate the origin of water masses was effective in characterizing tritium activities in the majority of the temporal events and provided strong arguments for the occurrence of high and low tritium activities. Water mass origins that originated in close proximity to the coast showed low tritium activities, presumably as a result of oceanic dilution, a phenomena evident in Australia and South Korea through the comparison of coastal and inland monitoring stations (Mair et al., 2013; Tadros et al., 2014). Comparatively, multiple trajectories that predicted water mass origins over the continent showed the highest tritium activities, confirming these phenomena are driven by oceanic dilution with HYSPLIT methods. This effect was also evident from the spatial analysis of water sources to precipitation in the Sierra Nevada, USA (Visser et al., 2018). Additionally, the altitude effect was evident and showed elevated tritium activities associated with trajectories with origins from higher altitudes (>4000 m) are capable of interacting more with stratospheric processes. The four snow samples collected in the study showed the highest tritium activities and all have origin altitudes above the confines of the model (>10 000 m). The altitude of air mass trajectories has not been analyzed before to explain tritium concentrations in precipitation (Visser et al., 2018). Although the incorporation of tritium from the stratosphere is complex (Aggarwal et al., 2016), we expect that altitude and the distinction between convective and stratiform precipitation will greatly improve our ability to predict tritium in precipitation. The seasonal effect on tritium activity is well characterized by water mass origins in summer and winter (Fig. 10), as generally higher tritium activities in summer months originate from lower latitudes but higher altitudes. Conversely, tritium activities are lower in winter months and originate from higher latitudes but lower altitudes. These findings rely on the higher temporal density of tritium samples that was not available in

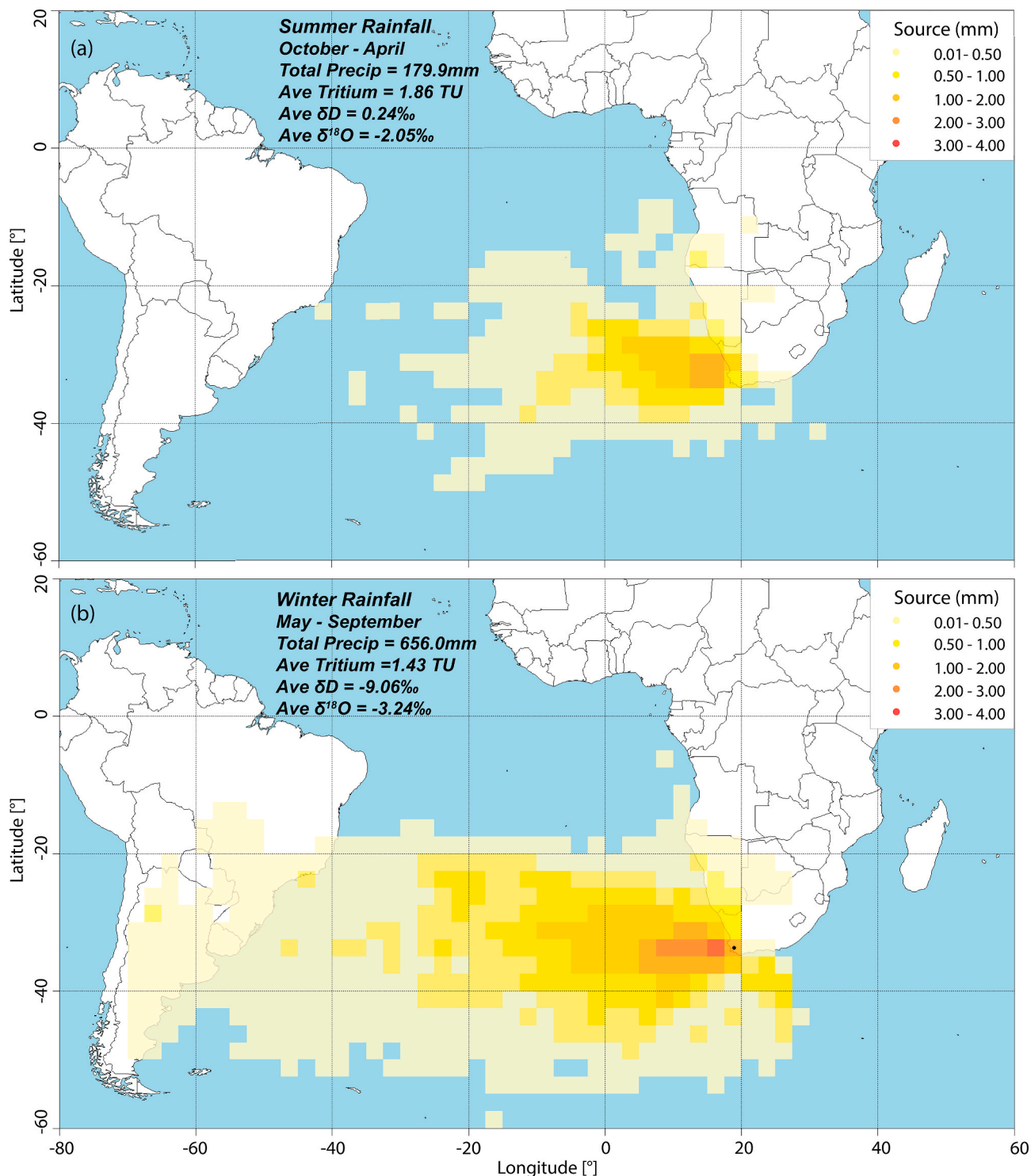


Fig. 10. Combined moisture origin heat maps of precipitation received in Paarl, Western Cape, in summer (a) and winter (b). Moisture sources are characterized by volume [mm] proportions of individual precipitation events and combined to show the moisture origins of the total precipitation received in a season.

previous studies (Unnikrishnan Warriier et al., 2013; Visser et al., 2018) that relied on aggregate samples of tritium in precipitation. It is also evident that the majority of precipitation received in Paarl originates from nearby off the coast of Cape Town (SW), and this indicates that relatively low mean annual tritium activities are predominantly caused by the oceanic dilution effect. Both the Sierra Nevada and the Western Cape receive a significant amount of precipitation from atmospheric rivers that have the ability to strongly dilute the original tritium content of the air mass. We expect that changes in the intensity and trajectories

of atmospheric rivers in future climates will also influence tritium in precipitation (Espinoza et al., 2018). The HYSPLIT modelling structure does not show distinct evidence of latitudinal effects before being corrected for seasonality at this location. Stronger latitudinal effects observed at the Sierra Nevada may have been correlated to enhanced atmospheric mixing over continental terrain at higher latitudes. The ability to explain variability of tritium in precipitation is justification to include water mass origin investigations for the purpose of hydrological and hydrogeological studies anywhere in the world.

5.3. Event based spatial variability of tritium in precipitation

In addition to seasonal variations of tritium activity, spatial variability is significant in large winter storms that provide the bulk of the Western Cape's annual precipitation (Ndebele et al., 2019). The two sampled storm events (June 2017 and 2018) have tritium activity ranges that exceed 2 TU and distributions almost as large as the temporal database (one year) collected in this study, with storm 1 (2017) having greater variability when compared to storm 2 (2018). Nevertheless, spatial distributions are practically random (Moran's $I = 0.03$) and show poor correlation to typical ranges of δD and $\delta^{18}O$ in precipitation as a result of altitude, rain out and temperature effects. The lack of spatial correlation suggests that the variability of tritium in a single storm is controlled by more than typical fractionation affects (continental/surface altitude). Rather, tritium activities show a stronger correlation to the moisture origin altitude of the storm air masses. Samples with elevated tritium activities precipitate from air-masses that have reached higher altitudes and are capable of entraining stratospheric water vapor (Ravishankara, 2012). This phenomena is evident in storm 1 where there is moderate correlation between the altitude of maximum moisture contribution and tritium activity ($r^2 = 0.506$). The altitudinal effect is a result of the storm morphology and can be explained by comparing trajectories with the frontal system. Water masses that originated from the low pressure center of an extratropical cyclonic system have elevated tritium signals, whereas sample sites that receive rainfall from the outer reaches of the storm front had lower tritium activities. This may be the result of two different processes: (1) increased interaction of the large cloud systems with the stratosphere in the low-pressure center, enriching the water mass with tritium and (2) increased uptake of oceanic water in the outward trajectories, resulting in the dilution of tritium activities.

When considering tritium in precipitation on a country-wide scale, the range of activities exceeds 10 TU and is the result of highly contrasting climatic conditions across the large country (Schulze and Maharaj, 2004). Rainfalls originating in the southern ocean initially rain out lower activities of tritium ($\sim 1-2$ TU), yet increase in activity in their north east trajectory across the country. The interior, especially in Gauteng and Limpopo, appears to have the highest tritium activities from weather systems, determined from HYSPLIT trajectories, migrating southward from the northern bordering countries. Distributions of sampling locations regionally are not ideal and many samples were only taken once, providing only a snapshot of what the likely averages of tritium activity might be. This is clear evidence that the scale at which tritium variability is investigated is critical as the conclusions on the cause of tritium variability of precipitation in the Western Cape is not applicable to the summer precipitation regions of the country.

5.4. Implications for hydrological studies

Tritium activities in the Western Cape varied significantly over short and long temporal ranges, as well as spatially across the province. As a region that has experienced drought conditions resulting in restrictions on domestic water supply (Baudoin et al., 2017), it is important that hydrological studies that use isotope tracers derived from precipitation are accurate. It is evident from this study, that if input tritium activities are not correctly constrained, modern recharge would be over-/underestimated. Although monthly tritium variability is controlled by macro processes, such as atmospheric turnover and seasonality, variation of daily rainfall is controlled by specific processes, such as ocean water dilution, continental recycling and altitudinal/latitudinal effects. This would suggest that comparable variability would be experienced in other regions of the world and would also need to be constrained before representative studies could be undertaken. Although many established GNIP stations have long-term records of tritium in precipitation, the nature of cumulative monthly samples may not constrain the potential tritium activity of recharge effectively. The capabilities of using

HYSPLIT trajectories to ascertain moisture origin are only tested in this paper to explain measured tritium activities. However, if calibrated correctly, HYSPLIT moisture origin could be used to predict the activity of tritium in precipitation and in turn characterize the expected tritium activity in past and future recharge events.

6. Conclusions

Analysis of 3H activity in 168 precipitation samples indicates that tritium activities in precipitation vary significantly not just between different rainfall seasons (approx. 1 TU), but also spatially during single storm events (>2 TU). It is also evident that tritium variability is likely controlled by seasonal changes in the type and amount of precipitation received. Rainfall origin of storms in summer and winter are distinctly different and result in varying mechanisms capable of incorporating and diluting tritium activity in precipitation. In South Africa in particular, precipitation received in the winter months that originated from the south-west in the Southern Ocean have, in general, lower tritium activities than summer precipitation originating from higher latitudes and altitudes. It is clear that storm behavior forms a major control on how and where moisture is incorporated and in turn large storm systems can develop variable tritium activities. Although not all tritium activities can be explained by interrogating the water mass origin, this study found that approximately 90% of tritium activities in daily precipitation can be completely or partially attributed to the origin of the water mass. Although monthly records of tritium activity around the world have been successful in identifying macro processes controlling tritium seasonality, other trends identified such as ocean water dilution, continental recycling and altitudinal/latitudinal effects are better characterized by interrogating HYSPLIT water mass origins of daily events. The consequence of underestimated variability of tritium in precipitation is that hydrological studies cannot effectively predict the variability of tritium in the hydrological cycle through runoff, recharge and discharge.

Declaration of competing interest

The authors declare that they have no known competing financial interests or personal relationships that could have appeared to influence the work reported in this paper.

Acknowledgements

We thank the Water Research Commission South Africa for initial funding support and the iPahakade program and National Research Foundation (NRF) South Africa for bursary support. The authors would like to acknowledge the assistance of the University of Utah's ITCE SPATIAL program for providing the training necessary to construct the model presented in this paper. This work is based on the research supported wholly/in part by the National Research Foundation of South Africa (Grant Number: 118594) and was partly supported by the European Union and the State of Hungary, co-financed by the European Regional Development Fund in the project of GINOP-2.3.2-15-2016-00009 'ICER'. Contributions by Lawrence Livermore National Laboratory (LLNL) authors under Contract DE-AC52-07NA27344, with funding from LDRD project 15-ERD-042. The stable isotope analyses were made in the framework of an exchange program between the universities of Stellenbosch and Lausanne, and the first author is grateful to IDYST and the University of Lausanne for their warm welcome and scientific exchange.

Appendix A. Supplementary data

Supplementary data to this article can be found online at <https://doi.org/10.1016/j.jenvrad.2020.106354>.

References

- Aggarwal, P.K., Romatschke, U., Araguas-Araguas, L., Belachew, D., Longstaffe, F.J., Berg, P., Schumacher, C., Funk, A., 2016. Proportions of convective and stratiform precipitation revealed in water isotope ratios. *Nat. Geosci.* 9, 624–629. <https://doi.org/10.1038/ngeo2739>.
- Baudoin, M.A., Vogel, C., Nortje, K., Naik, M., 2017. Living with drought in South Africa: lessons learnt from the recent El Niño drought period. *Int. J. Disaster Risk Reduct.* 23, 128–137. <https://doi.org/10.1016/j.ijdrr.2017.05.005>.
- Black, R.X., McDaniel, B.A., Robinson, W.A., 2006. Stratosphere-troposphere coupling during spring onset. *J. Clim.* 19, 4891–4901. <https://doi.org/10.1175/JCLI3907.1>.
- Blamey, R.C., Middleton, C., Lennard, C., Reason, C.J.C., 2017. A climatology of potential severe convective environments across South Africa. *Clim. Dynam.* 49, 2161–2178. <https://doi.org/10.1007/s00382-016-3434-7>.
- Blamey, R.C., Ramos, A.M., Trigo, R.M., Tomé, R., Reason, C.J.C., 2018. The influence of atmospheric rivers over the South Atlantic on winter rainfall in South Africa. *J. Hydrometeorol.* 19, 127–142. <https://doi.org/10.1175/JHM-D-17-0111.1>.
- Busenberg, E., Plummer, L.N., 2008. Dating groundwater with trifluoromethyl sulfurpentafluoride (SF₅CF₃), sulfur hexafluoride (SF₆), CF₃Cl (CFC-13), and CF₂Cl₂ (CFC-12). *Water Resour. Res.* 44. <https://doi.org/10.1029/2007WR006150>.
- Cartwright, I., Cendón, D., Currell, M., Meredith, K., 2017. A review of radioactive isotopes and other residence time tracers in understanding groundwater recharge: possibilities, challenges, and limitations. *J. Hydrol.* 555, 797–811. <https://doi.org/10.1016/j.jhydrol.2017.10.053>.
- Cartwright, I., Morgenstern, U., 2015. Transit times from rainfall to baseflow in headwater catchments estimated using tritium: the Owens River, Australia. *Hydrol. Earth Syst. Sci.* 19, 3771–3785. <https://doi.org/10.5194/hess-19-3771-2015>.
- Clark, I., 2015. *Groundwater Geochemistry and Isotopes*. CRC press.
- Clark, I.D., Fritz, P., 2013. *Environmental Isotopes in Hydrogeology*. CRC press.
- Cook, P.G., Solomon, D.K., 1997. Recent advances in dating young groundwater: chlorofluorocarbons, 3H/3He and 85Kr. *J. Hydrol.* 191, 245–265. [https://doi.org/10.1016/S0022-1694\(96\)03051-X](https://doi.org/10.1016/S0022-1694(96)03051-X).
- Darling, W.G., Goody, D.C., MacDonald, A.M., Morris, B.L., 2012. The practicalities of using CFCs and SF₆ for groundwater dating and tracing. *Appl. Geochem.* 27, 1688–1697. <https://doi.org/10.1016/j.apgeochem.2012.02.005>.
- Diamond, R.E., Harris, C., 2019. Stable isotope constraints on hydrostratigraphy and aquifer connectivity in the table mountain group. *S. Afr. J. Geol.* 122, 317–330. <https://doi.org/10.25131/sajg.122.0021>.
- Eastoe, C.J., Watts, C.J., Plouffe, M., Wright, W.E., 2012. Future use of tritium in mapping pre-bomb groundwater volumes. *Ground Water* 50, 87–93. <https://doi.org/10.1111/j.1745-6584.2011.00806.x>.
- Espinoza, V., Waliser, D.E., Guan, B., Lavers, D.A., Ralph, F.M., 2018. Global analysis of climate change projection effects on atmospheric rivers. *Geophys. Res. Lett.* 45, 4299–4308. <https://doi.org/10.1029/2017GL076968>.
- Gupta, P., Noone, D., Galewsky, J., Sweeney, C., Vaughn, B.H., 2009. Demonstration of high-precision continuous measurements of water vapor isotopologues in laboratory and remote field deployments using wavelength-scanned cavity ring-down spectroscopy (WS-CRDS) technology. *Rapid Commun. Mass Spectrom.* 23, 2534–2542. <https://doi.org/10.1002/rcm.4100>.
- Harms, P.A., Visser, A., Moran, J.E., Esser, B.K., 2016. Distribution of tritium in precipitation and surface water in California. *J. Hydrol.* 534, 63–72. <https://doi.org/10.1016/j.jhydrol.2015.12.046>.
- Harris, C., Burgers, C., Miller, J., Rawoof, F., 2010. O- and H-isotope record of Cape Town rainfall from 1996 to 2008, and its application to recharge studies of table mountain groundwater, South Africa. *S. Afr. J. Geol.* 113, 33–56. <https://doi.org/10.2113/gssajg.113.1.33>.
- Kalin, R.M., 2000. Radiocarbon dating of groundwater systems. In: *Environmental Tracers in Subsurface Hydrology*. Springer, pp. 111–144.
- Loosli, H.H., Lehmann, B.E., Smethie, W.M., 2000. Noble gas radioisotopes: 37 Ar, 85 Kr, 39 Ar, 81 Kr. In: *Environmental Tracers in Subsurface Hydrology*. Springer, pp. 379–396.
- Mair, A., Hagedorn, B., Tillery, S., El-Kadi, A.I., Westenbroek, S., Ha, K., Koh, G.W., 2013. Temporal and spatial variability of groundwater recharge on Jeju Island, Korea. *J. Hydrol.* 501, 213–226. <https://doi.org/10.1016/j.jhydrol.2013.08.015>.
- McGuire, K.J., McDonnell, J.J., 2006. A review and evaluation of catchment transit time modeling. *J. Hydrol.* 330, 543–563. <https://doi.org/10.1016/j.jhydrol.2006.04.020>.
- Ndebele, N.E., Grab, S., Turasie, A., 2019. Characterizing rainfall in the south-western Cape, South Africa: 1841–2016. *Int. J. Climatol.* 1–23. <https://doi.org/10.1002/joc.6314>.
- Nelson, S.T., 2000. A simple, practical methodology for routine VSMOW/SLAP normalization of water samples analyzed by continuous flow methods. *Rapid Commun. Mass Spectrom.* 14, 1044–1046.
- Palcsu, L., Major, Z., Köllő, Z., Papp, L., 2010. Using an ultrapure 4He spike in tritium measurements of environmental water samples by the 3He-ingrowth method. *Rapid Commun. Mass Spectrom.* 24, 698–704. <https://doi.org/10.1002/rcm.4431>.
- Palcsu, L., Morgenstern, U., Sültenfuss, J., Koltai, G., László, E., Temovskí, M., Major, Z., Nagy, J.T., Papp, L., Varlam, C., Faurescu, I., Túri, M., Rinyu, L., Czuppon, G., Botyán, E., Jull, A.J.T., 2018. Modulation of cosmogenic tritium in meteoric precipitation by the 11-year cycle of solar magnetic field activity. *Sci. Rep.* 8, 1–9. <https://doi.org/10.1038/s41598-018-31208-9>.
- Papp, L., Palcsu, L., Major, Z., Rinyu, L., Tóth, I., 2012. A mass spectrometric line for tritium analysis of water and noble gas measurements from different water amounts in the range of microlitres and millilitres noble gas measurements from different water amounts in the. *Isot. Environ.* 6016. <https://doi.org/10.1080/10256016.2012.679935>.
- Philippon, N., Rouault, M., Richard, Y., Favre, A., 2012. The influence of ENSO on winter rainfall in South Africa. *Int. J. Climatol.* 32, 2333–2347. <https://doi.org/10.1002/joc.3403>.
- Phillips, F.M., 2000. Chlorine-36. In: *Environmental Tracers in Subsurface Hydrology*. Springer, pp. 299–348.
- Ralph, F.M., Neiman, P.J., Wick, G.A., 2004. Satellite and CALJET aircraft observations of atmospheric rivers over the Eastern North Pacific Ocean during the winter of 1997/98. *Mon. Weather Rev.* 132, 1721–1745. [https://doi.org/10.1175/1520-0493\(2004\)132<1721:SACAOO>2.0.CO;2](https://doi.org/10.1175/1520-0493(2004)132<1721:SACAOO>2.0.CO;2).
- Ravishankara, A.R., 2012. Water vapor in the lower stratosphere. *Science* 337, 809–811. <https://doi.org/10.1126/science.1227004>, 80-.
- Reason, C.J.C., Rouault, M., 2005. Links between the Antarctic Oscillation and winter rainfall over western South Africa. *Geophys. Res. Lett.* 32, 1–4. <https://doi.org/10.1029/2005GL022419>.
- Rozanski, K., Gonfiantini, R., Araguas-Araguas, L., 1991. Journal of Physics G: nuclear and Particle Physics Related content Tritium in the global atmosphere: distribution patterns and recent trends. *J. Phys. G Nucl. Part. Phys.* 17, S523–S536.
- Scanlon, B.R., Healy, R.W., Cook, P.G., 2002. Choosing appropriate technique for quantifying groundwater recharge. *Hydrogeol. J.* 10, 18–39. <https://doi.org/10.1007/s10040-0010176-2>.
- Schulze, R.E., Maharaj, M., 2004. Development of a database of gridded daily temperatures for Southern Africa. *Water Res. Comm. Pretoria, RSA, WRC Rep.* 1156, 4.
- Stein, A.F., Draxler, R.R., Rolph, G.D., Stunder, B.J.B., Cohen, M.D., Ngan, F., 2015. NOAA's hybrid atmospheric transport and dispersion modeling system. *Bull. Am. Meteorol. Soc.* 96, 2059–2077. <https://doi.org/10.1175/BAMS-D-14-00110.1>.
- Stewart, M.K., Morgenstern, U., McDonnell, J.J., 2010. Truncation of stream residence time: how the use of stable isotopes has skewed our concept of streamwater age and origin. *Hydrol. Process.* 24, 1646–1659. <https://doi.org/10.1002/hyp.7576>.
- Synodinos, A.D., Tietjen, B., Lohmann, D., Jeltsch, F., 2018. The impact of inter-annual rainfall variability on African savannas changes with mean rainfall. *J. Theor. Biol.* 437, 92–100. <https://doi.org/10.1016/j.jtbi.2017.10.019>.
- Tadros, C.V., Hughes, C.E., Crawford, J., Hollins, S.E., Chisari, R., 2014. Tritium in Australian precipitation: a 50 year record. *J. Hydrol.* 513, 262–273. <https://doi.org/10.1016/j.jhydrol.2014.03.031>.
- Thatcher, L.L., 1962. The distribution of tritium fallout in precipitation over north America. *Int. Assoc. Sci. Hydrol. Bull.* 7, 48–58. <https://doi.org/10.1080/02626666209493255>.
- Unnikrishnan Warriar, C., Praveen Babu, M., Manjula, P., Shahul Hameed, A., 2013. Spatial and temporal variations of natural tritium in precipitation of southern India. *Curr. Sci.* 105, 242–248.
- Visser, A., Thaw, M., Esser, B., 2018. Analysis of air mass trajectories to explain observed variability of tritium in precipitation at the Southern Sierra Critical Zone Observatory, California, USA. *J. Environ. Radioact.* 181, 42–51. <https://doi.org/10.1016/j.jenvrad.2017.10.008>.
- Watson, A.P., Miller, J.A., Fleischer, M., de Clercq, W.P., 2018. Estimation of groundwater recharge via percolation outputs from a rainfall/runoff model for the Verlorenvlei estuarine system, west coast, South Africa. *J. Hydrol.* 558, 238–254. [https://doi.org/10.1016/S1532-0464\(03\)00032-7](https://doi.org/10.1016/S1532-0464(03)00032-7).
- Gleeson, T., Befus, K.M., Jasechko, S., Lujendijk, E., Cardenas, M.B., 2016. The global volume and distribution of modern groundwater. *Nat. Geosci.* 9, 161–164. <https://doi.org/10.1038/ngeo2590>.
- Jasechko, S., Perrone, D., Befus, K.M., Bayani Cardenas, M., Ferguson, G., Gleeson, T., Lujendijk, E., McDonnell, J.J., Taylor, R.G., Wada, Y., Kirchner, J.W., 2017. Global aquifers dominated by fossil groundwaters but wells vulnerable to modern contamination. *Nat. Geosci.* 10, 425–429. <https://doi.org/10.1038/ngeo2943>.
- MacMahon, D., 2006. Half-life evaluations for 3H, 90Sr, and 90Y. *Appl. Radiat. Isot.* 64, 1417–1419. <https://doi.org/10.1016/j.apradiso.2006.02.072>.

CHAPTER 3 MODERN AND FOSSIL GROUNDWATER

PAPER PUBLICATION HISTORY	
Title	Using tritium and radiocarbon activities to constrain modern and fossil groundwater mixing in southern Africa
Journal	Journal of Hydrology, IF =4.500 (2019)
Status	Submitted – under review
Authors and roles	J.D van Rooyen – PhD Candidate J.A. Miller – Primary Supervisor
Applicant Contribution	Collated data, constructed the models, interpreted results and wrote the manuscript.

Using Tritium and Radiocarbon Activities to Constrain Modern and Fossil Groundwater Mixing in Southern Africa

J.D. van Rooyen^a, J.A. Miller^a

a. Department of Earth Sciences, Faculty of Sciences, University of Stellenbosch, Private Bag X1, Matieland, 7601, South Africa. jvanrooyen21@gmail.com, jmiller@sun.ac.za

Correspondence: J.D. van Rooyen, jvanrooyen21@gmail.com, Department of Earth Sciences, Faculty of Sciences, University of Stellenbosch, Private Bag X1, Matieland, 7601, South Africa.

ARTICLE INFO

Keywords:

radiocarbon,
tritium, residence
time, SADC

ABSTRACT

Constraining the residence time of groundwater is an important step in numerous hydrogeological studies and development strategies. The use of radiocarbon (^{14}C – half-life = 5730 years) and tritium (^3H – half-life = 12.312 years) as residence time indicators has been extensively explored in the literature. The attenuation of the bomb pulse has returned the atmospheric abundance of ^{14}C and ^3H to background/naturals levels, particularly in groundwater within the southern hemisphere, allowing for new methods of interpretation to be explored. This study combines historical records of ^{14}C and ^3H in the atmosphere and soil with renewal rate and groundwater lumped parameter models to predict the abundance of ^{14}C and ^3H in groundwater over time. 624 groundwater samples from numerous studies, over four decades (1978-2019), in South Africa, Namibia, Botswana and Mozambique are collated to compare with predicted groundwater activities of ^{14}C and ^3H within the South African Development Community (SADC) region. Spatial datasets of carbonate bearing lithology, C_3/C_4 vegetation, summer/winter rainfall and coastal proximity are used to apply corrections to ^{14}C and ^3H data. Corrected values of ^{14}C and ^3H are compared with the theoretical abundance of these tracers, derived from lumped parameters models, to estimate the general mean residence times and extent of groundwater mixing between modern recharge and older groundwaters. This study found that corrected values produced varying mean residence times derived ^{14}C ages (500 - 28500 years) and a wide range of potentially mixed waters within each aquifer system (0 - 100% of tested wells) across the study area. The largest proportions of mixed groundwater, as well as the youngest mean residence times, are found in alluvial and primary fractured rock aquifers (e.g. western coast of South Africa and southern Mozambique). The smallest proportions of mixed groundwater were found in deep confined clay-rich aquifers as well as layered coal bearing carbonate sequences (e.g. Orapa, Malweve and Serowe, Botswana). Insights into the proportions of mixed groundwater and mean residence times can help assess hydrological resilience on a regional scale. As ^{14}C and ^3H activities decrease to background levels around the globe, similar studies will be more applicable in research and the development of groundwater strategies.

1. Introduction

An important component of understanding groundwater systems and their sustainability is constraining groundwater residence time (Gleeson et al., 2012; Turnadge and Smerdon, 2014). Radioactive tracer methods for determining residence times use a wide array of isotopes with varying half-lives e.g. ^{222}Rn with a half-life of 3.8 days to ^{36}Cl with a half-life of 301 000 years (Barbieri, 2019; Cartwright et al., 2017; Le Gal La Salle et al., 2001; Mook and Rozanski, 2000). Based on the

radioactive isotopes present in groundwater and their concentrations, the terms modern, young and fossil have been introduced into the literature as arbitrary groundwater age delineations. Modern represents groundwater with a residence time of <100 years, young represents residence time within the Holocene (100-12000 years) and fossil represents groundwater residence times in excess of ~12000 years or before the Holocene epoch (Jasechko et al., 2017). The temporal range of groundwater residence times, particularly in mixed systems, suggests that no single

Chapter 3 – Modern and Fossil Groundwater

radioactive isotope can be used to date all groundwaters or all components of a single system. As mixed groundwaters obtain isotopic abundances that are distinct from recharge waters as well as fossil groundwater. This concept was used to effectively delineate modern, Holocene and fossil groundwaters through known atmospheric abundances and measured groundwater abundances groundwater tracers by Jasechko, (2016). However, isotopically derived residence time estimates are affected by more than just decay constants, with local recharge, rock-water interaction and deep groundwater mixing mechanisms affecting the interpretation of calculated ages (Bethke and Johnson, 2008). Using multi-isotope methods, it is possible to make deductions about regional recharge/mixing mechanisms and the proportion of modern and fossil groundwater for any given region (Klump et al., 2008). This is particularly useful in regions where the hydrological system is poorly constrained and the impact of climate change and anthropogenic activities, such as agriculture, is not yet known.

Southern Africa relies heavily on groundwater for sustaining water supply, food security and supporting ecosystem function, particularly in the more arid regions of Southern African Development Community (SADC) (van Rooyen et al., 2020b; Villholth et al., 2013). Detailed open access isotope databases are still limited for major and minor aquifers within SADC and the regional prediction of modern groundwater proportion using isotopes would support groundwater management strategies. A better understanding of the accuracy of sustainable yield estimates for SADC groundwater is important in the effort to provide clean drinking water to the populace and in turn, limiting challenges associated with social inequality (Matchaya et al., 2018). Although this study was performed in southern Africa, the applicability of the model approach will grow as more areas of the world attenuate the 'bomb peak', allowing for the comparison of groundwater tracer activities with natural atmospheric abundances.

The most commonly used isotopes in residence time studies, which are produced by the interaction of cosmic radiation with atmospheric gases, are radiocarbon (^{14}C) and tritium (^3H) (A P Atkinson et al., 2014; Clark and Fritz, 2013). ^{14}C has a half-life of 5730 years and is well suited for identifying fossil groundwater components through recharge of precipitation over time spans as far back as 30 000 - 50 000 years (Bhandary et al., 2015), with the upper limit being somewhat optimistic in most natural systems (Cartwright et

al., 2017). However, recharge is not the only source of carbon in groundwater. The dissolution of limestone/calcite or carbonate rich-rocks, as well as other geogenic processes (e.g. methanogenesis), can release inorganic carbon that is absent of ^{14}C otherwise known as 'dead carbon' (Cartwright, 2010). Numerous studies have endeavoured to develop methods for calculation of accurate ^{14}C corrections in groundwater using $\delta^{13}\text{C}$ values (Clark and Fritz, 1997; Fontes and Garnier, 1979; Ingerson and Pearson, 1964), groundwater geochemistry (Coetsiers and Walraevens, 2009; Tamers, 1975) and/or mass transport models (El-Kadi et al., 2011). It is still not conclusive which method is the most appropriate and instead, methods cater to site specific environmental constraints and assumptions (Cartwright et al., 2013). Consequently, the calculation of ^{14}C ages of groundwater is complicated due to the fluctuation of atmospheric ^{14}C abundance, the nature of non-linear groundwater mixing and the dissolution of carbonate bearing material. Without correcting for these processes, it is difficult to constrain actual groundwater residence time using ^{14}C . Additionally, ^{14}C dating methods are less effective at predicting the residence time of younger waters (<200 years) and in turn cannot evaluate the modern groundwater component of any aquifer system (Cartwright, 2010).

Constraining modern recharge with ^3H , the radioactive isotope of hydrogen, is possible as ^3H is predominantly produced in the upper atmosphere and only produced in the subsurface in isolated areas (usually landfills and radioactive waste storage sites) or at negligible levels by geogenic processes (Andrews and Kay, 1982; Hughes et al., 2011; Robinson and Gronow, 1996). However, the calculation of residence time is possible when combining ^3H with its daughter isotope using the $^3\text{H}/\text{He}$ method, as the initial activity of ^3H in recharge is difficult to predict (Ekwurzel et al., 1994; Schlosser et al., 1989; Solomon and Sudicky, 1991). As noble gas (e.g. He) collection is difficult and laboratory access limited, many studies rather use ^3H as an indicator of modern recharge without calculating residence time. Yet, where the input activity of ^3H is well constrained, the residence time of modern groundwaters can be effectively constrained (Cartwright and Morgenstern, 2012; Le Gal La Salle et al., 2001). Although ^3H has, in previous studies, been used to identify water recharged in the last 50 years (largely due to the bomb pulse in the 1960s), recent studies that utilize background (natural) radioisotope levels have suggested that ^3H can still indicate modern recharge components even in older hydrologic systems (~100 years) (Cartwright and

Chapter 3 – Modern and Fossil Groundwater

Morgenstern, 2015; Morgenstern et al., 2010; Stewart, 2012). This is especially effective in the southern hemisphere, where the activity of ^3H has not only returned to background levels, but in the groundwater system as well (Cartwright et al., 2017; Morgenstern et al., 2010). Using mass balance, peak and storage methods, modern recharge (<100 years) can be effectively constrained using ^3H (Harvey et al., 2006; Li et al., 2019). Older groundwater bodies that have low levels of ^{14}C , still commonly contain detectable ^3H levels through modern recharge and hence calculated mean residence time of mixed groundwaters are often not representative of the entire groundwater system (A P Atkinson et al., 2014; Jasechko et al., 2017). Hence, while the predicted abundance of ^{14}C and ^3H rarely explains the measured abundance in a groundwater sample, the relative concentration of ^{14}C and ^3H in groundwater can still be used to assess groundwater mixing relationships.

Under simple groundwater flow conditions, ^3H decays out completely before any significant change in ^{14}C (~98 pmc if initial ^{14}C is 100 pmc). The deviation from the expected decay curve relationship between ^{14}C and ^3H in groundwater allows for the assessment of (1) mixing relationships albeit on qualitatively as ^3H and ^{14}C from two waters do not mix in a linear fashion, and/or (2) a significant change in recharge rate. In order to assess any deviation from the decay curve, a series of corrections would need to be considered for both ^{14}C

and ^3H initial activities in recharge. Correction methods typically need measured local input parameters, yet it is possible to predict plausible correction ranges for larger regions and aquifers by the regionalization of remote sensed and/or interpolated datasets (Still and Powell, 2010). While the correction of ^{14}C using $\delta^{13}\text{C}$ has been extensively investigated in the literature on a local scale, our understanding of the variability of ^3H in precipitation is poorly constrained. More recently, understanding the systems that control the abundance of ^3H in precipitation has been improved through atmospheric modelling techniques (e.g. HYSPLIT, Stein et al., 2015). This has facilitated the development of models that can effectively predict the relative abundance of ^3H in groundwater, in regions where the bomb peak has been sufficiently attenuated (van Rooyen et al., 2020a; Visser et al., 2018).

This study uses ^{14}C , $\delta^{13}\text{C}$ and ^3H to interpret the presence of groundwater mixing and the potential range of mean residence times of groundwater collected over four decades from four countries across the SADC region, namely Namibia, South Africa, Botswana and Mozambique (Fig.1). A large database (624 samples) of ^{14}C and ^3H activities in precipitation and groundwater from southern Africa was compiled and analysed to better understand: (1) the degree of natural attenuation of bomb pulse ^{14}C and ^3H in the southern hemisphere; (2) the applicability of ^{14}C and ^3H residence time

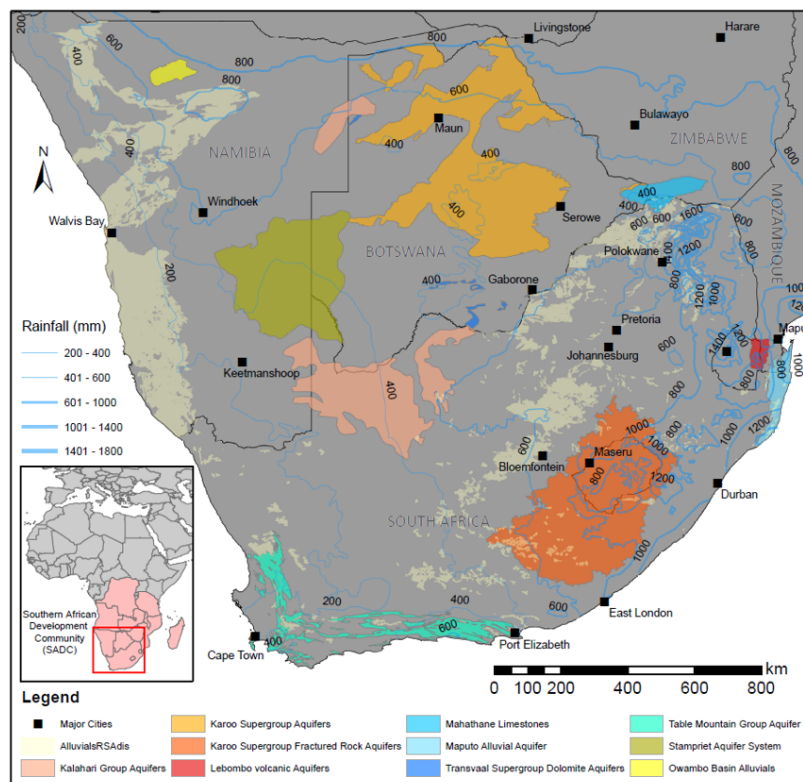


Figure 1 - The spatial distribution of alluvial and major rock aquifers that contain ^3H and ^{14}C reference data in relation to the SADC. Mean annual rainfall isohyets are included to give context to the large variability in regional recharge potential.

correction methods over a large spatial extent; and (3) the mixing proportions of modern recharge with fossil groundwaters of varying ages. Correction methods include: (1) the correction of initial ^{14}C for dissolved inorganic carbon (DIC) from carbonate dissolution, in open and closed systems, for spatial extents with diverse lithology (Cartwright, 2010) and (2) regions that receive variable ^3H activities in modern rainfall through seasonality and proximity to the ocean (van Rooyen et al., 2020a). To apply regional corrections, spatial data are grouped according to the abundance of carbonate bearing lithologies, the distribution of C₃/C₄ vegetation, sample proximity to the ocean and precipitation seasonality in each location and reported according to regional aquifers that samples were collected from (Fig.1) (Cobbing et al., 2008; Maria et al., 2012). Subsequently, the theoretical abundance of ^{14}C and ^3H in groundwater is predicted using renewal rate and groundwater flow models to better simulate attenuation, decay and mixing in the natural environment.

2. Methodology

The model approach used in this study predicts the presence of groundwater mixing and the potential range of mean residence times of regional groundwater by (Fig.2): (1) compiling groundwater reference data from previous studies in the SADC region, (2) constructing theoretical abundance curves of ^{14}C and ^3H in groundwater using atmospheric and soil records for determining the initial starting abundance in precipitation, (3) correcting the compiled groundwater ^{14}C data for open and closed system carbonate dissolution and the compiled groundwater ^3H data for variations in ^3H activity in precipitation and (4) using the predicted abundance curves to compare the corrected groundwater data, for each decadal time step from 1980-2020, to determine the presence and degree of groundwater mixing associated with the calculated groundwater mean residence times.

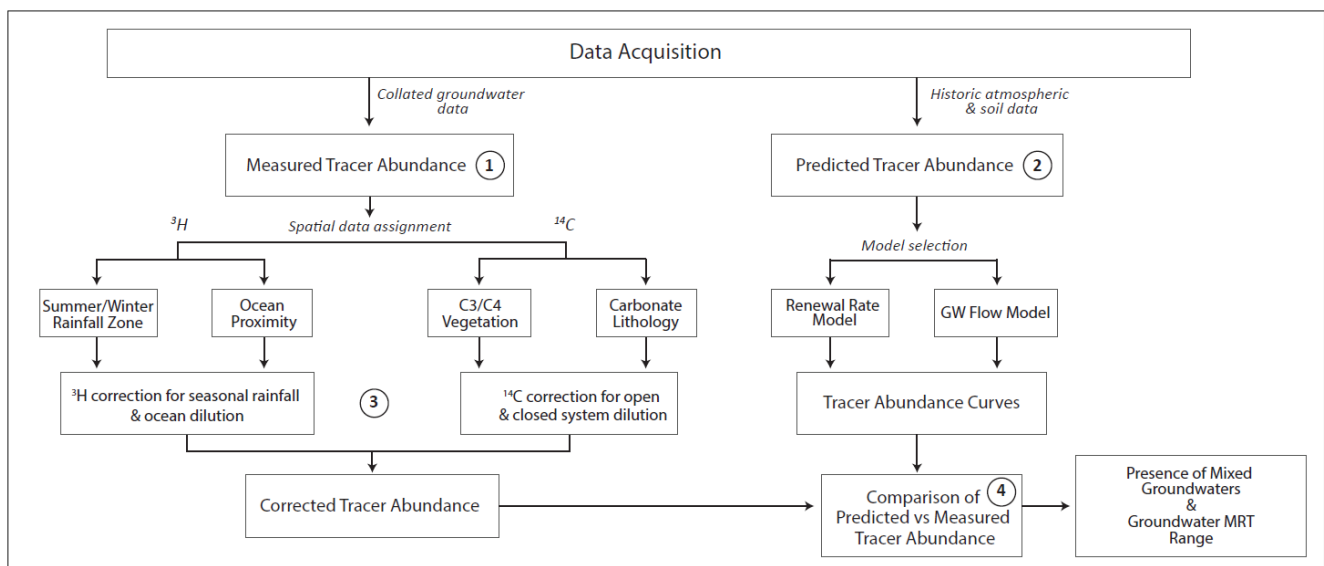


Figure 2 - Simplified model framework depicting the steps followed to predict the presence of mixed groundwater and the range of mean residence times (MRT) from historical atmospheric and soil data records and measured tracer abundances of ^{14}C and ^3H in groundwater.

2.1. Compilation of groundwater reference data

^{14}C and ^3H data, from across Namibia, Botswana, Mozambique and South Africa, were collated from published and unpublished literature (Appendix Table A1), producing 624 data points (Appendix Table A2). The collated database includes 540 samples with $\delta^{13}\text{C}$ values for correction of ^{14}C data. Although sample dates are spread across several decades, the data is not continuous and samples from each

individual borehole are, in every case, only sampled once. However, the measured ^{14}C and ^3H concentrations were analysed from the same sample. The data was separated into four decadal groups (1980-1989; 1990-1999; 2000-2009; and 2010-2019) to account for the natural attenuation of the bomb pulse experienced in the southern hemisphere. The data used in this study was compiled from data analysed at several different laboratories over the last few decades. As a result, the precision, accuracy and detection limits of the analysis are variable. The average standard deviation of

measurement uncertainty for ^{14}C and ^3H data are 0.90 and 0.22 respectively from 624 data points. Samples collected between 2000 and 2010 were analysed at a facility that had lower precision and accuracy for ^3H data (~ 0.1 TU).

The compiled groundwater data varies significantly between countries and decades. ^{14}C and ^3H measurements mostly fall within the predicted ranges for each decadal time step. Collated data sampled in: (1) South Africa ranged from 8.6 to 118.5 pmc (mean = 69.10, $n = 304$) for ^{14}C and ranged from 0 to 9.5 TU (mean = 1.07, $n = 304$) for ^3H ; (2) Namibia ranged from 0.0 to 106.1 pmc (mean = 42.57, $n = 150$) for ^{14}C and ranged from 0 to 5.3 TU (mean = 0.42, $n = 150$) for ^3H ; (3) Botswana ranged from 6.44 to 106.8 pmc (mean = 75.10, $n = 125$) for ^{14}C and ranged from 0.04 to 2.04 TU (mean = 0.38, $n = 125$) for ^3H and (4) Mozambique ranged from 0 to 109.10 pmc (mean = 69.10, $n = 45$) for ^{14}C and ranged from 0 to 7.00 TU (mean = 0.3, $n = 45$) for ^3H . Sample dates are not distributed equally between the four SADC countries and some studies only collected samples in one or two of the sampled decades. Samples from Mozambique were all collected in the late 2010s and the majority of samples in Botswana were collected in the 1990s. Namibian samples were mainly collected from 1990-2010 and only South African samples are well distributed across all four decades. Samples collected in the: (1) 1980s ranged from 2.59 to 118.50 pmc (mean = 64.20 pmc) for ^{14}C and ranged from 0 to 9.50 TU (mean = 1.15 TU) for ^3H ; (2) the 1990s data ranged from 0 to 110.30 pmc (mean = 47.08 pmc) for ^{14}C and ranged from 0 to 7 TU (mean = 0.57 TU) for ^3H ; (3) the 2000s data ranged from 0 to 109.49 pmc (mean = 47.57 pmc) for ^{14}C and ranged from 0 to 5.30 TU (mean = 0.46 TU) for ^3H and (4) the 2010s data ranged from 6.44 to 106.08 pmc (mean = 73.60 pmc) for ^{14}C and ranged from 0 to 3.22 TU (mean = 0.48 TU) for ^3H .

The spatial distribution of groundwater samples is clustered in the areas of interest of previous studies, largely correlated to major rock and alluvial aquifers across the region (Fig.1). Groundwater samples ($n = 47$) located in the Western Cape province of South Africa are mainly hosted in the Table Mountain Group, a fractured rock aquifer dominated by silicate host rocks. This aquifer system is also associated with the less productive, and lower quality, Malmesbury Group shale aquifer. Further north, on the west coast of the Northern Cape Province, groundwater samples ($n = 25$) are typically hosted in shallower alluvial systems underlain by a granitic aquifer system and the recharge mechanics of the region are still poorly constrained. Samples

collected in the northern reaches of the Northern Cape Province ($n = 183$), are typically hosted in perched interspersed paleo-river alluvial systems and deeper fractured rock aquifer systems underlain by basement granitoids. Groundwater samples collected from major inland rock aquifers in South Africa and Lesotho ($n = 41$), are hosted in fractured systems of sandstones and shales of the Karoo Supergroup, confined by volcanic sequences of the Drakensberg Group with interspersed perched alluvial systems. Groundwater samples collected from the southernmost region of Mozambique ($n = 45$), are hosted in two major hydrogeological regimes: (1) Low productivity basaltic and rhyolitic localized intergranular aquifers on the Lebombo Monocline and (2) large intergranular alluvial aquifers in valleys and floodplains. Sample locations in Namibia are distributed into three major systems: (1) the transboundary Stampriet Aquifer which extends across South Africa and Botswana ($n = 67$); (2) north-eastern low potential Kalahari Group aquifers, comprised of interspersed calcareous rocks and perched alluvial systems ($n = 47$) and; (3) northern limestone and dolomitic systems overlain by desert alluvials and salt pans ($n = 43$). Specific sample locations in Botswana are not disclosed in the original sources, only local areas/farms/mines, so samples are therefore grouped into the regions from where the studies were undertaken, of which there are five: (1) The Kalahari region in the south-west, comprised of low productivity calcareous rocks and interspersed alluvial systems ($n = 18$); (2) the Malweve and Tsokwane areas in the south where localized alluvial and low productivity clay-rich aquifers are dominant ($n = 21$); (3) the Meratswe Valley region that has deeper ($>200\text{m}$) fractured rock systems overlain by valley alluvial aquifers ($n = 44$); (4) the Orapa region dominated by deep confined clay-rich sequences and interspersed fissured systems ($n = 23$); and (5) the Mahathane/Serowe region that is a complex system of limestones and dolomites, coal beds and fractured rock aquifers ($n = 15$).

2.2. Construction of ^{14}C and ^3H abundance curves for southern Africa

Continuous temporal records of atmospheric and soil data associated with radionuclides, especially in southern Africa, are scarce. It was thus necessary to find a way to predict initial recharge activities of ^{14}C and ^3H across southern Africa. To do this, historical atmospheric and soil data for ^3H and ^{14}C compiled from multiple sources, were merged using a weighted moving average method to not bias individual databases. This method calculates the weighted

moving average from the previous temporal dates to estimate the likely average activity over the study area as well as extrapolate for missing data in the temporal record. Subsequently, theoretical groundwater flow is modelled either from established renewal rate methodologies (Le Gal La Salle et al., 2001) for shallow systems and recharge areas or with the use of the USGS developed TracerLPM software (Jurgens et al., 2012) to ensure consistency with comparable groundwater flow investigations worldwide (Cartwright et al., 2013; McGuire and McDonnell, 2006; Nimmo et al., 2005; Suckow et al., 2018; Turnadge and Smerdon, 2014).

2.2.1. Atmospheric and soil record

Atmospheric ^3H data was collected from six Global Network of Isotopes in Precipitation (GNIP) stations and ^{14}C data was compiled from established ^{14}C records from Wellington, New Zealand (Manning and Melhuish, 1994) and Heidelberg, Germany (Levin et al., 2013, 1995). Atmospheric records of ^{14}C and ^3H were extrapolated over years with no data, to better constrain the likely ‘bomb pulse’ signal in the southern African atmosphere over time. (Fig.3). Data prior to the bomb peak is assumed to be similar to current ambient levels, predicted by the above ^{14}C and ^3H atmospheric records

where the starting activities are modelled to be ~ 110 pmc and ~ 2 TU. Although this data is used to create curves intended to interpret samples over a large spatial and temporal extent, the resolution of available data at this time is not high enough to isolate specific recharge regions before correction. While atmospheric variation in ^{14}C is well documented, soil zone variations remain convoluted. The concentration of ^{14}C in the soil zone is derived from root respiration and a function of the oxidation of organic matter in the soils that are typically older (Cartwright et al., 2013). In order to successfully estimate soil zone ^{14}C , global records collected from Jenkinson et al., (1992); Kuc et al., (2004); Tipping et al., (2010) were used and extrapolated to the modern day for the purposes of this study. On this basis, ^{14}C in the soil zone ranged from ~ 95 pmc before the bomb pulse to around 115-130 pmc in the early 1990’s and decreased to ~ 110 pmc in the late 2000’s. It is also noted by the author that the interpretation of ^{14}C in soil, as well as the unsaturated zone, is likely more complicated than presented in this study (Meredith et al., 2016; Wood et al., 2015). Yet, without higher resolution data and knowledge of specific environmental data, these uncertainties can only be mitigated in future research.

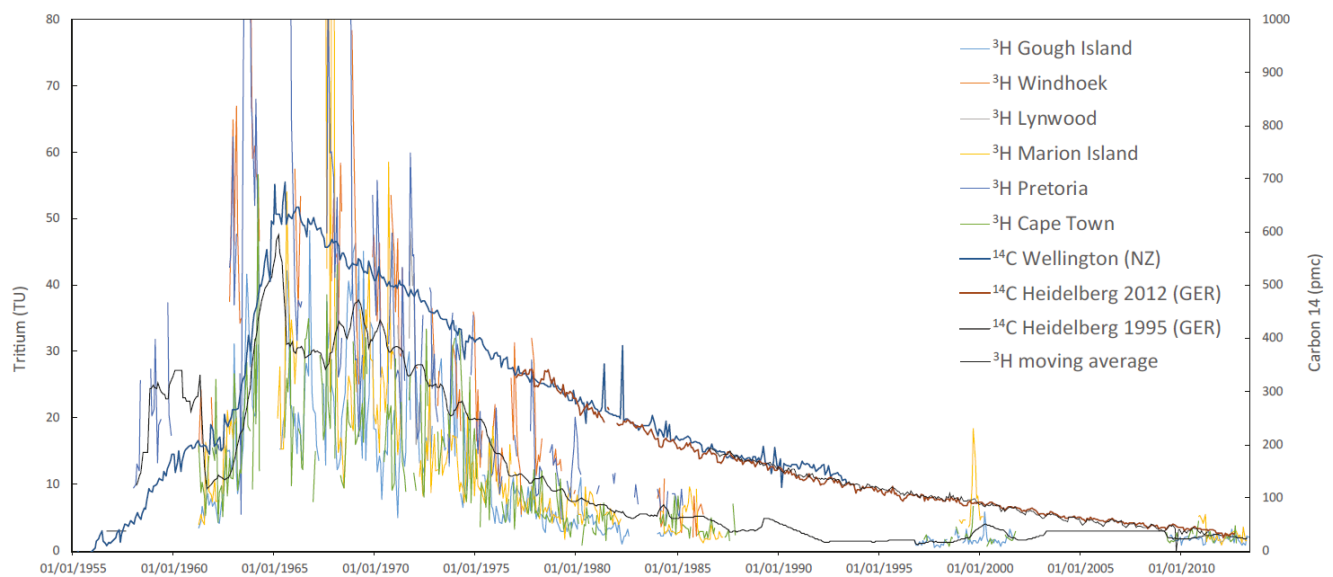


Figure 3 - The atmospheric record of ^{14}C and ^3H in precipitations from six GNIP stations for ^3H and three published records for ^{14}C . The weight moving average is calculated for ^3H activity (stippled black line).

2.2.2. Modelled ^{14}C and ^3H concentrations in groundwater

The rate of incorporation of ^{14}C and ^3H in recharge is similar and their relationship can be predicted over time for various recharge rates (Suckow et al., 2018). The abundance of ^{14}C and ^3H in recharge is predominantly dependent on the

atmospheric activities of individual tracers at the time of recharge. In order to model this interaction, La Gal La Salle et al. (2001) developed a renewal rate model that treats the top few meters of an aquifer as a reservoir that feeds the aquifer below and is in turn renewed by recharge water. The ^{14}C or ^3H concentration at time t (C_t) can be predicted according to Eq. (1) by calculating the effect of new recharge

(C_i), that has distinct ^{14}C and ^3H , on the previous year's recharge (C_{t-1}) according to the proportion of water replaced (R_n) and how much decay has occurred from a known decay constant λ :

$$C_t = (1 - R_n)C_{t-1}e^{-\lambda} + R_nC_i \quad (1)$$

Assuming that aquifers have a range of potential annual recharge rates (variable R_n values), the theoretical abundance of ^{14}C and ^3H in a groundwater body, that has a constant R_n can be predicted over time. This renewal rate model is only applicable for a single well-mixed homogeneous zone and is likely only representative of the top few meters of an aquifer or near the recharge source. Although this method is applicable in simple shallow systems, it is not likely representative of regional groundwater conditions.

To model recharge and flow of groundwater in natural systems, an exponential piston flow model (EPM) is used to predict the evolution of tracer abundances in the groundwater system. This is done using a lumped parameter model (LPM), which are mathematical models that determine the concentration of a tracer over a simplified groundwater flow path. This is done by setting an aquifer geometry and flow configuration to account for hydrodynamic dispersion or mixing within an aquifer, well bore, or discharge area. LPMs are generally used for determining ages for groundwater by including one or more residence time tracers and predicting mixing relationships of younger and older aquifer components.

The model was computed using TracerLPM, a python/VBA coded package developed by the USGS (Jurgens et al., 2012), using an adapted model that assumes a water sample from a borehole or well is a mixture of water from different lengths of flow paths with a range of residence times (Cook and Böhlke, 2000; Maloszewski and Zuber, 1993; Maloszewski and Zuber, 1982). This EPM model can be described as:

$$C_t = \int_0^\infty C_i(t - \tau)g(\tau)e^{-\lambda\tau}d\tau \quad (2)$$

where t is the time of observation, τ is the transit time, and $e^{-\lambda\tau}$ is the decay term of the tracer if it is not stable. $g(\tau)$ is the system response function described in Cook and Böhlke, 2000 and Zuber et al., 2005 and is given by:

$$g(\tau) = 0 \text{ for } \tau < T(1 - f) \quad (2a)$$

$$g(\tau) = (fT)^{-1}e^{\left(-\frac{\tau}{fT} + \frac{1}{1-f}\right)} \text{ for } \tau > T(1 - f) \quad (2b)$$

where T is the mean residence time of the water and f is the ratio of exponential flow to piston flow in the total water

flow ($f=0$ represents piston flow and $f=1$ represents exponential flow). Exponential flow models that were calculated using TracerLPM, used three 'f' ratios; $f=0.6$, $f=0.8$ and $f=1$, that represent the typical range of exponential flow seen in unconfined and semiconfined aquifers (Morgenstern et al., 2010; Stewart, 2012; Zuber et al., 2005). This f ratio is converted to an EPM ratio in the software which controls the contribution of piston flow to exponential flow conditions as described in Jurgens et al., (2012). The program predicts the theoretical tracer-tracer concentration of ^3H and ^{14}C in groundwater as a function of input and time.

LPMs that predict tracer behaviour in groundwater are most accurate with long term data, largely missing from Southern Africa, and preferably some known physical constraints on diffusion potential (difficult to quantify simply over the area of this study) (Lamontagne et al., 2015; Suckow et al., 2018). For the purpose of this study, an exponential piston flow model was used for aquifers of different mean residence times. This approach makes several assumptions: (1) the same amount of recharge is received each year and in the same location, thus even though flow paths are variable and of different residence time, recharge rates are consistent; (2) the interaction between aquicludes/aquitards and aquifers is negligible and does not affect the isotopic signature derived from recharge in a single aquifer; (3) the aquifer behaves as one homogenous body, transferring water with a constant hydraulic conductivity; and (4) the proportion of mixing between young and old water is constant throughout the aquifer and does not change along the flow path.

Based on the above approach, the predicted values for ^{14}C and ^3H in groundwater are significantly different for different decadal periods as a result of the bomb pulse and subsequent attenuation. Additionally, curves predicted with atmospheric records differ from those predicted with soil records, when using the simple renewal rate model (Fig.4a). The exponential piston flow models have, in general, a lower increase in predicted ^3H activity as predicted ^{14}C increases and do not reach as high a maximum ^3H content due to decay in the unsaturated zone (Fig.4b). Samples collected ~1980 are predicted to have ^{14}C values of as high as 130 pmc and ^3H up to 8 TU if the sample is representative of recharge from that time (residence time = ~0 years). The equivalent predicted values for samples collected ~1990 are 118 pmc and 3.5 TU respectively, for samples collected ~2000 the predicted values are 108 pmc and 1.9 TU respectively and samples collected after 2012 are predicted to be 110 pmc and

2 TU respectively. For the purpose of this study, only the exponential piston flow models are used to late predict the occurrence of mixing.

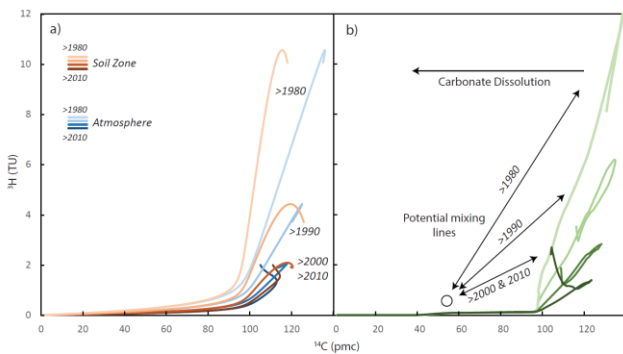


Figure 4 - Predicted activity of ^{14}C and ^3H from a renewal rate model (a) and exponential flow models (b). Atmospheric (blue) and Soil zone (brown) data was used for renewal rate models. Exponential flow models were calculated for $f=0.6$ (green), $f=0.8$ (blue) and $f=1$ (yellow). Lines for carbonate dissolution and decadal mixing of modern and fossil components are shown in panel b.

2.3. Correction of tracer activity in groundwater reference data

The abundance of ^{14}C and ^3H in groundwater is not only a function of the atmospheric abundance, recharge and subsequent decay but also other atmospheric, vadose zone and geogenic processes that contribute to, or dilute, the apparent tracer abundance. In order to interpret proportions of modern groundwater and fossil component ages that are more representative of the natural system, the compiled data was processed using several correction steps. This includes the correction of ^{14}C groundwater data for open and closed carbonate dissolution and ^3H groundwater data for the variation of ^3H activity in precipitation.

2.3.1. Open and closed system carbonate dissolution

There are several methods for the correction of the contribution of 'dead' carbon during recharge and subsurface flow currently in use in modern hydrology. Geochemical adjustment models attempt to correct the relative decrease of ^{14}C in DIC independently of the decay of ^{14}C and can only adjust for a younger ^{14}C residence time. Essentially, these models account for major carbonate reactions that occur in recharge and groundwater flow systems. The correction method employed here (Fontes and Garnier, 1979; Ingerson and Pearson, 1964) can be summarized by a 'q' value that represents the proportion of C derived by closed system dissolution of carbonate rock (dilution factor) described as:

$$q = \frac{\delta^{13}\text{C}_{\text{sample}} - \delta^{13}\text{C}_{\text{carbonate}}}{\delta^{13}\text{C}_{\text{recharge}} - \delta^{13}\text{C}_{\text{carbonate}}} \quad (3)$$

where 'sample' is the measured $\delta^{13}\text{C}$ value, 'carbonate' is the $\delta^{13}\text{C}$ value for the local carbonate lithology, 'recharge' is the initial $\delta^{13}\text{C}$ in the soil horizon and is largely controlled by root respiration processes and open system calcite dissolution. In this study, the potential dilution range of closed system dissolution was estimated by assigning $\delta^{13}\text{C}$ ranges for 'carbonate' and 'recharge' from the distribution of C4 dominant vegetation and carbonate bearing lithologies.

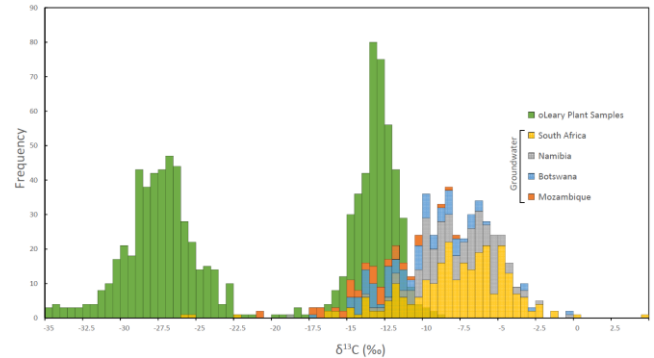


Figure 5 - The distribution of $\delta^{13}\text{C}$ in C₃ and C₄ plants (Green) (O'Leary, 1988) and in groundwater samples included in this study. Samples are stacked according to their country of origin.

The compiled groundwater $\delta^{13}\text{C}$ values in the dataset span the range of known values for C₃, CAM and C₄ photosynthetic pathways in plants (means of -25 ‰, -17 ‰ and -14 ‰ respectively) and typical marine derived carbonate rock (between -2 ‰ and +2 ‰). However, the mean value of -8.75 ‰ (median = -8.40 ‰ with a standard deviation of 3.61) is skewed to more positive values than values produced through C₄ photosynthesis, suggesting that carbonate dissolution plays a significant role in diluting initial $\delta^{13}\text{C}$ values and hence ^{14}C activities across the sample locations (Fig.5). In order to constrain the degree of closed system carbonate dissolution the distribution of carbonate bearing lithology and initial $\delta^{13}\text{C}$ values from vegetation type were assigned to each sample location. The spatial distribution of carbonate-dominated lithologies was compiled from regional geology maps by merging local carbonate-bearing formations into: (1) primary limestones and dolomites, (2) secondary calcareous sedimentary rocks and (3) coal-bearing lithologies for South Africa (Johnson et al., 2006), Namibia (Mendelsohn, 2002), Botswana (Key and Ayres, 2000) and Mozambique (Ruotoistenmäki, 2008) (Fig.6a). The variability of photosynthetic pathways is variable across southern Africa from C₃/CAM dominated regions in the west to C₄ dominated grasslands in the east. The relative proportion of C₄/CAM/C₃ type vegetation in

Chapter 3 – Modern and Fossil Groundwater

South Africa, which has recent published data, varies significantly across the country, particularly across winter and summer rainfall regions (from 14% C₄ in the south west to 67% C₄ in the north east)(Stock et al., 2004). Regional vegetation maps were used to estimate the likely dominance of C₃/CAM/C₄ plants at sample locations in South Africa (Rutherford and Mucina, 2006), Namibia (Mendelsohn, 2002), Botswana and Mozambique (Rutherford et al., 2005) (Fig6b). Although vegetation maps are not at a uniform resolution between countries in this study, the C₄ proportion distribution showed close correlation to both regional and larger scale assessments (Still and Powell, 2010; Stock et al., 2004).

Initial δ¹³C was predicted by assigning C₄ proportions from the spatial distribution of C₄ vegetation proportions. The likelihood of δ¹³C dilution was predicted through the presence of primary, secondary and coal-rich lithologies

assigned to the spatial locations of samples. Subsequently, a dilution line was drawn from the predicted initial δ¹³C soil value to the expected rock δ¹³C value range to assess the degree of open/closed system dissolution that has occurred (Fig.7). If the measured value fell to the left of the dilution line, where decay is predominant, the sample was corrected normally using the ‘q value’ and the predicted ¹⁴C-corrected residence time was used in the modern groundwater proportion prediction (Fig.7a). If the measured value fell to the right of the dilution line, then the ‘q value’ correction was adjusted by the degree of open/closed system dissolution based on the prevalence of local carbonate lithologies (Fig.7b). The distribution and potential contribution of natural gas exploration, methanogenesis and mantle derived CO₂ was not considered in this study. This approach was only adopted due to a lack of regional soil, carbonate rock and shallow groundwater δ¹³C data and is likely an over-simplification of the regional system.

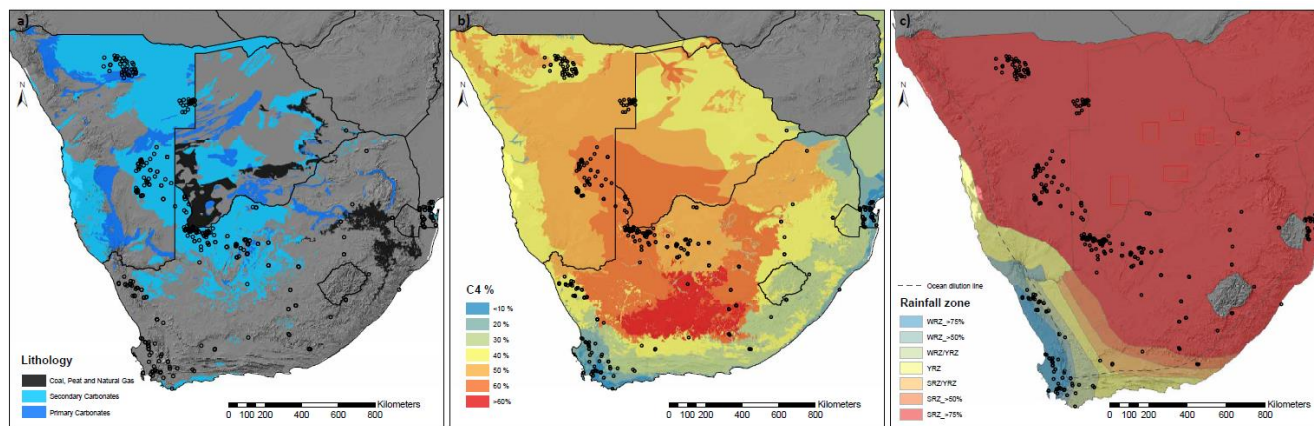


Figure 6 - The distribution of carbonate bearing lithologies: according to lithologies that contain significant coal deposits (black), secondary carbonate bearing rocks that contains calcareous rich sands and or clays (light blue) and primary carbonate rocks such as limestones, chert beds, marls and karstic aquifers (panel a), C₄ proportion of vegetation derived from satellite data, field observations and known plant distributions (panel b) and winter (WRZ) vs all year (YRZ) vs summer (SRZ) rainfall zones, represented as a percentages of consensus of previous literature that delineated rainfall zones in southern Africa (c), with reference to spatial groundwater data.

Namibia and Botswana had the highest proportion of samples taken in primary carbonate bearing regions (13 out of 150 samples and 11 out of 125 samples, respectively), followed by South African samples (18 out of 303 samples). Mozambique had no samples taken in carbonate-bearing regions and this is likely a function of the narrow geographic range over which these samples were collected (Fig.6a). A large number of South African and Namibian samples are located in secondary carbonate-bearing regions (167 out of 303 samples and 111 out of 150 samples, respectively). Conversely a lower number of samples in Botswana occur in secondary carbonate-bearing regions (36 out of 125 samples) and only 1 sample in Mozambique. 118 samples in South

Africa, 44 in Mozambique, 26 samples in Namibia and only 5 samples in Botswana occur in areas where there are no carbonate lithologies present.

Name	Number of wells	Mean 'q' values	Minimum 'q' value	Maximum 'q' value	Standard deviation of 'q' values
Western Cape TMG	20	0.60	0.24	1.17	0.23
West Coast South Africa	19	0.52	0.22	0.76	0.13
Southern Mozambique	44	0.58	0.33	0.88	0.12
Northern Cape	182	0.38	0.06	1.33	0.15
Stampriet	63	0.39	0.03	0.98	0.17
North east Namibia	44	0.42	0.22	0.53	0.09
Etoshia	42	0.38	0.22	0.55	0.08
Central South Africa	27	0.50	0.07	1.43	0.31
Malweve	15	0.49	0.01	0.81	0.25
Kalahari	11	0.47	0.18	0.74	0.16
Orapa	16	0.47	0.39	0.63	0.07
Kohlye Valley	15	0.67	0.34	0.93	0.15
Meratswe Valley	21	0.63	0.37	0.78	0.11
Serowe	15	0.56	0.41	0.66	0.08
Northern South Africa	11	0.39	0.18	0.73	0.18
Total/Average	545	0.50	0.22	0.86	0.15

Table 1 - Summary of 'q' values calculated per region with the number of well within each region.

The only samples that occur in coal-rich regions were found in Botswana (52 out of 125 samples). The distribution of $\delta^{13}\text{C}$ values is plotted against measured ^{14}C to show the potential dilution of initial ^{14}C by ‘dead’ carbon through open and closed carbonate dissolution, given that initial $\delta^{13}\text{C}$ is controlled by variable photosynthetic pathways (Fig.8). The degree of dilution is shown in the dilution lines between the known plant and rock contributions as q values calculated using Eq.3.

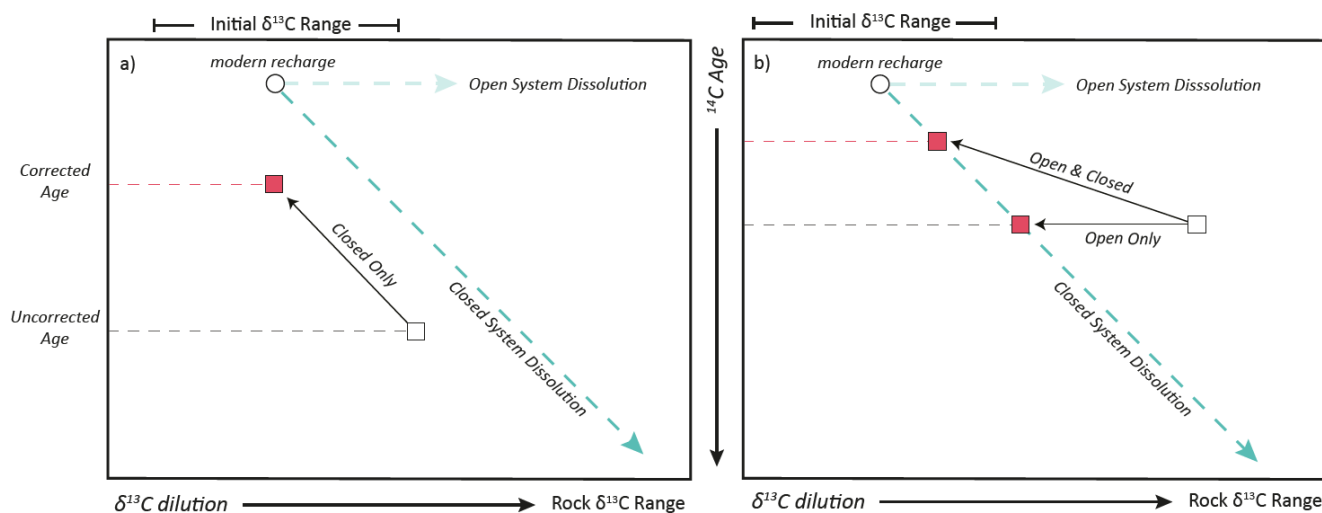


Figure 7 - Theoretical corrections scenarios for $\delta^{13}\text{C}/^{14}\text{C}$ that plot left (a) and right (b) of the closed system dissolution line. Uncorrected (white square) and corrected (red square) samples are connected by open, open & closed and closed system correction lines (black with arrow).

2.3.2. ^3H variability in recharge corrections

The variation of ^3H activity in rainfall is well documented in monthly GNIP and other global records (Cauquoin et al., 2015; Harms et al., 2016; Li and Si, 2018; C. V. Tadros et al., 2014; Zhai et al., 2013). Seasonality in ^3H activity usually results in lower activities in precipitation in the winter months and higher activities in precipitation during the summer months (Mair et al., 2013; van Rooyen et al., 2020a). This trend is evident in regions where summer and winter precipitation are, in general, generated by different processes, for example; a large frontal system developing from the coastal areas to orographic rainfall inland as a result of moisture recycling. Distinct rainfall origins in South Africa have been documented to show that the seasonal variation in ^3H activity between summer and winter rainfall can be as

The resultant data produced a large range of q values (0.01-0.98) with a mean q value of 0.44 ($n=545$). However, the variability of q values is substantially less when interpreted in the context of the spatial regions delineated in this study. The modal statistics of q values per region are summarised in table XX.

high as 1.3 TU, which has significant consequences for the long-term prediction of ^3H in groundwater (van Rooyen et al., 2020a). The data was categorized into predominantly summer, winter and all year rainfall regions depending on samples location, to account for seasonality of ^3H activity in precipitation (Fig.6c). Summer rainfall areas receive rainfall with elevated ^3H activities. Subsequently, the predicted initial/recharge activity was adjusted up to 1.3 TU, according to the rainfall region of the sample location. Another major contributing factor to the variability of ^3H in precipitation was the likelihood of ocean dilution and hence the proximity of the sample location to the ocean (Mair et al., 2013). For this reason, samples within 100km of the coastline, that experience the ocean dilution effect on initial ^3H activity, are corrected by increasing the initial ^3H activity by 1 TU (Fig.6c).

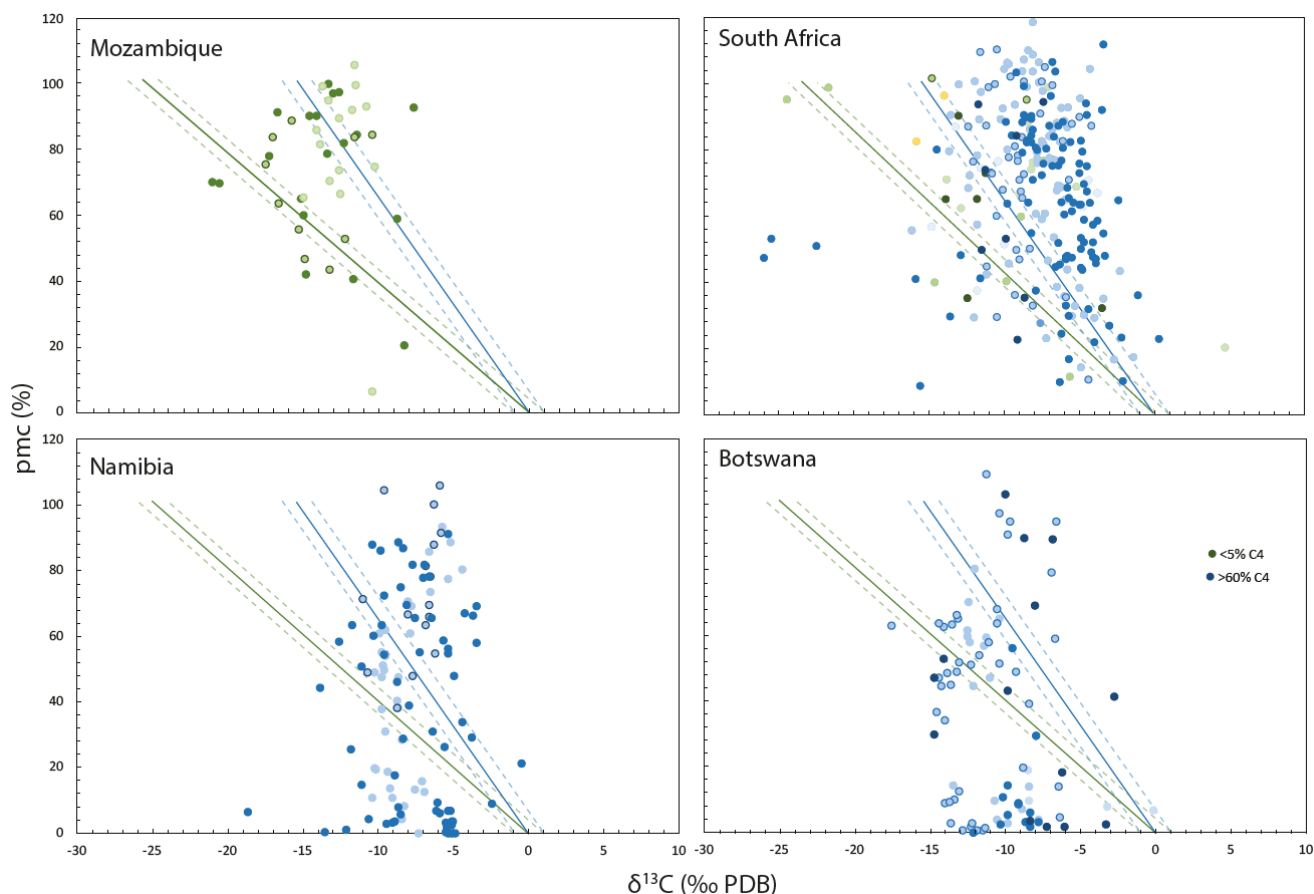


Figure 8 – $\delta^{13}\text{C}$ and ^{14}C of samples separate by country, dot colours are according to the proportion of C_4 in surface vegetation from <5% (Green) to 30% (yellow) >60% (blue). Dilution lines calculated using eq. 3 are shown for <5% C_4 (Green line) and >60% C_4 (blue line) with 5% range lines (stippled lines).

2.4. Predicting the occurrence of mixing between modern and fossil groundwater

The relationship between the mean residence time of groundwater and the activity of the chosen tracer, where tracer activity decreases with an increase in mean residence time, is non-linear. Each residence time tracer has different input functions and decay rates, resulting in different calculated mean residence times for the same sample depending on the chosen tracer (Cartwright et al., 2017). The resultant calculated mean residence time is less than the actual mean residence time. There are several possible explanations of different calculated mean residence times between tracers, including (1) the mixing of modern and fossil components, (2) heterogeneities in the aquifer that cause variable amounts of dispersion and (3) long borehole screens sampling multiple flow paths. Instead of attempting to calculate mean residence times of mixed waters, in a evidently complicated system, this approach compares measured tracer abundance to predicted tracer abundance in order to assess if groundwater is mixed between modern and fossil components or not. Furthermore, the calculated ^{14}C age

is reported as a potential range between corrected and uncorrected values as the regional context of this study cannot isolate the degree and extent of, if any, open/closed carbonate dissolution.

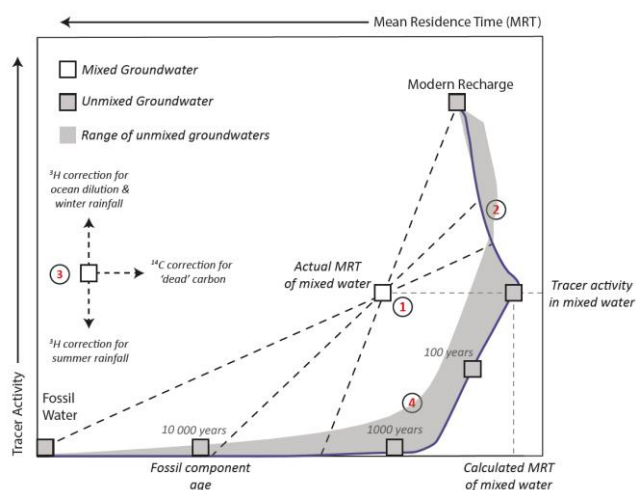


Figure 9 - Predicted mixed and unmixed groundwater (white and grey boxes) from actual mean residence time (MRT) in mixed water from corrected tracer input, using a tracer abundance curves. Dotted black lines represent the array of mixing scenarios, should the mixing be binary.

3. Results

Corrected values of ^{14}C and ^3H were assessed against theoretical abundances predicted by LPM techniques. The resultant comparisons suggest that almost half (49%) of the sampled boreholes showed significant mixing between modern and Holocene/fossil groundwaters. Uncorrected ^{14}C ages span a large range (modern to >50 000 years, mean = 7760 years), yet corrected ages, using calculated q values, predict ages from modern to >45 000 years (mean = 3340 years). Here, the calculated mean residence times and percentage of mixed wells were summarized in terms of regional zones associated with large rock and/or alluvial aquifer systems (Fig.11).

The highest percentage of mixed wells, as well as the youngest ranges of calculated (^{14}C) MRT's, were found in alluvial and primary fractured rock aquifers (e.g. western coast of South Africa and Mozambique). Samples in the Western Cape Province of South Africa indicated that 50.0% of wells showed significant mixing between modern and Holocene/fossil groundwaters and average MRTs range from 1420 (corrected) to 4550 (uncorrected) years old. Further north, on the west coast of the Northern Cape Province, groundwater samples indicated that all wells (100.0%) showed significant mixing and average MRTs range from 1170 (corrected) to 4120 (uncorrected) years. Groundwater samples collected in the southern-most region of Mozambique indicated that all wells (100.0%) showed significant mixing and average MRTs range from 1020 (corrected) to 3430 (uncorrected) years.

The lowest percentage of mixed wells/boreholes were found in deep confined clay-rich aquifers as well as layered

coal bearing carbonate sequences (e.g. Orapa, Malweve and Serowe, Botswana). Groundwater samples collected in the Orapa indicated that no wells (0.0%) showed significant mixing and average MRTs ranged from 22240 (corrected) to 28580 (uncorrected) years old. Groundwater samples collected in the Malweve and Tsokwane areas in southern Botswana indicated that 20.0% of wells/boreholes showed significant mixing and average MRTs ranged from 6570 (corrected) to 12270 (uncorrected) years old.. Groundwater samples collected in the Mahathane/Serowe regions on the eastern border with Zimbabwe indicated that only 6.7% of wells/boreholes showed significant signs of mixing and had an average MRT range of 6220 (corrected) to 10770 (uncorrected) years old.

The oldest average MRTs were found in regions with low productivity calcareous rock aquifers and interlayered confined systems (Stampriet, Kalahari and Meratswe Valley aquifer systems). Groundwater samples in the transboundary Stampriet aquifer, which extends from Namibia into South Africa and Botswana, which was estimated to have 34.9% of wells/boreholes that indicated significant mixing and average MRTs that ranged from 15704 (corrected) to 22090 (uncorrected) years old. Groundwater samples collected in the Kalahari region in the south-west of Botswana indicated that 46.2% of ewlls/boreholes showed significant mixing and average MRTs ranged from 12566 (corrected) to 18500 (uncorrected) years old. Groundwater samples collected in the Meratswe Valley region in central Botswana indicated that 19.0% of wells/boreholes showed significant mixing and average MRTs ranged from 9330 (corrected) to 12490 (uncorrected) years old.

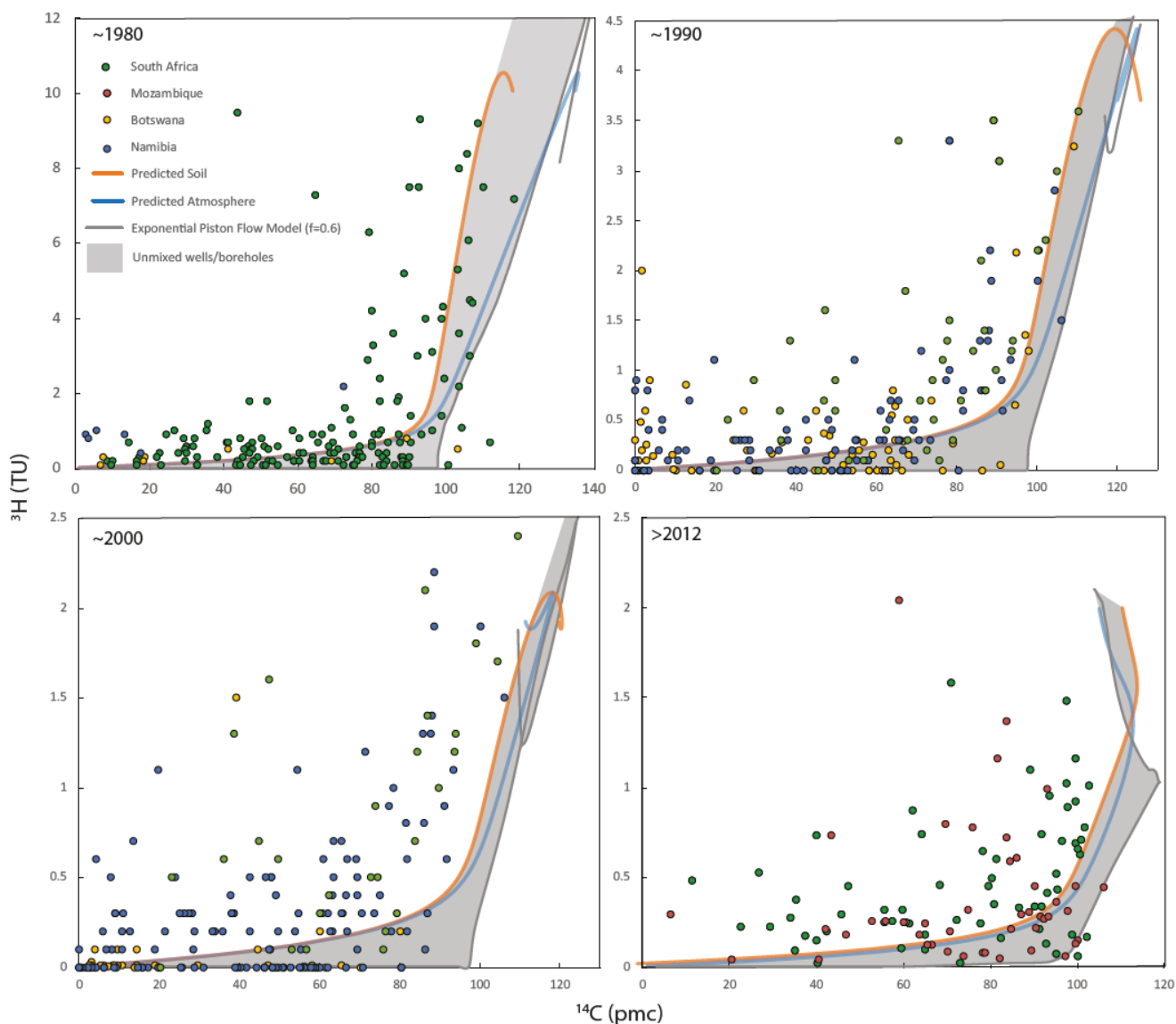


Figure 10 - Groundwater sample ^{14}C and ^3H separated into decadal groups with predicted atmospheric (blue line) and soil zone (orange line) renewal rate models and exponential flow model, $f=0.6$ (grey line). Ranges of unmixed groundwater are represented by transparent grey sections, delineated by the range of predicted abundance curves produced from renewal rate and groundwater flow models.

Intermediate proportions mixed wells and MRT ranges were found in the central regions of South Africa and the northern regions of Namibia. Samples collected in the northern reaches of the Northern Cape of South Africa indicated that 50.0% of wells/boreholes showed significant mixing and average MRTs ranged from 500 (corrected) to 4190 (uncorrected) years old.. Groundwater collected from major inland rock aquifers in South Africa and Lesotho indicated that 44.4% of wells/boreholes showed significant mixing and average MRTs ranged from 1030 (corrected) to

4870 (uncorrected) years old.. Groundwater samples collected from the northern most region of Namibia indicated that 78.6% of wells/boreholes showed significant mixing and average MRTs ranged from 1820 (corrected) to 5560 (uncorrected) years old.. Groundwater samples collected in the north-eastern low potential Kalahari Group aquifers of Namibia indicated that 29.5% of wells/boreholes showed significant mixing and average MRTs ranged from 1040 (corrected) to 17080 (uncorrected) years old..

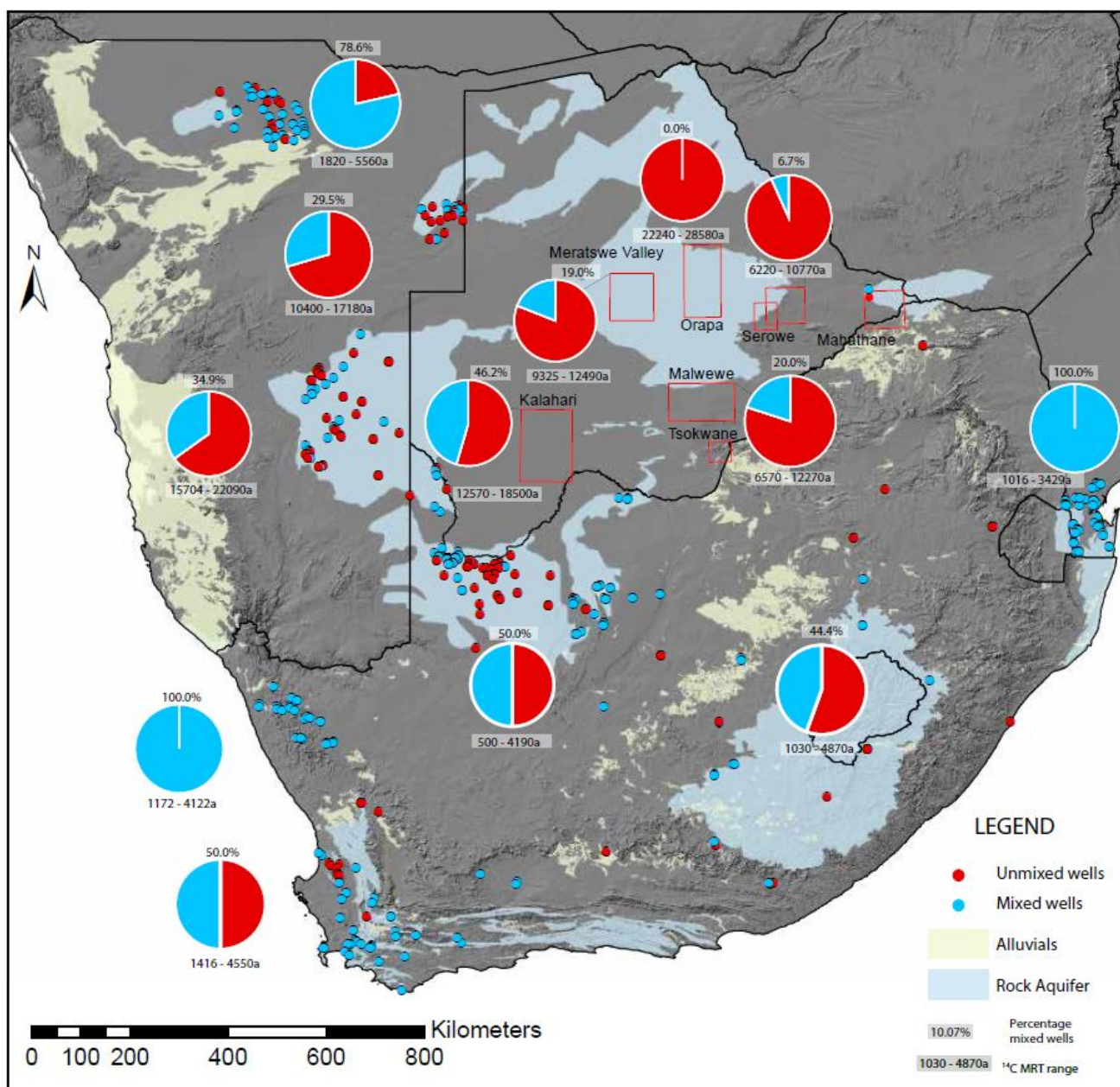


Figure 11 - The percentage of mixed wells (pie charts) with a range of MRTs for the given aquifer system. Samples with evidence of modern and Holocene/fossil groundwater mixing are coloured in blue whereas samples that indicated that no significant mixing are coloured in red.

4. Discussion

The use of isotopic tracers to predict the occurrence of groundwater mixing, between modern and Holocene/fossil groundwaters, is essential given the inherent difficulties associated with large-scale numerical modelling of recharge, base flow and discharge. The occurrence, distribution and longevity of modern groundwater is dependent on a myriad of environmental controls including climate fluctuations, long-term regional recharge patterns, aquifer mechanics and anthropogenic practices (Cuthbert et al., 2019; Gleeson et al., 2015, 2012; Jasechko et al., 2017). The construction of predicted abundance curves of ^{14}C and ^3H in groundwater

provides the opportunity to assess actual ^{14}C and ^3H tracer abundances in the context of modern and older groundwater mixing. It also highlights that the efficacy of modern groundwater distribution predictions is dependent on the appropriate correction of ^{14}C and ^3H abundances for atmospheric and rock-water (dilution) processes.

4.1. Predicting tracer abundance in recharge and flow over time

In this study, modern/fossil groundwater mixing predictions are implicitly dependent on the modelled abundance curve they were calculated from (Fig.4). It is evident from atmospheric and soil records that the bomb

pulse has a significant impact on the predicted groundwater abundances of ^{14}C and ^3H . These effects are less significant for more modern predicted curves (i.e. younger than the year 2000). When compared to the collated data in this study, atmospheric and soil abundance curves, predicted using the renewal rate model cannot estimate mixing proportion as measured tracer abundance falls outside of the model thresholds (Fig.10). This is a result of the inability of renewal rate models to incorporate groundwater flow paths of longer residence times. In contrast, EPM models predict tracer abundances that allow for the interpretation of a much larger portion of the collated data and can predict abundances in infinitely long groundwater flow paths. Hence, it is imperative that the appropriate groundwater flow model is selected before the prediction of mixing between modern and older groundwater components is undertaken. Similar tracer abundance investigations in other regions, which comprise of different hydrogeology and across different spatial scales, would benefit from numerically based groundwater flow predictions to supplement the lumped parameter models outlined in this study.

4.2. *The dissolution of 'dead' carbon*

The degree of open system dissolution in each country differs significantly, where South African ($n = 201$ of 304) and Namibian ($n = 46$ of 125) samples are more clearly affected by open system conditions (Fig.8). This is likely caused by the high proportion of samples taken from secondary carbonate systems, including carbonate-rich sediments in otherwise silicate dominated aquifers (e.g. the Northern Cape of South Africa). In samples with older ages, it is difficult to assess the degree of open system dissolution, as even when corrected under closed system conditions samples produce plausible mean residence times (e.g. Namibia and Botswana). It must also be noted that agricultural C_3 crops could be large contributors to groundwater $\delta^{13}\text{C}$ values in recharge, as these regions can represent significant zones of recharge in otherwise C_4 dominated regions (e.g. Mozambique). For samples less affected by open system conditions, where ^{14}C correction for closed system dissolution is appropriate, 'q' value corrections were applied ($n = 433$ of 624). This is representative of the distribution of carbonate-bearing lithologies across SADC as well as the measured $\delta^{13}\text{C}$ values, which indicate significant dissolution (Fig.5). In silicate-dominated aquifer systems, the efficacy of $\delta^{13}\text{C}$ derived corrections is less likely to produce representative MRTs. Even in environments where karstic systems and carbonate-bearing aquifers are prevalent

(Goldscheider et al., 2020; Stevanović, 2018), the degree of open vs closed system dissolution could be made more accurate if coupled with another isotopic or geochemical measurement, e.g. $^{87}\text{Sr}/^{86}\text{Sr}$ or HCO_3 (Cartwright, 2010; Cartwright et al., 2013).

4.3. *The variability of tritium in rainfall*

The indication of significant mixing in wells/boreholes assessed in this study is dependent on the accurate prediction of ^3H activity in recharge. Without the correction of ocean dilution and seasonal effects, the occurrence of significant mixing may be over or underestimated by up to ~8% although the mean discrepancy is 1.8%. The exact ^3H variability in precipitation is still poorly constrained across SADC. Samples collected in southern Mozambique and the Western Cape Province of South Africa experienced the highest degree of ocean dilution, resulting in likely underestimated modern groundwater proportions (Fig.6). Once corrected, samples showed significant increases in wells that showed mixing (Western Cape from 42 % to 50% and southern Mozambique from 89 % to 100 %). Samples in Botswana will likely reflect even lower proportions of mixed wells/boreholes if precipitation originates from the continental recycling of moisture, as this increased the ^3H activity in recharge (Harms et al., 2016; C. V. Tadros et al., 2014). Corrections associated with the seasonality of rainfall are limited by the current understanding of summer vs winter precipitation distributions, which may have changed significantly in the past century and are likely to evolve with climate change. Regions with improved ^3H data availability and continuity of records, will benefit from more representative initial ^3H predictions and in turn more representative predictions of groundwater mixing.

4.4. *The distribution of modern and fossil groundwater in southern Africa*

The heterogeneity of recharge and flow paths, combined with variable initial tracer abundances over time, make large-scale modern/fossil groundwater mixing estimates challenging (Hagedorn et al., 2018). The methods used to predict the modern component in groundwater systems vary with scale and hence catchment level quantitative investigations are ideal. Yet even on the global scale, isotopic investigations have proven to be useful, when assessing macro distributions of modern recharge and groundwater proportions (Gleeson et al., 2016). The distributions of modern groundwater mixing predicted in this study show larger scale trends, with higher proportions of mixing

Chapter 3 – Modern and Fossil Groundwater

predicted for the southwest coast of South Africa, southeast coast of Mozambique and most northern reaches of Namibia (Fig.11). Regional rainfall distributions correlated with elevated percentages of mixed wells in Mozambique and the Western Cape of South Africa yet did not correspond with lower proportions of mixed wells on the northwest coast and inland rock aquifers of South Africa. This may be a result of contrasting groundwater environments, where groundwater on the northwest coast is hosted in shallower, shorter flow path regimes as opposed to the deep fractured systems in the highlands of South Africa. Groundwater in central Namibia and Botswana have, in general, lower percentages of mixed wells and older fossil component residence times and are a result of low precipitation rates, high evaporation rates and less productive clay-rich aquifer systems. Older MRTs ages may also be a result of previously wetter climates experienced in the region (Lee-Thorp et al., 2001). A small portion samples, from Namibia and Botswana, exhibited MRTs that exceeded 50 000 years (n=45 of 624), yet the geological age and arid climate would suggest that a larger proportion of groundwater would be comprised of older recharge. Such fossil components, that exceed the longevity of ^{14}C , would be better constrained with a tracer of a longer half-life e.g. ^{81}Kr (half-life = 213 000 years) or ^{36}Cl (half-life = 301 000 years). Large aquifer systems, e.g. the Nubian and Intercalaire aquifers in North Africa and Great Artesian Basin in Australia, have identified groundwater of ages much older than the capabilities of ^{14}C allow with the use of ^{81}Kr , suggesting there could be an older component in SADC groundwater that this study cannot constrain (Collon et al., 2000; Matsumoto et al., 2020; Voss and Soliman, 2014).

Predicted mixing proportions have a significant impact on the interpretation of MRTs and in turn the availability of sustainable groundwater resources for agricultural and maintenance of the ecological reserve. The central regions of South Africa and Botswana are particularly dependent on groundwater to support agricultural activities (Giordano, 2006; Mukheibir, 2008; Puri and Aureli, 2005), leaving these regions, which have a low percentage of mixed wells, particularly vulnerable to groundwater depletion should the resource not be actively recharged to an equivalent rate of abstraction. Additionally, Botswana has a groundwater dependent ecology due to low surface water resources outside of the Okavango delta, which warrants prudence in the development of local groundwater resources (Timmermans and Meijerink, 1999). Conversely, some parts of northern Namibia likely have an under-utilized modern

groundwater resource as a result of less agricultural development in and around protected ecological reserves (Cunningham, 1997). If predicted climate change reduced water availability in the central and southwest SADC, modern groundwater mixing proportions are likely to decrease, increasing the groundwater vulnerability of these areas (van Rooyen et al., 2020b; Villholth et al., 2013). As current predictions indicate significant climate shift over the SADC, the vulnerability of groundwater will likely change accordingly, yet the long term effects of this change are still poorly understood.

4.5. *Global suitability and implications*

The proportions of mixed wells/boreholes in conjunction with ranges of MRTs, predicted in this study, give insights to regional hydrological resilience within the SADC. Where areas of high proportions of mixed wells and/or younger MRTs are likely renewing a larger portion of groundwater, or at a higher rate, than regions with low proportions of mixed wells and/or older MRTs. The model presented in this study highlights the potential for ^{14}C and ^3H tracers to constrain the presence modern groundwater mixing in data poor regions on a regional scale. However, the modelling approach would benefit from increased data availability and understanding of regional groundwater environments. Global aquifers, that have an abundance of groundwater data, could implement this model framework to produce results that are more robust. e.g. in Australia (A. P. Atkinson et al., 2014; Hu et al., 2019; C. V Tadros et al., 2014), North China (Changming et al., 2001; Zhai et al., 2013), North America (Scanlon et al., 2012; Sophocleous, 2005) and North Africa (Hamed et al., 2014; Voss and Soliman, 2014).

The presence of extensive groundwater mixing in the wells investigated in this study suggest that these aquifers may be vulnerable to modern contaminants from surface processes (Jasechko et al., 2017). The distribution of high percentages of modern groundwater mixing in well shows relatively good correlation with previous groundwater vulnerability estimates (Musekiwa and Majola, 2013; van Rooyen et al., 2020b). Although the emphasis of this study was related to the sustainability of SADC groundwater, the results are informative about groundwater quality risks in the region. Furthermore, the need for comprehensive isotope studies is pertinent to the application of tracer studies for both groundwater quality and quantity assessments in the future.

5. Conclusions

Assessment of the relationship between ^{14}C and ^3H can provide a clear distinction between modern and fossil components in groundwater. Groundwater within the extent of the study area is predicted to have extremely diverse proportions mixed wells (0.6 - 100%, mean = 42.7%) that correspond to a wide range of ^{14}C derived groundwater MRTs (500 - 28580 years). Areas of low proportions of mixed wells and older average MRT ranges are linked to areas of low mean annual rainfall as well as deep basement aquifers and clay rich aquifers of low productivity. Areas of higher proportions of mixed wells and younger average MRT ranges are synonymous with areas of increased mean annual rainfall as well as alluvial and fractured rock aquifers of higher productivity. Data compiled in this study indicate that simple renewal rate models from the atmospheric record alone cannot predict the activity of ^{14}C and ^3H and more representative groundwater flow models combined with soil records are necessary. Subsequently, corrections for both ^{14}C and ^3H are necessary to calculate representative proportions of modern groundwater. Traditional ^{14}C correction methods are only applicable in regions where significant closed system dissolution is occurring and open system dissolution needs to be incorporated to avoid under-estimating mean residence times. The degree and rate of ^{14}C dilution carries with it significant uncertainties and resultant ranges of MRTs are substantial. In older datasets, where regional soil and rock $\delta^{13}\text{C}$ data is not available, spatial vegetation and geological maps are useful in assessing the degree of carbon dilution (q value) from open/closed system dissolution of carbonate bearing lithologies, yet the natural system is likely more complicated than outlined in this study. The accuracy of modern groundwater mixing relationships estimation is dependent on the variation of ^3H in local rainfall over time, which is in turn impacted by the seasonality of rainfall and the potential for ocean dilution. Furthermore, modern recharge is not mixing with older waters of the same mean residence time and the fossil groundwater component varies across spatial regions. The use of isotope tracers, in particular ^{14}C and ^3H , is appropriate in regions where groundwater sustainability is poorly constrained, yet the model presented would benefit from specific records of local $\delta^{13}\text{C}$ values in recharge and rock-mass, $^3\text{H}/^{14}\text{C}$ variability in precipitation and groundwater renewal/flow rate.

Acknowledgements

We thank the Water Research Commission South Africa for initial funding support and the iPhakade program and National Research Foundation (NRF) South Africa for bursary support. A large portion of the data provided in this paper was kindly made available by Dr. Roger Diamond on behalf of the late Mr. Siep Talma. This work is based on the research supported wholly/in part by the *National Research Foundation of South Africa* (Grant Number: 118594) and the Southern African Science Centre for Climate Change and Adaptive Land Management (SASSCAL). Analysis was partly supported by the European Union and the State of Hungary, co-financed by the European Regional Development. This publication forms part of the output of the Biogeochemistry Research Infrastructure Platform (BIOGRIP) of the Department of Science and Innovation of South Africa. This contribution has an iPhakade publication number of 255.

References

- Aeschbach-Hertig, W., Gleeson, T., 2012. Regional strategies for the accelerating global problem of groundwater depletion. *Nat. Geosci.* 5, 853–861. <https://doi.org/10.1038/ngeo1617>
- Atkinson, A P, Cartwright, I., Gilfedder, B.S., Cendón, D.I., Unland, N.P., Hofmann, H., 2014. ^{14}C and ^3H to understand groundwater flow and recharge in an aquifer window. *Hydrol. Earth Syst. Sci* 18, 4951–4964. <https://doi.org/10.5194/hess-18-4951-2014>
- Atkinson, A. P., Cartwright, I., Gilfedder, B.S., Cendón, D.I., Unland, N.P., Hofmann, H., 2014. Using ^{14}C and ^3H to understand groundwater flow and recharge in an aquifer window. *Hydrol. Earth Syst. Sci.* 18, 4951–4964. <https://doi.org/10.5194/hess-18-4951-2014>
- Barbieri, M., 2019. Isotopes in hydrology and hydrogeology. *Water (Switzerland)* 11. <https://doi.org/10.3390/w11020291>
- Bethke, C.M., Johnson, T.M., 2008. Groundwater Age and Groundwater Age Dating. *Annu. Rev. Earth Planet. Sci.* 36, 121–152. <https://doi.org/10.1146/annurev.earth.36.031207.124210>
- Bhandary, H., Al-Senafy, M., Marzouk, F., 2015. Usage of Carbon Isotopes in Characterizing Groundwater Age, Flow Direction, Flow Velocity and Recharge Area. *Procedia Environ. Sci.* 25, 28–35. <https://doi.org/10.1016/j.proenv.2015.04.005>
- Cartwright, I., 2010. Using groundwater geochemistry and environmental isotopes to assess the correction of ^{14}C ages in a silicate-dominated aquifer system. *J. Hydrol.* 382, 174–187. <https://doi.org/10.1016/j.jhydrol.2009.12.032>

Chapter 3 – Modern and Fossil Groundwater

- Cartwright, I., Cendón, D., Currell, M., Meredith, K., 2017. A review of radioactive isotopes and other residence time tracers in understanding groundwater recharge: Possibilities, challenges, and limitations. *J. Hydrol.* 555, 797–811. <https://doi.org/10.1016/j.jhydrol.2017.10.053>
- Cartwright, I., Fifield, L.K., Morgenstern, U., 2013. Using ^3H and ^{14}C to constrain the degree of closed-system dissolution of calcite in groundwater. *Appl. Geochemistry* 32, 118–128. <https://doi.org/10.1016/j.apgeochem.2012.10.023>
- Cartwright, I., Morgenstern, U., 2015. Transit times from rainfall to baseflow in headwater catchments estimated using tritium: The Ovens River, Australia. *Hydrol. Earth Syst. Sci.* 19, 3771–3785. <https://doi.org/10.5194/hess-19-3771-2015>
- Cauquoin, A., Jean-Baptiste, P., Risi, C., Fourré, É., Stenni, B., Landais, A., 2015. The global distribution of natural tritium in precipitation simulated with an Atmospheric General Circulation Model and comparison with observations. *Earth Planet. Sci. Lett.* 427, 160–170.
- Changming, L., Jingjie, Y., Kendy, E., 2001. Groundwater exploitation and its impact on the environment in the North China Plain. *Water Int.* 26, 265–272. <https://doi.org/10.1080/02508060108686913>
- Clark, I.D., Fritz, P., 2013. *Environmental isotopes in hydrogeology*. CRC press.
- Coetsiers, M., Walraevens, K., 2009. A new correction model for ^{14}C ages in aquifers with complex geochemistry—application to the Neogene Aquifer, Belgium. *Appl. Geochemistry* 24, 768–776.
- Collon, P., Kutschera, W., Loosli, H.H., Lehmann, B.E., Purtschert, R., Love, A., Sampson, L., Anthony, D., Cole, D., Davids, B., Morrissey, D.J., Sherrill, B.M., Steiner, M., Pardo, R.C., Paul, M., 2000. ^{81}Kr in the Great Artesian Basin, Australia: A new method for dating very old groundwater. *Earth Planet. Sci. Lett.* 182, 103–113. [https://doi.org/10.1016/S0012-821X\(00\)00234-X](https://doi.org/10.1016/S0012-821X(00)00234-X)
- Cook, P.G., Böhlke, J.-K., 2000. Determining timescales for groundwater flow and solute transport, in: *Environmental Tracers in Subsurface Hydrology*. Springer, pp. 1–30.
- Cunningham, A.B., 1997. Landscape domestication and cultural change: Human ecology of the Cuvelai-Etoshia region. *Madoqua* 20, 37–48.
- Cuthbert, M.O., Gleeson, T., Moosdorf, N., Befus, K.M., Schneider, A., Hartmann, J., Lehner, B., 2019. Global patterns and dynamics of climate-groundwater interactions. *Nat. Clim. Chang.* 9, 137–141. <https://doi.org/10.1038/s41558-018-0386-4>
- Ekuruzel, B., Schlosser, P., Smethie, W.M., Plummer, L.N., Busenberg, E., Michel, R.L., Weppernig, R., Stute, M., 1994. Dating of shallow groundwater: Comparison of the transient tracers $^3\text{H}/^3\text{He}$, chlorofluorocarbons, and ^{85}Kr . *Water Resour. Res.* 30, 1693–1708. <https://doi.org/10.1029/94WR00156>
- El-Kadi, A.I., Plummer, L.N., Aggarwal, P., 2011. NETPATH-WIN: An interactive user version of the mass-balance model, NETPATH. *Groundwater* 49, 593–599.
- Fontes, J., Garnier, J., 1979. Determination of the initial ^{14}C activity of the total dissolved carbon: A review of the existing models and a new approach. *Water Resour. Res.* 15, 399–413.
- Giordano, M., 2006. Agricultural groundwater use and rural livelihoods in sub-Saharan Africa: A first-cut assessment. *Hydrogeol. J.* 14, 310–318. <https://doi.org/10.1007/s10040-005-0479-9>
- Gleeson, T., Alley, W.M., Allen, D.M., Sophocleous, M.A., Zhou, Y., Taniguchi, M., Vandersteen, J., 2012. Towards sustainable groundwater use: Setting long-term goals, backcasting, and managing adaptively. *Ground Water* 50, 19–26. <https://doi.org/10.1111/j.1745-6584.2011.00825.x>
- Gleeson, T., Befus, K.M., Jasechko, S., Luijendijk, E., Cardenas, M.B., 2016. The global volume and distribution of modern groundwater. *Nat. Geosci.* 9, 161–164. <https://doi.org/10.1038/ngeo2590>
- Gleeson, T., Befus, K.M., Jasechko, S., Luijendijk, E., Cardenas, M.B., 2015. The global volume and distribution of modern groundwater. *Nat. Geosci. Advance on*, 1–15. <https://doi.org/10.1038/ngeo2590>
- Goldscheider, N., Chen, Z., Auler, A.S., Bakalowicz, M., Broda, S., Drew, D., Hartmann, J., Jiang, G., Moosdorf, N., Stevanovic, Z., Veni, G., 2020. Global distribution of carbonate rocks and karst water resources. *Hydrogeol. J.* 28, 1661–1677. <https://doi.org/10.1007/s10040-020-02139-5>
- Hagedorn, B., Clarke, N., Ruane, M., Faulkner, K., 2018. Assessing aquifer vulnerability from lumped parameter modeling of modern water proportions in groundwater mixtures: Application to California's South Coast Range. *Sci. Total Environ.* 624, 1550–1560. <https://doi.org/10.1016/j.scitotenv.2017.12.115>
- Hamed, Y., Ahmadi, R., Hadji, R., Mokadem, N., Dhia, H. Ben, Ali, W., 2014. Groundwater evolution of the Continental Intercalaire aquifer of Southern Tunisia and a part of Southern Algeria: use of geochemical and isotopic indicators. *Desalin. Water Treat.* 52, 1990–1996. <https://doi.org/10.1080/19443994.2013.806221>
- Harms, P.A., Visser, A., Moran, J.E., Esser, B.K., 2016. Distribution of tritium in precipitation and surface water in California. *J. Hydrol.* 534, 63–72. <https://doi.org/10.1016/j.jhydrol.2015.12.046>

Chapter 3 – Modern and Fossil Groundwater

- Harvey, J.W., Newlin, J.T., Krupa, S.L., 2006. Modeling decadal timescale interactions between surface water and ground water in the central Everglades, Florida, USA. *J. Hydrol.* 320, 400–420. <https://doi.org/10.1016/J.JHYDROL.2005.07.024>
- Hu, K.X., Awange, J.L., Kuhn, M., Saleem, A., 2019. Spatio-temporal groundwater variations associated with climatic and anthropogenic impacts in South-West Western Australia. *Sci. Total Environ.* 696. <https://doi.org/10.1016/j.scitotenv.2019.133599>
- Hughes, C.E., Cendón, D.I., Harrison, J.J., Hankin, S.I., Johansen, M.P., Payne, T.E., Vine, M., Collins, R.N., Hoffmann, E.L., Loosz, T., 2011. Movement of a tritium plume in shallow groundwater at a legacy low-level radioactive waste disposal site in eastern Australia. *J. Environ. Radioact.* 102, 943–952. <https://doi.org/10.1016/j.jenvrad.2010.05.009>
- Ingerson, E., Pearson, F.J., 1964. Estimation of age and rate of motion of groundwater by the ^{14}C -method. *Recent Res. fields Atmos. Hydrosph. Nucl. geochemistry* 263–283.
- Jasechko, S., Perrone, D., Befus, K.M., Bayani Cardenas, M., Ferguson, G., Gleeson, T., Luijendijk, E., McDonnell, J.J., Taylor, R.G., Wada, Y., Kirchner, J.W., 2017. Global aquifers dominated by fossil groundwaters but wells vulnerable to modern contamination. *Nat. Geosci.* 10, 425–429. <https://doi.org/10.1038/ngeo2943>
- Jenkinson, D.S., Harkness, D.D., Vance, E.D., Adams, D.E., Harrison, A.F., 1992. Calculating net primary production and annual input of organic matter to soil from the amount and radiocarbon content of soil organic matter. *Soil Biol. Biochem.* 24, 295–308. [https://doi.org/10.1016/0038-0717\(92\)90189-5](https://doi.org/10.1016/0038-0717(92)90189-5)
- Johnson, M.R., Anhaeuser, C.R., Thomas, R.J., 2006. *The Geology of South Africa*. Geological Society of South Africa.
- Jurgens, B.C., Böhlke, J.K., Eberts, S.M., Survey, U.S.G., 2012. TracerLPM (Version 1): An Excel® workbook for interpreting groundwater age distributions from environmental tracer data. *Tech. Methods*. <https://doi.org/10.3133/tm4F3>
- Key, R.M., Ayres, N., 2000. The 1998 edition of the national geological map of Botswana. *J. African Earth Sci.* 30, 427–451.
- Klump, S., Grundl, T., Purtschert, R., Kipfer, R., 2008. Groundwater and climate dynamics derived from noble gas, ^{14}C , and stable isotope data. *Geology* 36, 395–398. <https://doi.org/10.1130/G24604A.1>
- Kuc, T., Gorczyca, Z., Kapusta, M., 2004. Carbon dynamics in soil recorded by ^{14}C : Model calculations. *Geochronometria* 23, 45–50.
- Lamontagne, S., Taylor, A.R., Battle-Aguilar, J., Suckow, A., Cook, P.G., Smith, S.D., Morgenstern, U., Stewart, M.K., 2015. River infiltration to a subtropical alluvial aquifer inferred using multiple environmental tracers. *Water Resour. Res.* 51, 4532–4549.
- Le Gal La Salle, C., Marlin, C., Leduc, C., Taupin, J.D., Massault, M., Favreau, G., 2001. Renewal rate estimation of groundwater based on radioactive tracers (^3H , ^{14}C) in an unconfined aquifer in a semi-arid area, Iullemeden basin, Niger. *J. Hydrol.* 254, 145–156. [https://doi.org/10.1016/S0022-1694\(01\)00491-7](https://doi.org/10.1016/S0022-1694(01)00491-7)
- Lee-Thorp, J., Holmgren, K., Lauritzen, S., Linge, H., Moberg, A., Partridge, T.C., Stevenson, C., Tyson, P.D., 2001. Rapid climate shifts in the southern African interior throughout the mid to late Holocene features of the index sequences in the U-series with in the upper mm section at higher resolution (continuous and the first transect (points, ---12 to 4 years ave. *Geophys. Res. Lett.* 28, 4507–4510.
- Levin, I., Graul, R., Trivett, N.B.A., 1995. Long-term observations of atmospheric CO_2 and carbon isotopes at continental sites in Germany. *Tellus B* 47, 23–34.
- Levin, I., Kromer, B., Hammer, S., 2013. Atmospheric $\delta^{14}\text{CO}_2$ trend in Western European background air from 2000 to 2012. *Tellus, Ser. B Chem. Phys. Meteorol.* 65. <https://doi.org/10.3402/tellusb.v65i0.20092>
- Li, Z., Jasechko, S., Si, B., 2019. Uncertainties in tritium mass balance models for groundwater recharge estimation. *J. Hydrol.* 571, 150–158. <https://doi.org/10.1016/j.jhydrol.2019.01.030>
- Li, Z., Si, B., 2018. Reconstructed precipitation tritium leads to overestimated groundwater recharge. *J. Geophys. Res. Atmos.* 123, 9858–9867.
- Mair, A., Hagedorn, B., Tillery, S., El-Kadi, A.I., Westenbroek, S., Ha, K., Koh, G.W., 2013. Temporal and spatial variability of groundwater recharge on Jeju Island, Korea. *J. Hydrol.* 501, 213–226. <https://doi.org/10.1016/j.jhydrol.2013.08.015>
- Maloszewski, P., Zuber, A., 1993. Tracer experiments in fractured rocks: matrix diffusion and the validity of models. *Water Resour. Res.* 29, 2723–2735.
- Maloszewski, P., Zuber, A., 1982. Determining the turnover time of groundwater systems with the aid of environmental tracers: 1. Models and their applicability. *J. Hydrol.* 57, 207–231.
- Manning, M.R., Melhuish, W.H., 1994. Atmospheric $\Delta^{14}\text{C}$ Record from Wellington (1954–1993). *Environmental System Science Data Infrastructure for a Virtual Ecosystem*
- Matchaya, G., Kaaba, O., Nhemachena, C., 2018. Justiciability of the Right to Water in the SADC Region: A Critical Appraisal. *Laws* 7, 18. <https://doi.org/10.3390/laws7020018>
- Matsumoto, T., Zouari, K., Trabelsi, R., Hillegonds, D., Jiang, W., Lu, Z.T., Mueller, P., Zappala, J.C., Araguás Araguás, L.J., Romeo, N., Agoun, A., 2020. Krypton-81 dating of the deep Continental Intercalaire aquifer with implications for

Chapter 3 – Modern and Fossil Groundwater

- chlorine-36 dating. *Earth Planet. Sci. Lett.* 535, 116120. <https://doi.org/10.1016/j.epsl.2020.116120>
- McGuire, K.J., McDonnell, J.J., 2006. A review and evaluation of catchment transit time modeling. *J. Hydrol.* 330, 543–563. <https://doi.org/10.1016/j.jhydrol.2006.04.020>
- Mendelsohn, J., 2002. *Atlas of Namibia: a portrait of the land and its people*. New Africa Books (Pty) Ltd.
- Mook, W., Rozanski, K., 2000. Environmental isotopes in the hydrological cycle. IAEA Publ. 39.
- Morgenstern, U., Stewart, M.K., Stenger, R., 2010. Dating of streamwater using tritium in a post nuclear bomb pulse world: Continuous variation of mean transit time with streamflow. *Hydrol. Earth Syst. Sci.* 14, 2289–2301. <https://doi.org/10.5194/hess-14-2289-2010>
- Mukheibir, P., 2008. Water resources management strategies for adaptation to climate-induced impacts in South Africa. *Water Resour. Manag.* 22, 1259–1276. <https://doi.org/10.1007/s11269-007-9224-6>
- Nimmo, J.R., Healy, R.W., Stonestrom, D.A., 2005. Aquifer Recharge. *Encycl. Hydrol. Sci.* 1–18. <https://doi.org/10.1002/0470848944.hsa161a>
- Puri, S., Aureli, A., 2005. Transboundary aquifers: A global program to assess, evaluate, and develop policy. *Ground Water* 43, 661–668. <https://doi.org/10.1111/j.1745-6584.2005.00100.x>
- Robinson, H.D., Gronow, J.R., 1996. Tritium levels in leachates and condensates from domestic wastes in landfill sites. *Water Environ. J.* 10, 391–398. <https://doi.org/10.1111/j.1747-6593.1996.tb00070.x>
- Ruotoistenmäki, T., 2008. Geophysical maps and petrophysical data of Mozambique 2008.
- Rutherford, M.C., Mucina, L., 2006. Biomes and bioregions of southern Africa: The vegetation of South Africa, Lesotho and Swaziland. *Strelitzia* 19, 31–51.
- Rutherford, M.C., O'farrel, P., Goldberg, K., Midgley, G.F., Powrie, L.W., Ringrose, S., MATHESON, W., Timberlake, J., 2005. SAFARI 2000 NBI vegetation map of the savannas of southern Africa. ORNL DAAC.
- Scanlon, B.R., Faunt, C.C., Longuevergne, L., Reedy, R.C., Alley, W.M., McGuire, V.L., McMahon, P.B., 2012. Groundwater depletion and sustainability of irrigation in the US High Plains and Central Valley. *Proc. Natl. Acad. Sci.* 109, 9320–9325. <https://doi.org/10.1073/pnas.1200311109>
- Schlosser, P., Stute, M., Sonntag, C., Otto Münnich, K., 1989. Tritogenic ^3He in shallow groundwater. *Earth Planet. Sci. Lett.* 94, 245–256. [https://doi.org/10.1016/0012-821X\(89\)90144-1](https://doi.org/10.1016/0012-821X(89)90144-1)
- Solomon, D.K., Sudicky, E.A., 1991. Tritium and Helium 3 Isotope Ratios for Direct Estimation of Spatial Variations in Groundwater Recharge. *Water Resour. Res.* 27, 2309–2319. <https://doi.org/10.1029/91WR01446>
- Sophocleous, M., 2005. Groundwater recharge and sustainability in the High Plains aquifer in Kansas, USA. *Hydrogeol. J.* 13, 351–365. <https://doi.org/10.1007/s10040-004-0385-6>
- Stein, A.F., Draxler, R.R., Rolph, G.D., Stunder, B.J.B., Cohen, M.D., Ngan, F., 2015. NOAA's hysplit atmospheric transport and dispersion modeling system. *Bull. Am. Meteorol. Soc.* 96, 2059–2077. <https://doi.org/10.1175/BAMS-D-14-00110.1>
- Stevanović, Z., 2018. Global distribution and use of water from karst aquifers. *Geol. Soc. Spec. Publ.* 466, 217–236. <https://doi.org/10.1144/SP466.17>
- Stewart, M.K., 2012. A 40-year record of carbon-14 and tritium in the Christchurch groundwater system, New Zealand: Dating of young samples with carbon-14. *J. Hydrol.* 430–431, 50–68. <https://doi.org/10.1016/j.jhydrol.2012.01.046>
- Still, C.J., Powell, R.L., 2010. Continental-scale distributions of vegetation stable carbon isotope ratios, in: *Isoscapes*. Springer, pp. 179–193.
- Stock, W.D., Chuba, D.K., Verboom, G.A., 2004. Distribution of South African C₃ and C₄ species of Cyperaceae in relation to climate and phylogeny. *Austral Ecol.* 29, 313–319. <https://doi.org/10.1111/j.1442-9993.2004.01368.x>
- Suckow, A., Raiber, M., Deslandes, A., Gerber, C., 2018. Constraining conceptual groundwater models for the Hutton and Precipice aquifers in the Surat Basin through tracer data Copyright and disclaimer, CSIRO: Land and Water.
- Tadros, C. V., Hughes, C.E., Crawford, J., Hollins, S.E., Chisari, R., 2014. Tritium in Australian precipitation: A 50 year record. *J. Hydrol.* 513, 262–273. <https://doi.org/10.1016/j.jhydrol.2014.03.031>
- Tadros, C. V., Hughes, C.E., Crawford, J., Hollins, S.E., Chisari, R., 2014. Tritium in Australian precipitation: A 50 year record. *J. Hydrol.* 513, 262–273.
- Tamers, M.A., 1975. Validity of radiocarbon dates on ground water. *Geophys. Surv.* 2, 217–239.
- Timmermans, W.J., Meijerink, A.M.J., 1999. Remotely sensed actual evapotranspiration: Implications for groundwater management in Botswana. *ITC J.* 1, 222–233. [https://doi.org/10.1016/S0303-2434\(99\)85016-8](https://doi.org/10.1016/S0303-2434(99)85016-8)
- Tipping, E., Chamberlain, P.M., Bryant, C.L., Buckingham, S., 2010. Soil organic matter turnover in British deciduous woodlands, quantified with radiocarbon. *Geoderma* 155, 10–18. <https://doi.org/10.1016/j.geoderma.2009.11.016>

- Turnadge, C., Smerdon, B.D., 2014. A review of methods for modelling environmental tracers in groundwater: Advantages of tracer concentration simulation. *J. Hydrol.* 519, 3674–3689. <https://doi.org/10.1016/j.jhydrol.2014.10.056>
- van Rooyen, J.D., Palcsu, L., Visser, A., Vennemann, T.W., Miller, J.A., 2020a. Spatial and temporal variability of tritium in precipitation in South Africa and its bearing on hydrological studies. *J. Environ. Radioact.* 106354. <https://doi.org/10.1016/j.jenvrad.2020.106354>
- van Rooyen, J.D., Watson, A.P., Miller, J.A., 2020b. Combining quantity and quality controls to determine groundwater vulnerability to depletion and deterioration throughout South Africa. *Environ. Earth Sci.* 79. <https://doi.org/10.1007/s12665-020-08998-1>
- Villholth, K.G., Tøttrup, C., Stendel, M., Maherry, A., 2013. Integrated mapping of groundwater drought risk in the Southern African Development Community (SADC) region. *Hydrogeol. J.* 21, 863–885. <https://doi.org/10.1007/s10040-013-0968-1>
- Visser, A., Thaw, M., Esser, B., 2018. Analysis of air mass trajectories to explain observed variability of tritium in precipitation at the Southern Sierra Critical Zone Observatory, California, USA. *J. Environ. Radioact.* 181, 42–51. <https://doi.org/10.1016/j.jenvrad.2017.10.008>
- Voss, C.I., Soliman, S.M., 2014. Le Système Aquifère Nubien fossile transfrontalier du Tchad, de l’Égypte, de la Lybie et du Soudan: Questions classiques de nappe souterraine, analyse hydrogéologique simplifiée et modélisation. *Hydrogeol. J.* 22, 441–468. <https://doi.org/10.1007/s10040-013-1039-3>
- Zhai, Y., Wang, J., Guo, H., Cao, Y., Teng, Y., 2013. Reconstruction and optimization of tritium time series in precipitation of Beijing, China. *Radiocarbon* 55, 67–79.
- Zuber, A., Witczak, S., Rózański, K., Śliwka, I., Opoka, M., Mochalski, P., Kuc, T., Karlikowska, J., Kania, J., Jackowicz-Korczyński, M., Duliński, M., 2005. Groundwater dating with ^3H and SF_6 in relation to mixing patterns, transport modelling and hydrochemistry. *Hydrol. Process.* 19, 2247–2275. <https://doi.org/10.1002/hyp.5669>

CHAPTER 4 TRITIUM IN GROUNDWATER

PUBLICATION HISTORY	
Title	Constraining the spatial distribution of tritium in groundwater across South Africa
Journal	Water resources research – open access journal IF=4.31 (2019)
Status	Submitted - under review
Authors and roles	<p>J.D. van Rooyen – PhD Candidate</p> <p>J.A. Miller – Primary Supervisor</p> <p>A.P Watson – Co-Author</p> <p>L. Palscu – Co-Author</p>
Applicant Contribution	Field sampling, data collation, model construction, statistical coding in R, interpretation of results and wrote the manuscript.

Constraining the Spatial Distribution of Tritium in Groundwater across South Africa

J.D. van Rooyen¹, A.P. Watson¹, L. Palcsu² and J.A. Miller¹

1. Department of Earth Sciences, Faculty of Sciences, University of Stellenbosch, Private Bag X1, Matieland, 7601, South Africa. jvanrooyen21@gmail.com, jmiller@sun.ac.za

2. Isotope Climatology and Environmental Research Centre (ICER), Institute for Nuclear Research, H-4026 Debrecen, Bem tér 18/c, Hungary. palcsu@atomki.mta.hu

Correspondence: J.D. van Rooyen, jvanrooyen21@gmail.com, Department of Earth Sciences, Faculty of Sciences, University of Stellenbosch, Private Bag X1, Matieland, 7601, South Africa.

ARTICLE INFO

ABSTRACT

Keywords:
tritium, modern
groundwater,
geostatistics,
South Africa

Tritium (^3H) has become synonymous with modern groundwater and is used in a myriad of applications, ranging from sustainability investigations to contaminant transport and groundwater vulnerability. This study uses measured ^3H groundwater activities from 722 samples locations across South Africa to construct a ^3H groundwater distribution surface. Environmental co-variables are tested using geostatistical analysis to constrain external controls on ^3H variability, namely: [1] depth to groundwater, [2] distance from the ocean and [3] summer vs winter rainfall proportion. The inclusion of co-variables in the 'fit' of residual variograms improved prediction variance significantly yet does not mitigate issues with sample density. The distribution of ^3H in groundwater surface agrees well to expected controls, with proximal (<100km) coastal regions, winter rainfall zones and higher depths to groundwater predicted to have lower ^3H activities. Conversely, inland localities with shallower depth to groundwater and/or summer rainfall are predicted to have elevated ^3H activities. High groundwater ^3H anomalies could potentially be attributed to uranium-bearing deposits, as geogenic production of ^3H amplifies the activity contributed through recharge. Some ^3H high and low anomalies cannot be explained by known phenomena and may simply be regions of variable recharge and/or longer isolated groundwater flow paths. Regions of active recharge are more vulnerable to climate change as well as modern pollution. Less actively recharged groundwater may be more resilient to climate change yet represents a potentially non-renewable resource for abstraction. The application of ^3H distributions in the assessment of hydrological resilience is pertinent to effective groundwater management studies.

1. Introduction

Groundwater represents the most abundant freshwater resource available to both humans and the environment (Gleeson et al., 2015), especially in semi-arid to arid regions where surface water is scarce (Schoups et al., 2005). Use of groundwater is rapidly increasing as a result of climate change as well as the need for increased food production due to population growth (Cuthbert et al., 2019; Díaz-Cruz and Barceló, 2008; Ferguson and Gleeson, 2012; Gleeson et al., 2015; Zhang et al., 2001). As a result, groundwater is becoming progressively more vulnerable to depletion and contamination (van Rooyen et al., 2020b; Villholth et al., 2013; Wada et al., 2010). As groundwater dependence increases, so does the need to understand a catchment's ability to absorb disturbance and maintain or quickly regain hydrologic function, known as a catchment's hydrological resilience (Mao et al., 2017). Additionally,

modern recharge mechanisms, which control a catchments hydrological resilience, are changing due to climate change, land use change and shifts in resource utilization (Meixner et al., 2016). In order to quantify the hydrological resilience of a catchment, a comprehensive understanding of the catchments hydrological structure, water balance, cyclical climate fluctuations and anthropogenic influence is typically needed. Yet, alternative methods that use environmental isotopes can provide an understanding of proportions of modern recharge and enable an early assessment of hydrological resilience without an abundance of data.

Progress in the field of spatial isotope statistics has validated the use of environmental isotopes in a myriad of applications (West et al., 2009). Conservative tracers (e.g. stable isotopes) of the hydrological cycle can determine spatial variations in recharge rates and zones (Vengosh et

al., 2002), water-rock interaction (Gillon et al., 2009), pollution potential (Hagedorn et al., 2018), aquifer connectivity and salinization processes (Bennetts et al., 2006). Although less common, non-conservative (e.g. radioactive isotopes) tracers have also been successfully used in spatial models to predict groundwater age distributions (Visser et al., 2016). Tritium (^3H), which has a half-life of 12.312 years (Lucas and Unterweger, 2000; MacMahon, 2006), has become synonymous with modern groundwater or groundwater that has been recharged within the last ~50-100 years (Hagedorn et al., 2018; Jasechko et al., 2017; Le Gal La Salle et al., 2001; Li et al., 2019; Palcsu et al., 2017; Samborska et al., 2013; Visser et al., 2016; Zuber et al., 2005). The popularity of methods that use ^3H was invigorated by the increase in atmospheric abundance of ^3H through thermonuclear bomb testing in the 1950s and 1960s (Schlosser et al., 1989). Subsequently, the attenuation of 'bomb' ^3H has resulted in modern precipitation only incorporating natural levels of ^3H , particularly in the southern hemisphere where the bomb peak was much lower (Stewart, 2012). As ^3H forms part of the water molecule, its behaviour in recharge is chemically conservative and radioactive decay is the predominant process controlling its abundance along a groundwater flow path. The assessment of natural levels of ^3H in recharge presents new challenges and opportunities in the prediction of the proportion and spatial distribution of modern groundwater (Morgenstern et al., 2010).

Recent research used ^3H data collected over diverse climatic and hydrogeological environments to estimate the global distribution and volume of modern groundwater (Gleeson et al., 2016). Yet, global investigations are less applicable at catchment scale, where seasonal fluctuation, land use change and shifts in resource use can disrupt the hydrological cycle. It is also evident that the variation of background ^3H in local rainfall is more significant than reported in older studies (Kern et al., 2020; van Rooyen et al., 2020a; Visser et al., 2018). Once ^3H reaches the subsurface through recharge, its abundance is predominantly dependent on decay as the subsurface production of ^3H is limited to areas nearby radioactive deposits, landfills or waste sites (Hughes et al., 2011). If an aquifer system does not contain detectable levels of ^3H , it is either no longer being actively recharged and/or the isolated flow path is long enough to allow for ^3H to decay below detection limits. The ability of ^3H to distinguish between modern and older groundwater provides insight

to how resilient an aquifer may be to disruptions in the hydrological cycle. Furthermore, evaluation of the distribution of modern groundwater via the use of ^3H is applicable for regions where physical groundwater monitoring is intermittent, inconsistent and/or sparse.

South Africa is a large country (1.22 million km^2) with a diverse climate that ranges from semi-arid to arid in the central and western reaches to sub-tropical on the east coast and temperate in the north-east. Rainfall seasonality is divided across the country into semi-distinct summer and winter rainfall regions (Roffe et al., 2019) (Fig.1). Mean annual rainfall ranges from <100 mm in the arid Northern Cape Province to a peak of 3500 mm in the high-altitude eastern interior (Schulze et al., 2006) (Fig.1). As a consequence, South Africa, by global standards, is a water scarce country and the agricultural industry as well as an increasing populace is dependent on sustained groundwater availability. Yet, a significant portion of the country's geology, is represented by large hard rock provinces that lack major groundwater aquifers (Basson et al., 1997). The largest aquifer system in South Africa is within the Karoo Basin and provides significant amounts of fresh water to an otherwise semi-arid region. Smaller aquifer systems occur in the Cape Fold Belt as well as in carbonate terrains of Limpopo and North West Provinces. Additionally, South Africa shares three major transboundary aquifer systems, the largest of which is the Stampriet aquifer between Namibia, Botswana and South Africa (Cobbing et al., 2008). Due to the heterogeneous nature of groundwater reservoirs in South Africa and increasing groundwater dependence, constraining the resilience of groundwater is important for effective groundwater management.

This study investigates the spatial distribution of ^3H in groundwater in South Africa through the statistical assessment of: [1] measured ^3H in groundwater ($n=722$), [2] local variability of ^3H in rainfall and [3] the impact of unsaturated zone travel time during recharge on ^3H activity. To assess the effect of ocean dilution and rainfall seasonality, localities of groundwater samples are grouped into regions where the activity of ^3H in recharge is expected to differ as a result of atmospheric processes. To estimate the effect of unsaturated zone travel time, depth to groundwater data are collated from South Africa's National Groundwater Archive (NGA) and modelled into a predictive static water level surface. Environmental co-variables are used to constrain external drift in predictions of ^3H in

groundwater, with the “drift” being the value of the co-variable identified to explain a portion of variance within the testing parameter, in this case ^3H . As temporal climate records are insufficient across most of Africa to assess climate change over the past century, tracers of the hydrological cycle contribute invaluable information to

policy makers (Niang et al., 2014). Understanding modern groundwater recharge is pertinent to assessing the effects of climate change on water resources, as well as groundwater mixing relationships and vulnerability estimates to both depletion and contamination.

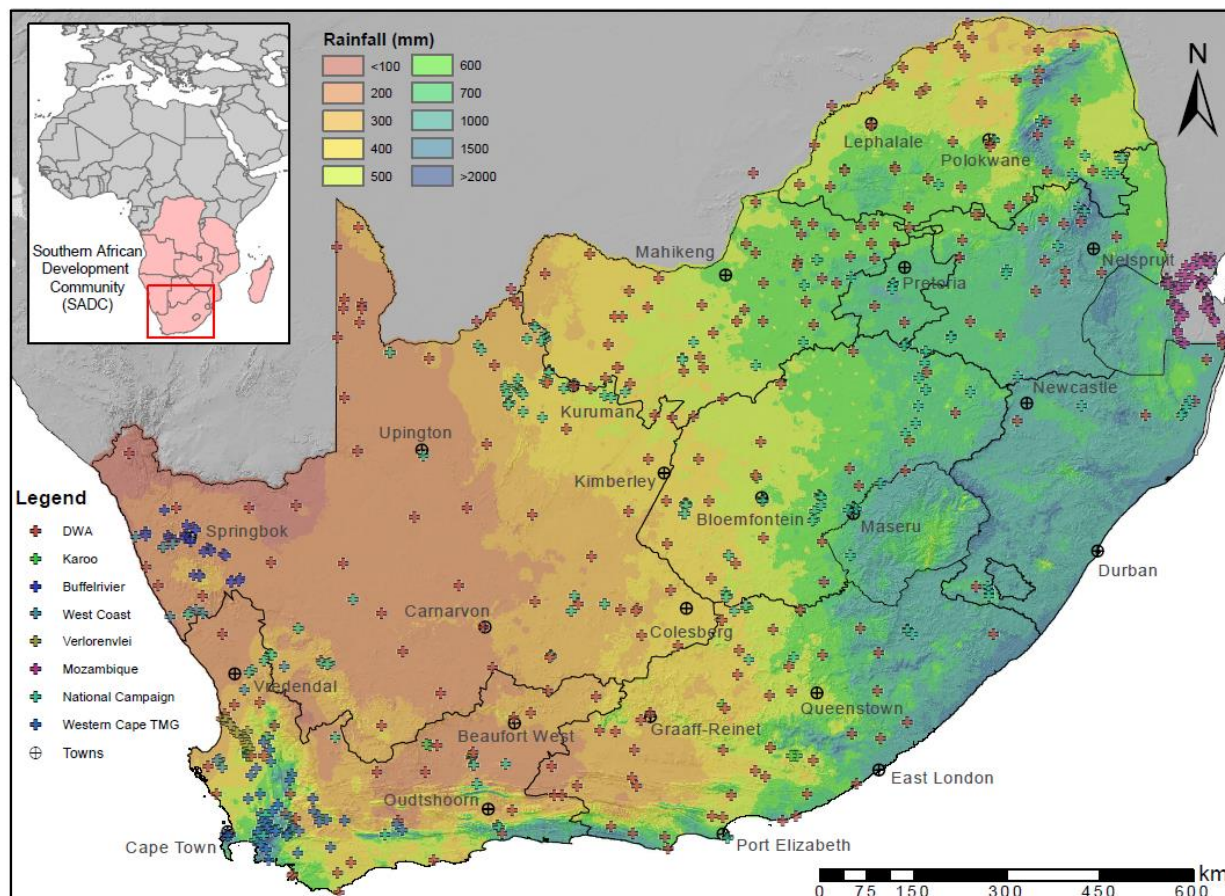


Figure 1 - The distribution of ^3H in groundwater sample locations as well as the major towns in South Africa. Mean annual precipitation is represented in mm in ten classes (Schulze et al., 2006).

2. Materials and methods

This study collected groundwater samples across South Africa in a series of sampling campaigns for the purpose of constraining the distribution of ^3H activity in groundwater. To improve the sample size and spatial distribution of samples used for interpolation, data from previous studies was incorporated into the dataset. Co-variables to ^3H data were determined from environmental data to remove any spatial structure that is dependent on factors other than the subsurface decay of ^3H . Following this approach, a ^3H distribution surface for South Africa was created using a Kriging with External Drift (KED) method and interpreted in the environmental context of South Africa.

2.1. Sampling strategy

Groundwater samples were collected during seven sampling campaigns across South Africa. These campaigns resulted in the collection of 446 samples (Fig.1). Sample groups were formed according to the sampling campaigns used to collect groundwater samples as follows: [1] west coast of South Africa (n=23), [2] Verlorenvlei RAMSAR protected catchment (n=19), [3] Buffelsrivier watershed (n=32), [4] Karoo basin (n=20), [5] Western Cape Table Mountain Group (n=59), [6] southern Mozambique (n=95) and, [7] ‘Know Your Water’ citizen science sampling campaign (n=198). Samples analysed for ^3H were collected in 1 liter polypropylene high density amber sampling bottles, completely filled to avoid atmospheric contamination. Additionally, all pumped well points were

sufficiently purged to ensure the groundwater sample was representative of the contributing aquifer. Detailed records of casing depths, screen lengths/depths and well depths were not always available, especially for older well points, the implications of which are explored in the discussion. Additional samples ($n=276$) (Fig.1) were collated from other unpublished research from a database of samples analysed by iThemba Labs (WITS), Johannesburg as well as a database provided by the South African Department of Water Affairs (DWA). All iThemba Labs samples were collected and analysed in 2006 and are available online as supplementary Table A.I.

2.2. Analysis

Groundwater samples collected from 2017-2019 were sent for analysis at the Isotope Climatology and Environmental Research Centre (ICER), Institute for Nuclear Research in Debrecen, Hungary. Analysis of ^3H at ICER was done using the ^3He e ingrowth method (Palcsu et al., 2010; Papp et al., 2012). This analysis involves degassing the water sample and measuring the newly produced ^3He gas from ^3H decay using a dual collector (noble gas) mass spectrometer, after a predetermined length of time. The method has a detection limit of 0.012 TU and expectation values are within 2 % for samples between 1 and 20 TU. ^3H measurement included in this study that were collated from other South African studies were analysed at iThemba labs (WITS) in Johannesburg, South Africa, using the liquid scintillation counter (LSC) and electrolytic enrichment method (Plastino et al., 2007). The method has a detection limit of 0.1 TU. Data included from other studies carries inherent uncertainties associated with spatial delineations and interpolated values, but this uncertainty is not constrained in the context of this study.

2.3. Measured ^3H in groundwater

Groundwater ^3H activities measured as part of this study had a mean ^3H activity of 0.64 TU ($n=446$) and a range of 0 – 3.5 TU. The standard deviation of the sample dataset was 0.63. Samples collected on the west coast sampling campaign had a mean ^3H activity of 0.68 TU and a range of 0 – 1.4 TU ($\sigma = 0.49$). Samples collected in the Verlorenvlei watershed had a mean ^3H activity of 0.19 TU and a range of 0 – 0.62 TU ($\sigma = 0.17$). Samples collected the Buffelsriver watershed are had a mean ^3H activity of 0.41 TU and a range of 0 – 1.58 TU ($\sigma = 0.40$). Samples collected in the central Karoo had a mean ^3H activity of 0.92 TU and a range of 0 – 3.50 TU ($\sigma = 0.93$). Samples collected in the

Western Cape sampling campaign had a mean ^3H activity of 0.73 TU and a range of 0 – 3.22 TU ($\sigma = 0.59$). Samples collected from the ‘Know Your Water’ citizen science sampling campaign had a mean ^3H activity of 0.82 TU and a range of 0 – 3.4 TU ($\sigma = 0.67$). Samples collected in southern Mozambique had a mean ^3H activity of 0.28 TU and a range of 0 – 2.04 TU ($\sigma = 0.36$). Samples collated from previous studies are well distributed across South Africa and had a mean ^3H activity of 1.26 TU and a range of 0 – 4.8 TU ($\sigma = 1.02$). The modal statistics are summarized in Figure 2. Measured groundwater ^3H activities summarized above are available online as supplementary Table A.II.

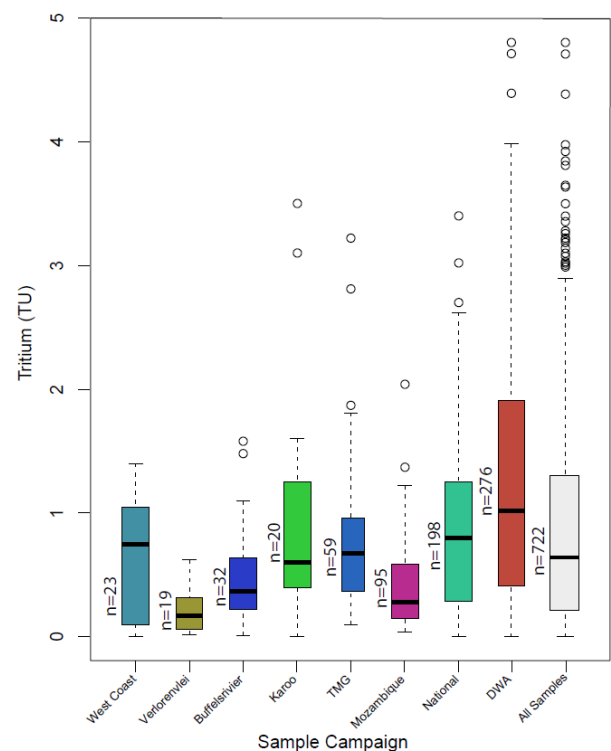


Figure 2 - Box plot showing the basic ^3H model statistics of the seven sampling campaigns used to collect groundwater in this study as well as the DWA database used to supplement the collected groundwater data.

2.4. Environmental co-variables

The co-variables investigated in this study were included from known controls on the activity of ^3H in groundwater (Harms et al., 2016; Visser et al., 2016). The co-variables used to assess external drift were identified as: [1] depth to groundwater, [2] distance from the ocean and [3] summer vs winter rainfall proportion. As the travel time of recharge in the unsaturated zone may result in significant decay of ^3H before it reaches the water table, it is important to remove this potential control, before

identifying the spatial structure of ^3H variability in groundwater. Although many collected samples have associated water level measurements taken during sample collection, these measurements are often not representative of the static water levels in the region or the aquifer. To mitigate assumptions made from spot sampling groundwater levels, a large national database (DWAF, 2004) ($n=126531$) of static water levels was used to interpolate a 'depth to groundwater' surface that predicted the static water level for the sample locations. This surface was produced using the same ordinary kriging methodology as other geo-spatial statistics in this study.

The background activity of ^3H in precipitation is largely controlled by the origin of the water mass that produces local precipitation (van Rooyen et al., 2020a; Visser et al., 2018). A HYSPLIT model, which calculates air mass trajectories, can be used to predict water mass origin and in turn, the likely effect on local ^3H activity in precipitation. Regions that have received rainfall predominantly in different times of the year, will be affected by intra-annual variability of ^3H due to seasonality. Summer vs winter rainfall zones are delineated into eight categories according to the combined agreement of previous delineations of winter summer rainfall zones (Roffe et al., 2019). Furthermore, coastal rainfall generally has lower ^3H activities due to the effect of ocean water dilution (van Rooyen et al., 2020a). The Euclidean distance to the ocean was calculated in ArcGIS to produce a 10×10 km grid to assess the control of ocean dilution.

2.5. Data pre-processing

To assess the degree of local spatial dependence of ^3H in groundwater, where samples collected closer in geographical space imply similar ^3H activities, the spatial autocorrelation of the dataset must be determined. This can be expressed as the strength of correlation depending on separation distance, where the correlation is expressed as the semivariance. Each pair of observations has an associated semivariance (γ) defined as:

$$\gamma(x_i, x_j) = \frac{1}{2}[z(x_i) - z(x_j)]^2 \quad (1)$$

where x is a specific geographical point and $z(x)$ is the associated attribute value, in this case ^3H in TU. A variogram cloud outlier detection procedure (Ploner, 1999) was applied to the collated ^3H database used in this study. The variogram cloud function reports the semivariance of point pairs within a particular neighbourhood radius. The

resultant pairs that deviate significantly from nearby observations, exceeding a semivariance of $\gamma=1$, were further investigated to constrain whether there could be a possible analytical error or if one sample was collected from a deeper confined aquifer system. To avoid samples being coupled with samples that were collected in a vastly different environment (subtropical vs semi-arid, coastal vs inland), the search neighbourhood was limited to the highest average variogram range ($\sim 200\text{km}$). Four sample point pairs were identified by creating a variogram cloud, which reports the average semivariance of sample point pairs within given search neighbourhood range and two of the eight investigated samples were removed as their measurement uncertainty was too high (>0.8 TU) (Fig.3).

The pairwise semivariances were then calculated for each sample location within the $\sim 200\text{km}$ search radius to group samples into search neighbourhoods. It was found that the standardized mean differences fell predominantly within ± 1 interval (88%) and only 12 samples fell outside the ± 5 interval range (1.6%). This range was used as the cut-off range for the possibility of erroneous data. The twelve identified samples were further interrogated yet were determined to be representative samples and thus included in further calculations.

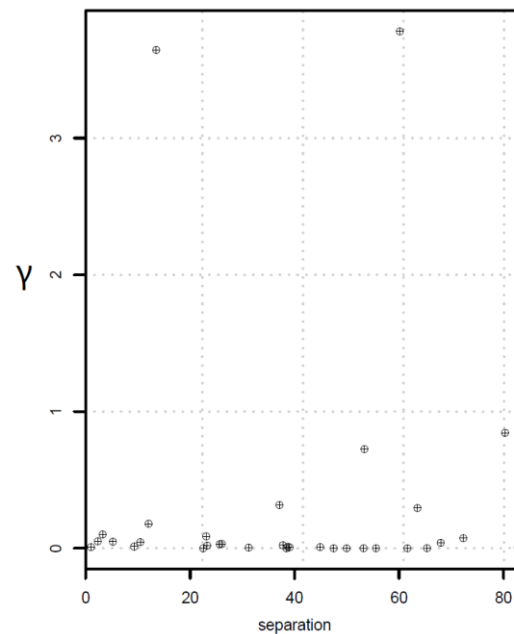


Figure 3 - The semivariance of point pairs computed as a variogram cloud in the data outlier analysis. Semivariance is represented as the average γ for a point pair as calculated in equation 1.

A similar outlier detection technique was applied to the collated groundwater levels database resulting in a small subset of readings excluded from further calculations

(0.17%). Previous research, that used global groundwater ^3H records, observed a robust trend in decreasing ^3H with depth to the groundwater as well as depth below the water table (Gleeson et al., 2016). The groundwater data in this study showed a similar pattern, yet where the depth to groundwater was shallower there was a significant variation in ^3H values (Fig.4). The heterogeneous distribution of hydraulic conductivities in shallow aquifers

in South Africa and significant variation in recharge ^3H activity are likely causes for the variation in shallower boreholes and suggest that the depth to the groundwater is not the only contributing factor to regional ^3H variability. These findings in the pre-processing analysis of data affirmed the inclusion for other atmospheric controls on ^3H variability to be included in interpolation techniques.

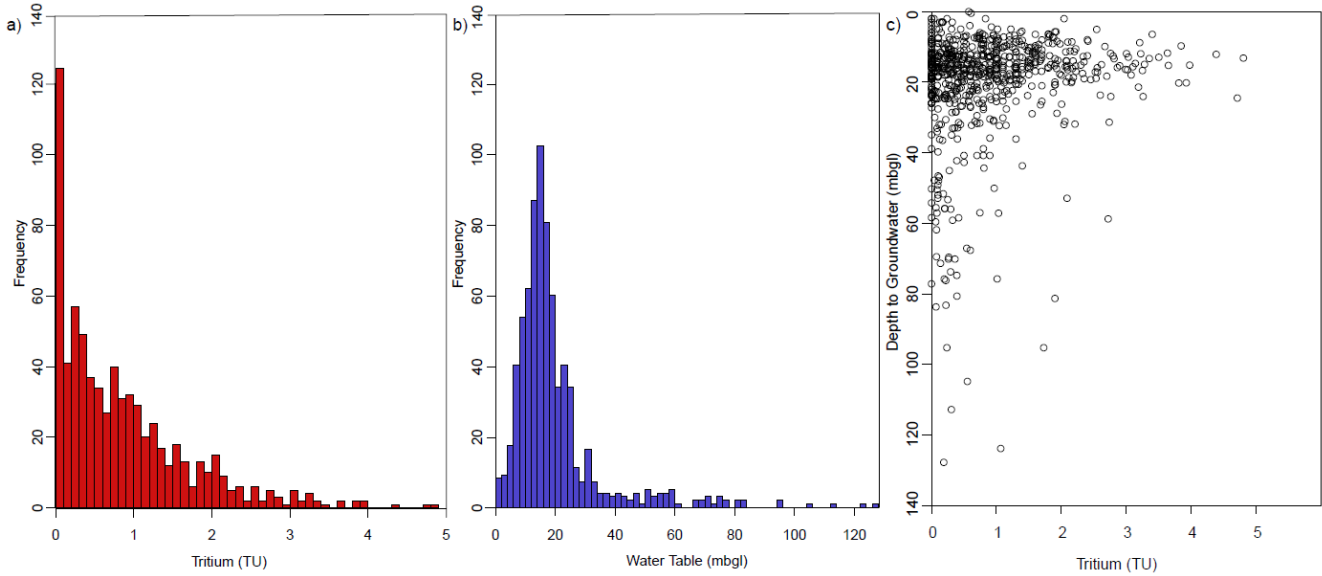


Figure 4 - The frequency distribution of a) measured ^3H (Tritium Units) in groundwater and b) the predicted depth to groundwater (meters below ground level) of all 722 samples. The relationship of ^3H and depth to groundwater is plotted in c).

2.6. Derivation of ^3H distribution surfaces

In order to relate the semivariances calculated in pre-processing, to the separation distance calculated from sample locality, an empirical variogram is used. The concept of displaying semivariances according to the separation distance was first proposed and calculated using the Matheron algorithm (Matheron, 1965). The empirical variogram, described as the average separation within some separation range, can be defined as:

$$\bar{\gamma}(h) = \frac{1}{2m(h)} \sum_{(i,j)|h_{ij} \in h} [z(x_i) - z(x_j)]^2 \quad (2)$$

where i,j represent the numbered point pair for which the semivariance is computed and h_{ij} is the separation distance between points i and j , h is the range of separations as defined by the histogram bins and $m(h)$ is the number of point-pairs in the bin corresponding to h . As is evident from the preprocessing procedure, some variation in ^3H in groundwater can be explained by the environmental co-variable. In order to remove variation attributed to the co-variable, variograms (Chilès, 2012) are constructed from the residual data, as described in Rossiter and Eda, (2019). A residual variogram is computed the

same as an empirical variogram, where $\gamma(h)$ is the semivariogram, and $Z(x)$ and $Z(x+h)$ are the values of a parameter sampled at a planar distance $|h|$ from each other:

$$\bar{\gamma}(h) = \frac{1}{2N(h)} \sum_{i=1}^{N(h)} [Z(x_i) - Z(x_i + h)]^2 \quad (3)$$

where $N(h)$ is the number of lag- h differences. This can be represented by the separation distance between two points, i.e. $nx(n-1)/2$, and n corresponds to the number of sampling locations at distance h . The fit parameters of a calculated variogram are describe as: [1] the nugget, which represents the variance at the given sample location and captures variability that is independent of spatial autocorrelation, [2] the sill, which is the maximum semivariance of the variogram model and is equal to the sum of the nugget and the partial sill, and [3] the range, which corresponds to the distance at which semivariance is no longer increasing and samples no longer display autocorrelation (Chilès, 2012). The fitting of a variogram model was performed by fitting the range and the sill to the given semivariance point-pairs by:

$$\gamma(h) = \begin{cases} c \cdot \left[\frac{2h}{3a} - \frac{1}{2} \left(\frac{h}{a} \right)^3 \right], & h < a \\ c, & h \geq a \end{cases} \quad (4)$$

where a is the range and c is the sill or maximum semivariance. The entire variogram is raised by the nugget variance. The variogram model was fitted to calculated semivariances for discrete lag intervals by the weighted least squares approach. This lag interval ranged from 10-25km depending on the ordinary or universal kriging method adopted.

For the geostatistical modelling of interpolated data (e.g. kriging), theoretical variograms were fitted to estimate an empirical variogram from the sample dataset. This empirical variogram was fit to have a maximum lag distance of 250 km with 11 equal interval bins (lags) in order to distribute equal sample observations per bin. The effective planar range (ae), which is equal to the distance in which autocorrelation is significant, was computed to be ~214km. Subsequently, residual variograms were prepared for KED, which are computed on a 10x10 km grid. The covariables included in this study were computed individually with TU to assess any improvement in the average semivariance of the semivariogram and the distribution of prediction variances of the interpolation.

3. Results

The obtained regional gridded ^3H activity in groundwater, independent of external drift, was computed from a fitted semivariogram model which had an average semivariance of 0.559 and planar distance of 214km (Fig.5a). The spatial prediction variance had a distribution localized to sample locations, where regions with few samples formed abrupt increases in variance near sample point locations. A notable increase in prediction variance was observed on the east coast of South Africa, where sample density was poor. Regions of elevated ^3H activity were localized to south central regions of the Karoo basin as well as the north eastern regions of the country. Many regions showed a random distribution of ^3H activity in groundwater, where erratic changes were observed over relatively short distances.

3.1. Prediction variances and external drift

The KED grid, produced with ‘depth to water’ as a covariable, was computed from a fitted Gaussian variogram model with an average semivariance of 0.542 and a planar distance of 89km (Fig.5b). Prediction variance was less localized and formed regional patterns around larger

distributions of sample density. High prediction variance regions remained prominent on the east coast and in the upper central Karoo. The KED prediction appeared more gradual in ^3H distributions with peaks and lows recurring gradually across the country. A similar decrease in average variance and planar distance was observed in KED grids produced with ‘Euclidean distance from ocean’ (Fig.5c) and ‘summer winter rainfall zone’ (Fig.5d). However, the KED grid, produced with ‘summer winter rainfall zone’ as a covariable, had a higher average semivariance of 0.547 and a planar distance of 90km. The KED grid, produced with ‘Euclidean distance from ocean’ as a covariable, had the lowest average semivariance of 0.539 and a planar distance of 89 km.

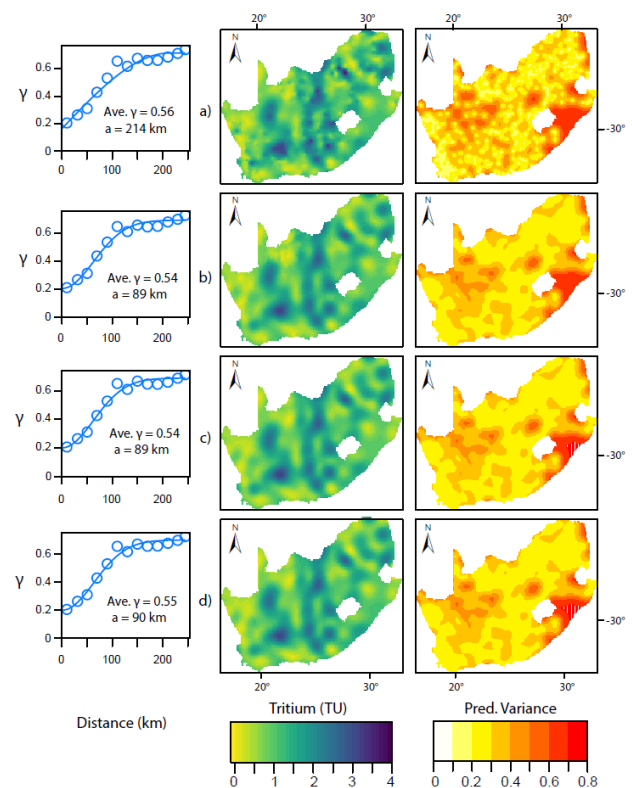


Figure 5 - The geostatistical results for variogram fit, predicted ^3H activity and prediction variance of a) the empirical calculation of ^3H distribution independent on external controls on activity and the residuals calculations of ^3H distribution dependent on external controls on activity for b) depth to water, c) summer vs winter rainfall and d) Euclidean distance from the ocean.

3.2. Predicted activity of ^3H in groundwater

Although the inclusion of environmental co variables greatly improved the prediction variance of ^3H , the regional distribution of ^3H was still heterogeneous across much of South Africa. The presented KED gridded values of ^3H in groundwater, which includes all environmental co-variables, ranged from <0.02 TU to > 3 TU. The highest

predicted ^3H activities were isolated to regions northwest of the town of Beaufort West and northeast of Kimberly (Fig.6). The northeast of the country near the town of Nelspruit as well as west of Pretoria, generally had elevated ^3H activities. The regions of lowest predicted ^3H activity occurred on the west and south coasts of South Africa as well as in the northern reaches of the central Karoo. The area around the town of Newcastle also showed low ^3H

activity in local groundwater. Coastal regions of South Africa had varying degrees of mid to low abundances of ^3H and showed partial correlation to South Africa's escarpment. The Karoo basin, which forms the largest aquifer system by extent, generally had higher, albeit variable, ^3H activities when compared to the rest of the country.

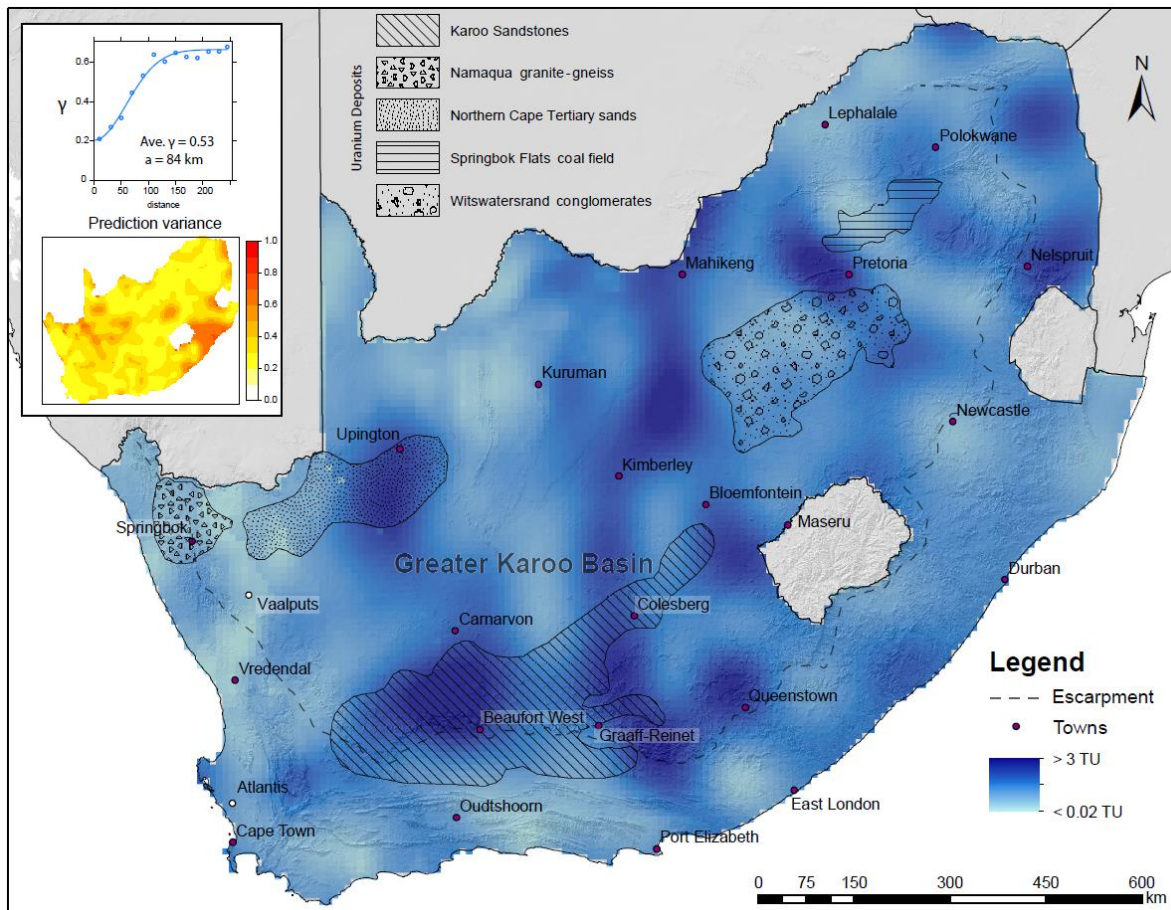


Figure 6 - The predicted distribution of ^3H in groundwater by KED with all environmental co-variables. The geostatistical results for variogram fit and prediction variance (top left) and the uranium deposit extents are overlaid onto the distribution surface as well as the location of the South African escarpment. Locations of interest are included for a radioactive waste disposal site (Vaalputs) and a managed aquifer recharge location (Atlantis).

4. Discussion

Predicting the distribution of ^3H activity in groundwater is essential for the assessment of regional recharge processes that effect both groundwater renewability (Gleeson et al., 2016) and modern pollution potential (Jasechko et al., 2017). Yet, regional predictions of groundwater ^3H activity can be affected by atmospheric, geographic and hydrogeological processes, including: [1] the variability of tritium in rainfall (van Rooyen et al., 2020a), [2] the decay of tritium in the unsaturated zone during recharge (Harvey et al., 2006; Le Gal La Salle et al., 2001) and, [3] the release of ^3H in the subsurface from

radioactive deposits (Dresel et al., 2000). The development of KED gridded distributions, that remove the spatial variance of environmental controls, allows for the assessment of: [1] the effective relationship between deeper groundwater wells/boreholes and ^3H activity, [2] the transfer or retention of atmospheric controls of ^3H activity in precipitation into the groundwater reservoir and, [3] the correlation of sites or natural features that might distort the atmospheric ^3H signal in groundwater.

4.1. Model validation and prediction variance

The performance of the KED model was tested via an out-of-sample verification, where random subsets of the testing data were excluded and then compared to the predicted surface. This was repeated fifteen times, in sample subsets of fifty, to produce a linear relationship of $R^2 = 0.554$ (Fig.7). The model prediction variance could be greatly improved with better sample distribution and density, as the current distribution is clustered as well as a better understanding of the actual water table rather than the calculated depth to groundwater. Similarly, the ^3H activities formed a clustered autocorrelation (Moran's $I = 0.25$). Given the z-score of 20.17, a metric of deviation from the mean, there is a less than 1% likelihood that this clustered pattern could be the result of random chance. An extensive autocorrelation analysis showed that regions of higher sample density were more likely to produce high-low/low-high outliers (Fig.8).

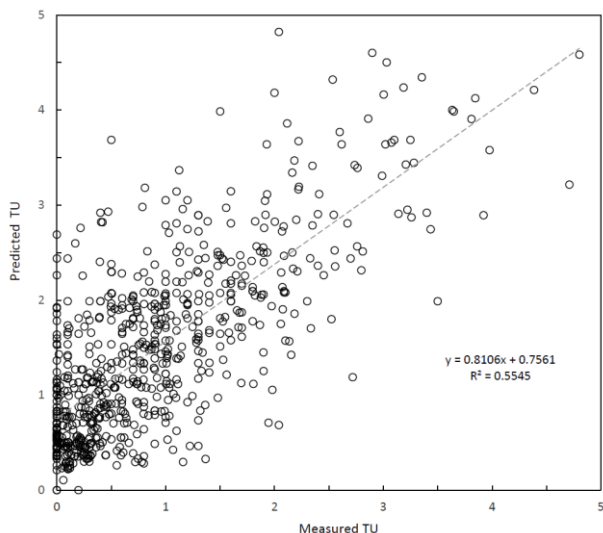


Figure 7 - Measured vs predicted ^3H activity in groundwater from the out-of-sample verification method.

Areas of high prediction variance were typically associated with areas of poor sample density, this was evident especially on the east coast of South Africa, as well as the northern central Karoo areas. In order to improve the predictive capabilities of this model, groundwater sampling would need to be done more rigorously in space and time to 'fill in' areas of poor sample density and assess the changes in ^3H activity over time. The depth to the groundwater had a significant effect on ^3H activity. It would therefore be essential to target regions with deeper groundwater wells to constrain this effect better and in turn calibrate the model for abrupt changes in groundwater

depth. Additionally, groundwater samples lack comprehensive data of borehole screens, leaving this predictive model to assume groundwater in South Africa behaves in one homogenous aquifer unit. Fortunately, this assumption is somewhat mitigated by the decay/flow relationship of tritium in groundwater, where long/slow flow paths will inherently have low ^3H activities, negating the need for aquifer separation in most cases. Nonetheless, a separated prediction for alluvial, unconfined and confined systems would improve the applicability for ^3H distributions in sustainability/resilience assessments.

4.2. Groundwater ^3H anomalies

Although the distribution of ^3H in groundwater, predicted by KED, was clustered and heterogeneous, the high and low anomalies in the data (Fig.8) correlated well to expected controls on the abundance of ^3H . The extensive high ^3H anomaly in the central Karoo has a distinct correlation with a large sandstone uranium province (Fig.6) (Kenan and Chirenje, 2016). Although the presence of uranium deposits is not typically associated with elevated groundwater ^3H activity, it has been reported that higher uranium concentrations were well correlated with ^3H in the Central Valley, California (Jurgens et al., 2010). Uranium deposits in South Africa could potentially produce significant amounts of ^3H through the decay, which has high concentrations of uranium in local groundwater (Dondo et al., 2010; Murray et al., 2015; Toens et al., 1998) and thus could elevate the natural signal contributed through recharge. Definitive evidence would need to be collected on ^3H production rates in uranium deposits in the region before confirming this contribution is sufficient. A similar phenomenon could be attributed to the alluvial uranium-rich deposits south of the town of Upington, where elevated tritium is predicted in a region of low rainfall (Fig.1) and a higher depth to groundwater (Fig.8). Conversely, the uranium-rich Witwatersrand conglomerates and the Springbok Flats coalfield, as well as South Africa's only radioactive waste disposal site (Vaalputs), correlate to low tritium anomalies, suggesting that groundwater ^3H activity is unaffected by the presence of uranium in these regions (Fig.6). The high anomaly above the town of Queenstown is not correlated to the presence of a uranium deposit, nor a known elevated activity in precipitation, and the region may simply experience higher rates of recharge than surrounding aquifers.

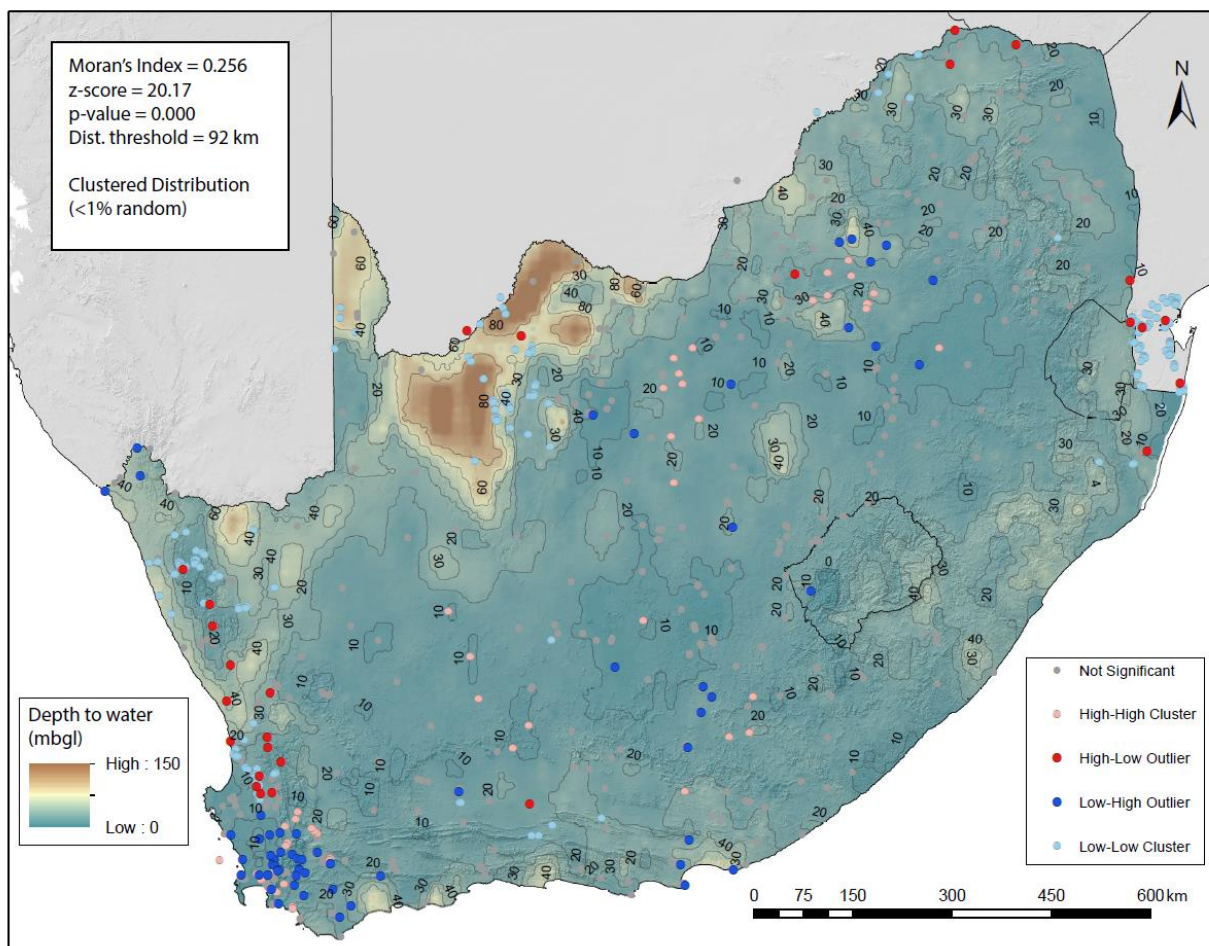


Figure 8 - Autocorrelation results for ^3H in groundwater which determines low and high clusters of samples as well as high-low and low-high outliers in the spatial dataset. Included are depth to water contours on the interpolated surface computed for this study.

4.3. ^3H and modern groundwater distributions

Modern recharge typically shares a similar ^3H activity to local precipitation available for recharge. Where groundwater ^3H anomalies cannot be explained by environmental factors that cause drift from recharge activities, active recharge is proportional to ^3H activity (Gleeson et al., 2016). The distribution of tritium in South African groundwater, unaffected by non-atmospheric ^3H , is somewhat consistent with the expected activity of ^3H in precipitation (van Rooyen et al., 2020a), where coastal regions have lower activity than inland regions (Fig.6). The effect of ocean water dilution in rainfall is not directly correlated with the distance from ocean of measured groundwater samples ($R^2 = 0.03$). However, coastal regions (<100 km from the ocean) generally have lower average ^3H activities that are not likely a result of less active recharge, as productive coastal aquifers are prevalent in South Africa (Pietersen et al., 2010). This would suggest that the effect of ocean dilution is experienced within a particular threshold of distance from the coast, potentially

the South African escarpment, but not further inland where terrestrial processes dominate (Fig.6).

It is not clear what effect groundwater abstraction has on ^3H activity, yet boreholes that are pumped excessively could induce the mixing of younger waters into deeper older systems, thus increasing ^3H activity (Visser et al., 2016). Anthropogenic influences, particularly dewatering of aquifers, on groundwater mixing could result in the overestimation of active recharge areas where groundwater use is particularly high. Conversely, managed aquifer recharge (MAR) programs would introduce ^3H faster than natural recharge processes, making measured ^3H activities non-representative. A known region of MAR, near Atlantis (Fig.6) is not predicted to have elevated ^3H activity and could be introducing ^3H at a localized scale too small for the resolution of this study.

Elevated ^3H activity within large aquifers in South Africa indicates that these groundwater resources are being actively recharged by modern precipitation. Research suggests that much of South Africa will experience less

frequent, but higher intensity, rainfall due to climate change (Schulze et al., 2010; Tadross et al., 2011). Consequently, these aquifers are particularly vulnerable to climate change, where changes in regional rainfall volumes and intensity will affect recharge (Taylor et al., 2013). Furthermore, areas of active recharge have a greater potential for contaminants to be transported into an aquifer. Regions where groundwater is abundant and aquifer yields are high, yet ^3H activity is low in relation to local rainfall, represent regions where recharge is less active and fossil groundwater is prevalent. Although older groundwater may have a lower sustainable yield, it is less likely to be immediately affected by climate change and may be more resilient to abrupt changes to the hydrological cycle. Furthermore, younger groundwater is not necessarily more sustainable as long groundwater flow paths could still be actively recharged by modern precipitation (Ferguson et al., 2020).

4.4. Current and future context of ^3H distributions

The distribution of ^3H in groundwater has been successfully used to predict modern groundwater distributions (Gleeson et al., 2016), deep groundwater contamination (Jasechko et al., 2017), groundwater contribution to streamflow (Morgenstern et al., 2010), pollutant transport from landfills (Robinson and Gronow, 1996), nuclear fall-out (Matsumoto et al., 2013) and groundwater vulnerability (van Rooyen et al., 2020b). Yet, the availability of ^3H activity distributions, as an interpolated surface, is uncommon or non-existent, as studies do not typically measure ^3H over large spatial extents with regular distributions. This may be a result of researches believing the applicability of ^3H in hydrological studies is dissipating with the attenuation of bomb peak activities (Rahn et al., 2017). However, with the progression of analytical techniques, the assessment of background levels of tritium presents new potential applications of ^3H in hydrology and related fields of study. It is postulated in this study that the presence of radioactive deposits (i.e. uranium) may have a substantial affect on ^3H activity, suggesting ^3H could have applications in exploration. Nonetheless, more robust interpretations of the above uses for ^3H distributions could be made with regular monitoring of well distributed samples locations, as were in California by Visser et al., (2016). A similar approach was undertaken in Kern et al., (2020), where temporal records of precipitation from multiple stations in

the Adriatic-Pannonian region were used to build isoscapes of ^3H in precipitation. The monitoring of environmental ^3H at such a resolution that isoscapes can be compared over time would require an improvement in local analytical capabilities in southern Africa.

5. Conclusions

Analysis of 722 data points across South Africa and southern Mozambique found that the spatial distribution of ^3H activities in groundwater was relatively heterogeneous. Yet, geostatistical analysis found that significant spatial structure can be attributed to environmental controls on activity other than subsurface decay. When excluded as external drift in universal kriging operations, environmental controls improve the average prediction semivariance by 0.03. Significant high ^3H anomalies in the predicted distribution in groundwater could be attributed to the presence of uranium rich deposits in the Karoo Basin sandstones and northern Karoo alluvial deposits, yet more evidence would need to be collected to propose this definitively. Notable areas of less active groundwater recharge occurred on the west coast of South Africa as well as the central and northern Karoo. Regions of more active recharge are noted in the north eastern areas of South Africa as well as the western borders of Lesotho. Regions of active recharge are more vulnerable to disruptions to the hydrological cycle as a result of climate change as well as the potential infiltration of contaminants into the groundwater system. Conversely, groundwater that is less actively recharge may be more resilient to climate change yet represents a potentially non-renewable resource for abstraction. The distribution of ^3H in groundwater surface developed in this study has potential applications in modern groundwater distribution, groundwater vulnerability and radioactive deposit investigations. Applications which are pertinent to the development of sustainable groundwater management strategies and hydrological resilience assessments.

Acknowledgements

We thank the Water Research Commission South Africa for initial funding support and the iPhakade program and National Research Foundation South Africa for bursary support. This work is also based on research supported in part by the National Research Foundation of South Africa (Grant number: 118594) and was partly supported by the European Union and the State of Hungary, co-financed by the European Regional Development Fund in the project of

GINOP-2.3.2-15-2016-00009 'ICER'. The authors would like to acknowledge the assistance of the University of Utah's ITCE SPATIAL program for providing the training necessary to construct the model presented in this paper. This publication forms part of the output of the Biogeochemistry Research Infrastructure Platform (BIOGRIP) of the Department of Science and Innovation of South Africa. This contribution has an iPhakade publication number of 257.

References

- Basson, M.S., Van Niekerk, P.H., Van Rooyen, J.A., 1997. Overview of water resources availability and utilisation in South Africa. Department of Water Affairs and Forestry.
- Bennetts, D.A., Webb, J.A., Stone, D.J.M., Hill, D.M., 2006. Understanding the salinisation process for groundwater in an area of south-eastern Australia, using hydrochemical and isotopic evidence. *J. Hydrol.* 323, 178–192. <https://doi.org/10.1016/j.jhydrol.2005.08.023>
- Böhlke, J.K., 2002. Groundwater recharge and agricultural contamination. *Hydrogeol. J.* 10, 153–179. <https://doi.org/10.1007/s10040-001-0183-3>
- Böhlke, J.K., Denver, J.M., 1995. Combined use of groundwater dating, chemical, and isotopic analyses to resolve the history and fate of nitrate contamination in two agricultural watersheds, Atlantic coastal plain, Maryland. *Water Resour. Res.* 31, 2319–2339.
- Chilès, J.-P., 2012. The Generalized Variogram 33.
- Cobbing, J.E., Hobbs, P.J., Meyer, R., Davies, J., 2008. A critical overview of transboundary aquifers shared by South Africa. *Hydrogeol. J.* 16, 1207–1214. <https://doi.org/10.1007/s10040-008-0285-2>
- Cuthbert, M.O., Gleeson, T., Moosdorf, N., Befus, K.M., Schneider, A., Hartmann, J., Lehner, B., 2019. Global patterns and dynamics of climate-groundwater interactions. *Nat. Clim. Chang.* 9, 137–141. <https://doi.org/10.1038/s41558-018-0386-4>
- Díaz-Cruz, M.S., Barceló, D., 2008. Trace organic chemicals contamination in ground water recharge. *Chemosphere* 72, 333–342. <https://doi.org/10.1016/j.chemosphere.2008.02.031>
- Dondo, C., Woodford, A.C., Murray, R., Nhleko, L.O., Gqiba, D., Chevallier, L., 2010. Flow conceptualisation, recharge and storativity determination in karoo aquifers, with special emphasis on Mzimvubu Keiskamma and Mvoti-Umzimkulu water management areas in the Eastern Cape and Kwazulu-Natal provinces of South Africa. WRC Rep.
- Dresel, P.E., Williams, B.A., Evans, J.C., Smith, R.M., Thompson, C.J., Hulstrom, L.C., Dresel, P.E., Williams, B.A., Evans, J.C., Smith, R.M., Thompson, C.J., Hulstrom, L.C., 2000. Evaluation of Elevated Tritium Levels in Groundwater Downgradient from the 618-11 Burial Ground Phase I Investigation.
- DWAF, 2004. Overview of the South African Water Sector. *Natl. water Resour. Strateg.* 1, 1–35.
- Ferguson, G., Gleeson, T., 2012. Vulnerability of coastal aquifers to groundwater use and climate change. *Nat. Clim. Chang.* 2, 342–345. <https://doi.org/10.1038/nclimate1413>
- Gillon, M., Barbecot, F., Gibert, E., Corcho Alvarado, J.A., Marlin, C., Massault, M., 2009. Open to closed system transition traced through the TDIC isotopic signature at the aquifer recharge stage, implications for groundwater ^{14}C dating. *Geochim. Cosmochim. Acta* 73, 6488–6501. <https://doi.org/10.1016/j.gca.2009.07.032>
- Gleeson, T., Befus, K.M., Jasechko, S., Luijendijk, E., Cardenas, M.B., 2016. The global volume and distribution of modern groundwater. *Nat. Geosci.* 9, 161–164. <https://doi.org/10.1038/ngeo2590>
- Gleeson, T., Befus, K.M., Jasechko, S., Luijendijk, E., Cardenas, M.B., 2015. The global volume and distribution of modern groundwater. *Nat. Geosci. Advance on*, 1–15. <https://doi.org/10.1038/ngeo2590>
- Hagedorn, B., Clarke, N., Ruane, M., Faulkner, K., 2018. Assessing aquifer vulnerability from lumped parameter modeling of modern water proportions in groundwater mixtures: Application to California's South Coast Range. *Sci. Total Environ.* 624, 1550–1560. <https://doi.org/10.1016/j.scitotenv.2017.12.115>
- Harms, P.A., Visser, A., Moran, J.E., Esser, B.K., 2016. Distribution of tritium in precipitation and surface water in California. *J. Hydrol.* 534, 63–72.
- Harvey, J.W., Newlin, J.T., Krupa, S.L., 2006. Modeling decadal timescale interactions between surface water and ground water in the central Everglades, Florida, USA. *J. Hydrol.* 320, 400–420. <https://doi.org/10.1016/J.JHYDROL.2005.07.024>
- Hughes, C.E., Cendón, D.I., Harrison, J.J., Hankin, S.I., Johansen, M.P., Payne, T.E., Vine, M., Collins, R.N., Hoffmann, E.L., Loosz, T., 2011. Movement of a tritium plume in shallow groundwater at a legacy low-level radioactive waste disposal site in eastern Australia. *J. Environ. Radioact.* 102, 943–952. <https://doi.org/10.1016/j.jenvrad.2010.05.009>
- Jasechko, S., Perrone, D., Befus, K.M., Bayani Cardenas, M., Ferguson, G., Gleeson, T., Luijendijk, E., McDonnell, J.J., Taylor, R.G., Wada, Y., Kirchner, J.W., 2017. Global aquifers dominated by fossil groundwaters but wells vulnerable to

- modern contamination. *Nat. Geosci.* 10, 425–429. <https://doi.org/10.1038/ngeo2943>
- Jurgens, B.C., Fram, M.S., Belitz, K., Burow, K.R., Landon, M.K., 2010. Effects of Groundwater Development on Uranium: Central Valley, California, USA. *Ground Water* 48, 913–928. <https://doi.org/10.1111/j.1745-6584.2009.00635.x>
- Kenan, A.O., Chirenje, E., 2016. Uranium in South Africa: Exploration and Supply Capacity. *Nat. Resour. Conserv.* 4, 25–33. <https://doi.org/10.13189/nrc.2016.040201>
- Kern, Z., Erdélyi, D., Vreča, P., Krajcar Bronić, I., Fórizs, I., Kanduč, T., Štok, M., Palcsu, L., Süveges, M., Czuppon, G., Kohán, B., Gábor Hatvani, I., 2020. Isoscape of amount-weighted annual mean precipitation tritium (^3H) activity from 1976 to 2017 for the Adriatic–Pannonian region – AP^3H_v1 database. *Earth Syst. Sci. Data* 12, 2061–2073. <https://doi.org/10.5194/essd-12-2061-2020>
- Le Gal La Salle, C., Marlin, C., Leduc, C., Taupin, J.D., Massault, M., Favreau, G., 2001. Renewal rate estimation of groundwater based on radioactive tracers (^3H , ^{14}C) in an unconfined aquifer in a semi-arid area, Iullemeden basin, Niger. *J. Hydrol.* 254, 145–156. [https://doi.org/10.1016/S0022-1694\(01\)00491-7](https://doi.org/10.1016/S0022-1694(01)00491-7)
- Li, Z., Jasechko, S., Si, B., 2019. Uncertainties in tritium mass balance models for groundwater recharge estimation. *J. Hydrol.* 571, 150–158. <https://doi.org/10.1016/j.jhydrol.2019.01.030>
- Lucas, L.L., Unterweger, M.P., 2000. Comprehensive Review and Critical Evaluation of the Half-Life of Tritium. *J. Res. Natl. Inst. Stand. Technol.* 105, 541–549. <https://doi.org/10.6028/jres.105.043>
- MacMahon, D., 2006. Half-life evaluations for ^3H , ^{90}Sr , and ^{90}Y . *Appl. Radiat. Isot.* 64, 1417–1419. <https://doi.org/10.1016/j.apradiso.2006.02.072>
- Mao, F., Clark, J., Karpouzoglou, T., Dewulf, A., Buytaert, W., Hannah, D., 2017. HESS Opinions: A conceptual framework for assessing socio-hydrological resilience under change. *Hydrol. Earth Syst. Sci.* 21, 3655–3670. <https://doi.org/10.5194/hess-21-3655-2017>
- Matheron, G., 1965. Les variables régionalisées et leur estimation: une application de la théorie des fonctions aléatoires aux sciences de la nature. Masson et CIE.
- Matsumoto, T., Maruoka, T., Shimoda, G., Obata, H., Kagi, H., Suzuki, K., Yamamoto, K., Mitsuguchi, T., Hagino, K., Tomioka, N., Sambandam, C., Brummer, D., Klaus, P.M., Aggarwal, P., 2013. Tritium in Japanese precipitation following the March 2011 Fukushima Daiichi Nuclear Plant accident. *Sci. Total Environ.* 445–446, 365–370. <https://doi.org/10.1016/j.scitotenv.2012.12.069>
- Meixner, T., Manning, A.H., Stonestrom, D.A., Allen, D.M., Ajami, H., Blasch, K.W., Brookfield, A.E., Castro, C.L., Clark, J.F., Gochis, D.J., Flint, A.L., Neff, K.L., Niraula, R., Rodell, M., Scanlon, B.R., Singha, K., Walvoord, M.A., 2016. Implications of projected climate change for groundwater recharge in the western United States. *J. Hydrol.* 534, 124–138. <https://doi.org/10.1016/j.jhydrol.2015.12.027>
- Morgenstern, U., Stewart, M.K., Stenger, R., 2010. Dating of streamwater using tritium in a post nuclear bomb pulse world: Continuous variation of mean transit time with streamflow. *Hydrol. Earth Syst. Sci.* 14, 2289–2301. <https://doi.org/10.5194/hess-14-2289-2010>
- Murray, R., Swana, K., Miller, J., Talma, S., Tredoux, G., Vengosh, A., Darrah, T., 2015. The Use of Chemistry, Isotopes and Gases as Indicators of Deeper Circulating Groundwater in the Main Karoo Basin: Report to the Water Research Commission. Water Research Commission.
- Niang, I., Ruppel, O.C., Abdrabo, M.A., Essel, A., Lennard, C., Padgham, J., Urquhart, P., 2014. Africa Climate Change 2014: Impacts, Adaptation, and Vulnerability. Part B: Regional Aspects. Contribution of Working Group II to the Fifth Assessment Report of the Intergovernmental Panel on Climate Change ed VR Barros et al.
- Palcsu, L., Kompár, L., Deák, J., Szucs, P., Papp, L., 2017. Estimation of the natural groundwater recharge using tritium-peak and tritium/helium-3 dating techniques in Hungary. *Geochem. J.* 51, 439–448. <https://doi.org/10.2343/geochemj.2.0488>
- Palcsu, L., Major, Z., Köllő, Z., Papp, L., 2010. Using an ultrapure ^4He spike in tritium measurements of environmental water samples by the ^3He -ingrowth method. *Rapid Commun. Mass Spectrom. An Int. J. Devoted to Rapid Dissem. Up-to-the-Minute Res. Mass Spectrom.* 24, 698–704.
- Papp, L., Palcsu, L., Major, Z., Rinyu, L., Tóth, I., 2012. A mass spectrometric line for tritium analysis of water and noble gas measurements from different water amounts in the range of microlitres and millilitres noble gas measurements from different water amounts in the. *Isot. environmental* 6016. <https://doi.org/10.1080/10256016.2012.679935>
- Pietersen, K., Kellgren, N., Roos, M., De Vries, P., 2010. Explanatory Brochure for the South African Development Community (SADC) Hydrogeological Map & Atlas. Explan. Broch. South African Dev. Community 1–51.
- Plastino, W., Chereji, I., Cuna, S., Kaihola, L., De Felice, P., Lupsa, N., Balas, G., Mirel, V., Berdea, P., Baciu, C., 2007. Tritium in water electrolytic enrichment and liquid scintillation

- counting. *Radiat. Meas.* 42, 68–73. <https://doi.org/10.1016/j.radmeas.2006.07.010>
- Ploner, A., 1999. The use of the variogram cloud in geostatistical modelling. *Environmetrics* 10, 413–437. [https://doi.org/10.1002/\(sici\)1099-095x\(199907/08\)10:4<413::aid-env365>3.0.co;2-u](https://doi.org/10.1002/(sici)1099-095x(199907/08)10:4<413::aid-env365>3.0.co;2-u)
- Rahn, P.H., Detwiler, A.G., Davis, A.D., 2017. Tritium in groundwater in the Black Hills of South Dakota. *Environ. Earth Sci.* 76, 1–11. <https://doi.org/10.1007/s12665-017-7082-y>
- Robinson, H.D., Gronow, J.R., 1996. Tritium levels in leachates and condensates from domestic wastes in landfill sites. *Water Environ. J.* 10, 391–398. <https://doi.org/10.1111/j.1747-6593.1996.tb00070.x>
- Roffe, S.J., Fitchett, J.M., Curtis, C.J., 2019. Classifying and mapping rainfall seasonality in South Africa: a review. *South African Geogr. J.* 101, 158–174. <https://doi.org/10.1080/03736245.2019.1573151>
- Rossiter, D.G., Eda, N., 2019. An introduction to (geo) statistics with R.
- Samborska, K., Rózkowski, A., Małoszewski, P., 2013. Estimation of groundwater residence time using environmental radioisotopes (^{14}C , T) in carbonate aquifers, southern Poland. *Isotopes Environ. Health Stud.* 49, 73–97. <https://doi.org/10.1080/10256016.2012.677041>
- Schlosser, P., Stute, M., Sonntag, C., Otto Münnich, K., 1989. Tritogenic ^3He in shallow groundwater. *Earth Planet. Sci. Lett.* 94, 245–256. [https://doi.org/10.1016/0012-821X\(89\)90144-1](https://doi.org/10.1016/0012-821X(89)90144-1)
- Schoups, G., Hopmans, J.W., Young, C.A., Vrugt, J.A., Wallender, W.W., Tanji, K.K., Panday, S., 2005. Sustainability of irrigated agriculture in the San Joaquin Valley, California. *Proc. Natl. Acad. Sci.* 102, 15352–15356. <https://doi.org/10.1073/pnas.0507723102>
- Schulze, R., Kunz, R., Knoesen, D., 2010. Atlas of climate change and water resources in South Africa. Water Res. Comm. Pretoria, Pretoria.
- Schulze, R.E., Lynch, S.D., Maharaj, M., 2006. Annual Precipitation. South African Atlas Climatol. Agrohydrology. Water Res. Comm. Pretoria, RSA, WRC Rep. 489/1/06, Section 6.2.
- Stewart, M.K., 2012. A 40-year record of carbon-14 and tritium in the Christchurch groundwater system, New Zealand: Dating of young samples with carbon-14. *J. Hydrol.* 430–431, 50–68. <https://doi.org/10.1016/j.jhydrol.2012.01.046>
- Tadross, M., Davis, C., Engelbrecht, F., Joubert, A., Archer, E.R.M., 2011. Regional scenarios of future climate change over southern Africa. CSIR.
- Taylor, R.G., Todd, M.C., Kongola, L., Maurice, L., Nahozya, E., Sanga, H., Macdonald, A.M., 2013. Evidence of the dependence of groundwater resources on extreme rainfall in East Africa. *Nat. Clim. Chang.* 3, 374–378. <https://doi.org/10.1038/nclimate1731>
- Toens, P.D., Standler, W., Wullschleger, N.J., 1998. The association of groundwater chemistry and geology with atypical lymphocytes (as a biological indicator) in the Pofadder area, North Western Cape, South Africa 64.
- van Rooyen, J.D., Palcsu, L., Visser, A., Vennemann, T.W., Miller, J.A., 2020a. Spatial and temporal variability of tritium in precipitation in South Africa and it's bearing on hydrological studies. *J. Environ. Radioact.* 106354. <https://doi.org/10.1016/j.jenvrad.2020.106354>
- van Rooyen, J.D., Watson, A.P., Miller, J.A., 2020b. Combining quantity and quality controls to determine groundwater vulnerability to depletion and deterioration throughout South Africa. *Environ. Earth Sci.* 79. <https://doi.org/10.1007/s12665-020-08998-1>
- Vengosh, A., Gill, J., Davisson, M.L., Hudson, G.B., 2002. A Multi-isotope (^3H , ^8B , ^87Sr , ^2H , ^{13}C) and Age Dating (^3H - ^3He , ^{14}C) Study of Ground Water from Salinas Valley California : Hydrochemistry, Dynamics, and Contamination Processes. *Water Resour. Res.* 38, 9 1–17. <https://doi.org/10.1029/2001WR000517>
- Villholth, K.G., Tøttrup, C., Stendel, M., Maherry, A., 2013. Integrated mapping of groundwater drought risk in the Southern African Development Community (SADC) region. *Hydrogeol. J.* 21, 863–885. <https://doi.org/10.1007/s10040-013-0968-1>
- Visser, A., Moran, J.E., Hillemonds, D., Singleton, M.J., Kulongoski, J.T., Belitz, K., Esser, B.K., 2016. Geostatistical analysis of tritium, groundwater age and other noble gas derived parameters in California. *Water Res.* 91, 314–330. <https://doi.org/10.1016/j.watres.2016.01.004>
- Visser, A., Thaw, M., Esser, B., 2018. Analysis of air mass trajectories to explain observed variability of tritium in precipitation at the Southern Sierra Critical Zone Observatory, California, USA. *J. Environ. Radioact.* 181, 42–51. <https://doi.org/10.1016/j.jenvrad.2017.10.008>
- Wada, Y., Van Beek, L.P.H., Van Kempen, C.M., Reckman, J.W.T.M., Vasak, S., Bierkens, M.F.P., 2010. Global depletion of groundwater resources. *Geophys. Res. Lett.* 37, 1–5. <https://doi.org/10.1029/2010GL044571>
- West, J.B., Bowen, G.J., Dawson, T.E., Tu, K.P., 2009. Isoscapes: understanding movement, pattern, and process on Earth through isotope mapping. Springer.

Chapter 4 – Tritium in Groundwater

Zhang, L., Dawes, W.R., Walker, G.R., 2001. Response of mean annual evapotranspiration to vegetation changes at catchment scale. *Water Resour. Res.* 37, 701–708.

Zuber, A., Witczak, S., Rózański, K., Śliwka, I., Opoka, M., Mochalski, P., Kuc, T., Karlikowska, J., Kania, J., Jackowicz-

Korczyński, M., Duliński, M., 2005. Groundwater dating with ^3H and SF_6 in relation to mixing patterns, transport modelling and hydrochemistry. *Hydrol. Process.* 19, 2247–2275. <https://doi.org/10.1002/hyp.5669>

CHAPTER 5 GROUNDWATER VULNERABILITY

PUBLICATION HISTORY	
Title	Combining quantity and quality controls to determine groundwater vulnerability to depletions and deterioration throughout South Africa
Journal	Environmental Earth Sciences IF=2.180 (2019)
Status	Published
Authors and roles	J.D. van Rooyen – PhD Candidate J.A. Miller – Primary Supervisor A.P Watson – Co-Author
Applicant Contribution	Field sampling, data collation, model development and construction, statistical coding in R, Interpretation of results and wrote the manuscript.

ORIGINAL ARTICLE

Combining quantity and quality controls to determine groundwater vulnerability to depletion and deterioration throughout South Africa

J. D. van Rooyen¹  · A. P. Watson¹  · J. A. Miller¹ Received: 13 August 2019 / Accepted: 13 May 2020
© Springer-Verlag GmbH Germany, part of Springer Nature 2020

Abstract

Groundwater vulnerability is normally associated with the potential for contamination, for example the DRASTIC approach, but the increasing importance of groundwater in human, agricultural, and industrial systems, implies that groundwater vulnerability is dependent on a range of other parameters and particularly parameters impacted by climate change. A robust method for evaluating groundwater vulnerability therefore requires the incorporation of multiple indices into one holistic evaluation. In this study, a model for groundwater vulnerability in South Africa was developed, calculating the combined weighted averages of nine spatial datasets; namely: (1) mean annual precipitation, (2) mean annual surface temperature, (3) tritium distribution in groundwater, (4) potential evaporation, (5) aquifer type and yield, (6) terrain slope, (7) electrical conductivity, (8) population density and (9) cultivated land use. The model was run through 36 different weighting scenarios and indicates that on average 22.4% of South Africa's groundwater is predicted to have a very high vulnerability to depletion in quantity and deterioration in quality (12.2% very low; 35.4% low; 16.8% moderate and 13.1% high). A single weighting scenario (M-I/C-2/P-2) was chosen that showed good alignment to the previous assessments that predicted that 20.9% of groundwater resources in South Africa have very high vulnerability (1.5% very low; 35.7% low; 24.9% moderate and 17.0% high). The model was adjusted to reflect climate conditions 50 years into the future, resulting in a 3% increase in very high vulnerability areas and a 6% decrease in low vulnerability areas. The results suggest that large areas of South Africa have high groundwater vulnerability, especially in areas where groundwater supplements domestic supply and agriculture. The implementation of this method to evaluate groundwater vulnerability across diverse natural environments and political boundaries will supplement comprehensive groundwater vulnerability assessments and the development of effective groundwater management policy.

Keywords Groundwater vulnerability · Climate change · GCM · GIS

Introduction

In the recent decades, changing climate patterns and increasing precipitation variability have seen groundwater abstraction on a global scale increase significantly (Green et al. 2011; Holman 2006; Richey et al. 2015; Smerdon

2017). Much of the increase in groundwater abstraction has occurred in highly concentrated areas to support urbanization and agricultural activities that provide food security (Famiglietti 2014). As a result, groundwater depletion, the permanent lowering of the water table due to over-abstraction is occurring across the globe (Treidel et al. 2011; Wada et al. 2010) at a range of scales from individual catchments (Tallaksen et al. 2009; Woldeamlak et al. 2007), to regional aquifer systems including transboundary aquifers (Changming et al. 2001; Hamed et al. 2014; Rodell et al. 2015; Scanlon et al. 2012). The consequences of groundwater over-abstraction have important implications for the management of aquifer systems, and have contributed significantly to how researchers think about groundwater sustainability, where sustainability is regarded as a volume concept i.e., is there sufficient groundwater to sustain society and the

✉ J. D. van Rooyen
16469003@sun.ac.za

A. P. Watson
awatson@sun.ac.za

J. A. Miller
jmiller@sun.ac.za

¹ Department of Earth Sciences, Faculty of Sciences,
University of Stellenbosch, Private Bag X1, Matieland 7601,
South Africa

environment (Aeschbach-Hertig and Gleeson 2012; Gorelick and Zheng 2015; Konikow and Kendy 2005). This has become even more critical as the realities of climate change become apparent and attention turns to hydrological resilience of the global water cycle.

The impact of climate change has become an increasingly important, but often overlooked factor in assessing groundwater sustainability (Döll 2009). This is partly because the impact of drought on groundwater is not visually apparent the way it is for a surface water reservoir. Drought most directly impacts young groundwater systems that are recently recharged by modern precipitation. It has a less immediate impact on older fossil groundwater systems that are typically isolated from modern climate fluctuations. As a result, differentiating between aquifers that are dominated by either modern groundwater or fossil groundwater has become an important component of global groundwater resource evaluation (Gleeson et al. 2015; Jasechko et al. 2017). Although, multiple methods have been used as modern water tracers, such as CFCs, SF₆ and environmental isotopes, differentiation of modern and fossil groundwater is often performed using a radioactive isotope to investigate residence time constraints. One of the most useful radioactive isotopes is tritium (³H) that has a half-life of only 12.43 years. Because the half-life is relatively short, the presence or absence of tritium has been used to differentiate modern (containing ³H) vs fossil groundwater (not containing ³H) (Gleeson et al. 2015). Because shallow groundwater is more likely to be actively recharged, tritium can also be used as a proxy for the potential for shallow groundwater to mix with older fossil groundwater, and in turn recharge larger, much older groundwater resources (Jasechko et al. 2017). The distinction between older, not actively recharged groundwater and shallow, actively recharged groundwater allows for the assessment of how vulnerable a groundwater resource is to depletion.

The concept of sustainability is generally seen as distinct from vulnerability, where vulnerability is regarded as a quality issue. Early development of methods for assessing groundwater vulnerability focused on an aquifers potential for contamination and produced the GOD rating system (Foster 1987) and DRASTIC method (Aller et al. 1987). Subsequently, other vulnerability evaluation methods have been adapted from these initial approaches (Civita 1994; Doerfliger and Zwahlen 1997; Stempvoort et al. 1993). Global studies on human adaptive strategies to climate change usually incorporate significant groundwater dependence (Adger et al. 2005; Agder and Nelly 1999; Kelly and Adger 2000), but methods that assess groundwater vulnerability to pollution are not suited for assessing the potential effect of climate change on groundwater depletion (Corniello et al. 1997). Additionally, the quality of a groundwater resource is not only dependent on anthropogenic pollutants/

contaminants, but also can deteriorate through natural processes, e.g., salinization (Vengosh 2013). In this respect, several studies have been successful in predicting groundwater depletion/deterioration through careful evaluation of historic land use change (Harbor 1994; Scanlon et al. 2005). Although efforts to assess groundwater vulnerability to contaminants, climate change, or land use change are justified independently, hydrological systems are dynamic and simultaneously vulnerable to both contamination and temporal climatic fluctuations. Potentially, the most holistic approaches are those that try to estimate groundwater drought risk as they incorporate meteorological, chemical and physical groundwater attributes as well as anthropogenic dependence and capacity over a variable timescale (Villholth et al. 2013).

This article presents a new holistic model for groundwater vulnerability, where vulnerability incorporates both depletion in groundwater quantity as well as a deterioration in quality. The model incorporates nine different spatial datasets of groundwater vulnerability controlling parameters, specifically including an isotope tracer (tritium) and uses a weighted index-overlay method to output the spatial distribution of groundwater vulnerability on a scale from 1 to 8, where 1 is least vulnerable and 8 is most vulnerable. The assessment is structured with multiple scenarios that focus on controls on either quantity or quality or both. Subsequently, parameters that directly relate to climate can be adjusted according to different global circulation models (GCMs) to predict the evolution of groundwater vulnerability with climate change. The model is applied to South Africa, where the recent drought conditions have brought the vulnerability of the groundwater system to the forefront of public discourse.

Much of this discourse centered on Cape Town, South Africa's largest coastal city, because of severe water shortages during the 2017–2018 summer, when it seemed possible that the city's water supply would run out. However, the water crisis represented only a small component of a much wider and longer drought crisis affecting large parts of the country. The City of Cape Town has put in place measures to augment the surface water supply with groundwater, but this has prompted heightened concerns about the long-term vulnerability of the local groundwater system to deterioration in both quantity and quality. In the past two decades, South Africa has developed two National Water Resource Strategies (NWRS). The first delineated nineteen water management areas (WMAs) in 2004 and the second implemented an amendment to reduce this to only nine Catchment Management Agencies (CMAs) in 2013 (Fig. 1). Both delineations overlap with provincial and municipal boundaries and in turn create a 'trans-boundary' like scenario, where authorities must deal with the disparities between the resource requirements of local populations and agricultural activities,

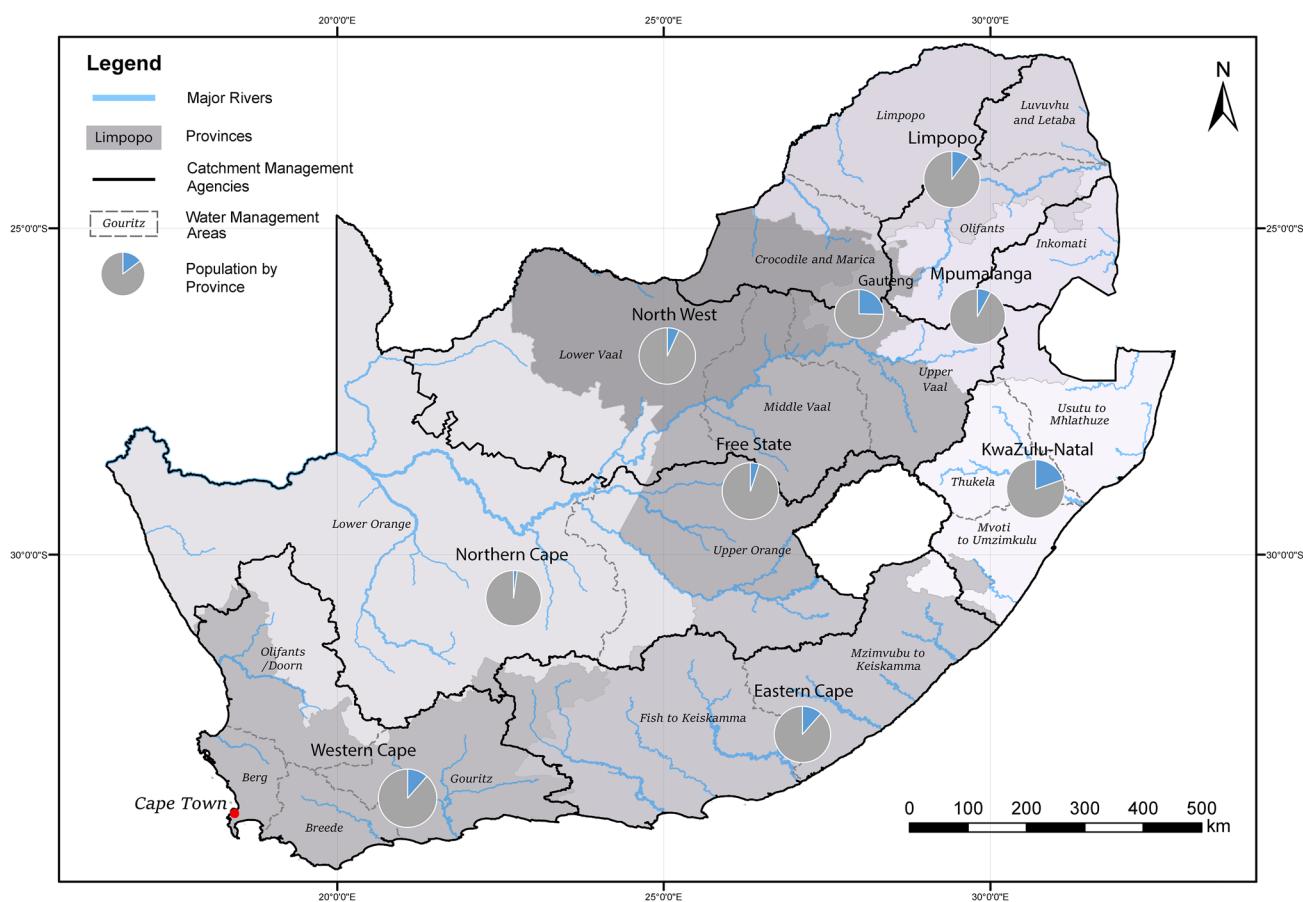


Fig. 1 Distribution of South Africa's population per province (grey shaded regions) represented as percentage of total population (Census 2011). South Africa is divided into nineteen water management areas (WMA's) according to NWRS-1 (stippled grey lines) and dark boundaries represent the revised nine Catchment Management

Agency (CMA) boundaries developed in NWRS-2. Major river systems are represented as the order of the river from source with varying thickness (note: some provincial boundaries are marked by major river systems)

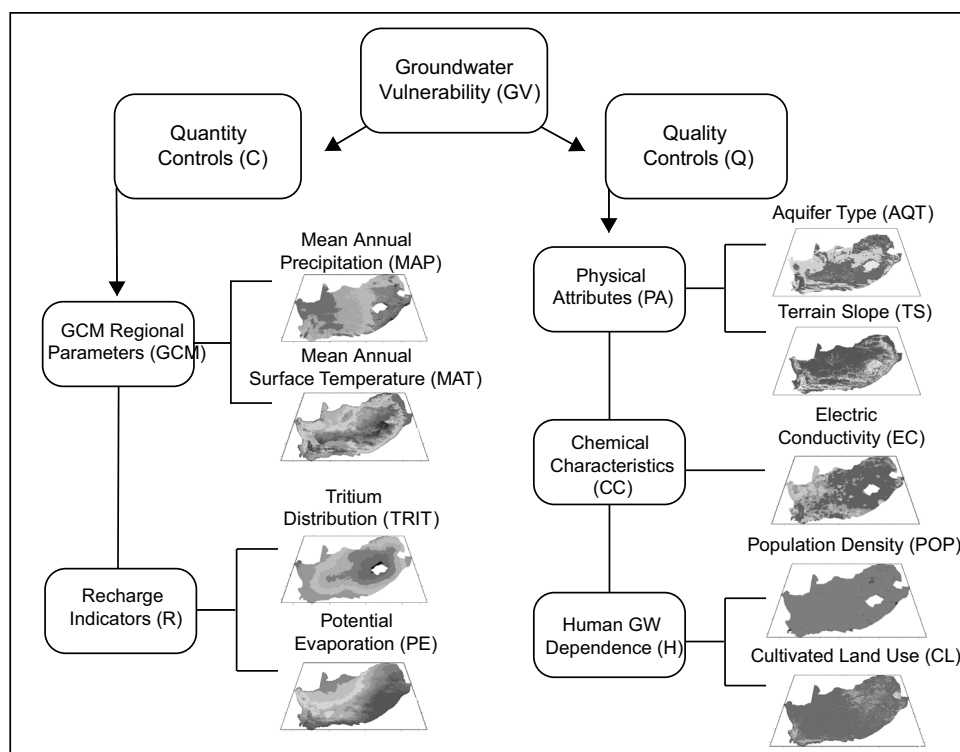
national resource strategies and the ecological reserve. To demonstrate the flexibility of this groundwater vulnerability model to evaluate these types of problems, this study applies the model to South Africa's complex water management agency framework and discusses how this relates to municipal and provincial boundaries (Fig. 1). The results can be directly translated to large-scale transboundary aquifer systems and provide a framework for future management of groundwater resources across the globe, whilst still being flexible enough to evaluate the groundwater vulnerability of a single urban center like the city of Cape Town.

Methodology

The groundwater vulnerability model identifies nine separate parameters derived from previous studies that have significant control on either the quantity or quality of a groundwater resource (Aller et al. 1987; Villholth et al. 2013). The

model allocates parameters to one of two groups, called major strategies in the model framework (Fig. 2): (1) a group associated with climatic conditions, which control the quantity of groundwater being actively recharged and (2) a group associated with factors that impact on groundwater quality, through the ease of infiltration, current groundwater quality and anthropogenic influences. The parameters were incorporated into frameworks that indicate: (1) how each parameter is grouped; (2) how the weighting of each group is allocated and (3) how the model sensitivity is calculated. The vulnerability is determined through iterative combinations of different subsection weightings and individual parameter weightings, taking into account errors associated with each model scenario and how these uncertainties are minimized in the selected scenario. This model differs from other popular approaches through the incorporation of a framework that investigates quantity and quality controls separately before combining them, as well as allowing for a variable weighting scheme of input parameters.

Fig. 2 Model framework of the thematic layers, divided into two major subheadings and five minor subheadings, representing major and minor strategies



Input parameters

The nine input parameters identified as significant controls on groundwater vulnerability are: (1) mean annual precipitation, (2) mean annual surface temperature, (3) tritium distribution in groundwater, (4) potential evaporation, (5) aquifer type and yield, (6) terrain slope, (7) electrical conductivity, (8) population density and (9) cultivated land use. The data source(s) for each parameter, including temporal and spatial resolution are given in Table 1. The nine input parameters are divided across five subheadings according to their collective contributions to the final groundwater vulnerability. The five subheadings, which in the model are described as minor strategies, are: (1) GCM regional parameters that indicate the current climate and in turn allude to the available water budget; (2) recharge indicators, that represent how actively recharged regions are and the potential for evaporation to limit this recharge; (3) physical attributes, that control how likely a contaminant, anthropogenic or natural, can infiltrate and be transported through the subsurface; (4) chemical characteristics, that indicate the degree to which groundwater quality has already deteriorated and (5) human groundwater dependence, that characterizes areas where human settlements and agriculture are likely to increase abstraction and contribute to groundwater deterioration. Owing to the spatial data in South Africa being relatively scarce, the reference periods of input data are not homogenous

(Table 1), but are within acceptable temporal ranges to be representative of current conditions.

GCM regional parameters

The available input into a regional water budget is strongly controlled by the amount of precipitation received in that region and is largely a function of regional climate. The mean annual surface temperature (MAT) has proven to be an effective indicator of the local climate and can be forecasted, along with mean annual precipitation (MAP), for different climate change scenarios (Alexander et al. 2006; Cannon 2015). Regional water budgets form a significant control on local groundwater quality through recharge that can either mobilize contaminants or dilute contaminated aquifers. Although these regional parameters are not directly representative of the vulnerability of groundwater water budgets, they are included as these parameters are the most reliably forecasted through established climate models (Smerdon 2017). MAP and MAT layers were acquired from the long-term mean of data collected between the years 1950 and 2000. Both datasets were produced in the South African Atlas of Climatology and Agrohydrology (Schulze et al. 2006; Schulze and Maharaj 2006a). The gridded datasets were developed using a geographically weighted regression approach and have a resolution of 1 arc minute.

Table 1 Data sources utilized in the modeling framework including the description of the data source utilized as well as the resolution, reference period and source of the data

Data set	Description	Resolution	Reference period	Source
Climatic indicators				
Rainfall	Long-term mean annual rainfall	1 Arc Minute	1950–2000	WRCa
Surface Temperature	Long-term mean annual temperature	1 Arc Minute	1950–2000	WRCb
Tritium distribution	The distribution of tritium activity in groundwater	1 km	2006	iThemba
Potential evaporation	A-pan equivalent reference potential evaporation	1 Arc minute	1970–1997	WRCc
Pollution potential				
Aquifer type	Aquifer type and yield	1:50 000		DWA
Terrain slope	Relative relief terrain	1 km		WRCd
Electric conductivity	Interpolated groundwater quality in EC ($\mu\text{S}/\text{cm}$)	100 m	1980–2004	NGA
Population density	Gridded population data	2 km	2005	NLC 2005
Cultivated land use	Gridded land use data	2 km	2000	FUNDISA
WRCa	Lynch, S. D. and Schulze, R. E. 2006. Rainfall Database. In: Schulze, R. E. (Ed) 2006. South African Atlas of Climatology and Agrohydrology. Water Research Commission, Pretoria, RSA, WRC Report 1489/1/06, Sect. 2.2			
WRCb	Schulze, R. E. and Maharaj, M. 2006. Temperature Database. In: Schulze, R. E. (Ed). 2006. South African Atlas of Climatology and Agrohydrology. Water Research Commission, Pretoria, RSA, WRC Report 1489/1/06, Sect. 2.1			
iThemba	Data collected but not published. Permission from iThemba LABS WITS			
WRCc	Schulze, R. E. and Maharaj, M. 2006. A-Pan Equivalent Reference Potential Evaporation. In: Schulze, R. E. (Ed). 2006. South African Atlas of Climatology and Agrohydrology Water Research Commission, Pretoria, RSA, WRC Report 1489/1/06, Sect. 13.2			
DWAa	Andiswa Matoti, Julian Conrad and Susan Jones, CSIR, 22 March 1999 Recompiled: August 2012 Directorate: Hydrological Services Sub-Directorate: Groundwater Information			
WRCd	Schulze, R. E. and Kruger, G.P. 2006. Terrain Morphology. In: Schulze, R. E. (Ed). 2006. South African Atlas of Climatology and Agrohydrology. Water Research Commission, Pretoria, RSA, WRC Report 1489/1/06, Sect. 3.2			
NGA	South African Department of Water Affairs National Groundwater Archive			
NLC	South African National land cover dataset			
FUNDISA	South African Census 2005			

Recharge indicators

Although the recharge can be estimated using a mass balance approach in data-rich areas (Mair et al. 2013), it is often difficult to characterize on a regional scale without reliable datasets of sufficient temporal and spatial resolution. It is therefore beneficial to have an alternative method for estimating how actively groundwater is being recharged, whilst still allowing for the inclusion of rainfall amount in the GCM regional parameters as a quantity control. The

activity of tritium in groundwater (TRIT) is a good indicator for how recently groundwater has been in contact with the atmosphere (Gleeson et al. 2015). In addition, potential evaporation (PE) is a reliable indication of the proportion of rainfall that remains to either feed surface water stores or recharge groundwater reserves (Mansour et al. 2018). Recharge indicators are incorporated through the inclusion of PE and TRIT. The A-pan equivalent reference potential evaporation is included as a recharge indicator (rather than in the GCM regional parameters) as it is empirically based

unlike estimated total evaporation (Schulze and Maharaj 2006b). The PE layer was developed using the A-pan evaporation method over 750 stations in South Africa (Schulze and Maharaj 2006a). The TRIT layer was produced from a South African Department of Water Affairs (DWA) groundwater dataset, measured by iThemba Labs, yielding 277 data points across South Africa. The layer was interpolated using an ordinary kriging model fitted against depth to the water table.

Physical attributes

Two physical attributes of the hydrogeological system have been included in the model framework under quality controls, namely: terrain slope (TS) and aquifer type/yield (AQT). Although TS is not equivalent to direct run-off, it can provide an indication of how likely it is for a contaminant to enter the system with high slope areas less likely to result in contaminants entering the groundwater system (Al-Zabet 2002). AQT can be used as a proxy for how rapidly a contaminant would be transported through the subsurface and is measured as hydraulic conductivity. In South Africa, the highest yielding aquifers are thick unconsolidated primary aquifers and represent areas vulnerable to surface/subsurface contamination and are capable of transporting contaminants faster. When combined with areas that have low relief (slope), these areas are normally indicative of high risk to a deterioration in quality. South Africa also has several major fractured rock aquifer systems that have relatively high yields, and represent an important fresh water resource to a large proportion of the agricultural sector (Robins et al. 2007). The AQT layer was developed by the South African Council for Scientific and Industrial Research (CSIR) (Andiswa et al. 2012). TS was computed from the SRTM 30 m mosaic of South Africa (Farr et al. 2007).

Chemical characteristics

In general, groundwater quality can be interpreted on a regional scale by using electrical conductivity (EC) as a proxy. EC represents an implicit analog for both natural and anthropogenic groundwater deterioration as it positively correlated with the concentration of ions (Liu et al. 2003). Groundwater quality in South Africa can be heterogeneous on a variety of scales and any dataset representing EC on a regional scale must accommodate this variability both spatially and temporally with sufficient sample density. Although EC can be controlled by both anthropogenic pollutants and natural dissolution of minerals, groundwater with EC values in excess of 'World Health Organization (WHO) standards are inappropriate for domestic and agricultural use (Gordon et al. 2008). For this reason, areas of high EC represent areas of high groundwater

vulnerability to further deterioration in quality. The EC distribution map was produced from a nationwide database of 49430 boreholes from the South African DWA National Groundwater Archive (NGA), with the input layer created using an ordinary kriging method.

Human groundwater dependence

Urbanization describes the global trend of population growth being focused in developed areas, resulting in increased stress on cities to maintain water distribution networks (Cohen 2006). Densely populated areas have a higher potential for both groundwater pollution and over-abstraction. However, densely populated areas are not the only ways in which humans interact with groundwater. Agricultural areas that exist to support population centres are high-end users of groundwater and are responsible for the strong correlation between groundwater depletion and cultivated land (Scanlon et al. 2012). Cultivated land also is susceptible to groundwater pollution because of the chemicals and agricultural waste that the industry uses and generates (Giordano 2006). South Africa has a large agriculture sector that uses ~70% of groundwater abstracted nationally and as a result cultivated land delineates an area of concern for both groundwater quantity and quality (DWA 2004). Population density (POP) and cultivated land (CL) layers were included from South Africa survey data (FUNDISA & NLC). Layers are produced as raster layers with a resolution of 2 km.

Model construction

The groundwater vulnerability model was constructed using a composite mapping analysis technique. This method superimposes input layers that have been reclassified and combines them through a predetermined linear algorithm that has an editable weighting scheme. The model construction was implemented in arc model builder (ArcGIS) in order to run batched calculations of multiple scenarios simultaneously, as well as output zonal statistics on each scenario. The ArcGIS model has the capability to be developed into a package for broader use. The framework was developed, with associated algorithms, to output a single groundwater vulnerability map measured in vulnerability index units which range from 1 to 8, where 8 is most vulnerable. Input parameters are reclassified according to their relative impacts on groundwater vulnerability. A major and minor strategy weighting regime was created for the current groundwater vulnerability in the research area. Subsequently, GCMs were chosen to evaluate the evolution of potential groundwater vulnerability 50 years into the future.

Model framework

Groundwater vulnerability (GV) as described in this framework is divided into two major strategies namely: (1) quantity controls (C) and (2) quality controls (Q) (Fig. 2). These major strategies are described as:

$$GV = q_C C + q_Q Q \quad (1)$$

where q is the associated weightings for major strategies subject to $q_C + q_Q = 1$. Each individual input parameter then forms part of a minor strategy within each of these major strategies according to:

$$C = v_{GCM} GCM + v_R R \quad (2)$$

$$Q = v_{PA} PA + v_{CC} CC + v_H H \quad (3)$$

where v is the weighting associated with each minor strategy, GCM is the GCM regional parameters, R is the recharge indicators, PA is the physical attributes, CC is the chemical characteristics and H is the human groundwater dependence and is subject to $v_{GCM} + v_R = 1$ and $v_{PA} + v_{CC} + v_H = 1$. Furthermore, each parameter has a weighting value w and reclassified vulnerability index I associated for each individual thematic layer described as:

$$GCM = w_{MAP} I_{MAP} + w_{MAT} I_{MAT} \quad (4)$$

$$R = w_{TRIT} I_{TRIT} + w_{PE} I_{PE} \quad (5)$$

$$PA = w_{AQT} I_{AQT} + w_{TS} I_{TS} \quad (6)$$

$$CC = w_{EC} I_{EC} \quad (7)$$

$$H = w_{POP} I_{POP} + w_{CL} I_{CL} \quad (8)$$

where MAP is mean annual precipitation, MAT is mean annual temperature, TRIT is distribution of tritium activities in groundwater, PE is potential evaporation, AQT is aquifer type, TS is terrain slope, EC is electric conductivity, POP is population density and CL is cultivated land use. The weighting of each individual parameter within each thematic layer is subject to the following:

$$w_{MAP} + w_{MAT} = 1.0 \quad (9)$$

$$w_{TRIT} + w_{PE} = 1.0 \quad (10)$$

$$w_{AQT} + w_{TS} = 1.0 \quad (11)$$

$$w_{POP} + w_{CL} = 1.0 \quad (12)$$

The model framework allows for weightings of major and minor strategies to be adjusted in order to produce a large number of individual scenarios (Table 2). The justification of how these weightings are set will change according to the objective of each investigation to which the model is applied.

Reclassification

Model parameters are reclassified according to a predetermined scheme that allows them to be comparable as a groundwater vulnerability index. Should input data not fit within the scheme, reclassification should be adjusted and justified for each specific study. This is to ensure that equation (1) does not contradict the constraints in equations (9–12). To do this, the reclassification scheme for each parameter was applied according to the potential impact a change would cause on the groundwater quantity and quality. Each input layer was reclassified to a vulnerability index scale from 1 to 8, with areas of low vulnerability being assigned 1 and those of high vulnerability being assigned 8 (Fig. 3). Each input layer was reclassified by either applying an equal interval weighting of the source data range or aligning to established ranges associated with the parameter. For example, the EC input thematic layer was reclassified to align with global WHO standards of water quality for potable and agricultural use (Gordon et al. 2008).

Weighting scenarios and selection

Three major strategies and seven minor strategies were developed by adjusting the weightings associated with the main headings and subheadings in the model framework. Major 1 (M-I) strategies equally weight quantity controls and quality controls whereas the M-II strategy favours quantity controls in a 3:1 ratio and the M-III strategy favours quality controls in a 3:1 ratio. Scenarios are then further divided by 3 minor strategies that adjust the weightings of parameters under quantity controls (C - n , where n is the strategy number) and 4 minor strategies that adjust weights of parameters under quality controls (Q - n , where n is the strategy number) (Table 2). C -1 and P -1 minor strategies equally weight the parameters whereas C -2/3 and P -2/3/4 minor strategies selectively increase the weightings of sub-sections individually. The specific combinations of major and minor strategies can be drawn from Table 2. The various combinations of major and minor strategy weightings produced 36 different weighting scenarios. The scenario selection process consists of: (1) sensitivity analysis feedback to determine if input layers are significant and (2) whether the study area is more vulnerable to controls from climate or contaminants or both. This study evaluates the vulnerability of groundwater to depletion and deterioration equally, and thus uses an M-I strategy.

Table 2 Major and minor strategy weightings that are possible in the 36 presented scenarios as well as the example scenario M-I/C-2/P-2

Minor-strategy	Minor subheadings	Major-strategy		
		M-I	M-II	M-III
		Quantity controls=0.5	Quantity controls=0.75	Quantity controls=0.25
		Quality controls=0.5	Quality controls=0.25	Quality controls=0.75
C-1	GCM regional parameters	0.5	0.5	0.5
C-2	Recharge indicators	0.5	0.5	0.5
C-3	GCM regional parameters	0.25	0.25	0.25
	Recharge indicators	0.75	0.75	0.75
Q-1	GCM regional parameters	0.75	0.75	0.75
	Recharge indicators	0.25	0.25	0.25
	Physical attributes	0.33	0.33	0.33
Q-2	Chemical characteristics	0.33	0.33	0.33
	Human GW dependence	0.33	0.33	0.33
	Physical attributes	0.6	0.6	0.6
Q-3	Chemical characteristics	0.2	0.2	0.2
	Human GW dependence	0.2	0.2	0.2
	Physical attributes	0.2	0.2	0.2
Q-4	Chemical characteristics	0.6	0.6	0.6
	Human GW dependence	0.2	0.2	0.2
	Physical attributes	0.2	0.2	0.2
	Chemical characteristics	0.2	0.2	0.2
	Human GW dependence	0.6	0.6	0.6

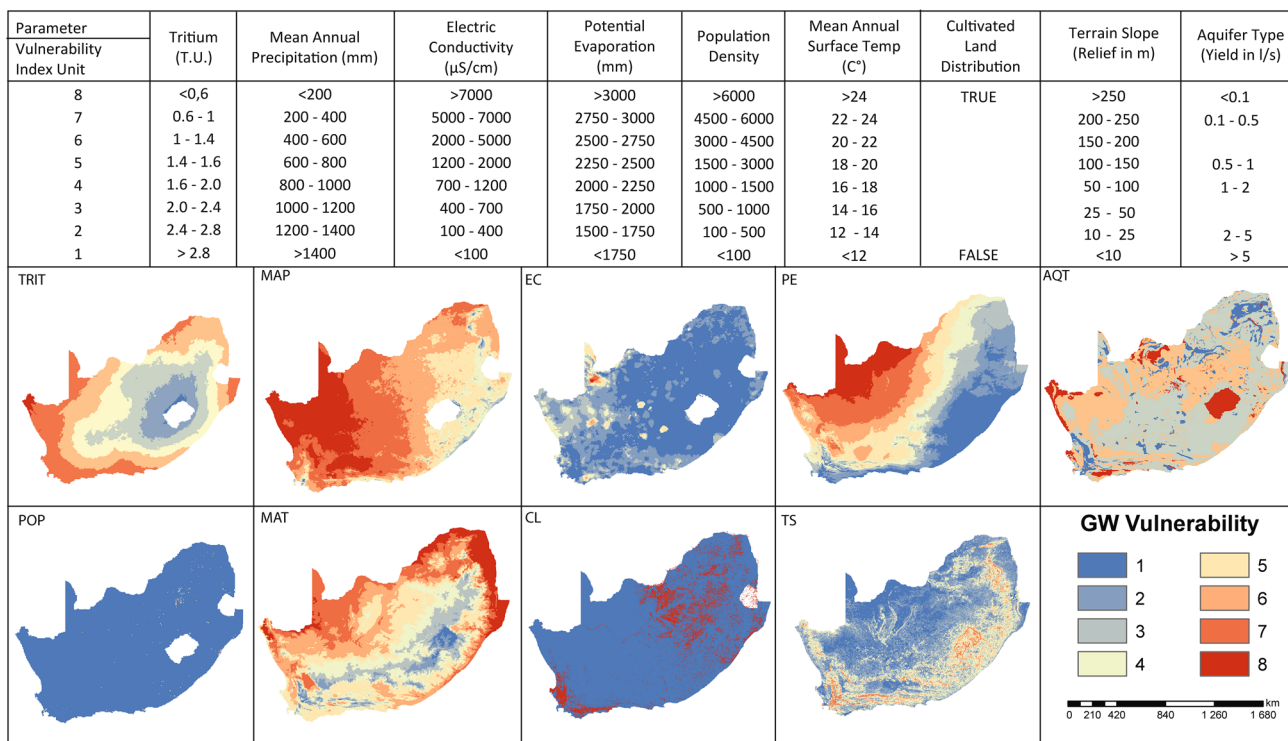


Fig. 3 Reclassification scheme used to calculate the vulnerability index for each input parameter on a scale of 1–8, with a visualization of reclassified thematic layers Each input variable was reclassified

on a predetermined linear scale that either applies an equal interval weighting of the source data range or aligns to typical reported ranges associated with the parameter

GCM climate scenarios

The longevity of a groundwater vulnerability assessment is dependent on how actively the equilibrium of the aquifer system is being disrupted. Anthropogenic influences usually occur over short time frames in relation to climate change, yet modern climate studies suggest that the difference in the rate of change is not as large as previously thought (Guermazi et al. 2019). Although quantifying these disruptions is inherently difficult to do with limited historical records of many of the input parameters, our ability to predict the evolution of regional climates has improved greatly, enabling researchers to forecast how water budgets may evolve over time (Archer et al. 2018; Mazzoni et al. 2018; Xie et al. 2015).

GCMs are used to predict the change in climate over time by using historical climate data and knowledge of atmospheric circulation to either predict or forecast the future change in climate. The models are generally developed to only adjust for the change in precipitation and surface temperature. There has been extensive debate about which GCM is the most accurate and the consensus depends on what the study is trying to achieve (Cannon 2015; Her et al. 2019; Hewitson and Crane 2006). For studies in southern Africa, the HadCM3 climate model is regarded as robust for climate change forecasts (Prescott et al. 2018; Tadross et al. 2005). Alternatively, it is possible to use an ensemble of various GCMs to better estimate climate change. In this study, three model input are used, namely: (1) the HadCM3 model, (2) an ensemble of the lowest predicted change GCMs and (3) an ensemble of the highest predicted change GCMs. These three models are then computed under two SRES (Special Report on Emission Scenarios) emission scenarios (A2 and B1). GCM output layers were downloaded from the IPCC Data Distribution Centre (<https://www.ipcc-data.org/>). These layers were calculated 50 years into the future to be more representative of groundwater timescales whilst still within prediction limits set by the IPCC. The issue of down-scaling is not tackled in this study as the inclusion of GCMs in the study is exclusively done to exhibit the ability of the model to incorporate future projections of climate change.

Sensitivity analysis

A univariate sensitivity analysis was performed to investigate the influence of each input parameter to the GWV model. The analysis was structured similar to established sensitivity analysis methods for index overlay methods, e.g. DRASTIC (Napolitano and Fabbri 1996), where one input parameter is adjusted/removed and the output compared to a base output where all parameters are weighted equally. The sensitivity analysis in this study is restricted to adjusting a single input parameter weighting at a time to evaluate how

sensitive the model output is to each parameter. A baseline output was created by equally weighting all the input parameters:

$$EQ_e = \sum_{j=1}^7 (W_j \times R_j) \quad (13)$$

where EQ_e is the equally weighted baseline, W_j is the weight factor and R_j is the vulnerability rating. Each input parameters is adjusted to create a skewed weighting (SW_i) by doubling a single parameter weighting (Eq. 14) and calculating the percentage change of the final output compared to an equal weighted base output (Eq. 15):

$$SW_i = \sum_1^6 (W_j \times R_j) + (2W_i \times R_i) \quad (14)$$

$$\%_{\text{change}} = \frac{EQ - SW_i}{EQ} \times 100 \quad (15)$$

Each skewed weighting layer is then normalized by calculating the number of cells that exceed 1 vulnerability index unit and dividing this by the total number of input cells and reported as a percentage value of cells sensitive to the testing parameter. This approach differs from more traditional approaches, that remove an entire input parameter at a time, by assessing if the doubling of a single parameters weighting, from the base weighting, results in an increase or decrease of > 1 vulnerability index unit. The sensitivity model framework (Fig. 4) was applied to the nineteen official WMAs in South Africa to determine individual parameter sensitivity per WMA. The study area was divided in this way to determine input sensitivities in a manner that is beneficial to water management authorities in South Africa.

The sensitivity of each input parameter is combined to visualize the total sensitivity of each gridded cell in the final MCE output (Fig. 5). Areas of low sensitivity are most likely a result of one input parameter having an anomalously high or low vulnerability for an area and; therefore, having an affect so large that other inputs are unlikely to change the final GWV. The total sensitivity of each WMA is divided into the percentage contribution of each input parameter to evaluate the specific contribution of each parameter on a smaller spatial scale (Fig. 6). This approach allows better assessment of vulnerabilities within a single WMA.

Results

The groundwater vulnerability model in this study produces maps of 36 model scenarios. Here we have chosen a scenario to present that best combines a strong alignment with previous studies and weightings that are not skewed

Fig. 4 Framework for the sensitivity analysis of groundwater vulnerability MCE methods. Adapted from Napolitano and Fabbri (1996)

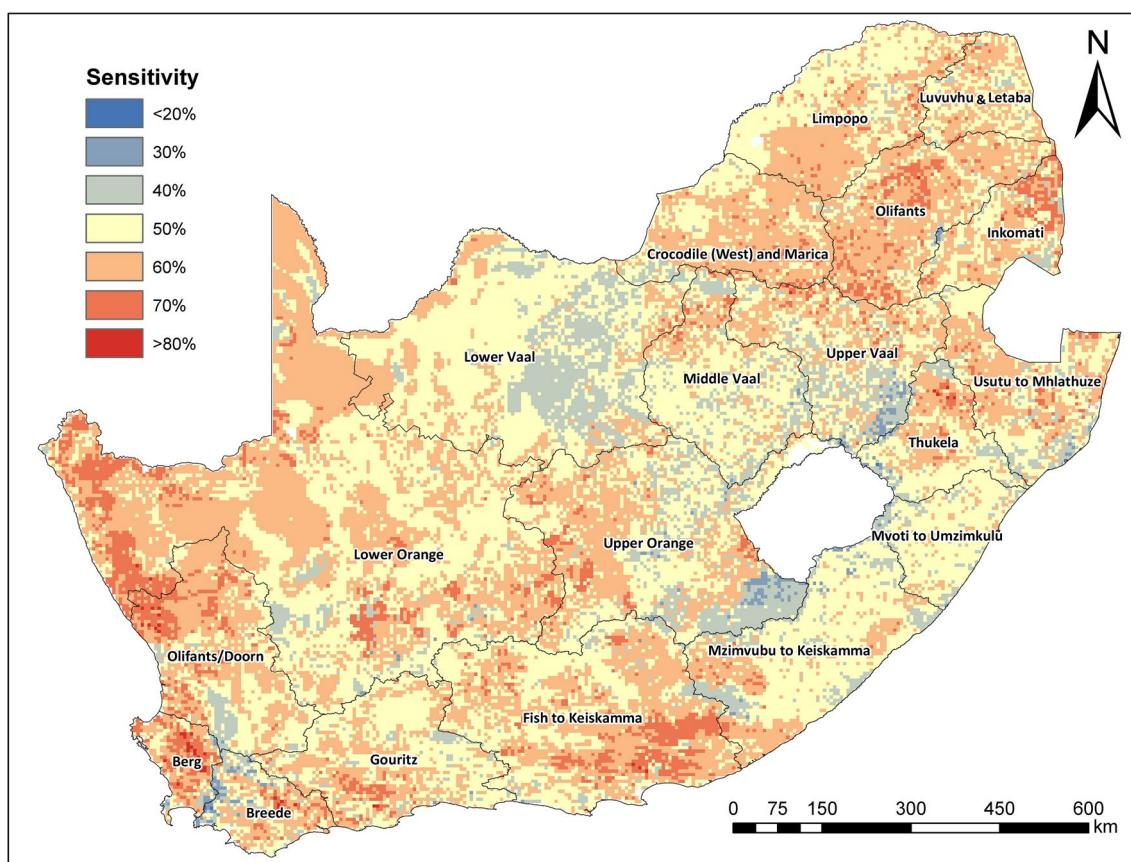
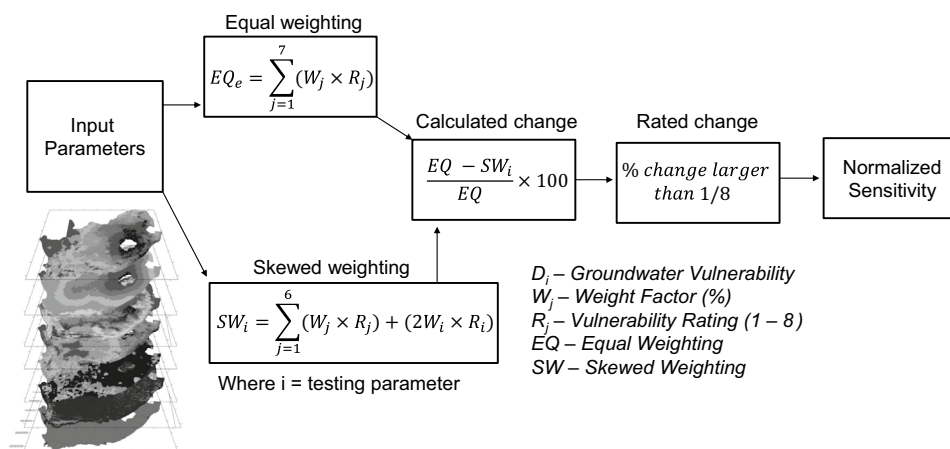


Fig. 5 Distribution of total sensitivity with the nineteen water management areas (WMAs) according to NWRS-1 for reference. Areas of low sensitivity are marked in blue and areas of high sensitivity in red

toward a particularly sensitive parameter (Fig. 7). This ensures that all data incorporated in the analysis is contributing to the output effectively without biasing the model towards any specific input. To illustrate the model, the results are reported in two spatial distributions: (1) South Africa as a whole and (2) the nineteen individual WMAs within South Africa's boundary as defined by NWRS-1.

Groundwater vulnerability

All 36 scenarios are visualized by plotting the data as mean percentage area of vulnerability from very low to very high (Fig. 8). In addition, ranges are included representing the minimum and maximum percentage of areas associated with each vulnerability range, as well as the base output,

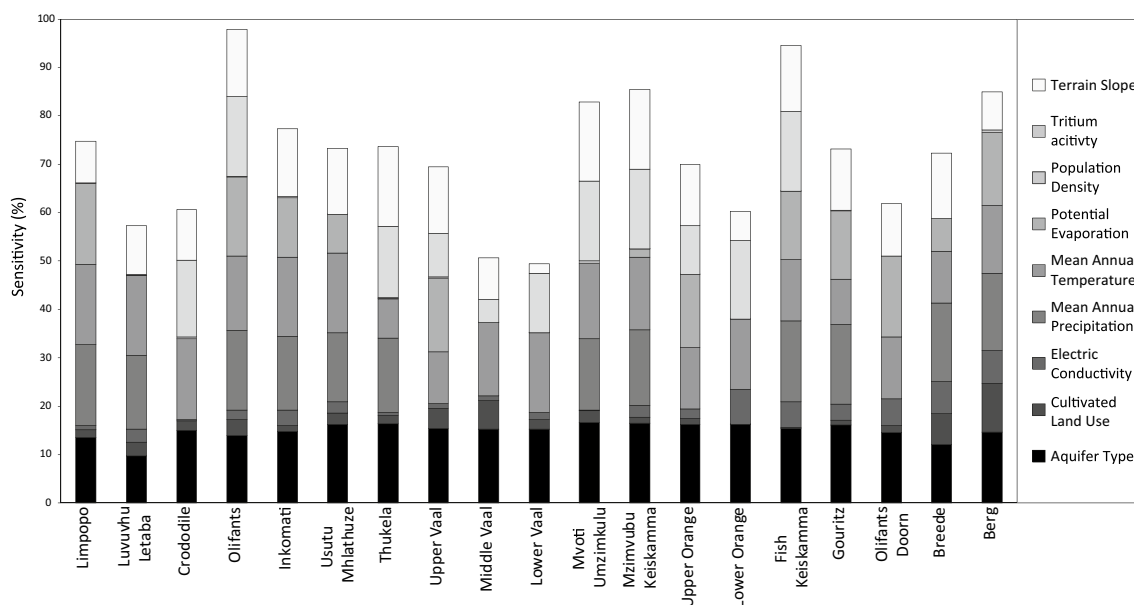


Fig. 6 Model sensitivity divided by parameter contribution to total sensitivity waterfront the nineteen management areas (WMA) defined in NWRs-1. The WMAs are organized from the north east of the country to the south west

which represents scenario MI/C-1/P-1 and the selected scenario MI/C-2/P-2 for reference against the mean. The mean groundwater vulnerability for all 36 scenarios differs significantly from the base scenario. For areas of very low GWV, the percentage of total land area in the base scenario was 2.79% and the mean of all scenarios was 12.2%, conversely the mean of all scenarios also predicted a larger percentage of very high vulnerability areas, from 14.6% (base) to 22.4% (mean). This is compensated by a smaller mean area of low, moderate and high vulnerability areas (Base: 40.2% low, 27.0% moderate, 15.5% high and Mean: 35.5% low, 16.8% moderate, 13.1% high).

The selected output is produced from scenario MI/C-2/P-2 (Fig. 9) and was chosen within the M-I major strategy to incorporate an equal weighting of quantity controls and quality controls, ensuring a more balanced evaluation. The selected scenario comprises 1.5% very low, 35.7% low, 24.9% moderate, 17.0% high and 20.9% very high vulnerability areas. The spatial distribution of groundwater vulnerability is skewed from higher vulnerability areas in the west and lower vulnerability areas in the east. A few exceptions include the Breede and Fish to Keiskamma WMAs in the south-west and the lower Vaal WMA in the north-western reaches of the country (Fig. 10).

Projected vulnerability

The model outputs can be forward projected for different time periods using different combinations of GCM

scenarios. In order to do this, an input scenario that has greater weightings on quantity controls was chosen to showcase the climatic change effect, in this case scenario MI/C-2/P-2. Figure 11 shows six possible outcomes under one GCM, two GCM ensembles and two emission scenarios projected 50 years into the future. The projected scenarios show an average increase in the total area of very high vulnerability from 25.6 to 28.7% and high vulnerability from 24.9% to 25.9. This is associated with an average decrease in the total area of low vulnerability from 19.3 to 15.7% and very low vulnerability from 0.9 to 0.5%. It also indicates that the low-emission scenarios (B1) represent less significant increases in very high vulnerability areas and a more significant increase in moderate zones. All high emission (A2) scenarios result in an increase in the area of very high vulnerability zones. The low GCM ensemble (A2) showed an anomalous increase in very high vulnerability areas from 25.6 to 41.0% (Fig. 12). Future predictions show substantially increased groundwater vulnerability in the central regions of the country as well as moderately increased groundwater vulnerability within the Western Cape and southern coastal areas. The northern boundary regions showed lower vulnerabilities in the projected model. The highest ensemble for future vulnerability to climate change showed the same regions of change, but with increased severity. In this weighting scenario, almost all of the western and central regions have high vulnerabilities and a smaller area of the eastern regions have low vulnerabilities.

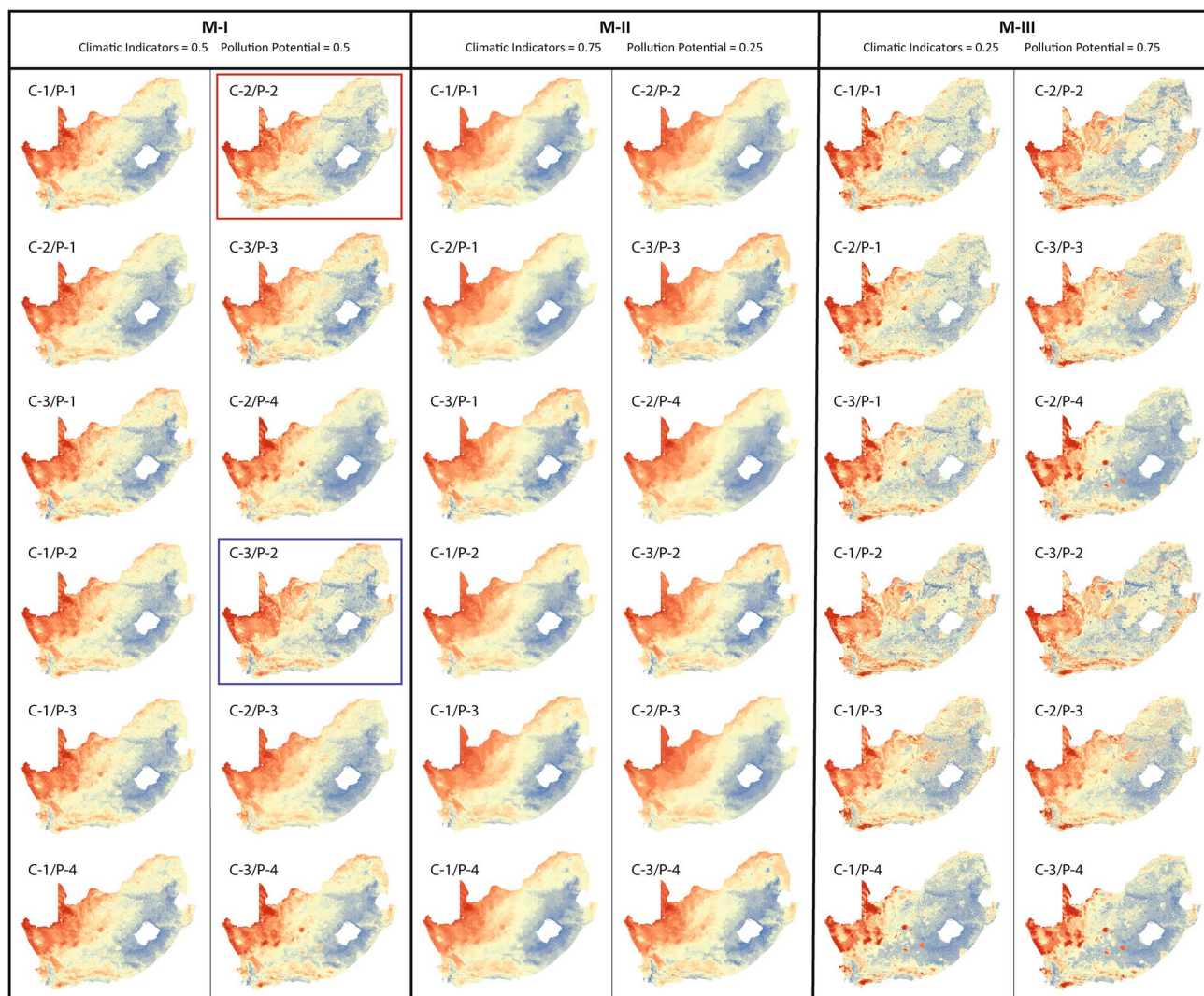


Fig. 7 Outputs of all 36 scenarios, grouped under the three major strategies and minor strategy combinations represented by individual maps as per Table 2. The selected scenario (MI/C-2/P-2), presented in text, is outlined in red and the projected scenario in Sect. 3.2 is highlighted in blue

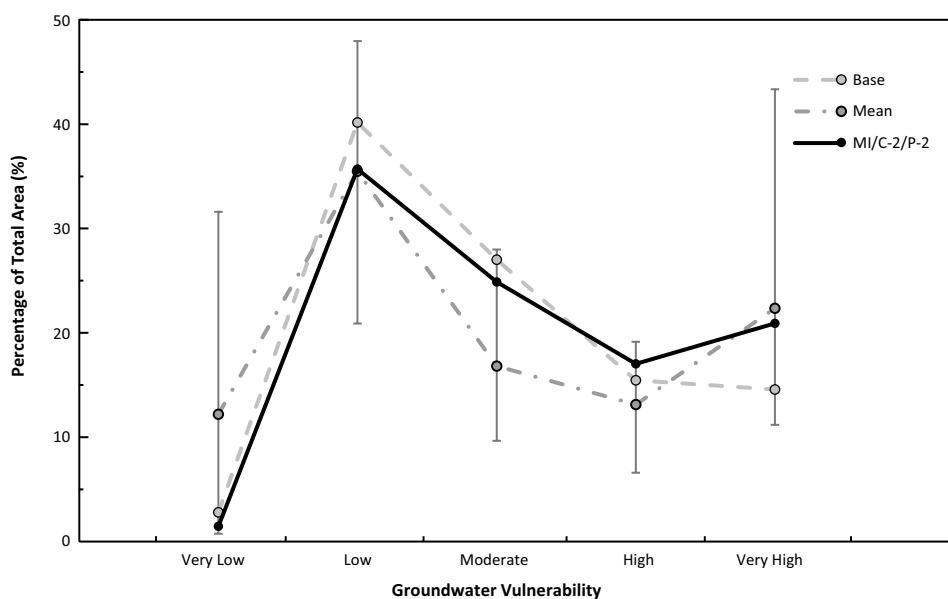
Parameter sensitivity

The results of the sensitivity analysis are shown in Table 3 and are presented alongside the effective weights of the model framework under the base scenario (MI/C-1/P-1) and the selected scenario (MI/C-2/P-2). The average sensitivities of each parameter across all nineteen WMAs show that eight of the nine input parameters are important to the final groundwater vulnerability output, with the exception of POP which has an average sensitivity of just 0.19%. The most sensitive parameters were MAT (20.2%) and AQT (21.4%), while the MAP (12.8%) and TRIT (10.9%) layers are the most variable with standard deviations > 10%. AQT, TS (16.1%), EC (4.02%), POP (0.19%) and CL (3.88%) all have a standard deviation of less than 5%, which suggests their sensitivity is relatively uniform across all nineteen WMAs.

Discussion

The model presented outlines the development of a new approach for assessing groundwater vulnerability to both deterioration and depletion. The model itself also has the capacity to be forecasted using climate data and can be optimized if the chosen field area has data available to perform a calibration step. Although not all input parameters have equal contributions to the final groundwater vulnerability index, the model sensitivity is assessed and discussed. In addition, it is not clear in which spatial extent vulnerabilities should be presented, yet national water management strategies that have more extensive data would lead to more robust modelling outputs. This may be aggravated by the heterogeneous nature of the distribution of groundwater vulnerabilities in regional investigations. The following discussion

Fig. 8 Percentage of total area of South Africa for five different categories of groundwater vulnerability (very low, low, moderate, high and very high) per unit area of the country as a whole. The results are presented as: (1) an equally weighted scenario or base scenario (light grey stippled); (2) the mean if all 36 scenarios (dark grey dot stippled) with range bars to show the ranges of included scenarios and (3) the selected MI/C-2/P-2 model scenario (solid black line)



highlights key distributions in the results, compares these sensitivity analysis results and evaluates the reliability of the groundwater vulnerability methodology and how it could contribute to constraining a regions hydrological resilience.

Model sensitivity

The sensitivity of each individual parameter is an indication of its potential to influence the final vulnerability scenario result. The results of the sensitivity analysis indicate that most parameters have significant contribution to the final groundwater vulnerability. EC, POP and CL are noticeably less sensitive. Although this may suggest that their contribution to overall groundwater vulnerability is low, their inclusion is still warranted, as areas with poor groundwater quality, a high population density and extensive agricultural activity, represent high-risk zones for groundwater. A robust scenario should align its effective weightings to the sensitivity of specific layers to generate the most representative output. However, if the model weightings are calibrated with the sensitivities, then it is not possible to independently compare multiple scenarios. If targeted vulnerabilities were included for each input parameter, these could be used to calibrate the model. Sensitivity has a regular spatial distribution of high and low sensitive areas across the country, indicating that the model does not suffer from a spatial bias across different climatic zones (Fig. 5). There are however WMAs that are more sensitive than others, with varying combinations of parameter sensitivities. More sensitive WMAs are those that are more likely to change their overall vulnerability severity and distribution if one or more input parameters change. This suggests that WMAs with lower sensitivities are potentially more resilient to the change of input parameters. Some

input parameters are uniformly sensitive across all WMAs (AQT, CL and MAT) and other input parameters have highly variable sensitivities (TS, TRIT, PE and EC) (Fig. 6). MAP shows high sensitivity in twelve WMAs and very low sensitivity in the other seven WMAs. The distribution of MAP sensitivity shows that high sensitivity areas are in the eastern and southern parts of South Africa while the less sensitive areas are in the northern and western areas. This is consistent with the change between semi-arid climates in the northern and western areas and more humid climates in the east. The Olifants, Mvoti Umzimkulu, Mzimvubu, Fish and Berg WMAs all show sensitivities above 80%, suggesting that these are most likely to change with a change in input parameters.

Comparison to other South African GWV assessments

In order to evaluate how representative the groundwater vulnerability model presented here is, the selected scenario MI/C-2/P-2 was compared to maps from the previous groundwater drought risk (Villholth et al. 2013) and DRASTIC style (Musekiwa and Majola 2013) investigations (Fig. 9). The models associated with the reference studies are constructed in a similar “multi criteria evaluation” method, with major differences in input datasets, reclassification of parameters and weighting scenarios. MI/C-2/P-2 generally aligns to the spatial distribution of groundwater vulnerability from previous studies but had some notable differences. Spatial differences between investigation techniques were prevalent in the Western Cape, where the MI/C-2/P-2 scenario identified the area of high groundwater vulnerability to be significantly larger than that of other methods. The

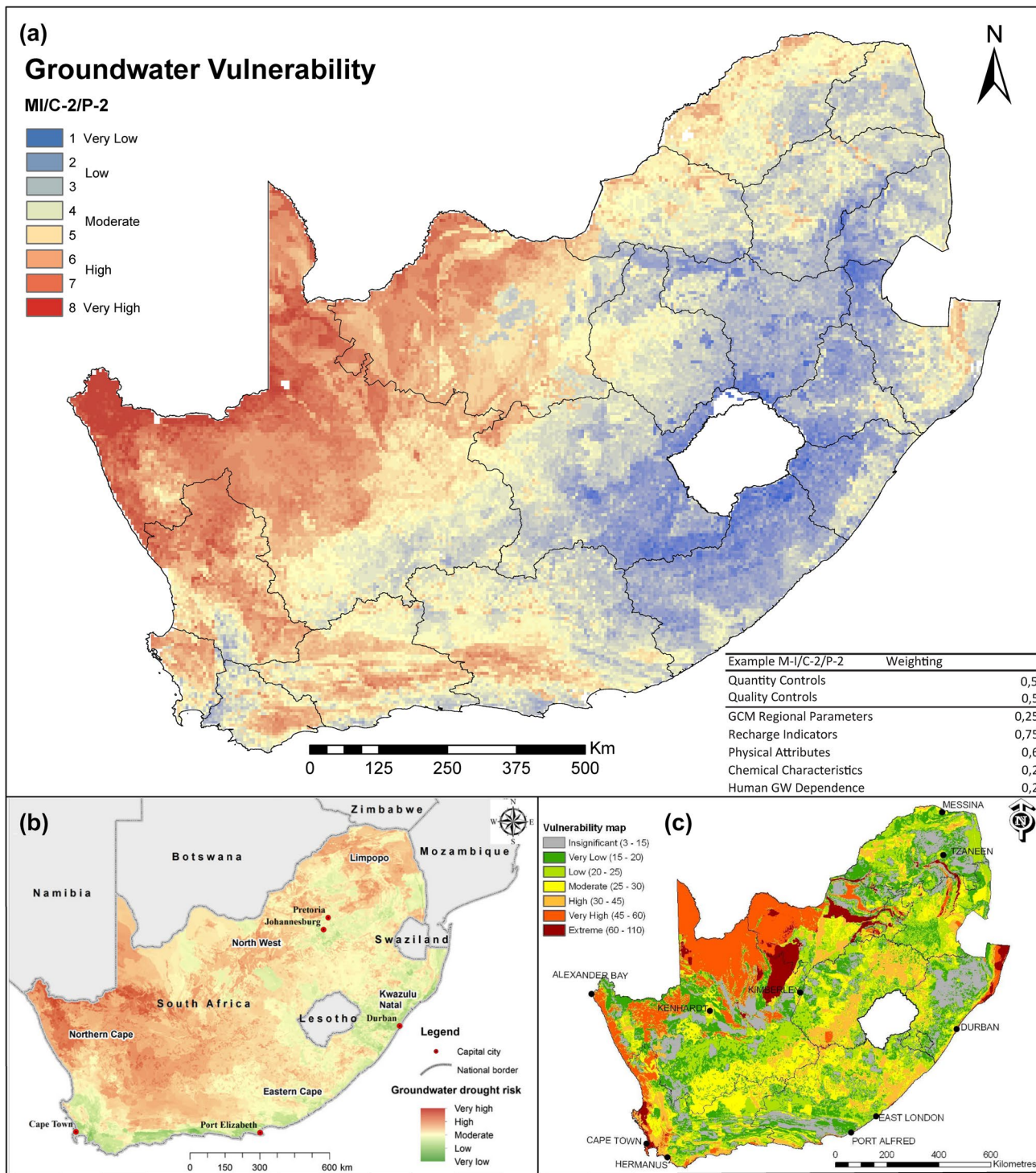


Fig. 9 Distribution of: **a** groundwater vulnerability from the selected scenario MI/C-2/P-2, where major strategies are weighted equally and minor strategies are skewed toward recharge indicators and physical attributes (water management areas shown for reference—thick

black lines); **b** groundwater drought risk produced from Villholth et al. (2013) and **c** DRASTIC groundwater vulnerability produced by Musekiwa and Majola (2013)

low groundwater drought risk previously predicted for the Western Cape is the result of low predicted climate sensitivity and productive aquifers with a high recharge potential.

The DRASTIC method agreed with high vulnerability zones, but MI/C-2/P-2 highlighted that the higher relief areas of the Western Cape, where rainfall is elevated, had decreased

Fig. 10 Groundwater vulnerability per water management area (WMA) produced from scenario MI/C-2/P-2 as a proportion of the total percentage vulnerability per area. WMAs west of 25° E generally have increased vulnerability than those east of 25E

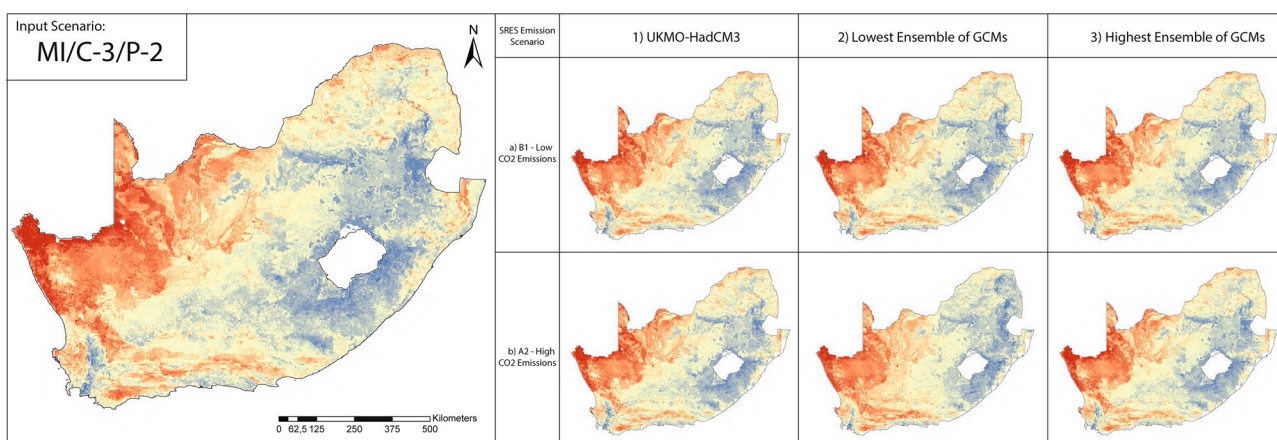
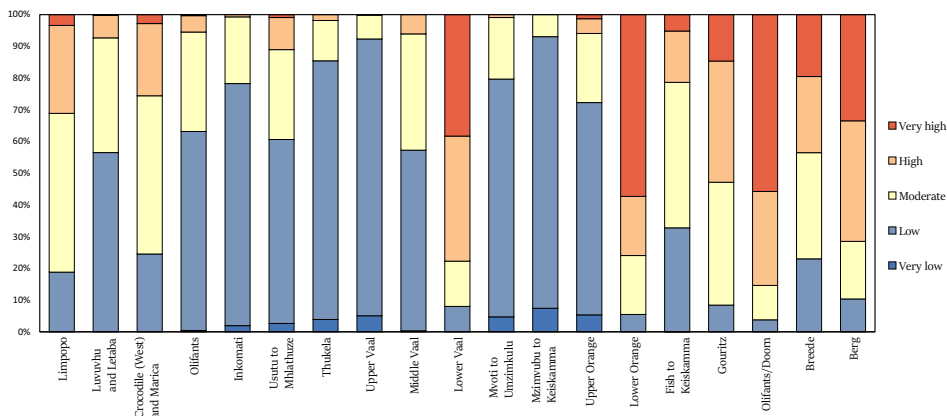


Fig. 11 Comparative map showing an example scenario output (left) MI/C-3/P-2 of current groundwater vulnerability with projected maps (50 years): (1) from the UKMO-HanCM3 GCM; (2) the lowest ensemble of 16 GCMs and (3) the highest ensemble of 16 GCMs.

Outputs for all prediction models are presented under two emission scenarios: **a** SRES B1 low CO₂ emissions and **b** SRES A2 high CO₂ emissions

Fig. 12 A combined plot of the percentage of total area of groundwater vulnerability for MI/C-3/P-2, with 6 projected scenarios developed from: (1) the UKMO-HanCM3 GCM; (2) the lowest ensemble of 16 GCMs and (3) the highest ensemble of 16 GCMs presented under two emission scenarios: **a** SRES B1 low CO₂ emissions and **b** SRES A2 high CO₂ emissions

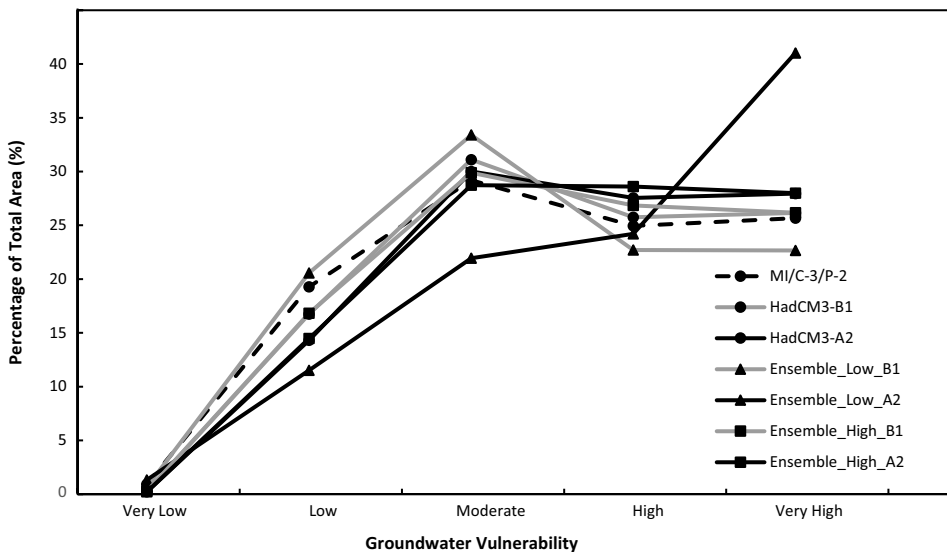


Table 3 Sensitivity analysis results presented with effective weights of the base output and the example output *MI/C-2/P-2*

Input data	Model weighting scheme			Sensitivity analysis results			
	Theoretical % (base)	Theoretical weight % (MI/C-2/P-2)	Average weight (%)	Standard deviation (%)	Median (%)	Minimum value (%)	Maximum value (%)
Mean annual precipitation	12.5	6.25	12.80	10.01	17.76	0.00	26.50
Mean annual temperature	12.5	6.25	20.19	6.08	18.84	11.06	33.22
Tritium distribution	12.5	18.75	10.94	10.17	12.86	0.00	26.94
Potential evaporation	12.5	18.75	10.53	9.53	10.87	0.00	26.90
Aquifer type	8.25	15	21.40	4.45	22.06	14.25	30.87
Terrain slope	8.25	15	16.05	4.37	17.57	4.00	22.40
Electric conductivity	16.5	10	4.02	3.23	2.99	0.13	11.85
Population density	8.25	5	0.19	0.20	0.12	0.00	0.61
Cultivated land use	8.25	5	3.88	3.37	3.02	0.09	11.94

groundwater vulnerability. Other notable differences in the DRASTIC evaluation include an extreme vulnerability (dark red) region in the northern central regions of South Africa (Fig. 9c). This extreme vulnerability region is a function of a large aquifer and a vadose zone that are both dolomitic. In the DRASTIC framework dolomite has a high rating and hence in areas where both the aquifer media and the vadose zone are dolomitic the vulnerability is extreme. For the northern areas of the Northern Cape and North West provinces (Lower Vaal and lower Orange WMAs) MI/C-2/P-2 and the DRASTIC model agree that groundwater has high vulnerabilities, but groundwater drought risk is moderate. This is directly linked to the presence of the deep and productive Stampriet Aquifer that flows south from the Okavango Delta in Botswana. Where there are major contrasting vulnerabilities between MI/C-2/P-2 and the DRASTIC output, they are not only a function of quantity controls but also that MI/C-2/P-2 investigates broad quality controls and not just anthropogenic pollution. The discrepancies between the two previous studies are a result of the potential for recharge, where groundwater drought risk values recharge as less vulnerable and DRASTIC values recharge as elevated potential for pollution. Larger spatial trends in the new model are comparable to the groundwater drought risk style investigation but smaller scale DRASTIC type anomalies are better defined in the new groundwater vulnerability model.

Assessing groundwater vulnerability

Globally, groundwater resources are dependent on physical and climatic constraints with major aquifers around the world affected by depletion (Scanlon et al. 2012) or a deterioration in quality (Mukherjee et al. 2006) or both. As a result, different major and minor strategy combinations would be suited to different regions. Areas, like the north of China, that face depletion issues (Feng et al. 2013) are focused on assessing aquifer vulnerability to depletion.

Areas battling with large scale pollution, similar to Bangladesh (Khan et al. 2019), are focused on assessing vulnerability to contamination. The nature of the model framework allows the user to output a multitude of different scenarios. Although this approach is dynamic and flexible, it is difficult to justify which scenario is the most appropriate for a given study aim. In order to do this effectively in South Africa, where groundwater can be scarce and have poor quality, an M–I major strategy must be used as it equally weights quantity controls and quality controls.

It is evident from model output MI/P-2/C-2, that large areas of South Africa (48%), have a high to very high groundwater vulnerability and these areas are found predominantly in the western parts of the country. This distribution is likely a function of arid climatic conditions as well as already poor groundwater quality (high EC). Although this region is not densely populated, it does represent an area where agricultural activity is strongly dependent on groundwater. The area surrounding Cape Town in the Western Cape (Berg and Breede WMAs) also shows high groundwater vulnerability. In the last four years, this area has experienced below average rainfall that has severely depleted surface water resources. During this time, local government has implemented emergency water supply schemes that include the utilization of groundwater resources to supplement surface water reservoirs. Many large urban centres around the world face similar conditions (Krueger et al. 2019). The eastern seaboard of Australia and the western seaboard of the United States have also in the recent years suffered from extreme drought conditions (Mann and Gleick 2015; Timbal and Fawcett 2013). In the South African context, the vulnerability assessment using MI/P-2/C-2 indicates that the region around Cape Town had high groundwater vulnerability even prior to the drought. This situation would likely be mimicked in Victoria (Australia) and California (United States). As conflict over water resources usually occurs after there has been significant threat to water supply, a framework to

assess groundwater vulnerability prior to this and therefore the capacity of groundwater to supplement urban and agricultural water supplies should be instrumental to all groundwater management policies.

Application to groundwater management

Although groundwater forms a major component of fresh water, the management of groundwater is still in the process of being holistically integrated into international water policy and legislation (Puri and Villholth 2018). Multi-agency initiatives have attempted to encourage riparian states to work together to develop effective transboundary groundwater management policies (Puri and Aureli 2005). These efforts have resulted in many countries around the world forming transboundary agreements on managing shared groundwater resources (Eckstein 2011; Villara and Ribeirol 2011). However, some of these agreements directly conflict with previously passed legislation on transboundary surface water resources (McCaffrey 2011). Many important transboundary aquifer systems are located in semi-arid and arid environments and abstraction from these aquifer systems has increased rapidly in recent years as a result of increased urbanization and agricultural food production (Wada and Heinrich 2013). Adaption to ongoing global environmental change varies significantly between different nation states (Biermann and Dingwerth 2004) and this serves to further increase the stress on groundwater resources, in part also because nation states can do little individually to mitigate against global processes.

South Africa is an example where transboundary aquifer systems complicate the development of effective groundwater management protocols (Cobbing et al. 2008). Aquifer systems shared with neighbouring countries are relatively data poor and WMAs within the country are not consistent with provincial boundaries. Although water resources are managed by the national government, decisions concerning local resources are implemented by local municipalities. In the development of the groundwater vulnerability model, the nine parameters that contribute to the modelling predictions on the vulnerability of groundwater resources, are managed at different scales and governmental levels within South Africa. Rainfall is regional and controlled largely by global scale processes whereas land use is often governed by local municipality policies. Accordingly, the management of groundwater resources is the responsibility of national government but is impacted by local government actions. The implications for this dichotomy in responsibilities can be seen in the way in which vulnerability is calculated in the original 19 WMAs as compared to the larger 9 CMAs. The variability in groundwater vulnerability between WMAs is significantly larger than in the CMAs meaning that should a groundwater management strategy be implemented in a

CMA and it would likely to protect one of the two (or more) WMAs within a CMA effectively. Conversely, if more conservative strategies were implemented, areas that have relatively low groundwater vulnerability might be under-utilized as a result.

As populations become more dependent on groundwater resources, either as a result of variable water budgets or population growth, the consequences of poor groundwater management become increasingly problematic (Adewoyin et al. 2016). The depletion and deterioration of groundwater resources has the potential to directly impact the viability of local agriculture that in turn can affect regional food security. In an effort to better cope with water scarcity and climate variability, the revised groundwater vulnerability assessment developed here provides new insights into how potential groundwater resources can and should be managed sustainably. In the context of food security, the vulnerability of the local and regional groundwater resource both at the present and into the future, should be considered to ensure, for example, that the correct types of crops are developed in specific regions. This model provides a useful tool to assess the ability of a catchment to adapt to a disturbance in quality and/or quantity and in turn better constrain regional hydrological resilience.

Conclusions

Increased groundwater abstraction on a global scale to support population growth and food security requires an effective method to assess groundwater vulnerability to both depletion and deterioration in quality. The approach presented here addresses issues surrounding broader concerns of groundwater vulnerability that more focused methods cannot constrain. The trade-off between pinpointing the primary driver of groundwater vulnerability and the holistic assessment of several vulnerability drivers is evident in the sensitivity analysis, where the groundwater vulnerability of any given area is controlled by different combinations of input parameters. Holistic regional groundwater vulnerability assessments that incorporate the differentiation between shallow, actively recharged groundwater and deeper, fossil groundwater represents a step forward in utilizing regional isotopic tracers in groundwater vulnerability assessments. The resultant output of groundwater vulnerability can be investigated across natural and legislative boundaries, providing a mechanism for baseline assessments of groundwater vulnerability in transboundary systems as well as predicting how these vulnerabilities will evolve into the future. By viewing the sustainability of groundwater in a shared light with the vulnerability of groundwater, there is an opportunity to develop adaptive and flexible groundwater management frameworks to prevent conflict over shared resources.

In addition, concerns surrounding how susceptible groundwater is to climate change can now be addressed in conjunction with traditional groundwater vulnerability assessments, mitigating the possibility of underestimating the vulnerability of a resource when developing management strategies. The implementation of this method to evaluate groundwater vulnerability across natural environments and political boundaries will be instrumental in the application of comprehensive groundwater vulnerability assessments and the development of effective groundwater management policy.

Acknowledgements We thank the Water Research Commission South Africa for initial funding support and the iPhakade program and National Research Foundation South Africa for bursary support. This work is also based on research supported in part by the National Research Foundation of South Africa (Grant number: 118594). The authors would like to acknowledge the assistance of the University of Utah's ITCE SPATIAL program for providing the training necessary to construct the model presented in this paper. We would also like to acknowledge Dr. Babetunde Abiodun, Department of Environmental & Geographical Science, University of Cape Town, for his input on climate modelling. This publication forms part of the output of the Biogeochemistry Research Infrastructure Platform (BIOGRIP) of the Department of Science and Innovation of South Africa. This contribution has an iPhakade publication number of 245.

References

- Adewoyin OO, Joel ES, Kayode OT (2016) Groundwater resource management: a way to reduce poverty in Africa. *Res J Appl Sci* 11:1465–1469
- Adger WN, Arnell NW, Tompkins EL (2005) Successful adaptation to climate change across scales. *Glob Environ Chang* 15:77–86. <https://doi.org/10.1016/j.gloenvcha.2004.12.005>
- Aeschbach-Hertig W, Gleeson T (2012) Regional strategies for the accelerating global problem of groundwater depletion. *Nat Geosci* 5:853–861. <https://doi.org/10.1038/ngeo1617>
- Agder NW, Nelly PM (1999) Social vulnerability to climate change and the architecture of entitlements. *Mitig Adapt Strateg Glob Chang*. <https://doi.org/10.1023/A:1009601904210>
- Al-Zabet T (2002) Evaluation of aquifer vulnerability to contamination potential using the DRASTIC method. *Environ Geol* 43:203–208. <https://doi.org/10.1007/s00254-002-0645-5>
- Alexander LV, Zhang X, Peterson TC, Caesar J, Gleason B, Klein Tank AMG, Haylock M, Collins D, Trewin B, Rahimzadeh F, Tagipour A, Rupa Kumar K, Revadekar J, Griffiths G, Vincent L, Stephenson DB, Burn J, Aguilar E, Brunet M, Taylor M, New M, Zhai P, Rusticucci M, Vazquez-Aguirre JL (2006) Global observed changes in daily climate extremes of temperature and precipitation. *J Geophys Res Atmos* 111:1–22. <https://doi.org/10.1029/2005JD006290>
- Aller L, Lehr JH, Petty R (1987) A standardized system to evaluate ground water pollution potential using hydrogeologic settings. *Natl Water Well Assoc*, Dublin
- Andiswa M, Conrad J, Jones S (2012) Aquifer type and yield, South Africa. *Orate Hydrol Serv Information, Groundw. CSIR.*, 22 March 1999.
- Archer ERM, Engelbrecht FA, Hänslér A, Landman W, Tadross M, Helmschrot J (2018) Seasonal prediction and regional climate projections for southern Africa. *Klaus Hess Publishers, Windhoek*
- Biermann F, Dingwerth K (2004) Global environmental change and the nation state. *Glob Environ Polit* 4:1–22. <https://doi.org/10.1162/152638004773730185>
- Cannon AJ (2015) Selecting GCM scenarios that span the range of changes in a multimodel ensemble: application to CMIP5 climate extremes indices. *J Clim* 28:1260–1267. <https://doi.org/10.1175/JCLI-D-14-00636.1>
- Census (2011) Statistics South Africa. *Census (2011). Stat South Africa* 78
- Changming L, Jingjie Y, Kendy E (2001) Groundwater exploitation and its impact on the environment in the North China plain. *Water Int* 26:265–272. <https://doi.org/10.1080/02508060108686913>
- Civita M (1994) *Le carte di vulnerabilita degli acquiferi all'inquinamento: teoria e pratica*. Quad di Tec di Prot Ambient Pitagora ed.
- Cobbing JE, Hobbs PJ, Meyer R, Davies J (2008) A critical overview of transboundary aquifers shared by South Africa. *Hydrogeol J* 16:1207–1214. <https://doi.org/10.1007/s10040-008-0285-2>
- Cohen B (2006) Urbanization in developing countries: current trends, future projections, and key challenges for sustainability. *Technol Soc* 28:63–80. <https://doi.org/10.1016/j.techsoc.2005.10.005>
- Corniello A, Ducci D, Napolitano P (1997) Comparison between parametric methods to evaluate aquifer pollution vulnerability using GIS: an example in the “Piana Campana”, southern Italy. *Eng Geol Environ Balkema, Rotterdam* 1721–1726.
- Doerfliger N, Zwahlen F (1997) EPIK: a new method for outlining of protection areas in karstic environment. In: Günay G, Jonshon A (ed) *International Symposium and Field Seminar on Karst waters and environmental impacts*. Balkema, Rotterdam. pp 117–123
- Doll P (2009) Vulnerability to the impact of climate change on renewable groundwater resources: a global-scale assessment. *Environ Res Lett*. <https://doi.org/10.1088/1748-9326/4/3/035006>
- DWAF (2004) Overview of the South African water sector. *Natl water Resour Strateg* 1:1–35
- Eckstein GE (2011) Managing buried treasure across frontiers: the international law of transboundary aquifers. *Water Int* 36:573–583. <https://doi.org/10.1080/02508060.2011.598642>
- Famiglietti JS (2014) The global groundwater crisis. *Nat Clim Chang* 4:945–948. <https://doi.org/10.1038/nclimate2425>
- Farr T, Rosen P, Caro E, Crippen R, Duren R, Hensley S, Kobrick M, Paller M, Rodriguez E, Roth L, Seal D, Shaffer S, Shimada J, Umland J, Werner M, Oskin M, Burbank D, Alsdorf D (2007) The shuttle radar topography mission. *Rev Geophys* 45:1–33. <https://doi.org/10.1029/2005RG000183.1>. INTRODUCTION
- Feng W, Zhong M, Lemoine JM, Biancale R, Hsu HT, Xia J (2013) Evaluation of groundwater depletion in North China using the gravity recovery and climate experiment (GRACE) data and ground-based measurements. *Water Resour Res* 49:2110–2118. <https://doi.org/10.1002/wrcr.20192>
- Foster S (1987) Fundamental concepts in aquifer vulnerability, pollution risk and protection strategy. *Vulnerability of soil and groundwater to pollutants, Proc Inf* 38:69–86. van Duijvenbooden W, van Waegeningh HG TNO Comm Hydrol Res Hague Vulnerabil, 69–86
- Giordano M (2006) Agricultural groundwater use and rural livelihoods in sub-Saharan Africa: a first-cut assessment. *Hydrogeol J* 14:310–318. <https://doi.org/10.1007/s10040-005-0479-9>
- Gleeson T, Befus KM, Jasechko S, Luijendijk E, Cardenas MB (2015) The global volume and distribution of modern groundwater. *Nat Geosci Adv*. <https://doi.org/10.1038/ngeo2590>
- Gordon B, Callan P, Vickers C (2008) WHO guidelines for drinking-water quality. *WHO Chron* 38:564. [https://doi.org/10.1016/S1462-0758\(00\)00006-6](https://doi.org/10.1016/S1462-0758(00)00006-6)
- Gorelick SM, Zheng C (2015) Global change and the groundwater-management challenge Steven. *Water Resour Res*. <https://doi.org/10.1002/2014WR016825>. Received

- Green TR, Taniguchi M, Kooi H, Gurdak JJ, Allen DM, Hiscock KM, Treidel H, Aureli A (2011) Beneath the surface of global change: impacts of climate change on groundwater. *J Hydrol* 405:532–560. <https://doi.org/10.1016/j.jhydrol.2011.05.002>
- Guermazi E, Milano M, Reynard E, Zairi M (2019) Impact of climate change and anthropogenic pressure on the groundwater resources in arid environment. *Mitig Adapt Strateg Glob Chang* 24:73–92. <https://doi.org/10.1007/s11027-018-9797-9>
- Hamed Y, Ahmadi R, Hadji R, Mokadem N, Dhia HB, Ali W (2014) Groundwater evolution of the continental intercalaire aquifer of Southern Tunisia and a part of Southern Algeria: use of geochemical and isotopic indicators. *Desalin Water Treat* 52:1990–1996. <https://doi.org/10.1080/19443994.2013.806221>
- Harbor JM (1994) A practical method for estimating the impact of land-use change on surface runoff, groundwater recharge and wetland hydrology. *J Am Plan Assoc* 60:95–108. <https://doi.org/10.1080/01944369408975555>
- Her Y, Yoo SH, Cho J, Hwang S, Jeong J, Seong C (2019) Uncertainty in hydrological analysis of climate change: multi-parameter vs. multi-GCM ensemble predictions. *Sci Rep* 9:1–22. <https://doi.org/10.1038/s41598-019-41334-7>
- Hewitson BC, Crane RG (2006) Consensus between GCM climate change projections with empirical downscaling: precipitation downscaling over South Africa. *Int J Climatol* 26:1315–1337. <https://doi.org/10.1002/joc.1314>
- Holman IP (2006) Climate change impacts on groundwater recharge-uncertainty, shortcomings, and the way forward? *Hydrogeol J* 14:637–647. <https://doi.org/10.1007/s10040-005-0467-0>
- Jasechko S, Perrone D, Befus KM, Bayani Cardenas M, Ferguson G, Gleeson T, Luijendijk E, McDonnell JJ, Taylor RG, Wada Y, Kirchner JW (2017) Global aquifers dominated by fossil groundwaters but wells vulnerable to modern contamination. *Nat Geosci* 10:425–429. <https://doi.org/10.1038/ngeo2943>
- Kelly PM, Adger WN (2000) Theory and practice in assessing vulnerability to climate change and facilitating adaptation. *Clim Change* 47:325–352. <https://doi.org/10.1023/A:1005627828199>
- Khan MR, Michael HA, Nath B, Huhmann BL, Harvey CF, Mukherjee A, Choudhury I, Chakraborty M, Ullah MS, Ahmed KM, Goodbred SL, Schlosser P, Bostick BC, Mailloux BJ, Ellis T, van Geen A (2019) High-arsenic groundwater in the southwestern bengal basin caused by a lithologically controlled deep flow system. *Geophys Res Lett* 46:13062–13071. <https://doi.org/10.1029/2019GL084767>
- Konikow LF, Kendy E (2005) Groundwater depletion: a global problem. *Hydrogeol J* 13:317–320. <https://doi.org/10.1007/s10040-004-0411-8>
- Krueger E, Rao PSC, Borchardt D (2019) Quantifying urban water supply security under global change. *Glob Environ Chang* 56:66–74. <https://doi.org/10.1016/j.gloenvcha.2019.03.009>
- Liu CW, Lin KH, Kuo YM (2003) Application of factor analysis in the assessment of groundwater quality in a blackfoot disease area in Taiwan. *Sci Total Environ* 313:77–89. [https://doi.org/10.1016/S0048-9697\(02\)00683-6](https://doi.org/10.1016/S0048-9697(02)00683-6)
- Mair A, Hagedorn B, Tillery S, El-Kadi AI, Westenbroek S, Ha K, Koh GW (2013) Temporal and spatial variability of groundwater recharge on Jeju Island. *Korea J Hydrol* 501:213–226. <https://doi.org/10.1016/j.jhydrol.2013.08.015>
- Mann ME, Gleick PH (2015) Climate change and California drought in the 21st century: Fig. 1. *Proc Natl Acad Sci* 112:3858–3859. <https://doi.org/10.1073/pnas.1503667112>
- Mansour MM, Wang L, Whiteman M, Hughes AG (2018) Estimation of spatially distributed groundwater potential recharge for the United Kingdom. *Q J Eng Geol Hydrogeol* 51:247–263. <https://doi.org/10.1144/qjegh2017-051>
- Mazzoni A, Heggy E, Scabbia G (2018) Forecasting water budget deficits and groundwater depletion in the main fossil aquifer systems in North Africa and the Arabian Peninsula. *Glob Environ Chang* 53:157–173. <https://doi.org/10.1016/j.gloenvcha.2018.09.009>
- McCaffrey SC (2011) The international law commission's flawed draft articles on the law of transboundary aquifers: the way forward. *Water Int* 36:566–572. <https://doi.org/10.1080/02508060.2011.597094>
- Mukherjee A, Sengupta MK, Hossain MA, Ahamed S, Das B, Nayak B, Lodh D, Rahman MM, Chakraborti D (2006) Arsenic contamination in groundwater: a global perspective with emphasis on the Asian scenario. *J Heal Popul Nutr* 24:142–163. <https://doi.org/10.2307/23499353?ref=search-gateway:803bb27ee5fb1f2d0cb0903413696e4c>
- Musekiwa C, Majola K (2013) Groundwater vulnerability map for South Africa. *South Afr J Geomat* 2:152–163
- Napolitano P, Fabbri AG (1996) Single-parameter sensitivity analysis for aquifer vulnerability assessment using DRASTIC and SINTACS. *IAHS Publ. Proc Rep Intern Assoc Hydrol Sci* 235:559–566
- Prescott CL, Dolan AM, Haywood AM, Hunter SJ, Tindall JC (2018) Regional climate and vegetation response to orbital forcing within the mid-Pliocene warm period: a study using HadCM3. *Glob Planet Change* 161:231–243. <https://doi.org/10.1016/j.gloplacha.2017.12.015>
- Puri S, Aureli A (2005) Transboundary aquifers: a global program to assess, evaluate, and develop policy. *Ground Water* 43:661–668. <https://doi.org/10.1111/j.1745-6584.2005.00100.x>
- Puri S, Villholth KG (2018) Governance and management of transboundary aquifers. *Adv Groundw Gov* 367–388.
- Richey AS, Thomas BF, Lo MH, Reager JT, Famiglietti JS, Voss K, Swenson S, Rodell M (2015) Quantifying renewable groundwater stress with GRACE. *Water Resour Res* 51:5217–5237. <https://doi.org/10.1002/2015WR017349>
- Robins NS, Chilton PJ, Cobbing JE (2007) Adapting existing experience with aquifer vulnerability and groundwater protection for Africa. *J Afr Earth Sci* 47:30–38. <https://doi.org/10.1016/j.jafrearsci.2006.10.003>
- Rodell M, Velicogna I, Famiglietti JS (2015) Satellite-based estimates of groundwater depletion in India. *Curr Sci* 109:610–617. <https://doi.org/10.1038/nature08238>
- Scanlon BR, Faunt CC, Longuevergne L, Reedy RC, Alley WM, McGuire VL, McMahon PB (2012) Groundwater depletion and sustainability of irrigation in the US High Plains and Central Valley. *Proc Natl Acad Sci* 109:9320–9325. <https://doi.org/10.1073/pnas.1200311109>
- Scanlon BR, Reedy RC, Stonestrom DA, Prudic DE, Dennehy KF (2005) Impact of land use and land cover change on groundwater recharge and quality in the southwestern US. *Glob Chang Biol* 11:1577–1593. <https://doi.org/10.1111/j.1365-2486.2005.01026.x>
- Schulze RE, Lynch SD, Maharaj M (2006) Annual precipitation. South African Atlas Climatol. *Agrohydrology*. *Water Res Comm Pretoria, RSA, WRC Rep.* 489/1/06, Section 6.2.
- Schulze RE, Maharaj M (2006a) Mean annual temperature. South African Atlas Climatol. *Agrohydrology*. *Water Res Comm Pretoria, RSA, WRC Rep.* 1489/1/06, Section 7.2. <https://doi.org/10.15713/ins.mmj.3>
- Schulze RE, Maharaj M (2006b) A-pan equivalent reference. South African Atlas Climatol. *Agrohydrology*. *Water Res. Comm. Pretoria, RSA, WRC Rep.* 1489/1/06, Section 13.2.
- Smerdon BD (2017) A synopsis of climate change effects on groundwater recharge. *J Hydrol* 555:125–128. <https://doi.org/10.1016/j.jhydrol.2017.09.047>
- Stempvoort DV, Ewert L, Wassenaar L (1993) Aquifer vulnerability index: a Gis-compatible method for groundwater vulnerability mapping. *Can Water Resour J* 18:25–37. <https://doi.org/10.4296/cwrj1801025>

- Tadross M, Jack C, Hewitson B (2005) On RCM-based projections of change in southern African summer climate. *Geophys Res Lett* 32:1–4. <https://doi.org/10.1029/2005GL024460>
- Tallaksen LM, Hisdal H, Lanen HAJV (2009) Space-time modelling of catchment scale drought characteristics. *J Hydrol* 375:363–372. <https://doi.org/10.1016/j.jhydrol.2009.06.032>
- Timbal B, Fawcett R (2013) A historical perspective on Southeastern Australian rainfall since 1865 using the instrumental record. *J Clim* 26:1112–1129. <https://doi.org/10.1175/JCLI-D-12-00082.1>
- Treidel H, Martin-Bordes JL, Gurdak JJ (2011) Climate change effects on groundwater resources: a global synthesis of findings and recommendations. CRC Press, Boca Raton
- Vengosh A (2013) Salinization and saline environments. Treatise on geochemistry. Elsevier Ltd., Amsterdam. <https://doi.org/10.1016/B978-0-08-095975-7.00909-8>
- Villara PC, Ribeiro WC (2011) The agreement on the guarani aquifer: a new paradigm for transboundary groundwater management? *Water Int* 36:646–660. <https://doi.org/10.1080/02508060.2011.603671>
- Villholth KG, Tøttrup C, Stendel M, Maherry A (2013) Integrated mapping of groundwater drought risk in the Southern African development community (SADC) region. *Hydrogeol J* 21:863–885. <https://doi.org/10.1007/s10040-013-0968-1>
- Wada Y, Heinrich L (2013) Assessment of transboundary aquifers of the world—vulnerability arising from human water use. *Environ Res Lett*. <https://doi.org/10.1088/1748-9326/8/2/024003>
- Wada Y, Van Beek LPH, Van Kempen CM, Reckman JWTM, Vasak S, Bierkens MFP (2010) Global depletion of groundwater resources. *Geophys Res Lett* 37:1–5. <https://doi.org/10.1029/2010GL044571>
- Woldeamlak ST, Batelaan O, De Smedt F (2007) Effects of climate change on the groundwater system in the Grote-Nete catchment. *Belgium Hydrogeol J* 15:891–901. <https://doi.org/10.1007/s10040-006-0145-x>
- Xie SP, Deser C, Vecchi GA, Collins M, Delworth TL, Hall A, Hawkins E, Johnson NC, Cassou C, Giannini A, Watanabe M (2015) Towards predictive understanding of regional climate change. *Nat Clim Chang* 5:921–930. <https://doi.org/10.1038/nclimate2689>

Publisher's Note Springer Nature remains neutral with regard to jurisdictional claims in published maps and institutional affiliations.

CHAPTER 6 CONCLUSIONS AND RECOMMENDATIONS

1. Synopsis

Understanding the resilience and vulnerability of water resources is integral to the development of sustainable groundwater management strategies. Constraining hydrological resilience typically requires a comprehensive understanding of the physical hydrogeologic environment and vulnerability assessments have, in the past, focussed on the contamination of resources (e.g. DRASTIC). In regions where monitoring data is scarce and the regional environment is heterogenous, conventional approaches are difficult to perform. The use of isotope tracers, as an alternative to numerical approaches, has been proven effective in the prediction of groundwater residence times and recharge rates (Bethke and Johnson, 2008; Cartwright, 2010; Cartwright et al., 2017; Turnadge and Smerdon, 2014). Although researchers have used ^3H to interpret modern groundwater distributions on a global scale (Gleeson et al., 2016), regional and local variations of ^3H in precipitation and groundwater remain unclear. Furthermore, ^3H as a residence time indicator is incapable of constraining mixing relationships of modern and fossil groundwaters and a residence time indicator on older groundwater is necessary. This thesis investigates the variability of ^3H in precipitation, both spatially and temporally for South Africa, by constraining the correlation of water mass origin with the ^3H activity of local rainfall (Chapter 2). With a better understanding of local and seasonal variability of ^3H in South African precipitation, the theoretical abundance of ^3H and ^{14}C is predicted using lumped parameter models to assess the proportion of modern groundwater present in major southern African aquifers as well as the age of the fossil mixing component (Chapter 3). The distribution of ^3H in groundwater across South Africa is modelled to assess the degree at which variability of ^3H in precipitation is transferred into the groundwater system, the effect of transport through the unsaturated zone and to isolate how actively recharged groundwater is (Chapter 4). Ultimately, the distribution of ^3H in groundwater across South Africa is used as a recharge indicator in a novel approach to assess groundwater vulnerability to both a decrease in quantity and a deterioration in quality (Chapter 5).

2. Major contributions

The development and application of a model, that uses information derived from HYSPLIT, to assess the dependence of ^3H variability in daily rainfall on a local and regional scale, constrained processes that control ^3H variability that has previously not been addressed. This study not only showed that the variability of ^3H in precipitation in South Africa is significant on a seasonal and regional scale as was predicted in California by Visser et al., (2018), but also between daily precipitation and within large storm events. Where differences in the water mass origin of summer and winter rainfall, as well as coastal and inland precipitation, entrain and dilute the atmospheric activity differently. The effect of origin altitude of precipitation was constrained for the first time and modelled data showed compelling evidence of elevated tritium present in precipitation formed at higher altitudes. It is imperative that the input of ^3H into groundwater is not assumed to be uniform over a local scale nor over different seasons, particularly for hydrological studies that use the activity of ^3H in groundwater for residence time and recharge assessments.

By understanding the mechanisms that control the variability of ^3H in precipitation, the atmospheric record obtained from GNP monthly stations in the SADC region can be appropriately adjusted over a regional context. Where previous studies have used the closest precipitation ^3H record to the field area (A. P. Atkinson et al., 2014; Cartwright et al., 2013), this model approach included the potential for spatial and temporal variability of ^3H in local precipitation. This in turn, combined with atmospheric and soil records of ^{14}C in the southern hemisphere, was used to predict the modern proportions and fossil mixing component ages of groundwater in southern Africa for the first time on a regional scale. The model, based on lumped parameter modelling methodology, incorporated a thorough evaluation of open carbonate dissolution potential without access to measured ^{13}C in soil and the subsurface, that dilutes the ^{14}C relative abundance. Regions of higher modern groundwater proportions represent more sustainable reserves yet may be vulnerable to climate change as well as modern contaminants. Groundwater in the Western Cape of South Africa, which has been targeted for supply to curtail water shortages, is one such example and caution must be taken to forecast how this resource will be affected by climate change, land use change and a shift in resource dependence. This

Chapter 6 – Conclusions and Recommendations

been targeted for supply to curtail water shortages, is one such example and caution must be taken to forecast how this resource will be affected by climate change, land use change and a shift in resource dependence. This novel approach enabled the characterization of mixed and unmixed systems, and the ages of the fossil groundwater they are mixed with and in turn, strengthened the understanding of regional hydrological resilience in southern Africa.

As groundwater ^3H activities are not monitored in South Africa, there is no data available to predict the distribution and temporal change of ^3H activity on a regional scale. The collection of regional groundwater samples, supplemented by a successful citizen science campaign and collated with data provided from the Department of Water Affairs, produced the largest known dataset of groundwater ^3H activities in South Africa. The geostatistical interrogation of ^3H in South African groundwater identified significant spatial structure dependence on ^3H variability in precipitation and the impact of travel time through the unsaturated zone. Distributions and relationships of modern groundwater were akin to those predicted in California (Visser et al., 2016), where shallower depth to groundwater and productive aquifers, in regions that received more frequent rainfall had elevated tritium activities. These findings are particularly important in predicting the spatial distribution of ^3H in groundwater accurately and in turn assessing how ^3H activity is related to aquifer vulnerability, sustainability, recharge locations and mechanisms, and the anthropogenic impact on recharge in South Africa.

As South Africa becomes more dependent on groundwater resources and these resources are put under further stress through changes in climate, the continual exploration for shale gas and augmentation of groundwater to curtail the effects of drought, the need for groundwater assessment tools has never been greater. As the region lacks much of the data needed to perform a regional numerical assessment on groundwater recharge and flow mechanics, the establishment of regional distributions on ^3H in groundwater provides an important recharge indicator across South Africa. The vulnerability, sustainability and resilience of groundwater is now at the forefront of water resource management strategies in South Africa. As vulnerability assessments are generally focussed on pollution potential (Aller et al., 1987; Napolitano and Fabbri, 1996; Stempvoort et al., 1993) or drought risk (Villholth et al., 2013) independently, the resources needed to constrain vulnerability to several risks is difficult and potentially conflicting. The development, review and application of a novel groundwater vulnerability assessment, that encompasses quantity and quality risks, provides a holistic understanding of South African groundwater resource vulnerability.

3. Recommendations and future work

The collection, analysis and interpretation of tracer data in southern Africa, in both precipitation and groundwater, has enabled this study to investigate the intricacies associated with using ^3H and ^{14}C isotopes in regional hydrological studies. The development of several model approaches to fulfil the aims and objectives of this study was integral to the contributions that this research has made to the scientific community. However, there are limitations and questions pertaining to the collected datasets and model frameworks that could be addressed in future research:

- 3.1. The availability of isotope data in both precipitation and groundwater is limited in southern Africa. As the region acquires a larger capacity to analyse stable and radio isotopes in both higher volume and precision, so the likelihood of reliable monitoring data increases. The methods outlined in this study are dependent on reliable and comprehensive datasets. Although our efforts have vastly improved our current understanding of tracer distributions, predicted variability and fluxes of these tracers, future research would benefit from complete temporal and higher density spatial records of tracer abundance.
- 3.2. The calculations of water mass transport in chapter 2 cannot constrain the recycling of moisture within the air column during transport and isotopic signals may change significantly over a ‘water parcel’s’ trajectory. Improvements to the prediction of moisture flux within a water parcel would be beneficial. Furthermore, the current model bounds are limited to an upper altitude of 10km and the origin of South African snow fall, which measured to have the highest ^3H activity of all precipitation samples, could not be constrained as the moisture origins were predicted to fall above the upper limits of the model. This approach would benefit from the inclusion of a strato-tropospheric mixing model to better constrain high altitude trajectories.
- 3.3. The prediction of mixing between modern and fossil groundwater in chapter 3 is dependent on numerous variables that contain several assumptions in this study due to data scarcity, including: [1] the initial ^3H activity in recharge is

Chapter 6 – Conclusions and Recommendations

assumed to be similar to a weighted moving average of local GNIP stations, adjusted for known controls on ^3H activity; [2] the degree of open system dissolution of carbonate material is related to the presence of carbonate material and measured $\delta^{13}\text{C}$; [3] the dilution factor of samples that are predicted to have undergone closed system dissolution is calculated from predicted initial (soil) and carbonate rock $\delta^{13}\text{C}$ values; [4] all groundwater flow across the region is homogenised in the LPM methodology to behave similar to an exponential piston flow model with an f value of 0.6; [5] percentages of mixed wells and ranges of fossil ages are predicted from abundance curves that use ^{14}C atmospheric and soil records not from South Africa. The predictions and assumptions should be mitigated, largely through data availability, to improve the robustness of predictions made in chapter 3.

- 3.4. The ranges of ^{14}C mean residence times calculated in chapter 3 are relatively young compared to the upper bounds of calculated ^{14}C ages from a smaller portion of the dataset. Additionally, some individual samples are absent of ^{14}C , which suggests that the selected tracers in this study may not constrain the upper boundary of ages correctly. Future research should consider including a residence time tracer with a longer lifespan than ^{14}C to account for fossil waters older than ~50 000 years in these isolated cases.
- 3.5. Although the prediction residuals of ^3H distribution in groundwater in chapter 4 were acceptable, large areas of high prediction variance were concerning. These are directly attributed to poor sample density and a result of either limited sampling resources or unreliable citizen science collection campaigns. Although citizen science collection was integral in the sampling process, improvements could be made to the creation of awareness and commitment of volunteers.
- 3.6. The most significant limitation to groundwater collected in this study is the lack of information about well screen depths, wider water tables, casing depths and water levels of sampled wells. The result of which is a lack of distinction between aquifers in a single location or mixing between multiple aquifers within the well casing. Although this is somewhat mitigated by the behaviour of ^3H in the subsurface, the distinction of aquifers would be beneficial in future research endeavours.
- 3.7. As the groundwater vulnerability model presented in chapter 5 is novel and has only been applied in a South African context, the testing of parameter sensitivity and input parameter relevance in other regions and environments would greatly benefit the model framework and scenario selection process. As data for the outlined input parameters is not always available, a reassessment of what are the strongest controls on output vulnerability could be beneficial in certain environments. The forecasting of vulnerabilities should be done with the latest climate modelling techniques (e.g. RCM downscaling), and bias the climate projection to align with local climatic conditions (Gudmundsson et al., 2012), to predict a more representative evolution of groundwater vulnerability over time.

References

- Aller, L., Lehr, J. H., & Petty, R. (1987). A Standardized System to Evaluate Ground Water Pollution Potential Using Hydrogeologic Settings. In National Water Well Association (p. 20). <http://rdn.bc.ca/cms/wpattachments/wpID3175atID5999.pdf>
- Atkinson, A. P., Cartwright, I., Gilfedder, B. S., Cendón, D. I., Unland, N. P., & Hofmann, H. (2014). Using ^{14}C and ^3H to understand groundwater flow and recharge in an aquifer window. *Hydrology and Earth System Sciences*, 18(12), 4951–4964. <https://doi.org/10.5194/hess-18-4951-2014>
- Bethke, C. M., & Johnson, T. M. (2008). Groundwater Age and Groundwater Age Dating. *Annual Review of Earth and Planetary Sciences*, 36(1), 121–152. <https://doi.org/10.1146/annurev.earth.36.031207.124210>
- Cartwright, I. (2010). Using groundwater geochemistry and environmental isotopes to assess the correction of ^{14}C ages in a silicate-dominated aquifer system. *Journal of Hydrology*, 382(1–4), 174–187. <https://doi.org/10.1016/j.jhydrol.2009.12.032>
- Cartwright, I., Cendón, D., Currell, M., & Meredith, K. (2017). A review of radioactive isotopes and other residence time tracers in understanding groundwater recharge: Possibilities, challenges, and limitations. *Journal of Hydrology*, 555, 797–811. <https://doi.org/10.1016/j.jhydrol.2017.10.053>
- Cartwright, I., Fifield, L. K., & Morgenstern, U. (2013). Using ^3H and ^{14}C to constrain the degree of closed-system dissolution of calcite in groundwater. *Applied Geochemistry*, 32, 118–128. <https://doi.org/10.1016/j.apgeochem.2012.10.023>
- Gleeson, T., Befus, K. M., Jasechko, S., Luijendijk, E., & Cardenas, M. B. (2016). The global volume and distribution of modern groundwater. *Nature Geoscience*, 9(2), 161–164. <https://doi.org/10.1038/ngeo2590>
- Gudmundsson, L., Bremnes, J. B., Haugen, J. E., & Engen-Skaugen, T. (2012). Downscaling RCM precipitation to the station scale using statistical transformations—a comparison of methods. *Hydrology and Earth System Sciences*, 16(9), 3383–3390.

Chapter 6 – Conclusions and Recommendations

Napolitano, P., & Fabbri, A. G. (1996). Single-parameter sensitivity analysis for aquifer vulnerability assessment using DRASTIC and SINTACS. *IAHS Publications-Series of Proceedings and Reports-Intern Assoc Hydrological Sciences*, 235(235), 559–566.

Stempvoort, D. Van, Ewert, L., & Wassenaar, L. (1993). Aquifer Vulnerability Index: a Gis - Compatible Method for Groundwater Vulnerability Mapping. *Canadian Water Resources Journal*, 18(1), 25–37. <https://doi.org/10.4296/cwrj1801025>

Turnadge, C., & Smerdon, B. D. (2014). A review of methods for modelling environmental tracers in groundwater: Advantages of tracer concentration simulation. *Journal of Hydrology*, 519(PD), 3674–3689. <https://doi.org/10.1016/j.jhydrol.2014.10.056>

Villholth, K. G., Tøttrup, C., Stendel, M., & Maherry, A. (2013). Integrated mapping of groundwater drought risk in the Southern

African Development Community (SADC) region. *Hydrogeology Journal*, 21(4), 863–885. <https://doi.org/10.1007/s10040-013-0968-1>

Visser, A., Moran, J. E., Hillemonds, D., Singleton, M. J., Kulongoski, J. T., Belitz, K., & Esser, B. K. (2016). Geostatistical analysis of tritium, groundwater age and other noble gas derived parameters in California. *Water Research*, 91, 314–330. <https://doi.org/10.1016/j.watres.2016.01.004>

Visser, Ate, Thaw, M., & Esser, B. (2018). Analysis of air mass trajectories to explain observed variability of tritium in precipitation at the Southern Sierra Critical Zone Observatory, California, USA. *Journal of Environmental Radioactivity*, 181(June 2017), 42–51. <https://doi.org/10.1016/j.jenvrad.2017.10.008>

APPENDIX

The appendix consists of data or supplementary material included in the online publication of the journal articles. These are separated into the four chapters. The chapter 2 (paper 1) appendix consists of three tables: [1] Analysis results of samples collected in Paarl, Western Cape, [2] Analysis results of samples collected in single storm events and [3] Analysis results of regional samples. The chapter 3 (paper 2) appendix consists of two tables: [1] ^{14}C and ^3H data, from across Namibia, Botswana, Mozambique and South Africa, collated from published and unpublished literature producing 624 data points and [2] the data sources from which the collated data was acquired. The chapter 4 (paper 3) appendix consists of two tables: [1] Analysis results of samples collected in by authors over seven sampling campaigns and [2] Analysis results of samples collated by iThemba LABS and the Department of Water Affairs (DWA). Any data or material not supplied in this appendix is available upon request or is published in research outside the scope of this thesis. The appendix is ordered accordingly below:

Sample Name	Time	Date	Tritium (TU)	TU		
				Uncertainty	d 2H	d 18O
JAR009	Daytime	03 October 2017	1.60		11.0	-0.64
JAR010	08:00	03 November 2017	3.53		3.1	-1.96
JAR014	08:00	21 November 2017	0.62		10.7	2.03
JAR015	08:00	10 February 2018	0.96	0.03		
JAR027	08:00	12 April 2018	4.02	0.10		
JAR028	08:00	06 April 2018	1.17	0.04		
JAR029	08:00	18 April 2018	1.28	0.06	11.3	-0.42
JAR030	08:00	30 March 2018	2.96	0.08		
JAR031	08:00	29 March 2018	2.33	0.08		
JAR040	08:00	26 April 2018	1.94		-19.3	-4.74
JAR041	08:00	02 May 2018	3.00			
JAR042	08:00	27 April 2018	1.85	0.07		
JAR043	08:00	26 April 2018	1.86	0.23	-6.1	-3.56
JAR044	08:00	08 May 2018	0.93		-18.3	-3.97
JAR045	08:00	28 April 2018	1.46	0.06	-5.6	-3.76
Jar18302	8:30-10:00	14 June 2018	1.20	0.06	-16.2	-3.80
Jar18303	22:00-00:00	14 June 2018	0.98	0.05	-14.9	-3.84
Jar18304	8:30-10:30	16 June 2018	1.50	0.08	-16.6	-4.22
Jar18305	12:00-14:00	14 June 2018	1.91	0.04	-9.8	-3.30
Jar18306	14:00-18:00	14 June 2018	1.45		-35.0	-6.37
Jar18307	7:00-9:00	16 June 2018	3.27	0.49	-11.5	-3.76
Jar18308	22:00	16 June 2018	0.91	0.03	-16.6	-4.41
Jar18309	22:30	16 June 2018	1.32	0.06	-16.7	-4.16
Jar18310	10:30	15 June 2018	1.28	0.06	-18.8	-5.42
Jar18311	08:00	22 June 2018	1.28	0.05		
Jar18312	14:30 - 16:30	15 June 2018	0.99	0.05	-7.4	-2.30
Jar18313	06:30 - 08:30	15 June 2018	1.12	0.03	-18.4	-5.29
Jar18314	18:30 - 10:30	15 June 2018	0.93	0.05	-9.9	-3.18
Jar18315	08:00	15 June 2018	1.43	0.06	-19.9	-5.44
Jar18316	08:30 - 10:30	15 June 2018	1.12	0.06	-14.2	-5.04
Jar18317	08:00	18 June 2018	1.13	0.05	-10.1	-3.87
Jar18318	16:30 - 18:30	15 June 2018	1.07	0.03	-11.5	-3.40
Jar18319	08:00	20 June 2018	1.15	0.06	-2.1	-2.29
Jar18320	09:00	01 July 2018	1.08	0.05	0.7	-1.39
Jar18321	08:00	03 July 2018	2.33	0.08	-34.9	-6.97
Jar18322	09:00	30 June 2018	1.61	0.06	-10.2	-2.98
Jar18323	08:00	28 June 2018	1.23	0.07	-15.1	-3.30
Jar18324	08:30	02 July 2018	1.70	0.06		
Jar18325	12:30 - 14:30	15 June 2018	1.33	0.04	7.8	-1.43
Jar18326	08:00	27 June 2018	1.17	0.04	-14.4	-4.00
Jar18327	08:00	24 June 2018	0.79	0.05	7.8	-1.43
Jar18335	18:15	14 July 2018	1.72	0.07	-16.0	-4.09
Jar18336	08:00	12 July 2018	2.27	0.16	12.8	-1.53
Jar18341	07:00	22 May 2018	1.33	0.07	-2.5	-1.37
Jar18342	08:00	24 May 2018	0.69	0.05	-6.6	-3.68
Jar18343	08:00	01 June 2018	0.87	0.06	-15.6	-3.68
Jar18345	17:00	09 June 2018	0.96	0.03	-6.0	-3.28
Jar18346	17:00	06 September 2018	0.87	0.06	-5.9	-2.23
Jar18347	22:00	21 May 2018	2.28	0.16	2.2	-1.32

Jar18348	08:00	05 August 2018	0.45	6.43	-6.5	-3.04
Jar18349	10:00	03 June 2018	0.96	0.05	6.0	-2.24
Jar18350	08:00	29 May 2018	1.30	0.06	-8.9	-3.16
Jar18368	09:00	07 August 2018	2.06	0.07	-19.7	-3.92
Jar18369	08:00	01 August 2018	2.13	0.05	7.9	-1.35
Jar18371	10:00	28 July 2018	1.81	0.05	5.3	-1.90
Jar18372	08:00	06 August 2018	1.82	0.04	17.3	2.88
Jar18394	08:00	27 August 2018	1.64	0.12		
Jar18395	07:00	03 September 2018	2.88	0.16		
Jar18396	07:00	27 August 2018	1.87	0.14		
Jar18397	08:00	14 August 2018	2.17	0.14		
Jar18398	08:30	08 September 2018	2.94	0.08		
Jar18399	11:00	15 September 2018	1.21	0.14		
Jar18400	08:00	23 August 2018	2.78	0.23		
Jar18401	08:00	17 September 2018	1.49	0.07		
Jar18402	08:00	19 September 2018	1.10	0.13		
Jar18403	08:00	13 September 2018	1.74	0.13		
Jar18405	07:30	28 August 2018	1.91	0.08		
Jar18406	08:00	20 August 2018	1.94	0.15		
Jar18407	08:00	06 September 2018	3.48	0.09		
Jar18408	08:00	18 September 2018	1.13	0.11		
Jar18409	08:00	20 August 2018	2.54	0.14		
Jar18410	08:00	05 September 2018	2.00	0.13		
JAR18422	08:00	16 August 2018	1.55	0.07		
JAR18423	08:00	27 September 2018	1.48	0.14		
JAR18424	08:00	28 September 2018	1.10	0.06		
JAR18425	08:00	02 October 2018	2.59	0.17		
JAR18426	08:00	15 October 2018	1.98	0.29		

Sample Name	Date	Town	Lat	Long	Tritium (TU)	d 2H	d 18O
Storm 1							
YADSTEL007	07 June 2017	Stellenbosch	-33.9265	18.86831	0.37	13.0	0.97
YADWC035	07 June 2017	Het Kruis	-32.59137	18.74936	1.24	-6.5	-3.74
YADWC036	07 June 2017	Vanrynsdorp	-31.6089	18.7397	0.85		-4.54
YADWC037	07 June 2017	Robertson	-33.80022	19.87989	1.97	-37.8	-7.61
YADWC32	07 June 2017	Porterville	-33.01472	18.99353	1.20	-7.2	-2.44
Jar18330	08 June 2017	Napier	-34.47242	19.89592	2.02	-33.9	-6.95
YADWC01	08 June 2017	Vyeboom	-34.06667	19.11667	1.70	-16.4	-5.76
YADWC03	08 June 2017	Cape Town	-34.11232	18.84921	1.00	-18.8	-5.14
YADWC04	08 June 2017	Cape Town	-33.94139	18.70664	0.80	-18.4	-5.03
YADWC05	08 June 2017	Cape Town	-33.89748	19.15233	0.90	-24.4	-5.72
YADWC06	08 June 2017	Paarl	-33.78124	19.00157	2.10	-28.9	-7.03
YADWC07	08 June 2017	Villiersdorp	-34.07806	19.28917	0.60	-31.9	-6.84
YADWC08	08 June 2017	Potervillie	-33.36086	19.06422	0.90	-33.3	-7.85
YADWC10	08 June 2017	Paarl	-33.72974	18.96377	0.80	-19.6	-5.02
YADWC11	08 June 2017	Bettys bay	-34.34747	18.92051	1.10	-14.5	-3.95
YADWC12	08 June 2017	Stellenbosch	-33.9265	18.86831	1.50	-23.6	-5.61
YADWC14	08 June 2017	Hermanus	-34.38172	19.24187	1.90	-15.6	-4.68
YADWC15	08 June 2017	Tulbaugh	-33.283	19.1434	1.60	-18.8	-4.73
YADWC16	08 June 2017	Cape Town	-34	18.7393	1.80	-18.0	-4.66
YADWC17	08 June 2017	Paarl	-33.79827	18.96778	1.60	-21.5	-5.23
YADWC18	08 June 2017	Bonnievale	-33.51281	19.1764	2.20	-19.9	-5.48
YADWC19	08 June 2017	Cape Town	-29.70237	17.66586	0.90	-35.5	-6.42
YADWC20	08 June 2017	Bettys bay	-34.34747	18.92051	0.80	-14.0	-4.21
YADWC22	08 June 2017				0.00	-14.6	-3.54
YADWC23	08 June 2017	Lamberts bay	-32.1	18.3	1.10	1.0	-1.86
YADWC24	08 June 2017	Darling	-33.9289	18.41725	1.00	-10.4	-3.84
YADWC25	08 June 2017	Cape Town	-33.986	18.47212	1.10	-20.7	-4.70
YADWC26	08 June 2017	Clanwilliam	-32.19758	18.89674	1.10	2.7	-1.57
YADWC27	08 June 2017	Hermanus	-34.4092	19.25044	1.70	-20.8	-5.66
YADWC28	08 June 2017	Yzerfontein	-33.35986	18.15917	1.00	-32.1	-5.37
YADWC29	08 June 2017	Yzerfontein	-33.35986	18.15917	0.80	-16.2	-5.07
YADWC30	08 June 2017	Piketberg	-32.91161	18.75534	0.60	-15.2	-4.03
YADWC31	08 June 2017	Ket Kruis	-32.59642	18.68565	0.90	0.3	-2.15
YADWC33	08 June 2017	Porterville	-33.01472	18.99353	1.50	-15.1	-5.05
YADWC34	09 June 2017	Porterville	-33.01472	18.99353	1.10	-28.3	-5.19
Storm 2							
Jar18331	13 June 2018	Klipheuwel	-33.72401	18.07082	0.46	-19.3	-4.29
Jar18305	14 June 2018	Paarl	-33.73476	18.95879	1.91	-9.8	-3.30
Jar18302	14 June 2018	Paarl	-33.73476	18.95879	1.17	-16.2	-3.80
Jar18303	14 June 2018	Paarl	-33.73476	18.95879	0.98	-14.9	-3.84
Jar18306	14 June 2018	Paarl	-33.73476	18.95879	1.45	-35.0	-6.37
Jar18332	14 June 2018	Kuilsrivier	-33.92444	18.67156	1.47	-19.9	-5.35
Jar18352	14 June 2018	Stellenbosch	-33.92655	18.86833	1.45	-23.0	-6.20
Jar18356	14 June 2018	melkbosstrand	-33.71299	18.44829	0.37	-11.3	-4.06
Jar18310	15 June 2018	Paarl	-33.73476	18.95879	1.26	-18.8	-5.42
Jar18312	15 June 2018	Paarl	-33.73476	18.95879	0.99	-7.4	-2.30
Jar18313	15 June 2018	Paarl	-33.73476	18.95879		-18.4	-5.29
Jar18314	15 June 2018	Paarl	-33.73476	18.95879	0.91	-9.8	-3.18
Jar18316	15 June 2018	Paarl	-33.73476	18.95879	1.12	-14.2	-5.04
Jar18315	15 June 2018	Paarl	-33.73476	18.95879	1.43	-19.9	-5.44
Jar18325	15 June 2018	Paarl	-33.73476	18.95879	1.33	7.8	-1.43

Jar18318	15 June 2018 Paarl	-33.73476	18.95879	1.07	-11.5	-3.40
Jar18333	15 June 2018 Franschoek	-33.9187	19.11956	1.31	-39.3	-8.66
Jar18337	15 June 2018 Franschoek	-33.90406	19.11971	1.33	-23.1	-4.96
Jar18307	16 June 2018 Paarl	-33.73476	18.95879	3.27	-11.4	-3.76
Jar18308	16 June 2018 Paarl	-33.73476	18.95879	0.91	-16.5	-4.41
Jar18304	16 June 2018 Paarl	-33.73476	18.95879	1.50	-16.5	-4.22
Jar18309	16 June 2018 Paarl	-33.73476	18.95879	1.32	-16.6	-4.16
Jar18328	16 June 2018 Pniel	-33.8975	18.95236	1.31	-18.9	-5.06
Jar18334	16 June 2018 Franschoek	-33.9187	19.11956	0.96		
Jar18338	16 June 2018 Franschoek	-33.90406	19.11971	0.82	-4.9	-3.93
Jar18374	16 June 2018 Paarl	-33.78069	19.00429			
Jar18375	16 June 2018 Paarl	-33.78069	19.00429	1.29	-14.1	-3.53
Jar18339	17 June 2018 Bainskloof	-33.61777	19.10045	1.30	-22.1	-5.92
Jar18340	17 June 2018 Bainskloof	-33.61777	19.10045	1.34	-21.6	-6.39
JAR18421	17 June 2018 Paarl	-33.67579	18.9762	0.94		
Jar18317	18 June 2018 Paarl	-33.73476	18.95879	1.13	-10.0	-3.87
Jar18353	19 June 2018 Stellenbosch	-33.92655	18.86833	1.03	-2.3	-1.81
Jar18372	19 June 2018 Somerset West	-34.05785	18.81708	1.82	3.8	-2.76
Jar18373	19 June 2018 Somerset West	-34.05785	18.81708	1.20	17.0	3.07

Sample Name	Date	Town	Lat	Long	Tritium (TU)	d 2H	d 18O
JAR004	20 March 2018	Beaulieu	-25.9822	28.0722	4.55	19.91	3.06
JAR005	21 November 2017	Riverby	-33.6758	18.9762	1.70	-21.10	-5.73
JAR006	13 February 2018	Amatoni	-33.9379	18.8518	2.48	15.16	2.59
JAR007	13 February 2018	Amatoni	-33.9379	18.8518	2.71	-37.04	-6.59
JAR008	13 February 2018	Amatoni	-33.9379	18.8518	2.82		
JAR011	11 April 2017	Riverby	-33.6758	18.9762	1.83		
JAR012	20 November 2017	Amatoni	-33.9379	18.8518	2.30	-18.36	-5.28
JAR013	02 October 2018	Riverby	-33.6758	18.9762	1.29		
JAR016	19 April 2018	Riverby	-33.6758	18.9762	0.80		
JAR017	22 March 2017	Trollope Farm	-24.6743	27.5020	1.52		
JAR018		Uvongo	-30.8427	30.3839	0.61		
JAR032	15 October 2017	Stellenbosch	-33.9266	18.8683	1.60		
JAR033	25 September 2017	Stellenbosch	-33.9266	18.8683	1.25		
JAR034	21 November 2017	Stellenbosch	-33.9266	18.8683	1.88		
JAR035	30 November 2017	Stellenbosch	-33.9266	18.8683	2.98		
JAR037	21 March 2018	Beaulieu	-25.9822	28.0722	3.01	9.87	0.76
JAR038	18 April 2018	Beaulieu	-25.9822	28.0722	8.09		
JAR039	05 August 2018	Amatoni	-33.9379	18.8518	0.91		
JAR046	04 March 2018	Uvongo	-30.8427	30.3839	1.05		
JAR047	24 March 2018	Uvongo	-30.8427	30.3839	2.96		
JAR18301	03 July 2018	Matroosberg	-33.3866	19.6687	2.56	-57.37	10.96
Jar18329	06 July 2017	Napier	-34.4724	19.8959	1.40	-14.77	-4.80
jar18351	08 July 2018	Stellenbosch	-33.9266	18.8683	1.11	-15.67	-6.36
Jar18355	08 July 2018	Robertson	-33.8015	19.8847	2.49	-24.87	-4.42
Jar18357	03 June 2018	40 Truter Street	-33.8015	19.8847	1.11	-15.43	-4.36
Jar18358	22 July 2018	Arangieskop	-33.7161	19.8771	1.41	-28.38	-6.27
Jar18359	08 July 2018	40 Truter Street	-33.8015	19.8847	2.68	-9.55	-4.27
Jar18362	08 September 2018	40 Truter Street	-33.8015	19.8847	2.27	-7.36	-3.90
Jar18363	06 October 2018	40 Truter Street	-33.8015	19.8847	1.30	-1.65	-0.82
Jar18364	04 August 2018	40 Truter Street	-33.8015	19.8847	4.06	-8.29	-3.21
Jar18365	04 August 2018	40 Truter Street	-33.8015	19.8847	3.90	-15.13	-6.27
Jar18367	02 July 2018	40 Truter Street	-33.8015	19.8847	2.57	-40.99	-8.53
Jar18378	22 May 2018	Stellenbosch	-33.9266	18.8683	1.49	1.71	-1.58
Jar18379	24 May 2018	Stellenbosch	-33.9265	18.8683	0.58	-5.29	-4.34
Jar18380	28 May 2018	Stellenbosch	-33.9266	18.8683	1.03	-0.60	-2.48
Jar18381	01 June 2018	Stellenbosch	-33.9266	18.8683	0.88	-1.29	-2.24
JAR18412	26 August 2018	Geology Dept	-33.9321	18.8625	2.68		
JAR18413	28 March 2018	Summerstrand, PE	-33.9899	25.6639	1.16		
JAR18414	09 August 2018	Summerstrand, PE	-33.9899	25.6639	3.14		
JAR18415	08 September 2018	Summerstrand, PE	-33.9899	25.6639	2.81		
JAR18416	03 September 2018	Summerstrand, PE	-33.9899	25.6639	5.45		
JAR18417	27 August 2018	Matroosberg	-33.3600	19.6255	4.72		
JAR18418	17 August 2018	Near Matroosberg	-33.3152	19.5819	2.73		
JAR18419	26 September 2018	Arangieskop	-33.7161	19.8771	5.88		
JAR18420	26 August 2018	Geology Dept	-33.9321	18.8625	1.60		
JAR18427	26 August 2018	Robertson Farm	-33.7671	19.8659	3.61		
JAR18428	26 August 2018	40 Truter Street	-33.8015	19.8847	4.10		
JAR18430	05 September 2018	40 Truter Street	-33.8015	19.8847	3.26		
JAR18431	06 October 2018	Uvongo	-30.8427	30.3839	1.87		
JAR18432	06 October 2018	Uvongo	-30.8427	30.3839	1.49		
JAR18433	07 December 2018	Namaquasfontein	-32.7194	18.7043	2.09		
JAR18434	12 June 2018	Kersefontein	-32.9029	18.3306	1.97		
JAR18435	12 July 2018	Kersefontein	-32.9029	18.3306	1.82		
JAR18436	12 August 2018	Kersefontein	-32.9029	18.3306	1.80		
JAR18437	12 July 2018	Riebeck Kasteel	-33.3838	18.9144	1.18		
River 13		Riverby	-33.6758	18.9762	0.55	-35.05	-6.04
YAD007	30 May 2017	Loeriesfontein	-30.9770	19.4463	1.29	-3.95	-5.02
YAD008	30 May 2017	Upington	-28.4745	21.2614	2.26	-13.86	-2.87

YAD010	18 March 2017	Kuruman	-27.4389	23.4338	3.66	29.63	3.28
YAD012	10 April 2017	Taken in the field	-27.5540	24.1830	1.60	1.40	-1.03
YAD015	05 April 2017	Roodepoort	-25.8449	28.1537	12.20	-12.02	-2.66
YAD016	01 April 2017	Roodepoort	-25.8449	28.1537	1.65	-30.60	-6.10
YAD019	04 December 2017	Bela-bela	-24.8709	28.1512	1.70	-15.31	-3.65
YAD020 (Timbavati)	15 April 2017	Timbavati	-24.3807	31.2608	1.33	-4.37	-2.88
YAD025	18 April 2017	Vryheid	-27.7571	30.7933	2.19	-7.43	-3.35
YAD030		Mclear	-31.0076	28.2796	1.40	-14.85	-4.22
YAD032	24 March 2017	Gariiep Dam	-30.7167	25.7500	2.63	21.20	-0.43
YADSTEL001	15 July 2017	Stellenbosch	-33.9265	18.8683	2.03		-5.40
YADSTEL002	08 October 2017	Stellenbosch	-33.9265	18.8683	1.06	-4.68	-2.59
YADSTEL003	15 August 2017	Stellenbosch	-33.9265	18.8683	1.87	-8.21	-3.86
YADSTEL004	21 August 2017	Stellenbosch	-33.9265	18.8683	1.57	-12.57	-3.26
YADSTEL005	29 August 2017	Stellenbosch	-33.9265	18.8683	1.59	7.09	-0.86
YADSTEL006	29 August 2017	Stellenbosch	-33.9265	18.8683	2.21	17.91	0.65
YADWC02	06 March 2018	Paarl	-33.7297	18.9638	0.70	5.55	-1.39
YADWC09	06 November 2018	Paarl	-33.7297	18.9638	0.80	-40.18	-6.88
YADWC13	06 November 2018	Stellenbosch	-33.9265	18.8683	0.60	-16.14	-2.98

Sample period	Reference
1969	Vogel, J.C, Thilo L and Van Dijken M 1974. Determination of groundwater recharge with tritium. <i>Journal of Hydrology</i> 23 , 131-140.
1969	Vogel, J.C. and Bredenkamp, D.B. A study of the subterranean water in the Southern Kalahari with the aid of Carbon-14 dating and isotope analysis. Pretoria:NPRL, CSIR. , 1969.
1970	Jennings, Verhagen, Sellschop. The contribution of environmental tritium measurements to some geohydrological problems in Southern Africa. DGS report 3273-1
1974	Vogel, J.C. and van Urk, H. Isotopic composition of groundwater in semi-arid regions of Southern Africa. <i>J Hydrol</i> 25:23-36, 1975.
1974	Verhagen, B.T., Mazor, E., and Sellschop, J.P.F. Radiocarbon and tritium evidence for direct recharge to groundwater in the northern Kalahari. <i>Nature</i> 249:643-644, 1974.
1974	Jennings CMH, 1974. The hydrogeology of Botswana. PhD thesis University of Natal, Pietermaritzburg
1975	Hutton, L.G. & Dincer, T. (1976): Chemistry and stable isotope composition of Okavango Delta waters. Investigation of the Okavango Delta as a Primary Water Resource for Botswana. UNDP/FAO, AG:DP/BOT/71/506, Technical Note 23.
1976	Mazor, E., Verhagen, B.T., Sellschop, J.P.F., Jones, M.T., Robins, N.E., Hutton, L., and Jennings, C.M.H. (1977). Northern Kalahari groundwaters: Hydrologic, isotopic and chemical studies at Orapa, Botswana. <i>J Hydrol</i> 34:203-234.
1977	Verhagen, B.Th., Smith, P.E., McGeorge, I. and Dziembowski, Z.M. (1979) Tritium profiles in Kalahari sands as a measure of rain recharge. <i>Isotope Hydrology</i> 1978 Vol.II. IAEA-SM-228. 733-751. IAEA,Vienna.
1979	Mazor, E., Bielsky, M., Verhagen, B.T., Sellschop, J.P.F., Hutton, L., and Jones, M.T. Chemical composition of groundwaters in the vast Kalahari Flatland. <i>J Hydrol</i> 48:147-165, 1980.
1979	Dziembowski ZM, Verhagen BT, Salgado HR, Smith PE, Erasmus CJH & McGeorge IB (1979). Ground water studies in the Gamogara catchment. Report to the Water Research Commission. Nuclear Physics Research Unit, Johannesburg.
1980	Vogel, J.C, Talma, AS and Heaton, THE (1981). Gaseous nitrogen as evidence for denitrification in groundwater. <i>J. Hydrol.</i> 50, 191-200.
1981	Huyser, D.J., 1982. The Chemical Quality of the Underground Waters of South-West Africa/Namibia (in Afrikaans). Vol 1-3, Dept. Wat. Aff., Pretoria/Windhoek.
1982	Heaton, T.H.E., Talma, A.S., Vogel, J.C., 1983. Origin and history of nitrate in confined groundwater in the Western Kalahari. <i>J. Hydrol</i> 62, 243 -262.
1982	Vogel, J.C, Talma, AS and Heaton, THE (1982). The age and isotopic composition of groundwater in the Stampriet artesian basin, SW Africa. CSIR Research Report.
1982	Mazor, E. Rain recharge in the Kalahari a note on some approaches. <i>J Hydrol</i> 55:137 144, 1982.
1982	Foster, S.S.D., Bath, A.H., Farr, J., and Lewis, W.J. The likelihood of active groundwater recharge in the Botswana Kalahari. <i>J Hydrol</i> 55:113-136, 1982.

- 1982 Verhagen, B.T. (1982) The isotope hydrology of ground waters of the Kalahari, Gordonia. In: Ground Water '82. Abstract. Johannesburg: Geol. Soc. S.Afr. Ground Water Div., 117-122.
- 1983 Heaton, T.H.E., 1984. Sources of the nitrate in phreatic groundwater in the Western Kalahari. *J. Hydrol.* 67, 249-259.
- 1983 Verhagen, B Th. (1983) Environmental Isotope Study of a Ground Water Supply Project in the Kalahari of Gordonia. International Symposium on Isotope Hydrology in Water resources Development. IAEA-SM-2701, Vienna, Austria
- 1984 Verhagen, B.T. (1985) Rain recharge to Kalahari ground waters as revealed in a wellfield. In: Groundwater 1985, Programme and extended abstracts of a symposium, Johannesburg: Geological Society of South Africa, p. 114-116
- 1984 De Vries, J.J., 1984: Holocene depletion and active recharge of the Kalahari groundwaters: a review and an indicative model. *J. Hydrol.* 70, 221-232.
- 1985 Verhagen, B.T. 1987. Environmental isotopes suggest a recharge model for the well field supplying Jwaneng Mine, Botswana. In: *Isotopes Techniques in the Water Resources Development*, Vienna: IAEA.
- 1985 Levin, M, Talma, AS and Vogel, JC (1985). Geohydrological investigation of an uranium anomaly near Vanzylsrus in the northern Cape Province. *Trans. geol. Soc. S. Afr.* 88, 529-540.
- 1985 Verhagen, B.T. Isotope hydrology of ground waters of the Kalahari, Gordonia. *Trans geol Soc S Afr* 88(3):517-522, 1985.
- 1987 Swedish Geological (1988). Serowe: Groundwater resources evaluation project. Final Report CTB No 10/2/7/84-85 to BGS, Botswana. 286pp. SGAB International, Stockholm
- 1988 Verhagen, B.T. and Brook, M.C. (1989) The isotope hydrology of the northern well field, Jwaneng diamond mine, Botswana. In: *Proc Symp: Ground Water and Mining, Randburg*: p. 161-169.
- 1988 Phofuetsile Thesis UCL 1988. Hydrochemistry of the Groundwater in the Kalahari-south western Botswana.
- 1989 Verhagen, B.T. Isotope hydrology of the Kalahari: Recharge or no recharge? *Palaeoecology of Africa* 21:143-158, 1990.
- 1990 Verhagen, B.T. (1991) Detailed geohydrology with environmental isotopes – A case study at Serowe, Botswana. *Isotope Techniques in Water Resources Development 1991*; IAEA-SM-319. 345-362. IAEA, Vienna.
- 1991 Gieske, A. (1992). Dynamics of Groundwater Recharge: A Case Study in Semi Arid Eastern Botswana. Free University, Amsterdam.
- 1991 BRGM (1991). Evaluation of groundwater resources (GS10): Letlhakeng-Botlhapatlou groundwater project, main report. BRGM, Orleans, France.
- 1991 Verhagen BT. Detailed geohydrology with environmental isotopes: a case study at Serowe, Botswana. IAEA-SM-319/25
- 1991 SMEC, WLPU, SGAB (1991) Botswana national water master plan study. Final report to DWA, (LCCN 95980213). Gaborone.
- 1992 BRGM Mmamabula Groundwater resources investigation: Phase II Khurutse area. Report to DGS, tender TB 10/2/3/90-91, 1994
- 1993 Water Surveys Botswana. Groundwater Potential Survey Middelpits/Makopong TGLP areas, Report to DGS tender TB 10/2/8/91-92

- 1994 Verhagen, B.Th., 1995. Semiarid zone groundwater mineralization processes as revealed by environmental isotope studies. In: Application of Tracers in Arid Zone Hydrology, Adar, E., Leibundgut, C., 245-266. IAHS Publ. 232
- 1994 DWA., 1994: Palla-Road Groundwater Resources Investigation. Phase 1. CBT 10/3/26/91-92. Final Report. Appendix 10. Environmental Impact Assessment.
- 1994 Molebatsi, T. (1994) Occurrence and origin of saline groundwaters of the Tsabong Region, south-west Botswana. Thesis submitted in partial fulfilment of M.Sc. Degree, University College London.
- 1994 Van Rensburg HJJ and Bush RA, (1994). Jwaneng northern wellfield - modelling of groundwater flow with optimized management recommendations on wellfield utilization. Anglo American Corporation, Report CED/029/04
- 1994 Carney, J.N., Aldiss, D.T. and Lock, N.P. (1994) The geology of Botswana. Bulletin 37. Geological Survey of Botswana.
- 1994 Geoflux (1994) Groundwater potential survey. Toteng/Sehitwa TGLP area. TB 10/2/90-91. Final report to Geological Survey Dept. Vol.1 232 pp. Gaborone
- 1994 Morosini, M., 1996. Chemical-isotopic character, origin and evolution of groundwater in western Ghanzi District, Botswana. Dept. Geol. Surv., Lobatse, Botswana. 56p, figures and tables.
- 1995 Bredenkamp, D.B., Botha, L.J., van Tonder, G.J., and van Rensburg, H.J. (1995). Manual on Quantitative Estimation of Groundwater Recharge and Aquifer Storativity. Pretoria: Water Research Commission. TT 73/95.
- 1995 Gieske, A. Hydrodynamics of ¹⁴C analysis in unconfined aquifers. In: Groundwater '95, Midrand:Ground Water Division of the Geol Soc of S Afr, 1995,
- 1995 Verhagen, B.T., Levin, M., Farr, J., and Gumiremhete, R. Groundwater recharge in the Kalahari: unravelling the evidence from Jwaneng mine to Palla Road, Botswana. Ground Water '95. In: Conf. on Ground water Recharge and Rural Water Supply, Midrand, South Africa, 1995.
- 1995 Verhagen, B.T., Marobela, C., Sawula, G., and Kgarebe, B. Geohydrological and mineralisation studies with environmental isotopes in a large Kalahari ranching development. In: Isotopes in Water Resources Management. Procs Symposium, Vienna: IAEA, 1995, p. 91 106.
- 1995 Nijsten GJ and Beekman HE (1997). Groundwater recharge and resources assessment in the Botswana Kalahari – Groundwater flow study in the Letlhakeng-Botlhapatlou area. GRES II project: technical report, Dept of geological Survey, Lobatse; University of Botswana, Gaborone: Free University Amsterdam, Netherlands.
- 1996 Beekman, H.E., Gieske, A. and Selaolo, E.T. (1996) GRES – groundwater recharge studies in Botswana (1987-1996). Botswana Journal of Earth Sciences, V 3, pp. 1-17.
- 1996 Morosini, M., 1996b: Chemical-Isotopic Character, Origin and Evolution of Groundwater in Western Ghanzi District, Botswana. Hydrogeochemical Report for the TGLP Ghanzi/Makunda Groundwater Survey. Department of Geological Survey.

- 1996 Verhagen, B. Th., Marobela, C., Sawula, G. and Kgarebe, B. (1996) Geohydrological and mineralization studies with environmental isotopes in a large Kalahari ranching development. *Isotopes in Water Resources Development*. IAEA-SM-336.91-105. IAEA, Vienna.
- 1996 Stute, M and Talma, AS (1998). Glacial temperatures and moisture transport regimes reconstructed from noble gases and ^{18}O in Stampriet aquifer, Namibia. In: *Isotope Techniques in the Study of Environmental Change: Proceedings of Symposium SM-349, 14-18 April 1997*. 307-318. IAEA, Vienna, 932pp.
- 1997 Beekman HE and Selaolo ET (1997). Groundwater recharge and resources assessment in the Botswana Kalahari – Hydrochemical, isotope and noble gases tracer study in the Letlhakeng-Botlhapatlou area. GRES II project: technical report, Dept of geological Survey, Lobatse; University of Botswana, Gaborone: Free University Amsterdam, Netherlands.
- 1997 Tredoux, G and Talma, AS (1997). Maun Groundwater Development Project: Hydrochemistry and Environmental Isotopes. Report to Eastend Investments, Botswana. CSIR contract report ENV/S-C97092.
- 1997 Beekman HE, Selaolo ET, van Elswijk, R, Lenderink N and Obakeng, OTO (1997). Groundwater recharge and resources assessment in the Botswana Kalahari – Chloride and isotope profiling studies in the Letlhakeng-Botlhapatlou area and the Central Kalahari. GRES II project: technical report, Dept of geological Survey, Lobatse; University of Botswana, Gaborone: Free University Amsterdam, Netherlands.
- 1997 Verhagen, B.Th., Bredenkamp, D.B., Janse van Rensburg, H. and Farr, J. (1999). Recharge quantification with radiocarbon: independent corroboration in three Karoo aquifer studies in Botswana. *International Symposium on Isotope Techniques in Water Resources Development and Management*. IAEA-SM-361. IAEA, Vienna
- 1998 Selaolo, E.T., (1998) Tracer studies and groundwater recharge assessment in the eastern fringe of the Botswana Kalahari. Published PhD thesis Free University Amsterdam, the Netherlands.
- 1998 G Tredoux, M Masie & AS Talma. Characterisation of the Shashe river aquifer system by means of hydrochemistry and stable isotopes. "Groundwater in Arid Climates". Conference at the University of Botswana, Gaborone, 23-25 June 1998.
- 1998 Schaffner B, Chen YY, Kelepile T, Kinzelbach W, Carlsson L and Mannathoko I, (2000). Scientific support for sustainable groundwater management: A modelling study in Botswana using environmental tracers. In: Sililo, O. (ed), *Groundwater: Past Achievements and Future Challenges*, 291-296, Balkema, Rotterdam, 2000 1144p.
- 1999 Beekman HE, Selaolo ET and de Vries JJ (1999). Groundwater recharge and resources assessment in the Botswana Kalahari. GRES II project: executive summary, Dept of geological Survey, Lobatse; University of Botswana, Gaborone: Free University Amsterdam, Netherlands.
- 1999 Wrabel J 1999. Estimation of groundwater recharge in semi-arid Namibia using the Chloride-Mass-Balance-Approach (in German). PhD thesis, Univ Wurzburg. Published in *Hydrogeologie und Umwelt*, Vol 16, 1-155.
- 1999 Talma, A.S. and Vogel, J.C. 2001. Isotopic and Chemical signatures of water in the Transvaal Dolomite springs. Report to the Water Research Commission. CSIR Report ENV-PC-2001/040. Pretoria.

- 2000 De Vries, J.J., Simmers, I., 2002. Groundwater recharge: an overview of processes and challenges. *Hydrogeol. J.* 10, 5-17.
- 2001 Chilume, C.J., 2001: Hydrogeological Assessment of the South-western Karoo basin. A case study from Lokalane, Botswana.
- 2001 Resources Services, 2001: Tsabong Groundwater Investigation Assessment and Development. Final Report. Department of Water Affairs. Gaborone. Botswana.
- 2001 Wellfield Consulting Services (WCS), 2001: Hunhukwe/Lokalane Groundwater Survey Project (TB 10/2/1/98-99), Wellfield Consulting Services, Final Report submitted to the Department of Geological Survey, Lobatse, Botswana.
- 2001 Department of Water Affairs (2001) Final Report, Tsabong groundwater investigation, assessment, and development project (TB10/3/24/98-99). Resources Services, Gaborone, Botswana.
- 2001 Xu Y and Beekman HE (eds) 2003. Groundwater recharge estimation in southern Africa. UNESCO IHP series 64, UNESCO, Paris, 207p.
- 2002 JICA, 2002: The Groundwater Potential Evaluation and Management Plan in the Southeast Kalahari (Stampriet) Artesian Basin in the Republic of Namibia, Final Report submitted to the Department of Water Affairs, Namibia.
- 2002 Kirchner, J., Tredoux, G., Wierenga, A., and Christelis, G., 2002: Applying environmental isotopes to a Hydrogeological model of the Stampriet Artesian Basin. IAEA regional model project RAF/8/029. Department of Water Affairs, Windhoek.
- 2002 Department of Water Affairs 2002. Tsabong Groundwater Resources Investigation. Final report produced by Resource Services, Gaborone.
- 2002 Palla-Road Groundwater Resources Investigation. Phase 1. CBT 10/3/26/91-92. Final Report. Appendix 10. Environmental Impact Assessment.
- 2002 DWA/BGR 2004. Groundwater investigations in the Eiseb graben. Main hydrogeological report. Report of Technical Cooperation Project No. 2001.2475.0, Volume IV.GW.3.1. Windhoek, Namibia.
- 2003 Rahube, 2003. Recharge and Groundwater resources evaluation of the Lokalane-Ncojane Basin (Botswana) using numerical modeling. MSc thesis
- 2003 Wellfields Consulting Services. 2003. Werda-Mabutsane-Sekoma TGLP groundwater Survey (Project 10/2/18/2000-2001). Report to DGS, Lobatsi
- 2003 Geoflux. 2003. Bokspits TGLP area groundwater potential survey. Report to DGS, Lobatsi
- 2003 Stadler, S, von Hoyer, M & Himmelsbach, T, 2005. Natural nitrate in the Ntane sandstone aquifer: Origin, fate and impacts on groundwater management. In: *Environmental Geology in Semi-Arid Environments*, Vogel, H., Chilume, C., 113-120, Dept. Geol. Surv., Lobatse. 289p.
- 2004 Kulongoski JT, Hilton DR and Selaolo ET, 2004. Climate variability in the Botswana Kalahari from the late Pleistocene to the present day. *Geophysical Research Letters* 31, L10204.
- 2004 Stadler, S. 2006. Investigation of natural processes leading to nitrate enrichment in aquifers of semi-arid regions. Ph.D. Thesis., Dept Appl. Geol., Univ. Karlsruhe. Available as: *Schriftenreihe angewandte Geologie Karlsruhe* (2006) 71. 238p.

- 2005 Tredoux, G., Engelbrecht, J.F.P., Talma, A.S., 2005. Nitrate in groundwater in arid and semi-arid parts of southern Africa. In: *Environmental Geology in Semi-Arid Environments*, Vogel, H., Chilume, C., (eds), 121-133, Dept. Geol. Surv., Lobatse. 289p
- 2005 Talma, A.S., Tredoux, G., 2005. Isotopic source identification of nitrate in the groundwater of semi-arid southern Africa. In: *Environmental Geology in Semi-Arid Environments*, Vogel, H., Chilume, C., 92-102, Dept. Geol. Surv., Lobatse. 289p.
- 2005 Wrabel, J. 2005. Investigation of the processes leading to nitrate enrichment in the Kamtsas quartzite aquifer, Namibia. In: *Environmental Geology in Semi-Arid Environments*, Vogel, H., Chilume, C., 134-139, Dept. Geol. Surv., Lobatse. 289p.
- 2005 Cheney CS, Rutter HK, Farr JL and Phofuetsile P. 2006. Hydrological potential of the deep Ecca aquifer of the Kalahari, Botswana. *Quarterly Journal of Engineering Geology and Hydrogeology*, 39, 303-312.
- 2006 Sarma D, Simmonds ALE, Talma AS, Tredoux G and Moehadu OM (2006). Hydrochemical evolution and recharge of groundwater in the Olifantshoek Sequence Quartzite aquifer near Tsabong, Southwestern Botswana. Proc Conf of the Hydrological Association of Namibia, Windhoek, 23-25 March 2006.
- 2006 Verhagen, BT and Butler, MJ (2006). Long-term data series and the hydrological model of Jwaneng mine northern wellfield. In: *Isotope assessment of Long term groundwater exploitation*, TECDOC 1507. International Atomic Energy Agency, Vienna.
- 2006 Verhagen, B.T. and Butler, M.J. (2006). Long-term isotope data series and the hydrological model of Jwaneng mine northern well field. In: *Isotopic assessment of long term groundwater exploitation*, IAEA-TECDOC 1507, 97-125, International Atomic Energy Agency, Vienna..
- 2006 Sarma D, Simmonds ALE, Talma AS, Tredoux G and Moehadu OM (2006). Hydrochemical evolution and recharge of groundwater in the Olifantshoek Sequence Quartzite aquifer near Tsabong, Southwestern Botswana. Proc Conf of the Hydrological Association of Namibia, Windhoek, 23-25 March 2006.
- 2006 Obakeng, OT, 2007. Soil moisture dynamics and evapotranspiration at the fringe of the Botswana Kalahari. PhD thesis, Free University Amsterdam. 225pp.
- 2007 DWA. 2007. Kang-Phuduhudu regional groundwater resources investigation and development project. Final report by Wellfields Consulting Services
- 2007 M Schwiede 2007. Nitrogen Dynamics and Nitrate Leaching from sandy Soils of the semi-arid Kalahari, Botswana. Ph.D. thesis, Univ Hannover.
- 2007 DWA. Matsheng groundwater development project. Draft final report by Water Resouces Consultants
- 2008 Stadler, S., Osenbrück, K., Knöller, K., Suckow, A., Sültenfuß D., J., Oster, H., Himmelsbach, T., Hötzl, H., 2008. Understanding the origin and fate of nitrate in groundwater of semi-arid environments. *J. Arid Env.* 72 (10), 1830-1842.

- 2008 Osenbrück, K., Stadler, S., Sültenfuß, J., Suckow, A., Weise, S. M., 2009: Impact of recharge variations on water quality as indicated by excess air in groundwater of the Kalahari, Botswana. *Geoch. Cosmoch. Acta* 73, 911–922 .
- 2009 Talma, A.S., Tredoux, G. Engelbrecht, J.H.P., 2009. Behaviour of nitrogen in the unsaturated zone in southern Africa. In: *Application of Isotopes to the Assessment of Pollutant Behaviour in the Unsaturated Zone for Groundwater Protection*, TECDOC-1618, IAEA, Vienna
- 2009 Stadler, S., Osenbrück, K., Duijnsveld, W.H.M., Schwiede, M., and Böttcher, J., 2010b. Linking chloride mass balance infiltration rates with chlorofluorocarbon and SF6 groundwater dating in semi-arid settings: potential and limitations– *Isotopes in Environmental and Health Studies* 46 (3): 312 - 324.
- 2010 Stadler, S., Osenbrück, K., Suckow, A., Himmelsbach, T., Hötzl, H., 2010a. Groundwater flow regime, recharge and regional-scale solute transport in the semi-arid Kalahari of Botswana derived from isotope hydrology and hydrochemistry - *Journal of Hydrology* 388 (2010) 291–303.
- 2010 Stadler, S., Talma, A.S., Tredoux, G., Wrabel, J. 2012. Identification of sources and infiltration regimes of nitrate in the semi-arid Kalahari: Regional differences and implications for groundwater management. *Water SA* 38(2), 213-224

Serial	Country	Radiocarbon	RadiocarbonSD	Tritium	TritiumSD	Carbon13
20	BW	1.60	1.50	0.00	0.10	-8.30
21	BW	0.00	1.50	0.00	0.10	-12.10
32	BW	39.20	0.40	1.50	0.20	-8.40
40	BW	9.00	0.30	0.30	0.20	-14.00
41	BW	14.20	0.30	0.10	0.20	-13.40
42	BW	3.70	0.40	0.00	0.20	-10.50
56	BW	53.00	1.00	7.00	2.00	-14.10
57	BW	29.80	0.80	0.00		-14.70
62	BW	47.00	0.80	0.00		-14.70
67	BW	68.10	0.30	0.15	0.10	-10.50
68	BW	51.60	0.30	0.00	0.15	-10.37
69	BW	19.80	0.10	0.00	0.25	-8.78
70	BW	13.90	0.10	0.00	0.15	-6.41
71	BW	0.60		0.00	0.10	-12.84
72	BW	79.20	0.40	0.27	0.12	-6.87
73	BW	9.90	0.40	0.00	0.12	-13.33
74	BW	63.90	0.20	0.55	0.40	-10.53
75	BW	62.50	0.30	0.00	0.12	-14.09
76	BW	1.80		0.00	0.10	-12.29
77	BW	65.00	0.20	0.05	0.10	-13.09
78	BW	51.80	0.20	0.05	0.10	-13.07
79	BW	48.90	0.20	0.00	0.10	-13.21
80	BW	97.20	0.30	1.35	0.25	-10.40
81	BW	63.60	0.20	0.10	0.10	-14.37
82	BW	63.30	0.20	0.00	0.10	-13.51
83	BW	66.30	0.30	0.00	0.15	-13.19
84	BW	58.10	0.30	0.00	0.15	-11.11
86	BW	2.60		0.10	0.10	-13.57
87	BW	9.20	0.10	0.15	0.10	-13.63
88	BW	0.60		0.10	0.10	-11.49
89	BW	0.50		0.00	0.10	-11.86
90	BW	59.00	0.20	0.15	0.10	-6.69
91	BW	94.70	0.30	0.65	0.20	-9.62
93	BW	48.90	0.30	0.15	0.12	-9.25
94	BW	90.80	0.30	0.05	0.35	-9.82
101	BW	36.60	0.20	0.28	0.14	-14.57
104	BW	47.00	0.80	0.37	0.14	-14.36
107	BW	45.10	0.20	0.60	0.35	-13.57
108	BW	54.00	0.20	0.15	0.10	-11.72
109	BW	51.10	0.30	0.00	0.09	-12.29
111	BW	12.60	0.10	0.86	0.10	-13.03
112	BW	2.60	0.10	0.26	0.13	-12.19
113	BW	4.50	0.10	0.14	0.08	-6.35
115	BW	48.40	0.40	0.35	0.12	-13.80
116	BW	1.30		0.48	0.14	-11.28
117	BW	44.60	0.30	0.00	0.13	-14.20
120	BW	34.10	0.20	0.16	0.16	-14.00
123	BW	63.10	0.20	0.20	0.10	-17.49
124	BW	109.10	0.60	3.25	0.15	-11.22

125	BW	94.80	0.60	2.18	0.15	-6.59
1631	BW	56.00	0.90	0.01	0.01	-9.50
1632	BW	3.80	0.80	0.10	0.30	-7.80
1633	BW	2.60	0.50	0.00	0.30	-9.80
1634	BW	59.90	1.10	0.20	0.30	-12.50
1635	BW	9.50	1.30	0.10	0.30	-10.70
1636	BW	13.80	0.60	0.00	0.30	-8.40
1637	BW	47.00	1.00	0.01	0.01	-11.00
1638	BW	80.20	1.50	0.20	0.30	-12.00
1639	BW	80.50	1.40	0.00	0.30	-12.00
1640	BW	70.20	1.20	0.00	0.30	-12.40
1641	BW	44.50	1.10	0.10	0.30	-12.10
1642	BW	58.00	7.20	0.01	0.01	-12.30
1643	BW	56.90	1.30	0.00	0.30	-11.40
1644	BW	29.60	0.70	0.01	0.01	-7.90
1645	BW	61.50	1.60	0.00	0.30	-12.50
1646	BW	59.40	1.00	0.00	0.30	-11.20
1647	BW	65.30	1.00	0.01	0.02	-10.40
1649	BW	7.20	0.50	0.01	0.01	-8.90
1650	BW	14.20	0.40	0.01	0.01	-9.80
1651	BW	2.90	0.40	0.03	0.02	-7.80
1652	BW			0.01	0.01	
1653	BW	5.10	0.70	0.01	0.01	-9.80
1654	BW	10.50	0.40	0.01	0.01	-10.10
1655	BW	2.40	0.40	0.01	0.01	-10.30
1656	BW	6.00	0.40	0.01	0.01	-8.30
1657	BW	8.40	0.40	0.01	0.01	-9.10
1659	BW	18.80	0.60	0.01	0.01	-8.50
1660	BW	9.40	0.60	0.01	0.01	-8.40
1661	BW	8.70	0.40	0.01	0.01	-9.10
1662	BW	3.10	0.40	0.01	0.02	-8.60
1663	NAM	30.90	1.90	0.00	0.20	-9.46
1664	NAM	12.50	1.60	0.20	0.20	-6.87
1665	NAM	53.90	2.10	0.20	0.20	-9.52
1666	NAM	40.20	2.00	0.00	0.20	-8.74
1667	NAM	15.80	1.70	0.00	0.20	-7.08
1668	NAM	63.30	2.20	0.50	0.20	-9.72
1669	NAM	19.60	1.70	0.00	0.20	-10.24
1670	NAM	10.70	1.60	0.20	0.20	-10.33
1671	NAM	62.10	2.20	0.00	0.20	-9.50
1672	NAM	47.50	2.00	0.10	0.20	-8.67
1673	NAM	47.40	2.00	0.10	0.20	-9.70
1674	NAM	60.90	2.20	0.60	0.20	-7.81
1675	NAM	49.00	2.10	0.00	0.20	-10.18
1676	NAM	62.00	2.20	0.30	0.20	-9.65
1677	NAM	49.70	2.50	0.20	0.20	-9.60
1678	NAM	13.50	1.70	0.70	0.20	-9.17
1679	NAM	18.70	1.70	0.10	0.20	-9.35
1680	NAM	0.00	1.50	0.10	0.20	-7.32
1681	NAM	60.70	2.20	0.30	0.20	-9.88

1682	NAM	55.20	2.10	0.10	0.20	-9.73
1683	NAM	51.10	2.10	0.00	0.20	-9.65
1695	NAM	38.00	0.30	0.30		-8.66
1701	NAM	19.50	0.80	1.10		-10.10
1713	NAM	13.20	0.70	0.90		-7.50
1725	NAM	37.60	0.27	0.40		-9.70
1726	NAM	28.20	0.24	0.30		-8.40
1728	NAM	4.00	0.09	0.60		-8.40
1729	NAM	8.00	0.11	0.10		-8.20
1732	NAM	10.80	0.18	0.30		-9.00
1754	NAM	73.50	2.30	0.30	0.20	-6.50
1755	NAM	80.50	2.40	0.00	0.20	-4.40
1756	NAM	69.30	2.30	0.40	0.20	-7.80
1757	NAM	70.50	2.30	0.30	0.20	-8.00
1758	NAM	85.80	2.40	1.30	0.20	-6.60
1775	NAM	93.50	2.50	1.10	0.20	-5.70
1776	NAM	77.30	2.30	0.90	0.20	-5.30
1777	NAM	88.60	2.40	1.90	0.20	-5.20
1778	NAM	100.20	2.50	1.90	0.20	-6.30
1779	NAM	78.30	2.40	3.30	0.20	-6.50
1780	NAM	66.70	2.20	0.20	0.10	-8.00
1786	NAM	71.30	0.50	1.20		-11.00
1792	NAM	49.00	0.40	0.40		-10.70
1793	NAM	38.00	0.25	0.30		-8.70
1794	NAM	69.40	0.38	0.50		-6.60
1795	NAM	54.70	0.49	0.30		-6.20
1819	NAM	106.10	2.60	1.50	0.20	-5.90
1820	NAM	86.00	2.40	0.80	0.20	
1821	NAM	81.50	2.40	0.80	0.20	-6.80
1822	NAM	104.50	2.60	2.80	0.20	-9.60
1823	NAM	63.50	2.20	0.70	0.20	-6.80
1824	NAM	91.60	2.50	0.60	0.20	-5.80
1825	NAM	88.00	2.50	1.40	0.20	-6.30
1827	NAM	48.00	2.10	0.50	0.20	-7.70
1828	NAM	65.80	2.30	0.30	0.20	-6.60
1829	NAM	26.20	1.80	0.30	0.20	-5.60
1830	NAM	81.70	2.40	0.60	0.20	-6.90
1833	NAM	65.50	2.20	0.70	0.20	-6.40
1875	NAM	78.30	2.40	1.00	0.20	-6.60
1876	NAM	65.40	2.20	0.30	0.20	-7.50
1877	NAM	91.10	2.50	0.90	0.20	-5.30
1878	NAM	69.40	2.30	0.10	0.10	-8.10
1879	NAM	88.50	2.40	2.20	0.20	-8.60
1880	NAM	87.80	2.40	1.30	0.20	-10.40
1885	NAM	54.50	0.40	1.10		-9.60
1998	BW	58.00	2.20	0.10	0.20	
1999	BW	60.10	2.20	0.00	0.20	
2000	BW	57.80	2.20	0.10	0.20	
2001	BW	58.20	2.20	0.00	0.20	
2002	BW	26.90	1.90	0.60	0.20	

2003	BW	27.90	1.90	0.20	0.20	
2004	BW	54.70	2.20	0.30	0.20	
2005	BW	24.40	1.90	0.30	0.20	
2006	BW	0.00	1.50	0.30	0.20	
2007	BW	67.90	2.30	0.50	0.20	
2008	BW	61.50	2.20	0.00	0.20	
2009	BW	0.00	1.50	0.00	0.20	
2010	BW	86.50	2.50	0.00	0.20	
2011	BW	51.00	2.10	0.00	0.20	
2012	BW	64.80	2.30	0.30	0.20	
2013	BW	55.10	2.20	0.30	0.10	
2016	BW	57.40	2.20	0.10	0.10	
2017	BW	73.80	2.40	0.70	0.20	
2018	BW	29.90	2.20	0.00	0.20	
2019	BW	64.20	2.20	0.80	0.20	
2020	BW	61.70	2.20	0.00	0.20	
2021	BW	98.00	2.50	1.20	0.20	
2022	BW	53.90	2.20	0.00	0.16	
2023	BW	56.80	2.20	0.27	0.16	
2024	BW	76.50	2.50	0.00	0.16	
2025	BW	66.80	2.20	0.29	0.16	
2026	BW	63.30	2.20	0.00	0.15	
2027	BW	64.60	2.20	0.64	0.18	
2028	BW	55.60	2.20	0.20	0.20	
2035	BW	69.30	0.50	0.20	0.20	-8.00
2036	BW	6.80	0.50	0.10	0.20	-0.10
2037	BW	7.60	0.50	0.30	0.20	-3.20
2039	BW	89.40	0.40	0.00	0.20	-6.80
2041	BW	41.20	0.80	0.50	0.20	-2.70
2042	BW	18.30	0.60	0.20	0.20	-6.20
2044	BW	18.80	0.60	0.00	0.20	-7.60
2051	BW	103.20	1.10	0.50	0.20	-10.00
2053	BW	89.60	0.80	0.80	0.20	-8.70
2074	BW	42.20	0.50	0.00	0.30	
2075	BW	18.60	0.80	0.30	0.20	
2077	BW	43.00	0.50	0.30	0.20	-9.80
2079	BW	1.60	0.40	2.00	0.30	-7.20
2081	BW	3.60	0.40	0.90	0.30	-8.30
2082	BW	1.50	0.40	0.20	0.30	-6.00
2083	BW	2.30	0.40	0.60	0.30	-3.30
2131	RSA	75.10	0.80	0.10	0.20	-6.80
2132	RSA	90.90	1.20	0.00	0.20	-7.60
2133	RSA	82.60	0.80	0.00	0.20	-6.10
2134	RSA	53.50	1.00	0.00	0.20	-6.70
2135	RSA	37.40	1.10	0.00	0.20	-7.90
2136	RSA	62.70	1.40	0.00	0.20	-4.80
2137	RSA	63.90	0.80	0.20	0.20	-4.30
2138	RSA	72.30	0.50	0.10	0.20	-7.50
2139	RSA	53.10	0.90	0.00	0.40	-9.90
2140	RSA	98.90	0.70	4.00	0.20	-7.10

2141	RSA	27.60	0.60	0.40	0.20	-7.60
2142	RSA	88.40	0.90	0.20	0.10	-9.90
2143	RSA	88.30	0.90	0.10	0.10	-8.80
2144	RSA	77.20	0.80	0.00	0.20	-7.80
2145	RSA	103.70	1.20	3.60	0.40	-8.80
2146	RSA	76.90	0.80	0.00	0.20	-6.80
2147	RSA	93.60	1.00	0.90	0.30	-9.30
2148	RSA	89.90	0.70	0.10	0.20	-5.00
2149	RSA	51.40	0.70	0.10	0.20	-10.00
2150	RSA	75.20	0.40	0.10	0.20	-6.40
2151	RSA	59.00	0.40	0.20	0.20	-7.50
2152	RSA	100.60	0.70	0.10	0.50	-7.50
2153	RSA	73.10	0.80	0.30	0.60	-10.90
2158	RSA	107.20	1.20	4.40	0.40	-8.70
2159	RSA	79.40	0.80	6.30	0.70	-4.80
2160	RSA	72.90	0.70	1.60	0.40	-5.00
2161	RSA	76.50	0.80	0.30	0.20	-10.40
2162	RSA	47.60	0.60	0.50	0.20	-5.90
2163	RSA	47.90	0.60	0.00	0.30	-5.80
2165	RSA	70.80	0.70	0.50	0.50	-4.40
2166	RSA	84.30	0.60	0.00	0.20	-8.20
2167	RSA	58.80	0.60	0.20	0.30	-4.70
2168	RSA	52.00	0.40	0.00	0.20	-4.70
2169	RSA	47.50	0.90	0.10	0.30	-5.70
2171	RSA	86.20	0.90	2.10	0.40	-8.30
2172	RSA	38.60	0.60	1.30	0.30	-6.50
2173	RSA	111.80	2.70	0.70	0.40	-3.40
2174	RSA	92.00	1.10	0.00	0.20	-3.50
2175	RSA	87.80	0.50	0.70	0.40	-5.50
2176	RSA	74.10	1.20	1.30	0.20	-8.20
2178	RSA	93.10	1.20	9.30	0.90	-4.00
2180	RSA	63.40	0.80	0.00	0.20	-4.90
2181	RSA	67.40	0.90	0.00	0.20	-4.50
2186	RSA	103.60	1.10	2.20	0.40	-6.60
2187	RSA	106.50	1.40	3.00	0.60	-6.80
2188	RSA	69.90	0.70	0.40	0.20	-4.60
2189	RSA	69.20	0.70	1.10	0.40	-6.40
2190	RSA	70.90	0.90	0.00	0.30	-8.10
2191	RSA	81.70	0.80	0.40	0.40	-7.40
2192	RSA	86.00	0.80	3.60	0.50	-8.10
2193	RSA	32.90	0.60	0.10	0.20	-8.10
2194	RSA	32.90	0.70	0.30	0.40	-5.90
2195	RSA	16.70	0.50	0.20	0.40	-5.70
2196	RSA	9.80	0.80	0.10	0.20	-6.30
2197	RSA	47.90	0.60	0.00	0.10	-3.30
2199	RSA	66.90	0.40	0.20	0.40	-3.80
2200	RSA	61.40	0.60	0.40	0.40	-5.50
2201	RSA	47.40	0.70	0.50		-5.50
2202	RSA	43.80	0.60	0.20	0.50	-5.80
2204	RSA	63.70	0.80	0.20	0.10	-9.80

2205	RSA	49.00	0.90	0.30	0.40	-4.20
2206	RSA	44.50	0.80	0.10	0.30	-6.60
2208	RSA	24.40	0.40	0.90	0.20	-6.20
2209	RSA	50.10	0.50	0.80	0.20	-8.30
2210	RSA	70.90	0.70	0.20	0.30	-5.70
2211	RSA	60.60	0.80	0.40	0.10	-7.90
2212	RSA	54.80	0.60	0.10	0.30	-8.20
2213	RSA	64.00	0.70	0.10	0.30	-8.40
2214	RSA	89.30	0.90	0.10	0.30	-8.20
2215	RSA	67.70	0.90	0.20	0.20	-6.50
2216	RSA	87.20	0.80	1.90	0.20	-6.40
2217	RSA	60.70	0.80	0.00	0.30	-7.30
2218	RSA	63.40	1.00	0.00	0.20	-5.00
2219	RSA	45.30	0.50	0.30	0.20	-6.30
2220	RSA	76.60	0.20	0.40	0.30	-7.10
2221	RSA	77.50	0.50	0.30	0.20	-7.00
2222	RSA	99.20	0.90	4.30	0.30	-8.70
2223	RSA	103.30	1.30	5.30	0.50	-9.20
2224	RSA	64.70	1.00	7.30	0.50	-2.40
2225	RSA	118.50		7.20	0.70	-8.10
2226	RSA	110.00	1.30	7.50	0.80	-8.40
2227	RSA	79.90	0.80	4.20	0.70	-7.80
2228	RSA	80.30	0.60	3.30	0.50	-7.20
2229	RSA	106.40	1.20	4.50	0.40	-7.70
2230	RSA	103.60	0.80	8.00	0.50	-8.10
2232	RSA	82.70	0.90	0.00	0.20	-4.90
2233	RSA	82.30	0.90	0.10	0.20	-5.60
2234	RSA	108.70	0.40	9.20	0.90	-8.10
2235	RSA	76.70	0.50	0.60	0.20	-6.20
2236	RSA	43.70	0.50	9.50	0.80	-4.80
2238	RSA	68.70	0.70	0.00	0.40	-6.20
2239	RSA	80.50	0.40	0.00	0.30	-6.10
2240	RSA	96.20	0.40	1.00	0.40	-6.90
2241	RSA	21.80	0.80	0.30	0.30	-4.00
2242	RSA	26.80	0.60	1.00	0.20	-3.00
2243	RSA	90.50	0.80	0.70	0.40	-4.50
2244	RSA	47.60	0.70	0.70	0.30	-4.10
2245	RSA	10.10	1.00	0.20	0.20	-2.10
2246	RSA	86.80	0.80	1.80	0.40	-5.80
2247	RSA	65.00	0.60	0.00	0.20	-5.90
2248	RSA	35.00	0.40	0.00	0.20	-3.40
2249	RSA	75.80	0.50	0.40	0.20	-5.00
2250	RSA	51.80	0.40	1.80	0.30	-6.40
2251	RSA	82.50	0.50	1.00	0.20	-6.30
2252	RSA	88.40	0.90	0.00	0.20	-6.10
2253	RSA	50.80	0.80	0.10	0.20	
2257	RSA	68.50	0.50	0.60	0.30	-5.80
2260	RSA	88.70	0.90	5.20	0.60	-6.00
2262	RSA	23.20	0.80	0.10	0.30	-2.20
2263	RSA	82.00	0.80	0.90	0.50	-5.90

2266	RSA	83.90	0.50	0.40	0.20	-6.70
2271	RSA	66.70	0.90	0.90	0.30	-9.00
2273	RSA	52.00	0.50	0.50	0.20	-4.10
2276	RSA	53.30	0.30	0.20	0.10	-4.90
2277	RSA	57.30	0.50	0.30	0.20	-4.10
2279	RSA	38.20	0.50	0.30	0.20	-5.00
2280	RSA	30.10	0.30	0.40	0.30	-4.70
2281	RSA	54.70	0.50	0.60	0.20	-3.40
2282	RSA	64.00	0.40	0.90	0.30	-5.40
2283	RSA	58.50	0.40	1.00	0.20	-3.80
2284	RSA	50.00	0.60	0.00	0.20	-4.90
2285	RSA	75.00	0.40	0.90	0.20	-4.50
2286	RSA	87.20	0.70	0.00	0.20	-4.20
2287	RSA	76.60	0.40	0.30	0.20	-7.40
2288	RSA	22.80	0.50	0.40	0.20	0.30
2289	RSA	14.20	0.40	0.70	0.20	-4.90
2293	RSA	82.60	0.40	0.00	0.20	-7.50
2294	RSA	16.60	0.60	0.10	0.20	-2.70
2295	RSA	82.80	0.80	0.30	0.20	-8.50
2297	RSA	90.20	0.50	7.50	0.50	-8.20
2299	RSA	79.10	0.70	2.90	0.40	-8.80
2301	RSA	44.30	0.60	0.80	0.20	-4.90
2302	RSA	41.10	0.60	0.70	0.30	-11.60
2303	RSA	80.00	0.50	0.60	0.30	-9.80
2305	RSA	60.30	0.60	0.20	0.20	-6.30
2309	RSA	29.70	0.60	0.20	0.20	-5.50
2310	RSA	32.80	0.40	0.10	0.20	-5.30
2312	RSA	46.50	0.50	0.60	0.30	-7.10
2314	RSA	43.30	2.00	0.10	0.20	-2.30
2315	RSA	86.20	0.70	0.10	0.20	-6.80
2316	RSA	87.20	0.70	0.90	0.30	-7.00
2318	RSA	69.60	1.80	0.70	0.30	-4.70
2320	RSA	31.80	0.60	0.60	0.30	-4.40
2323	RSA	51.90	0.50	0.20	0.20	
2324	RSA	32.10	0.80	0.80	0.30	-3.50
2325	RSA	104.40	1.00	1.10	0.20	-4.30
2326	RSA	33.60	0.70	0.00	0.20	
2328	RSA	29.20	0.60	0.80	0.40	-4.00
2329	RSA	92.60	0.80	7.50	0.60	-6.20
2330	RSA	17.30	0.40	0.30	0.40	-1.40
2332	RSA	79.20	0.70	0.30	0.30	-7.80
2335	RSA	76.00	0.40	0.20	0.20	-7.80
2336	RSA	84.10	1.10	0.20	0.50	-7.00
2337	RSA	76.80	0.60	0.30	0.40	-6.60
2338	RSA	48.10	1.50	0.20	0.20	-12.90
2339	RSA	40.90	1.00	0.70	0.30	-15.90
2341	RSA	47.00	0.60	0.40	0.30	-3.90
2342	RSA	35.40	0.70	1.00	0.30	-5.90
2343	RSA	10.50	0.50	0.00	0.20	-4.40
2344	RSA	90.50	0.50	1.40	0.30	-8.70

2345	RSA	82.20	1.00	2.40	0.40	-8.50
2346	RSA	82.20	0.60	1.80	0.40	-8.20
2347	RSA	106.30	1.20	6.10	0.60	-9.80
2349	RSA	105.90	1.20	8.40	0.70	-9.70
2350	RSA	99.00	0.70	1.40	0.30	-8.50
2351	RSA	88.10	0.30	0.30	0.30	-6.50
2354	RSA	36.00	0.50	0.60	0.20	-1.10
2356	RSA	92.50	0.80	3.00	0.40	-10.10
2357	RSA	76.20	0.60	0.00	0.20	-8.10
2358	RSA	90.00	0.60	0.30	0.20	
2359	RSA	88.40	0.70	0.30	0.20	-8.40
2360	RSA	65.40	0.60	0.70	0.20	-5.70
2361	RSA	64.10	0.90	0.30	0.30	-6.20
2362	RSA	84.30	0.40	0.70	0.30	-9.50
2363	RSA	8.60	0.40	0.20	0.30	-15.60
2364	RSA	60.40	0.30	0.80	0.30	-6.00
2365	RSA	94.40	0.40	4.00	0.40	-7.40
2366	RSA	82.80	0.40	0.00	0.20	-8.40
2367	RSA	50.90	0.40	0.60	0.20	-22.50
2368	RSA	99.50	0.70	2.40	0.40	-6.80
2370	RSA	80.00	0.50	0.70	0.20	-14.50
2372	RSA	96.30	0.60	3.10	0.40	-14.00
2373	RSA	83.20	0.90	0.10	0.20	-13.60
2375	RSA	68.80	0.40	0.40	0.20	-5.20
2377	RSA	29.60	0.50	0.50	0.20	-13.60
2378	RSA	75.80	0.50	0.10	0.20	-7.40
2380	RSA	80.60	0.30	0.90	0.30	-7.90
2382	RSA	29.80	0.80	0.60	0.30	-5.70
2383	RSA	73.10	0.80	0.30	0.20	-16.40
2384	RSA	46.90	0.50	1.80	0.40	-5.90
2385	RSA	35.70	0.30	1.20	0.40	-6.00
2386	RSA	45.70	0.50	0.50	0.20	-3.90
2389	RSA	86.97	0.54	0.80	0.20	-12.40
2390	RSA	67.88	0.52	0.30	0.20	-10.10
2391	RSA	76.40	1.24	0.20	0.20	-12.07
2395	RSA	78.22	0.61	1.50	0.20	-9.10
2396	RSA	100.62	0.56	2.20	0.20	-8.70
2397	RSA	98.90	2.64	1.80	0.30	-11.06
2403	RSA	87.29	0.56	0.80	0.20	-11.20
2404	RSA	76.59	0.54	1.10	0.20	-9.10
2405	RSA	45.58	0.43	0.00	0.10	-9.70
2406	RSA	102.05	0.57	2.30	0.20	-9.60
2411	RSA	77.71	0.54	1.30	0.20	-9.70
2412	RSA	29.45	0.71	0.90	0.20	-10.50
2413	RSA	44.70	0.60	0.70	0.20	-11.17
2439	RSA	67.36	0.51	1.80	0.20	-8.90
2440	RSA	72.77	0.43	0.50	0.20	-10.82
2479	RSA	81.04	0.42	0.70	0.20	-9.30
2480	RSA	83.80	1.58	0.70	0.20	-8.84
2481	RSA	60.00	1.14	0.30	0.20	-10.52

2482	RSA	36.11	0.41	0.30	0.10	-9.30
2485	RSA	100.33	0.56	2.20	0.20	-7.70
2486	RSA	104.40	1.13	1.70	0.30	-10.00
2488	RSA	49.73	0.44	0.90	0.20	-9.20
2489	RSA	65.42	0.56	3.30	0.30	-8.80
2490	RSA	46.84	0.42	0.70	0.20	-9.00
2491	RSA	109.49	0.83	2.40	0.30	-11.60
2493	RSA	110.30	0.69	3.60	0.30	-10.50
2497	RSA	70.86	0.36	0.70	0.20	-9.00
2498	RSA	72.57	0.52	0.20	0.20	-8.70
2500	RSA	104.98	0.61	3.00	0.30	-7.30
2501	RSA	99.80	0.90	2.90	0.30	-10.62
2614	NAM	19.80	1.70	0.00	0.20	-6.82
2615	NAM	15.80	1.70	0.00	0.20	-6.21
2616	NAM	48.30	2.10	0.00	0.20	-8.87
2617	NAM	66.60	2.20	0.40	0.20	-10.61
2618	NAM	70.70	2.30	0.00	0.20	-9.61
2619	NAM	46.30	2.00	0.00	0.20	-9.70
2620	NAM	46.50	2.00	0.50	0.20	-9.27
2621	NAM	62.50	2.20	0.20	0.20	-10.23
2622	NAM	57.80	2.20	0.00	0.20	-7.44
2623	NAM	49.50	2.10	0.00	0.20	-9.87
2624	NAM	39.30	2.00	0.00	0.20	-11.98
2625	NAM	35.60	1.90	0.20	0.20	-9.99
2626	NAM	28.60	1.80	0.20	0.20	-10.49
2627	NAM	2.00	1.50	0.00	0.20	-5.27
2628	NAM	33.30	1.90	0.20	0.20	-9.50
2629	NAM	10.70	1.60	0.10	0.20	-6.41
2630	NAM	5.70	1.60	0.20	0.20	-4.87
2631	NAM	52.80	2.10	0.00	0.20	-6.44
2632	NAM	0.00	1.40	0.00	0.20	-5.32
2633	NAM	42.50	2.00	0.20	0.20	-6.72
2634	NAM	41.80	2.00	0.00	0.20	-9.41
2635	NAM	27.30	1.80	0.30	0.20	-9.02
2639	NAM	25.30	1.80	0.00	0.20	-9.42
2640	NAM	42.50	2.00	0.50	0.20	
2641	NAM	24.90	1.80	0.30	0.20	
2646	NAM	28.40	1.80	0.10	0.20	
2663	NAM	72.40	0.50	2.20		-9.60
2664	NAM	17.69	0.28	0.40		-8.90
2665	NAM	5.68	0.22	1.00		-8.50
2666	NAM	3.29	0.20	0.80		-8.90
2668	NAM	2.59	0.15	0.90		-9.40
2697	NAM	57.90	2.20	0.10	0.10	-3.41
2698	NAM	0.00	1.50	0.10	0.20	-5.35
2699	NAM	0.10	1.50	0.90	0.20	-5.47
2700	NAM	2.20	1.50	0.00	0.20	-5.11
2701	NAM	3.10	1.50	0.80	0.20	-5.47
2777	NAM	9.00	1.60	0.30	0.20	-2.42
2780	NAM	21.30	1.80	0.20	0.20	-0.48

2781	NAM	9.20	1.60	0.00	0.20	-6.02
2803	NAM	6.60	1.60	0.10	0.20	-5.29
2807	NAM	28.90	1.90	5.30	0.30	-3.77
2808	NAM	33.90	1.90	0.20	0.20	-4.37
2811	NAM	50.70	0.36	0.00	0.20	-11.10
2812	NAM	66.90	2.30	0.60	0.20	-4.26
2816	NAM	69.10	2.30	0.60	0.20	-3.44
2817	NAM	1.80	1.50	0.00	0.20	-5.43
2862	NAM	6.00	1.60	0.00	0.20	-5.88
2882	NAM	58.80	2.20	0.00	0.20	-5.61
2883	NAM	56.10	2.20	0.00	0.20	-5.34
2884	NAM	58.40	2.20	0.00	0.20	-12.55
2888	NAM	17.10	1.80	0.00	0.20	
2889	NAM	38.80	2.00	0.00	0.20	
2890	NAM	48.20	2.10	0.00	0.20	
2907	NAM	24.00		0.50		
2912	NAM	0.00	1.50	0.80	0.20	-5.09
2913	NAM	6.60	1.60	0.50	0.20	-6.09
2914	NAM	0.00	1.50	0.10	0.20	-4.89
2915	NAM	30.70	1.90	0.00	0.20	-6.38
2916	NAM	3.30	1.50	0.00	0.20	-5.04
2917	NAM	6.70	1.60	0.40	0.20	-5.16
2920	NAM	3.30	1.50	0.40	0.20	-5.06
2922	NAM	14.60	0.30	0.00	0.20	-11.10
2923	NAM	60.10	0.50	0.00	0.20	-10.30
2924	NAM	0.25	0.20	0.00	0.20	-13.50
2925	NAM	44.10	0.40	0.00	0.20	-13.80
2926	NAM	4.00	0.20	0.00	0.20	-10.60
2928	NAM	3.00	0.20	0.00	0.20	-9.00
2929	NAM	55.20	0.45	0.00	0.20	-7.20
2931	NAM	25.47	0.33	0.00	0.20	-11.80
2933	NAM	0.85	0.18	0.00	0.20	-12.10
2934	NAM	66.40	2.30	0.00	0.20	-3.65
2935	NAM	47.90	2.10	0.50	0.20	-4.93
2936	NAM	54.87	0.47	0.00	0.20	-5.30
2938	NAM	6.19	0.22	0.00	0.20	-18.60
2948	NAM	77.70	0.50	0.20	0.20	-7.00
2950	NAM	28.80	0.40	0.00	0.20	-8.30
2952	NAM	86.90	0.60	0.30	0.20	-8.30
2954	NAM	38.70	0.30	0.30	0.20	-7.90
2957	NAM	81.86	0.70	0.20	0.20	-7.70
2960	NAM	7.66	0.18	0.50	0.20	-8.60
2963	NAM	86.27	0.55	0.10	0.20	-9.80
2966	NAM	74.90	0.40	0.40	0.20	-8.50
2967	NAM	63.20	0.50	0.40	0.20	-9.70
2973	NAM	63.25	0.13	0.20		-11.70
2974	NAM	46.15	0.39	0.00		-8.70
2979	NAM	8.60	1.60	0.00	0.20	-6.73
BFB1	RSA	20.20		0.00		4.70
BFB2	RSA	62.30		0.40		-12.88

BT18VL03	RSA	95.11	0.25	0.07		
BT18VL05	RSA	90.22	0.27	0.34		
BT18VL06	RSA	65.05	0.39	0.10		
BT18VL07	RSA	72.93	0.23	0.02		
BT18VL08	RSA	65.09	0.37	0.18		
BT18VL11	RSA	59.77	0.32	0.32		
BT18VL12	RSA	35.13	0.22	0.09		
BT18VL13	RSA	40.24	0.21	0.02		
BT18VL14	RSA	82.50	0.25	0.16		
BT18VL15	RSA	98.73	0.47	0.18		
BT18VL17	RSA	95.17	0.43	0.52		
CRS1	RSA	23.00		0.50		-7.20
DRB4	RSA	90.50		3.10		-13.56
FLB5	RSA	94.00		1.30		-4.56
FLS1	RSA	47.30		1.60		-26.00
Jar18383	RSA	39.89	0.17	0.73	0.09	-14.64
Jar18384a	RSA	11.39	0.09	0.48	0.09	-5.63
JV18BR05	RSA	57.37	0.29	0.26	0.05	-11.80
JV18BR07	RSA	78.26	0.30	0.64	0.15	-11.80
JV18BR10	RSA	100.02	0.41	0.06		
JV18CD02	RSA	100.78	0.36	0.71	0.04	
JV18KK01	RSA	71.02	0.28	1.58	0.11	-13.84
JV18KK02	RSA	99.73	0.34	0.92	0.09	-13.03
JV18KK03	RSA	55.60	0.23	0.32	0.14	-16.16
JV18KK05	RSA	95.50	0.42	0.43	0.06	-4.95
JV18KK06	RSA	68.41	0.18	0.46	0.09	-12.39
JV18KK07	RSA	97.76	0.21	0.89	0.09	-7.44
JV18KK08	RSA	29.29	0.12	0.22	0.07	-12.01
JV18KK09	RSA	22.60	0.10	0.22	0.08	-9.12
JV18KK10	RSA	35.26	0.12	0.37	0.07	-8.65
JV18KK11	RSA	42.29	0.13	0.20	0.10	-11.20
JV18KK13	RSA	97.44	0.39	1.48	0.11	-11.56
JV18KK14	RSA	89.13	0.19	1.10	0.08	-11.67
JV18KZ01	RSA	92.75	0.29	0.13	0.06	-5.76
JV18KZ02	RSA	37.40	0.21	0.17	0.06	-11.80
JV18NB01	RSA	72.18	0.31	0.26	0.03	-12.31
JV18NB02	RSA	100.66	0.38	0.63	0.04	-11.96
JV18NB03	RSA	91.26	0.33	0.21	0.04	
JV18NB04	RSA	80.86	0.32	0.35	0.05	
JV18SK01	RSA	47.21	0.22	0.45	0.16	
JV18SP01	RSA	61.38	0.23	0.24	0.05	
JV18SP02	RSA	79.55	0.25	0.45	0.06	-13.66
LRB2	RSA	84.20		1.20		-9.19
MWB2	RSA	86.90		1.40		-13.25
RRB1	RSA	74.40		0.50		-11.57
RWB1c	RSA	73.90		0.90		-11.27
RWB5	RSA	93.70		1.20		-11.73
SH18001	MOZ	86.05	0.30	0.61		-14.10
SH18002	MOZ	6.44	0.08	0.29		-10.39
SH18003	MOZ	73.82	0.23	0.06		-12.58

SH18004	MOZ	60.06	0.22	0.25		-14.90
SH18005	MOZ	65.07	0.21	0.24		-15.08
SH18008	MOZ	82.17	0.27	0.05		-12.24
SH18009	MOZ	59.01	0.21	2.04		-8.72
SH18014	MOZ	40.47	0.19	0.04		-11.63
SH18015	MOZ	20.38	0.11	0.04		-8.23
SH18020	MOZ	70.27	0.26	0.09		-20.95
SH18021	MOZ	78.26	0.25	0.08		-17.24
SH18024	MOZ	69.73	0.24	0.80		-20.51
SH18029	MOZ	78.76	0.34	0.08		-13.35
SH18030	MOZ	100.04	0.26	0.15		-13.28
SH18031	MOZ	91.53	0.27	0.28		-16.68
SH18032	MOZ	84.52	0.26	0.59		-11.36
SH18033	MOZ	93.10	0.24	0.99		-7.64
SH18034	MOZ	97.30	0.28	0.06		-12.98
SH18035	MOZ	90.31	0.24	0.45		-14.09
SH18036	MOZ	90.55	0.27	0.22		-14.54
SH18037	MOZ	97.73	0.25	0.31		-12.60
SH18039	MOZ	106.08	0.27	0.45		-11.54
SH18040	MOZ	99.64	0.25	0.45		-13.65
SH18041	MOZ	99.71	0.26	0.13		-11.47
SH18042	MOZ	92.35	0.25	0.27		-11.69
SH18043	MOZ	95.24	0.25	0.36		-13.25
SH18044	MOZ	89.57	0.26	0.09		-12.55
SH18045	MOZ	93.35	0.25	0.28		-10.76
SH18047	MOZ	66.62	0.25	0.12		-12.51
SH18048	MOZ	65.40	0.25	0.12		-14.90
SH18049	MOZ	74.95	0.33	0.32		-10.19
SH18050	MOZ	70.66	0.27	0.20		-13.23
SH18052	MOZ	81.70	0.29	1.16		-13.81
SH18053	MOZ	83.83	0.31	0.72		-16.97
SH18054	MOZ	75.78	0.27	0.78		-17.48
SH18082	MOZ	42.19	0.19	0.21	0.05	-14.79
SH18084	MOZ	84.66	0.32	0.21	0.05	-10.37
SH18085	MOZ	88.95	0.36	0.30	0.05	-15.69
SH18086	MOZ	43.38	0.17	0.74	0.06	-13.19
SH18088	MOZ	55.74	0.20	0.25	0.06	-15.23
SH18089	MOZ	52.86	0.19	0.25	0.06	-12.18
SH18091	MOZ	46.68	0.18	0.18	0.06	-14.89
SH18092	MOZ	83.85	0.28	1.37	0.08	-11.58
SH18093	MOZ	63.66	0.22	0.18	0.06	-16.58
SH18R01	MOZ	87.09	0.30	0.29		
VBB1	RSA	49.70		0.60		-11.50
VFB1	RSA	53.10		0.10		-25.50
VFB2	RSA	89.70		1.00		-8.58
WP 502	RSA	89.20		3.50		-10.25
WP 508	RSA	56.70		0.10		-14.84
ZH18001	RSA	97.89	0.45	2.94		
?H18-BD00:	RSA	62.12	0.19	0.87	0.13	
?H18-BD00:	RSA	91.84	0.21	0.33	0.05	

ZH18-C001	RSA	23.10	0.11	3.22		
ZH18-C002	RSA	94.31	0.22	2.81		
ZH18-DD00	RSA	99.55	0.23	1.16	0.10	
ZH18-DD00	RSA	99.52	0.24	0.69	0.10	
ZH18-FH00	RSA	96.56	0.23	0.70	0.09	
ZH18-FH00	RSA	26.65	0.11	0.52	0.11	
ZH18-FH00	RSA	86.60	0.21	0.33	0.08	
ZH18-MONO	RSA	55.49	0.18	0.25	0.06	
ZH18-PV00	RSA	59.55	0.18	0.10		
ZH18-SW00	RSA	102.25	0.24	0.17		
ZH18-SW00	RSA	102.62	0.25	1.01		
ZH18-VD00	RSA	97.40	0.22	1.02		
ZH18-VD00	RSA	93.19	0.22	0.41	0.06	
ZH18-VD00	RSA	81.41	0.29	0.60	0.08	
ZH19-CAL00	RSA	60.43		0.25	0.04	
ZH19-CAL00	RSA	45.60		0.29	0.04	
ZH19-CD00	RSA	77.75		0.24	0.11	
ZH19-FH00	RSA	100.08		0.66	0.11	
ZH19-FH00	RSA	91.79		0.74	0.12	
ZH19-MAL00	RSA	33.94		0.27	0.03	
ZH19-MB00	RSA	40.09		0.15	0.03	
ZH19-STB00	RSA	80.46		0.50	0.11	
ZHKB001	RSA	93.64	0.35	0.95	0.08	
ZHKB002	RSA	64.32	0.25	0.74	0.07	
ZHR001	RSA	101.57	0.36	0.78	0.08	-14.82

Sample Name	Lat	Long	Student	Project	Tritium (TU)	TU Error
DWA 234	-22.4156	29.2094	Mike Butler	DWA	0.28	0.16
DWA 266	-22.5289	30.6800	Mike Butler	DWA	0.00	0.20
DWA 440	-22.5556	29.0142	Mike Butler	DWA	0.26	0.17
DWA 267	-22.5692	28.6219	Mike Butler	DWA	0.00	0.16
DWA 268	-22.5703	28.6222	Mike Butler	DWA	0.00	0.15
DWA 265	-22.6075	30.1747	Mike Butler	DWA	0.02	0.20
DWA 222	-22.6789	29.1006	Mike Butler	DWA	1.25	0.19
DWA 263	-22.8556	28.2028	Mike Butler	DWA	0.92	0.20
DWA 262	-22.9058	30.1806	Mike Butler	DWA	0.00	0.20
DWA 441	-23.0300	29.8447	Mike Butler	DWA	0.37	0.17
DWA 455	-23.0678	27.9986	Mike Butler	DWA	0.31	0.15
DWA 436	-23.1625	28.5350	Mike Butler	DWA	0.32	0.15
DWA 435	-23.2225	28.4508	Mike Butler	DWA	0.38	0.15
DWA 438	-23.3611	29.3428	Mike Butler	DWA	0.96	0.20
DWA 264	-23.6356	30.2817	Mike Butler	DWA	0.73	0.20
DWA 233	-23.6906	27.7453	Mike Butler	DWA	0.00	0.16
DWA 269	-23.8189	30.1569	Mike Butler	DWA	1.90	0.23
DWA 442	-23.9283	28.9269	Mike Butler	DWA	1.48	0.21
DWA 250	-23.9506	30.6133	Mike Butler	DWA	1.87	0.23
DWA 257	-23.9925	29.4650	Mike Butler	DWA	0.87	0.17
DWA 270	-24.2944	28.0911	Mike Butler	DWA	0.38	0.16
DWA 271	-24.3233	28.0986	Mike Butler	DWA	0.64	0.18
DWA 542	-24.3411	27.3617	Mike Butler	DWA	0.62	0.18
DWA 254	-24.3644	30.2975	Mike Butler	DWA	0.29	0.15
DWA 439	-24.3903	26.0406	Mike Butler	DWA	2.04	0.22
DWA 444	-24.4556	28.5689	Mike Butler	DWA	0.11	0.16
DWA 454	-24.5450	26.7083	Mike Butler	DWA	0.97	0.18
DWA 453	-24.7561	30.0194	Mike Butler	DWA	1.20	0.20
DWA 446	-24.8719	29.7519	Mike Butler	DWA	0.22	0.16
DWA 544	-24.8847	28.2894	Mike Butler	DWA	0.07	0.15
DWA 545	-24.8858	28.2917	Mike Butler	DWA	0.10	0.15
DWA 259	-25.0922	30.7853	Mike Butler	DWA	1.37	0.18
DWA 280	-25.1089	26.6569	Mike Butler	DWA	0.50	0.18
DWA 241	-25.1206	27.7861	Mike Butler	DWA	0.00	0.16
DWA 279	-25.1219	26.9036	Mike Butler	DWA	0.60	0.18
DWA 223	-25.1592	27.6017	Mike Butler	DWA	0.42	0.16
DWA 377	-25.1717	20.3222	Mike Butler	DWA	0.29	0.18
DWA 281	-25.2792	26.7364	Mike Butler	DWA	0.53	0.17
DWA 225	-25.3519	29.0669	Mike Butler	DWA	0.77	0.17
DWA 255	-25.4083	28.0817	Mike Butler	DWA	0.41	0.15
DWA 240	-25.4258	31.9583	Mike Butler	DWA	2.06	0.21
DWA 373	-25.4603	20.0106	Mike Butler	DWA	0.00	0.24
DWA 274	-25.5408	26.0797	Mike Butler	DWA	1.03	0.18
DWA 380	-25.5453	23.6731	Mike Butler	DWA	0.24	0.18
DWA 244	-25.6131	29.0297	Mike Butler	DWA	0.04	0.22
DWA 245	-25.6569	30.2611	Mike Butler	DWA	0.00	0.16
DWA 398	-25.8378	23.0247	Mike Butler	DWA	0.19	0.15
DWA 277	-25.9086	24.6728	Mike Butler	DWA	1.90	0.22
DWA 231	-25.9094	27.0358	Mike Butler	DWA	0.00	0.16

DWA 227	-25.9569	30.5606	Mike Butler	DWA	0.63	0.17
DWA 283	-25.9817	26.1892	Mike Butler	DWA	0.39	0.16
DWA 356	-26.0642	22.5303	Mike Butler	DWA	0.00	0.16
DWA 379	-26.0944	24.2431	Mike Butler	DWA	0.50	0.18
DWA 372	-26.2036	20.1142	Mike Butler	DWA	0.00	0.23
DWA 370	-26.2050	22.5725	Mike Butler	DWA	0.55	0.28
DWA 514	-26.2544	26.8022	Mike Butler	DWA	1.01	0.20
DWA 397	-26.2822	20.3656	Mike Butler	DWA	0.60	0.18
DWA 357	-26.2847	22.6167	Mike Butler	DWA	0.31	0.16
DWA 273	-26.3150	27.8019	Mike Butler	DWA	0.25	0.16
DWA 404	-26.3408	20.3700	Mike Butler	DWA	0.54	0.16
DWA 371	-26.3447	20.1053	Mike Butler	DWA	0.22	0.25
DWA 358	-26.4256	22.2325	Mike Butler	DWA	0.20	0.24
DWA 350	-26.5228	26.1789	Mike Butler	DWA	0.87	0.20
DWA 387	-26.5344	25.8017	Mike Butler	DWA	1.30	0.20
DWA 403	-26.5500	20.3333	Mike Butler	DWA	0.75	0.16
DWA 419	-26.5853	26.9153	Mike Butler	DWA	0.43	0.15
DWA 247	-26.7311	29.6211	Mike Butler	DWA	1.87	0.21
DWA 349	-26.8575	23.9403	Mike Butler	DWA	0.74	0.19
DWA 291	-27.0872	32.6050	Mike Butler	DWA	0.11	0.15
DWA 378	-27.2017	24.0808	Mike Butler	DWA	1.48	0.21
DWA 407	-27.2683	28.5561	Mike Butler	DWA	1.48	0.19
DWA 365	-27.4633	23.4369	Mike Butler	DWA	0.41	0.26
DWA 376	-27.6333	20.1167	Mike Butler	DWA	0.54	0.19
DWA 395	-27.8819	24.6144	Mike Butler	DWA	0.17	0.18
DWA 290	-27.8989	31.7234	Mike Butler	DWA	0.92	0.19
DWA 286	-27.9734	29.8630	Mike Butler	DWA	0.00	0.21
DWA 341	-28.0958	23.3322	Mike Butler	DWA	0.70	0.19
DWA 409	-28.2783	26.1511	Mike Butler	DWA	1.90	0.23
DWA 406	-28.3036	22.1736	Mike Butler	DWA	1.01	0.18
DWA 355	-28.4483	17.0042	Mike Butler	DWA	0.33	0.16
DWA 421	-28.6719	27.4303	Mike Butler	DWA	1.02	0.19
DWA 417	-28.7678	26.0700	Mike Butler	DWA	0.40	0.16
DWA 518	-29.1411	25.3925	Mike Butler	DWA	0.55	0.19
DWA 381	-29.1897	19.4203	Mike Butler	DWA	0.36	0.18
DWA 390	-29.2283	17.6881	Mike Butler	DWA	0.36	0.17
DWA 393	-29.2292	18.7358	Mike Butler	DWA	0.27	0.15
DWA 383	-29.2306	21.8878	Mike Butler	DWA	0.63	0.17
DWA 374	-29.3275	22.8375	Mike Butler	DWA	0.77	0.27
DWA 335	-29.7364	17.6281	Mike Butler	DWA	1.95	0.22
DWA 385	-29.9331	23.6972	Mike Butler	DWA	0.38	0.17
DWA 396	-30.0172	19.0506	Mike Butler	DWA	0.09	0.16
DWA 352	-30.0403	20.1044	Mike Butler	DWA	1.03	0.20
DWA 363	-30.0900	17.2436	Mike Butler	DWA	0.00	0.23
DWA 422	-30.2528	25.4342	Mike Butler	DWA	0.74	0.16
DWA 344	-30.3528	17.4233	Mike Butler	DWA	0.39	0.19
DWA 401	-30.3553	21.7733	Mike Butler	DWA	1.53	0.21
DWA 185	-30.3747	29.2625	Mike Butler	DWA	0.36	0.16
DWA 200	-30.4256	24.8422	Mike Butler	DWA	1.16	0.23
DWA 333	-30.6319	23.5056	Mike Butler	DWA	0.80	0.17

DWA 408	-30.7156	26.7147	Mike Butler	DWA	0.38	0.15
DWA 334	-30.7558	20.6597	Mike Butler	DWA	1.66	0.19
DWA 511	-30.8667	25.5869	Mike Butler	DWA	0.80	0.20
DWA 212	-31.2961	25.8303	Mike Butler	DWA	0.75	0.27
DWA 187	-31.3294	27.8558	Mike Butler	DWA	0.00	0.23
DWA 186	-31.3756	27.0447	Mike Butler	DWA	1.93	0.23
DWA 556	-31.4567	19.7747	Mike Butler	DWA	0.00	0.16
DWA 191	-31.6528	25.8153	Mike Butler	DWA	0.67	0.23
DWA 557	-32.0583	18.8894	Mike Butler	DWA	1.70	0.22
DWA 568	-32.0869	18.5247	Mike Butler	DWA	0.22	0.18
DWA 207	-32.2144	22.8189	Mike Butler	DWA	1.12	0.28
DWA 596	-32.2156	18.3789	Mike Butler	DWA	0.50	0.18
DWA 562	-32.3008	18.3686	Mike Butler	DWA	0.66	0.17
DWA 591	-32.3944	20.6569	Mike Butler	DWA	2.40	0.18
DWA 174	-32.4772	24.0467	Mike Butler	DWA	0.87	0.20
DWA 213	-32.5100	27.4672	Mike Butler	DWA	1.53	0.30
DWA 195	-32.5806	27.8828	Mike Butler	DWA	0.99	0.23
DWA 599	-32.6803	21.4644	Mike Butler	DWA	1.40	0.18
DWA 555	-32.7403	19.0356	Mike Butler	DWA	0.28	0.16
DWA 575	-32.7747	21.9800	Mike Butler	DWA	1.60	0.18
DWA 586	-32.8222	18.9486	Mike Butler	DWA	1.90	0.18
DWA 585	-32.8300	18.7694	Mike Butler	DWA	1.30	0.18
DWA 203	-32.8911	26.9081	Mike Butler	DWA	0.00	0.23
DWA 574	-32.9828	18.1428	Mike Butler	DWA	1.80	0.18
DWA 573	-33.0683	21.2925	Mike Butler	DWA	1.40	0.18
DWA 577	-33.0700	20.5886	Mike Butler	DWA	1.60	0.18
DWA 182	-33.1233	26.2094	Mike Butler	DWA	1.93	0.24
DWA 197	-33.2369	27.5342	Mike Butler	DWA	0.74	0.23
DWA 214	-33.2617	24.3508	Mike Butler	DWA	0.00	0.25
DWA 201	-33.3703	26.8167	Mike Butler	DWA	0.00	0.23
DWA 601	-33.3847	18.2678	Mike Butler	DWA	1.00	0.18
DWA 178	-33.3911	25.7206	Mike Butler	DWA	1.00	0.20
DWA 593	-33.3986	23.1550	Mike Butler	DWA	0.20	0.18
DWA 221	-33.3989	23.2733	Mike Butler	DWA	0.18	0.16
DWA 594	-33.6119	22.5483	Mike Butler	DWA	0.00	0.18
DWA 566	-33.6650	19.2664	Mike Butler	DWA	0.92	0.18
DWA 219	-33.7000	25.4381	Mike Butler	DWA	0.24	0.24
DWA 548	-33.7300	19.4156	Mike Butler	DWA	0.30	0.16
DWA 581	-33.7656	20.1175	Mike Butler	DWA	0.00	0.18
DWA 598	-33.7658	20.9000	Mike Butler	DWA	0.60	0.18
DWA 582	-33.8353	22.3344	Mike Butler	DWA	0.90	0.18
DWA 193	-33.8419	23.9808	Mike Butler	DWA	0.00	0.23
DWA 567	-33.9483	22.4022	Mike Butler	DWA	1.70	0.18
DWA 198	-33.9558	24.2956	Mike Butler	DWA	1.40	0.23
DWA 209	-34.1728	24.8083	Mike Butler	DWA	0.39	0.25
DWA 588	-34.3361	21.4111	Mike Butler	DWA	0.90	0.18
DWA 587	-34.3783	20.2150	Mike Butler	DWA	0.90	0.18
DWA 570	-34.5444	19.3722	Mike Butler	DWA	1.02	0.18
DWA 590	-34.8017	20.0394	Mike Butler	DWA	1.30	0.18

Sample Name	Lat	Long	Student	Project	Tritium (TU)	TU Error
JV18KK08	-30.3113	18.4799	Jani van Gend	Buffelsrivier	0.22	0.16
JV18KK10	-30.2913	18.5870	Jani van Gend	Buffelsrivier	0.37	0.25
JV18KK11	-30.2845	18.4844	Jani van Gend	Buffelsrivier	0.20	0.24
JV18KK09	-30.2626	18.6099	Jani van Gend	Buffelsrivier	0.22	0.20
JV18KK01	-30.2319	18.0291	Jani van Gend	Buffelsrivier	1.58	0.20
JV18KK02	-30.2101	17.9339	Jani van Gend	Buffelsrivier	0.92	0.16
JV18KK03	-30.1969	18.0132	Jani van Gend	Buffelsrivier	0.32	0.15
JV18KK12	-29.9247	18.3929	Jani van Gend	Buffelsrivier	0.01	0.21
JV18KK13	-29.9108	18.3661	Jani van Gend	Buffelsrivier	1.48	0.19
JV18KK14	-29.9102	18.3662	Jani van Gend	Buffelsrivier	1.10	0.15
JV18KK07	-29.8717	18.0802	Jani van Gend	Buffelsrivier	0.89	0.21
JV18KK04	-29.8489	18.1915	Jani van Gend	Buffelsrivier	0.46	0.19
JV18KK05	-29.8304	18.1755	Jani van Gend	Buffelsrivier	0.43	0.26
JV18KK06	-29.8202	18.1332	Jani van Gend	Buffelsrivier	0.46	0.19
JV18SP02	-29.7135	17.8919	Jani van Gend	Buffelsrivier	0.45	0.18
JV18BR10	-29.7019	17.6645	Jani van Gend	Buffelsrivier	0.06	0.19
JV18BR07	-29.6754	17.5731	Jani van Gend	Buffelsrivier	0.64	0.21
JV18NB01	-29.6726	17.8131	Jani van Gend	Buffelsrivier	0.26	0.19
JV18NB03	-29.6530	17.8124	Jani van Gend	Buffelsrivier	0.21	0.23
JV18BR05	-29.6342	17.5630	Jani van Gend	Buffelsrivier	0.26	0.18
JV18KZ02	-29.6326	17.2405	Jani van Gend	Buffelsrivier	0.17	0.16
JV18NB04	-29.6226	17.8286	Jani van Gend	Buffelsrivier	0.35	0.19
JV18NB02	-29.6175	17.8059	Jani van Gend	Buffelsrivier	0.63	0.16
JV18KZ01	-29.5843	17.2414	Jani van Gend	Buffelsrivier	0.13	0.19
JV18CD02	-29.5179	17.9385	Jani van Gend	Buffelsrivier	0.71	0.18
JV18SP01	-29.4852	17.8357	Jani van Gend	Buffelsrivier	0.24	0.17
JV18SK01	-29.2694	17.5107	Jani van Gend	Buffelsrivier	0.45	0.15
JV18BR09	-29.1757	17.3339	Jani van Gend	Buffelsrivier	0.08	0.02
JV18BR19	-29.0515	17.1200	Jani van Gend	Buffelsrivier	0.09	0.02
JV18SP03	-28.9272	16.9061	Jani van Gend	Buffelsrivier	0.31	0.04
WP 508	-32.8510	21.9566	Kelly Swana	Karoo	0.10	0.02
BFB2	-32.8318	26.6229	Kelly Swana	Karoo	0.40	0.05
BFB1	-32.8264	26.6706	Kelly Swana	Karoo	0.00	0.01
RRB1	-32.8203	26.5883	Kelly Swana	Karoo	0.50	0.06
WP 505	-32.8180	21.9683	Kelly Swana	Karoo	0.40	0.05
WP 502	-32.8105	21.9703	Kelly Swana	Karoo	3.50	0.36
MWB2	-32.6560	21.3025	Kelly Swana	Karoo	1.40	0.15
CRS1	-32.1355	25.6260	Kelly Swana	Karoo	0.50	0.06
DRB4	-32.0860	25.5878	Kelly Swana	Karoo	3.10	0.32
RWB1c	-30.8660	25.5874	Kelly Swana	Karoo	0.90	0.10
RWB5	-30.8588	25.5832	Kelly Swana	Karoo	1.20	0.13
ANBH1	-30.7272	26.7282	Kelly Swana	Karoo	0.10	0.02
ANS1	-30.7153	26.7150	Kelly Swana	Karoo	0.50	0.06
LRB2	-30.6855	25.9610	Kelly Swana	Karoo	1.20	0.13
VBB1	-30.6833	25.9305	Kelly Swana	Karoo	0.60	0.07
VFB2	-29.9292	25.6795	Kelly Swana	Karoo	1.00	0.11
VFB1	-29.9180	25.6749	Kelly Swana	Karoo	0.10	0.02
FLB5	-28.7943	26.0917	Kelly Swana	Karoo	1.30	0.14
FLS1	-28.7682	26.0697	Kelly Swana	Karoo	1.60	0.17

SH18032	-26.8433	32.2846	Sabine Henry	Mozambique	0.59	0.07
SH18011	-26.8420	32.8800	Sabine Henry	Mozambique	0.96	0.11
SH18010	-26.8347	32.8835	Sabine Henry	Mozambique	0.09	0.02
SH18012	-26.8328	32.8840	Sabine Henry	Mozambique	0.61	0.07
SH18034	-26.8305	32.2366	Sabine Henry	Mozambique	0.06	0.02
SH18033	-26.8235	32.2437	Sabine Henry	Mozambique	0.99	0.11
SH18008	-26.7520	32.8259	Sabine Henry	Mozambique	0.05	0.02
SH18009	-26.7458	32.8320	Sabine Henry	Mozambique	2.04	0.21
SH18031	-26.6888	32.1800	Sabine Henry	Mozambique	0.28	0.04
SH18035	-26.6725	32.1821	Sabine Henry	Mozambique	0.45	0.06
SH18030	-26.6584	32.1845	Sabine Henry	Mozambique	0.15	0.03
SH18014	-26.5299	32.7212	Sabine Henry	Mozambique	0.04	0.01
SH18015	-26.5067	32.7101	Sabine Henry	Mozambique	0.04	0.01
SH18036	-26.5001	32.2127	Sabine Henry	Mozambique	0.22	0.03
SH18016	-26.4980	32.7128	Sabine Henry	Mozambique	0.32	0.04
SH18037	-26.4483	32.2739	Sabine Henry	Mozambique	0.31	0.04
SH18039	-26.4401	32.2425	Sabine Henry	Mozambique	0.45	0.05
SH18R01	-26.4400	32.2426	Sabine Henry	Mozambique	0.29	0.04
SH18038	-26.4220	32.2630	Sabine Henry	Mozambique	0.59	0.07
SH18005	-26.3836	32.6308	Sabine Henry	Mozambique	0.24	0.03
SH18006	-26.3808	32.6318	Sabine Henry	Mozambique	0.13	0.02
SH18004	-26.3733	32.6208	Sabine Henry	Mozambique	0.25	0.04
SH18003	-26.3675	32.6457	Sabine Henry	Mozambique	0.06	0.02
SH18041	-26.3359	32.1677	Sabine Henry	Mozambique	0.13	0.02
SH18040	-26.3359	32.1677	Sabine Henry	Mozambique	0.45	0.06
SH18029	-26.3244	32.5668	Sabine Henry	Mozambique	0.08	0.02
SH18017	-26.2361	32.6220	Sabine Henry	Mozambique	0.17	0.03
SH18018	-26.2281	32.6211	Sabine Henry	Mozambique	0.16	0.03
SH18027	-26.2208	32.6189	Sabine Henry	Mozambique	0.31	0.04
SH18024	-26.1988	32.6123	Sabine Henry	Mozambique	0.80	0.09
SH18065	-26.1190	32.1421	Sabine Henry	Mozambique	0.33	0.04
SH18059	-26.0454	32.1985	Sabine Henry	Mozambique	1.22	0.13
SH18057	-26.0433	32.2600	Sabine Henry	Mozambique	0.75	0.08
SH18058	-26.0375	32.1952	Sabine Henry	Mozambique	0.09	0.02
SH18061	-26.0341	32.1675	Sabine Henry	Mozambique	0.24	0.03
SH18022	-26.0195	32.5239	Sabine Henry	Mozambique	0.15	0.03
SH18025	-26.0162	32.5285	Sabine Henry	Mozambique	0.80	0.09
SH18021	-26.0154	32.5261	Sabine Henry	Mozambique	0.08	0.02
SH18020	-25.9994	32.5396	Sabine Henry	Mozambique	0.09	0.02
SH18042	-25.9958	32.2925	Sabine Henry	Mozambique	0.27	0.04
SH18045	-25.9924	32.2933	Sabine Henry	Mozambique	0.28	0.04
SH18047	-25.9902	32.0413	Sabine Henry	Mozambique	0.12	0.02
SH18052	-25.9901	32.0120	Sabine Henry	Mozambique	1.16	0.13
SH18053	-25.9878	32.0193	Sabine Henry	Mozambique	0.72	0.08
SH18048	-25.9868	32.0378	Sabine Henry	Mozambique	0.12	0.02
SH18046	-25.9770	32.0900	Sabine Henry	Mozambique	0.55	0.07
SH18054	-25.9752	32.0264	Sabine Henry	Mozambique	0.78	0.09
SH18051	-25.9739	32.0023	Sabine Henry	Mozambique	0.11	0.02
SH18001	-25.9550	32.5949	Sabine Henry	Mozambique	0.61	0.07
SH18091	-25.9241	32.5435	Sabine Henry	Mozambique	0.18	0.03

SH18050	-25.9235	32.0267	Sabine Henry	Mozambique	0.20	0.03
SH18089	-25.9228	32.5435	Sabine Henry	Mozambique	0.25	0.04
SH18088	-25.9224	32.5438	Sabine Henry	Mozambique	0.25	0.04
SH18087	-25.9221	32.5440	Sabine Henry	Mozambique	0.11	0.02
SH18092	-25.9175	32.5267	Sabine Henry	Mozambique	1.37	0.15
SH18049	-25.9138	32.0286	Sabine Henry	Mozambique	0.32	0.04
SH18002	-25.8958	32.3888	Sabine Henry	Mozambique	0.29	0.04
SH18043	-25.8660	32.2879	Sabine Henry	Mozambique	0.36	0.05
SH18044	-25.8527	32.2195	Sabine Henry	Mozambique	0.09	0.02
SH18093	-25.6864	32.5171	Sabine Henry	Mozambique	0.18	0.03
SH18078	-25.6832	32.6651	Sabine Henry	Mozambique	1.02	0.11
SH18081	-25.6636	32.6256	Sabine Henry	Mozambique	0.62	0.07
SH18082	-25.6533	32.5970	Sabine Henry	Mozambique	0.21	0.03
SH18083	-25.6407	32.5877	Sabine Henry	Mozambique	0.37	0.05
SH18084	-25.6117	32.5892	Sabine Henry	Mozambique	0.21	0.03
SH18086	-25.6096	32.6708	Sabine Henry	Mozambique	0.74	0.08
SH18085	-25.6025	32.5891	Sabine Henry	Mozambique	0.30	0.04
SH18064	-25.6025	32.5891	Sabine Henry	Mozambique	0.30	0.04
Jar18392	-34.0586	18.8178	J van Rooyen	National Campaign	0.23	0.17
Jar18393	-34.0586	18.8178	J van Rooyen	National Campaign	0.24	0.27
Jar18385	-34.0091	25.6657	J van Rooyen	National Campaign	0.67	0.22
Jar18386	-34.0091	25.6657	J van Rooyen	National Campaign	2.06	0.17
Jar18382	-34.0003	25.6781	J van Rooyen	National Campaign	0.95	0.16
JVR18SU001	-33.9936	18.9514	J van Rooyen	National Campaign	0.80	0.20
Jar18411	-33.9652	20.7044	J van Rooyen	National Campaign	0.40	0.23
Jar18388	-33.9024	19.1562	J van Rooyen	National Campaign	1.98	0.16
Jar18390	-33.8656	22.3615	J van Rooyen	National Campaign	1.12	0.19
Jar18384a	-33.7855	19.7548	J van Rooyen	National Campaign	0.48	0.21
Jar18383	-33.6958	19.7452	J van Rooyen	National Campaign	0.73	0.16
JAR019	-33.6758	18.9762	J van Rooyen	National Campaign	0.53	0.23
JV17098	-33.2355	22.0320	J van Rooyen	National Campaign	1.00	0.17
JV17097	-33.2335	22.0335	J van Rooyen	National Campaign	1.00	0.15
JV17096	-32.9690	21.9967	J van Rooyen	National Campaign	0.90	0.19
JV17094	-32.9689	21.9854	J van Rooyen	National Campaign	0.10	0.20
JV17094b	-32.9689	21.9854	J van Rooyen	National Campaign	0.00	0.27
JV17095	-32.9463	22.4505	J van Rooyen	National Campaign	0.10	0.23
JV17001	-32.5586	19.9885	J van Rooyen	National Campaign	0.10	0.23
JV17002	-32.5584	18.9885	J van Rooyen	National Campaign	0.00	0.16
JV17003	-31.6163	18.7360	J van Rooyen	National Campaign	0.80	0.23
JV17004	-31.5871	18.7802	J van Rooyen	National Campaign	0.40	0.22
JV17010	-31.4981	19.8746	J van Rooyen	National Campaign	1.20	0.18
JV17011	-31.4854	19.9010	J van Rooyen	National Campaign	0.80	0.28
JV17009	-31.4830	19.7937	J van Rooyen	National Campaign	0.00	0.18
JV17005	-31.4591	18.9560	J van Rooyen	National Campaign	1.10	0.17
JV17084	-31.4330	25.9757	J van Rooyen	National Campaign	0.60	0.18
JV17083	-31.3919	26.6285	J van Rooyen	National Campaign	1.50	0.20
JV17093	-31.3780	23.1152	J van Rooyen	National Campaign	1.60	0.30
JV17092	-31.3757	23.1131	J van Rooyen	National Campaign	1.10	0.23
JV17007	-31.3655	19.0677	J van Rooyen	National Campaign	0.60	0.18
JV17006	-31.3636	19.0261	J van Rooyen	National Campaign	0.20	0.16

JV17008	-31.3487	19.0508	J van Rooyen	National Campaign	0.70	0.18
JV17082	-31.0707	28.3482	J van Rooyen	National Campaign	1.10	0.18
JV17080	-31.0091	28.2779	J van Rooyen	National Campaign	1.30	0.18
JV17080A	-31.0091	28.2779	J van Rooyen	National Campaign	1.50	0.23
JV17081	-31.0084	28.2776	J van Rooyen	National Campaign	0.20	0.18
JV17079	-31.0076	28.2796	J van Rooyen	National Campaign	0.60	0.18
JV17012	-30.9770	19.4463	J van Rooyen	National Campaign	0.90	0.18
JV17013	-30.9768	19.4485	J van Rooyen	National Campaign	0.70	0.24
JV17091	-30.7365	23.4054	J van Rooyen	National Campaign	0.00	0.23
JV17090	-30.7351	23.4056	J van Rooyen	National Campaign	0.20	0.25
JV17085	-30.7327	25.7675	J van Rooyen	National Campaign	0.60	0.23
JV17086	-30.6427	25.9308	J van Rooyen	National Campaign	0.80	0.18
JV17088	-30.6280	23.8869	J van Rooyen	National Campaign	1.30	0.20
JV17089	-30.6262	23.8872	J van Rooyen	National Campaign	0.50	0.18
JV17087	-30.6243	25.9296	J van Rooyen	National Campaign	2.10	0.16
JV17014	-30.5604	20.2396	J van Rooyen	National Campaign	0.30	0.18
JV17245	-30.5188	25.6524	J van Rooyen	National Campaign	1.80	0.18
JV17244	-30.5169	25.6660	J van Rooyen	National Campaign	1.80	0.24
JV17074	-30.5142	23.4521	J van Rooyen	National Campaign	0.30	0.16
JV17075	-30.5138	29.4507	J van Rooyen	National Campaign	0.60	0.18
JV17243	-30.4575	25.6364	J van Rooyen	National Campaign	1.60	0.18
JV17077	-30.4520	29.4487	J van Rooyen	National Campaign	1.50	0.18
JV17076	-30.3769	29.4330	J van Rooyen	National Campaign	0.70	0.23
JV17219	-29.9154	27.4474	J van Rooyen	National Campaign	0.50	0.18
JV17242	-29.9126	25.6809	J van Rooyen	National Campaign	0.80	0.23
JV17226	-29.4246	26.8958	J van Rooyen	National Campaign	1.20	0.25
JV17227	-29.3897	26.9213	J van Rooyen	National Campaign	1.00	0.18
JV17241	-29.3192	25.0501	J van Rooyen	National Campaign	1.00	0.18
JV17238	-29.3154	25.0171	J van Rooyen	National Campaign	1.10	0.18
JV17230	-29.2897	26.9213	J van Rooyen	National Campaign	1.20	0.18
JV17225	-29.2733	27.4095	J van Rooyen	National Campaign	0.90	0.19
JV17223	-29.2464	27.5294	J van Rooyen	National Campaign	1.30	0.19
JV17224	-29.2464	27.5294	J van Rooyen	National Campaign	1.30	0.19
JV17222	-29.2396	27.5109	J van Rooyen	National Campaign	1.80	0.19
JV17221	-29.2237	27.4850	J van Rooyen	National Campaign	0.90	0.19
JV17220	-29.2203	27.4899	J van Rooyen	National Campaign	1.10	0.19
JV17235	-29.1933	25.0642	J van Rooyen	National Campaign	0.90	0.19
JV17228	-29.1924	27.0213	J van Rooyen	National Campaign	1.00	0.19
JV17239	-29.1819	25.0804	J van Rooyen	National Campaign	1.10	0.19
JV17236	-29.1809	25.0399	J van Rooyen	National Campaign	1.50	0.19
JV17237	-29.1740	25.0589	J van Rooyen	National Campaign	1.60	0.17
JV17240	-29.1726	25.0593	J van Rooyen	National Campaign	1.50	0.16
JV17234	-29.1388	26.1751	J van Rooyen	National Campaign	1.30	0.14
JV17233	-29.1386	26.1747	J van Rooyen	National Campaign	1.30	0.14
JV17229	-29.0839	27.0258	J van Rooyen	National Campaign	1.90	0.20
JV17231	-29.0615	27.0105	J van Rooyen	National Campaign	1.70	0.18
JV17232	-29.0514	26.9907	J van Rooyen	National Campaign	0.50	0.06
JV17216	-28.8838	27.8810	J van Rooyen	National Campaign	2.10	0.22
JV17217	-28.8773	27.8683	J van Rooyen	National Campaign	0.90	0.10
JV17218	-28.8770	27.8683	J van Rooyen	National Campaign	1.00	0.11

JV17015	-28.4745	21.2614	J van Rooyen	National Campaign	2.60	0.27
JV17215	-28.1678	28.2387	J van Rooyen	National Campaign	0.90	0.10
JV17214	-28.0145	28.3912	J van Rooyen	National Campaign	0.70	0.08
JV17020	-27.9236	22.9801	J van Rooyen	National Campaign	0.90	0.10
JV17073	-27.8870	32.2351	J van Rooyen	National Campaign	0.00	0.01
JV17072	-27.8746	32.2537	J van Rooyen	National Campaign	0.00	0.01
Jv17md31	-27.8407	22.7045	J van Rooyen	National Campaign	0.09	0.02
JV17068	-27.7571	30.7933	J van Rooyen	National Campaign	0.70	0.08
JV17213	-27.7531	28.4343	J van Rooyen	National Campaign	0.50	0.06
Jv17md14	-27.7440	22.4991	J van Rooyen	National Campaign	0.11	0.02
Jv17md16	-27.7420	22.4841	J van Rooyen	National Campaign	0.20	0.03
Jv17md17	-27.7418	22.4842	J van Rooyen	National Campaign	0.21	0.03
Jv17md13	-27.7413	22.4928	J van Rooyen	National Campaign	0.18	0.03
Jv17md18	-27.7153	22.4810	J van Rooyen	National Campaign	0.42	0.05
Jv17md15	-27.7084	22.5191	J van Rooyen	National Campaign	0.10	0.02
JV17070	-27.6932	32.3544	J van Rooyen	National Campaign	0.30	0.04
JV17069	-27.6931	32.3545	J van Rooyen	National Campaign	0.90	0.10
JV17025	-27.6448	23.9783	J van Rooyen	National Campaign	1.00	0.11
JV17024	-27.6138	23.8866	J van Rooyen	National Campaign	2.20	0.23
Jv17md03	-27.5952	22.4734	J van Rooyen	National Campaign	0.27	0.04
Jv17md04	-27.5842	22.4761	J van Rooyen	National Campaign	0.26	0.04
Jv17md05	-27.5839	22.4751	J van Rooyen	National Campaign	0.36	0.05
Jv17md32	-27.5833	22.7054	J van Rooyen	National Campaign	0.10	0.02
JV17026	-27.5540	24.1830	J van Rooyen	National Campaign	1.90	0.20
JV17028	-27.5532	29.1813	J van Rooyen	National Campaign	0.30	0.04
Jv17md01	-27.5478	22.6851	J van Rooyen	National Campaign	0.12	0.02
Jv17md06	-27.5389	22.6678	J van Rooyen	National Campaign	0.04	0.01
JV17211	-27.5253	28.5366	J van Rooyen	National Campaign	1.70	0.18
Jv17md07	-27.5227	22.6629	J van Rooyen	National Campaign	0.10	0.02
JV17212	-27.5168	28.5332	J van Rooyen	National Campaign	1.60	0.17
Jv17md28	-27.5059	22.4476	J van Rooyen	National Campaign	0.22	0.03
JV17021	-27.5029	23.2883	J van Rooyen	National Campaign	0.80	0.09
JV17022	-27.5005	23.2935	J van Rooyen	National Campaign	0.00	0.01
Jv17md02	-27.4971	22.6284	J van Rooyen	National Campaign	0.25	0.04
Jv17md33	-27.4963	22.6332	J van Rooyen	National Campaign	0.09	0.02
Jv17md30	-27.4786	22.5957	J van Rooyen	National Campaign	0.30	0.04
Jv17md29	-27.4646	22.4459	J van Rooyen	National Campaign	0.39	0.05
JV17023	-27.4304	23.4450	J van Rooyen	National Campaign	0.70	0.08
Jv17md27	-27.4060	23.0057	J van Rooyen	National Campaign	0.19	0.03
Jv17md25	-27.3831	23.0634	J van Rooyen	National Campaign	0.21	0.03
Jv17md26	-27.3828	23.0640	J van Rooyen	National Campaign	0.25	0.04
Jv17md23	-27.3822	23.0649	J van Rooyen	National Campaign	0.10	0.02
Jv17md24	-27.3818	23.0646	J van Rooyen	National Campaign	0.07	0.02
Jv17md22	-27.3817	23.0643	J van Rooyen	National Campaign	0.08	0.02
Jv17md34	-27.3725	22.6352	J van Rooyen	National Campaign	0.10	0.02
JV17210	-27.3528	28.4387	J van Rooyen	National Campaign	1.70	0.18
JV17067	-27.3314	29.8679	J van Rooyen	National Campaign	0.80	0.09
Jv17md19	-27.2616	23.0777	J van Rooyen	National Campaign	0.59	0.07
Jv17md20	-27.2444	23.0864	J van Rooyen	National Campaign	0.59	0.07
Jv17md21	-27.2295	23.0815	J van Rooyen	National Campaign	0.05	0.01

JV17032	-27.1669	26.0706	J van Rooyen	National Campaign	0.70	0.08
JV17209	-27.1332	28.5239	J van Rooyen	National Campaign	0.50	0.06
JV17031	-27.0909	25.0131	J van Rooyen	National Campaign	0.90	0.10
JV17029	-27.0617	25.0172	J van Rooyen	National Campaign	1.30	0.14
JV17030	-27.0617	25.0117	J van Rooyen	National Campaign	0.80	0.09
JV17016	-26.9823	20.7809	J van Rooyen	National Campaign	0.50	0.06
JV17017	-26.9823	20.7809	J van Rooyen	National Campaign	0.80	0.09
JV17019	-26.9805	20.7808	J van Rooyen	National Campaign	0.70	0.08
JV17018	-26.9803	20.7808	J van Rooyen	National Campaign	0.90	0.10
JV17207	-26.9677	28.5335	J van Rooyen	National Campaign	2.40	0.25
JV17208	-26.9604	28.5373	J van Rooyen	National Campaign	1.70	0.18
Jv17md11	-26.9416	22.0980	J van Rooyen	National Campaign	0.07	0.02
Jv17md12	-26.8844	22.0539	J van Rooyen	National Campaign	0.39	0.05
JV17205	-26.8763	28.2279	J van Rooyen	National Campaign	1.60	0.17
JV17204	-26.8744	28.2276	J van Rooyen	National Campaign	1.30	0.14
JV17202	-26.8597	28.2326	J van Rooyen	National Campaign	0.00	0.01
JV17206	-26.8495	28.2599	J van Rooyen	National Campaign	1.50	0.16
JV17203	-26.8486	28.2472	J van Rooyen	National Campaign	0.20	0.03
JV17033	-26.8392	26.7577	J van Rooyen	National Campaign	0.40	0.05
JV17201	-26.8355	25.1730	J van Rooyen	National Campaign	1.60	0.17
Jv17md36	-26.8107	22.9694	J van Rooyen	National Campaign	1.03	0.11
Jv17md35	-26.7959	23.0072	J van Rooyen	National Campaign	0.08	0.02
Jv17md37	-26.7787	23.0317	J van Rooyen	National Campaign	0.32	0.04
Jv17md08	-26.7724	22.7616	J van Rooyen	National Campaign	0.08	0.02
Jv17md38	-26.7716	23.0296	J van Rooyen	National Campaign	0.07	0.02
JV17066	-26.7693	28.9005	J van Rooyen	National Campaign	0.40	0.05
JV17065	-26.7562	28.9101	J van Rooyen	National Campaign	3.40	0.35
Jv17md10	-26.7135	23.0170	J van Rooyen	National Campaign	0.08	0.02
Jv17md09	-26.6044	22.8758	J van Rooyen	National Campaign	0.07	0.02
JAR022	-26.0606	28.0530	J van Rooyen	National Campaign	2.62	0.27
JV17035	-26.0047	26.7806	J van Rooyen	National Campaign	0.90	0.10
JV17036	-26.0042	26.7774	J van Rooyen	National Campaign	1.10	0.12
JAR021	-25.9840	28.0571	J van Rooyen	National Campaign	1.93	0.20
JAR020	-25.9809	28.0713	J van Rooyen	National Campaign	3.02	0.31
JV17034	-25.8909	27.4591	J van Rooyen	National Campaign	1.10	0.12
JV17064	-25.8447	29.7028	J van Rooyen	National Campaign	1.30	0.14
JV17063	-25.8010	29.7170	J van Rooyen	National Campaign	0.10	0.02
JV17062	-25.7958	29.7070	J van Rooyen	National Campaign	0.70	0.08
JV17037	-25.6383	26.9620	J van Rooyen	National Campaign	0.10	0.02
JV17038	-25.6332	26.9643	J van Rooyen	National Campaign	2.70	0.28
JV17039	-25.6331	26.9644	J van Rooyen	National Campaign	0.00	0.01
JV17061	-25.4378	30.4459	J van Rooyen	National Campaign	1.00	0.11
JV17060	-25.4375	30.4482	J van Rooyen	National Campaign	1.10	0.12
JV17058	-24.9328	30.8414	J van Rooyen	National Campaign	0.50	0.06
JV17059	-24.8851	30.7486	J van Rooyen	National Campaign	1.20	0.13
JV17040	-24.5512	28.7207	J van Rooyen	National Campaign	0.50	0.06
JV17057	-24.4024	30.6538	J van Rooyen	National Campaign	0.10	0.02
JV17056	-24.3807	31.2608	J van Rooyen	National Campaign	1.30	0.14
JV17054	-24.3763	31.1608	J van Rooyen	National Campaign	1.70	0.18
JV17055	-24.3755	31.1687	J van Rooyen	National Campaign	1.00	0.11

JV17050	-24.1695	31.3877	J van Rooyen	National Campaign	0.30	0.04
JV17052	-24.1662	31.3507	J van Rooyen	National Campaign	0.40	0.05
JV17051	-24.1648	31.3714	J van Rooyen	National Campaign	1.60	0.17
JV17053	-24.1574	31.3494	J van Rooyen	National Campaign	1.00	0.11
JV17049	-24.1560	31.3988	J van Rooyen	National Campaign	1.30	0.14
JV17047	-24.1514	31.3859	J van Rooyen	National Campaign	0.70	0.08
JV17048	-24.1421	31.3841	J van Rooyen	National Campaign	2.30	0.24
JV17046	-24.1362	30.8425	J van Rooyen	National Campaign	0.70	0.08
JV17041	-23.9176	29.5317	J van Rooyen	National Campaign	1.00	0.11
JV17042	-23.8943	29.5234	J van Rooyen	National Campaign	1.40	0.15
JV17044	-23.6247	30.1989	J van Rooyen	National Campaign	0.60	0.07
JV17045	-23.6233	30.1985	J van Rooyen	National Campaign	0.80	0.09
JV17043	-23.6205	30.1998	J van Rooyen	National Campaign	0.10	0.02
JAR024	-23.6178	30.2011	J van Rooyen	National Campaign	2.29	0.24
JAR025	-23.6151	30.2025	J van Rooyen	National Campaign	0.90	0.10
JAR026	-23.6123	30.2038	J van Rooyen	National Campaign	1.95	0.20
Jar18387	-23.6096	30.2052	J van Rooyen	National Campaign	1.40	0.15
Jar18389a	-23.6069	30.2065	J van Rooyen	National Campaign	0.41	0.05
Jar18391	-23.6042	30.2078	J van Rooyen	National Campaign	1.66	0.18
BT18VL19	-32.8272	18.7297	Britt Turner	Verlorenvlei	0.31	0.24
BT18VL18	-32.8239	18.7200	Britt Turner	Verlorenvlei	0.33	0.18
BT18VL16	-32.8219	18.7078	Britt Turner	Verlorenvlei	0.62	0.18
BT18VL17	-32.8219	18.7142	Britt Turner	Verlorenvlei	0.52	0.22
BT18VL15	-32.8150	18.7083	Britt Turner	Verlorenvlei	0.18	0.16
BT18VL10	-32.7181	18.7492	Britt Turner	Verlorenvlei	0.06	0.15
BT18VL11	-32.6811	18.7178	Britt Turner	Verlorenvlei	0.32	0.22
BT18VL13	-32.6489	18.6919	Britt Turner	Verlorenvlei	0.02	0.16
BT18VL12	-32.6483	18.6875	Britt Turner	Verlorenvlei	0.09	0.17
BT18VL07	-32.5581	18.6708	Britt Turner	Verlorenvlei	0.02	0.16
BT18VL06	-32.4974	18.5624	Britt Turner	Verlorenvlei	0.10	0.16
BT18VL08	-32.4822	18.7164	Britt Turner	Verlorenvlei	0.18	0.18
BT18VL05	-32.4728	18.5309	Britt Turner	Verlorenvlei	0.34	0.23
BT18VL04	-32.3773	18.4638	Britt Turner	Verlorenvlei	0.31	0.28
BT18VL02	-32.3161	18.3982	Britt Turner	Verlorenvlei	0.04	0.20
BT18VL03	-32.3156	18.3970	Britt Turner	Verlorenvlei	0.07	0.18
BT18VL01	-32.3139	18.4170	Britt Turner	Verlorenvlei	0.02	0.16
BT18VL14	-32.2881	18.3353	Britt Turner	Verlorenvlei	0.16	0.16
AP16Gbr03	-32.9925	18.3498	Alice Petronio	West Coast	1.00	0.16
AP16Gbr01	-32.8875	18.2721	Alice Petronio	West Coast	1.20	0.20
AP16Gbr02	-32.8695	18.3136	Alice Petronio	West Coast	1.40	0.17
AP16Gvv01	-32.5622	18.6752	Alice Petronio	West Coast	0.90	0.16
AP16GVV04	-32.3650	18.4547	Alice Petronio	West Coast	0.70	0.15
AP16Gor01	-31.8719	18.6714	Alice Petronio	West Coast	0.00	0.20
AP16Gor04	-31.5283	19.2461	Alice Petronio	West Coast	0.80	0.19
AP16Ggr05	-30.8099	17.5980	Alice Petronio	West Coast	1.40	0.20
AP16Ggr04	-30.7847	17.8549	Alice Petronio	West Coast	0.10	0.20
AP16Ggr01	-30.7614	18.0718	Alice Petronio	West Coast	0.10	0.17
AP16Gbf01	-30.7454	17.8769	Alice Petronio	West Coast	0.80	0.15
AP16Ggr03	-30.7454	17.8769	Alice Petronio	West Coast	0.60	0.15
AP16Ggr02	-30.7119	17.9691	Alice Petronio	West Coast	1.30	0.15

AP16Gbf02	-29.8032	17.4929	Alice Petronio	West Coast	0.00	0.20
AP16Gbf03	-29.7988	17.4928	Alice Petronio	West Coast	0.30	0.20
AP16Gbf04	-29.7488	17.6367	Alice Petronio	West Coast	1.00	0.16
AP16Gbf05	-29.6616	17.5813	Alice Petronio	West Coast	1.00	0.23
AP16Gbf06	-29.6608	17.5827	Alice Petronio	West Coast	0.10	0.21
AP16BF01	-29.6459	17.0965	Alice Petronio	West Coast	0.10	0.23
AP16Gbf07	-29.5823	17.2427	Alice Petronio	West Coast	0.40	0.17
AP16Gbf08	-29.5823	17.2427	Alice Petronio	West Coast	1.30	0.16
B41	-24.6614	15.9832	Alice Petronio	West Coast	1.10	0.18
AP16TS07	-24.6613	15.9833	Alice Petronio	West Coast	0.00	0.18
B32	-24.6476	15.7855	Alice Petronio	West Coast	0.00	0.15
AP16TS04	-24.6174	15.9889	Alice Petronio	West Coast	0.10	0.22
AP16TS03	-24.5292	10.3004	Alice Petronio	West Coast	0.90	0.16
S84	-24.4630	16.2373	Alice Petronio	West Coast	1.00	0.18
S83	-24.4624	16.2378	Alice Petronio	West Coast	0.80	0.20
B45	-24.4437	16.1718	Alice Petronio	West Coast	0.00	0.16
AP16TS02	-24.4419	16.1718	Alice Petronio	West Coast	0.20	0.15
NDL-B59	-24.1169	15.9056	Alice Petronio	West Coast	0.00	0.15
B37	-24.0791	16.0561	Alice Petronio	West Coast	1.20	0.18
AP15TD05	-23.9867	16.1168	Alice Petronio	West Coast	0.00	0.18
B05	-23.9821	16.8599	Alice Petronio	West Coast	1.20	0.16
NNL-B09	-23.9796	15.8518	Alice Petronio	West Coast	1.10	0.18
AP16TD03	-23.9744	15.9566	Alice Petronio	West Coast	0.20	0.16
AP16TD04	-23.9744	15.9567	Alice Petronio	West Coast	0.00	0.18
AP16KR01	-23.6363	15.1806	Alice Petronio	West Coast	1.60	0.17
AP16KR02	-23.5617	15.0399	Alice Petronio	West Coast	0.60	0.17
AP16KR03	-23.5616	15.0354	Alice Petronio	West Coast	1.30	0.15
AP16KR04	-23.1973	14.6641	Alice Petronio	West Coast	0.00	0.21
Jar18360	-33.7480	19.8618	Zita Harillal	Western Cape TMG	1.36	0.15
ZH19-KM001	-34.3371	19.0237	Zita Harillal	Western Cape TMG	0.82	0.09
ZH19-CAL002	-34.2303	19.4379	Zita Harillal	Western Cape TMG	0.29	0.04
ZH18-GRB001	-34.1842	18.9851	Zita Harillal	Western Cape TMG	1.53	0.16
ZH19-CAL001	-34.1516	19.9156	Zita Harillal	Western Cape TMG	0.25	0.03
ZH18-SW002	-34.1300	18.9113	Zita Harillal	Western Cape TMG	1.01	0.11
ZH19-SW003	-34.0895	18.8586	Zita Harillal	Western Cape TMG	0.77	0.09
ZH18-SW001	-34.0579	18.8171	Zita Harillal	Western Cape TMG	0.17	0.03
ZHKB001	-33.9906	18.4330	Zita Harillal	Western Cape TMG	0.95	0.11
ZHKB002	-33.9902	18.4330	Zita Harillal	Western Cape TMG	0.74	0.08
ZH18-VD001	-33.9835	19.2857	Zita Harillal	Western Cape TMG	1.02	0.11
ZH18-VD003	-33.9717	19.2938	Zita Harillal	Western Cape TMG	0.60	0.07
ZH19-TM001	-33.9693	18.3979	Zita Harillal	Western Cape TMG	1.87	0.20
ZH18-VD002	-33.9526	19.3152	Zita Harillal	Western Cape TMG	0.41	0.05
ZH18-SU002	-33.9406	18.8701	Zita Harillal	Western Cape TMG	1.11	0.12
ZH18-SU001	-33.9349	18.8756	Zita Harillal	Western Cape TMG	1.01	0.11
ZH18-SU003	-33.9330	18.8609	Zita Harillal	Western Cape TMG	0.27	0.04
ZH19-STB001	-33.9305	18.8693	Zita Harillal	Western Cape TMG	0.50	0.06
ZH19-FH007	-33.9247	18.9230	Zita Harillal	Western Cape TMG	0.66	0.08
ZH19-FH008	-33.9229	18.9222	Zita Harillal	Western Cape TMG	0.74	0.08
ZH19-VD004	-33.9214	19.4680	Zita Harillal	Western Cape TMG	0.50	0.06
ZH18-FH003	-33.9181	19.1216	Zita Harillal	Western Cape TMG	0.33	0.04

ZH18-BD002	-33.8956	20.9535	Zita Harillal	Western Cape TMG	0.33	0.04
ZH19-FH006	-33.8857	19.0021	Zita Harillal	Western Cape TMG	1.81	0.19
ZH19-VD005	-33.8825	19.3742	Zita Harillal	Western Cape TMG	0.12	0.02
ZH19-FH005	-33.8781	19.0123	Zita Harillal	Western Cape TMG	0.73	0.08
ZH18-FH001	-33.8732	19.0475	Zita Harillal	Western Cape TMG	0.70	0.08
ZH18-FH002	-33.8643	19.0144	Zita Harillal	Western Cape TMG	0.52	0.06
ZH18-PE001	-33.8618	22.3515	Zita Harillal	Western Cape TMG	0.41	0.05
ZH19-VD006	-33.8574	19.3657	Zita Harillal	Western Cape TMG	0.41	0.05
ZH18-BD001	-33.8255	20.8735	Zita Harillal	Western Cape TMG	0.87	0.10
ZH19-FH004	-33.8086	18.9755	Zita Harillal	Western Cape TMG	1.03	0.11
ZH18-ROB001	-33.7856	19.7554	Zita Harillal	Western Cape TMG	0.48	0.06
ZH18-DB004	-33.7855	19.0024	Zita Harillal	Western Cape TMG	0.54	0.06
ZH18-DB003	-33.7854	19.0027	Zita Harillal	Western Cape TMG	0.95	0.11
ZH18-DB002	-33.7853	19.0031	Zita Harillal	Western Cape TMG	0.82	0.09
ZH18-MON001	-33.7662	20.1171	Zita Harillal	Western Cape TMG	0.25	0.03
ZH19-RV001	-33.7192	19.3380	Zita Harillal	Western Cape TMG	1.02	0.11
ZH18-DK001	-33.6979	19.7474	Zita Harillal	Western Cape TMG	0.73	0.08
ZHR001	-33.6756	18.9760	Zita Harillal	Western Cape TMG	0.78	0.09
ZH19-W001	-33.6698	18.9094	Zita Harillal	Western Cape TMG	0.36	0.05
ZH19-NY001	-33.6350	19.6726	Zita Harillal	Western Cape TMG	0.46	0.06
ZH19-BK001	-33.6335	19.0695	Zita Harillal	Western Cape TMG	0.97	0.11
ZH19-BK002	-33.5427	19.1585	Zita Harillal	Western Cape TMG	1.25	0.13
ZH19-MAL001	-33.4470	18.7260	Zita Harillal	Western Cape TMG	0.27	0.04
ZH18-DD001	-33.4407	19.6596	Zita Harillal	Western Cape TMG	1.16	0.13
ZH18-DD002	-33.4406	19.6636	Zita Harillal	Western Cape TMG	0.69	0.08
ZH19-RBK001	-33.3857	18.8959	Zita Harillal	Western Cape TMG	0.38	0.05
ZH18-C002	-33.1764	19.3212	Zita Harillal	Western Cape TMG	2.81	0.29
ZH19-MB001	-33.1174	18.7603	Zita Harillal	Western Cape TMG	0.15	0.02
ZH18-C001	-33.0899	19.3529	Zita Harillal	Western Cape TMG	3.22	0.33
ZH18-PV001	-33.0028	18.8418	Zita Harillal	Western Cape TMG	0.10	0.02
ZH19-PV002	-32.9077	19.0547	Zita Harillal	Western Cape TMG	0.87	0.10
ZH19-CD004	-32.7407	19.0395	Zita Harillal	Western Cape TMG	0.29	0.04
ZH19-CD003	-32.6316	18.9509	Zita Harillal	Western Cape TMG	0.43	0.05
ZH19-CD002	-32.6299	18.9475	Zita Harillal	Western Cape TMG	0.37	0.05
ZH19-CD001	-32.5530	19.0201	Zita Harillal	Western Cape TMG	0.24	0.03
ZH18001	-32.5530	19.0201	Zita Harillal	Western Cape TMG	2.94	0.30